Synthesis, reactions and redox properties of 1,4-dihydro-1,4-diphosphinines and related P/Si- and P/Ge-compounds

Dissertation

zur

Erlangung des Doktorgrades (Dr. rer. nat.)

der

Mathematisch-Naturwissenschaftlichen Fakultät

der

Rheinischen Friedrich-Wilhelms-Universität Bonn

Vorgelegt von

Mridhul Ram Kottayil Madam Ramachandran

aus Kerala, India

Bonn, 2023

Angefertigt mit Genehmigung der Mathematisch-Naturwissenschaftlichen Fakultät der Rheinischen Friedrich-Wilhelms-Universität Bonn

Hiermit versichere ich, dass die vorgelegte Arbeit persönlich, selbständig und ohne Benutzung anderer als der angegebenen Hilfsmittel angefertigt wurde und alle Quellen kenntlich gemacht wurden.

''Excellence is a continuous process and not an accident''

-Dr. A. P. J. Abdul Kalam

Some of the results of this Thesis were previously published

1. M. R. K. Ramachandran, G. Schnakenburg, M. Majumdar, Z. Kelemen, D. Gál, L. Nyulászi, R. T. Boeré and R. K. Streubel, Reversible Redox Chemistry of Anionic Imidazole-2-thione-Fused 1,4-Dihydro-1,4-diphosphinines, *Inorg. Chem.* **2022**, *61*, 4639–4646, DOI: 10.1021/ acs.inorgchem.1c03620.

2. M. R. K. Ramachandran, P. C. Brehm, G. Schnakenburg, T. Sasamori, R. T. Boeré and R. Streubel, P-Centred redox reactions of a 1,4-dihydro-1,4-phosphasiline, *Dalton Trans.* **2023**, *52*, 7948–7956, DOI: 10.1039/D3DT00850A.

3. D. Welideniya, M. R. K. Ramachandran, T. Kalisch and R. Streubel, New frontiers: 1,4-diphosphinines and P-bridged bis(NHCs), *Dalton Trans.* **2021**, *50*, 9345–9366, DOI: 10.1039/ D1DT01624E.

Conference contributions

1. *Preparation and reactivity studies of 1,4–diphosphinines*, **M. R. K. Ramachandran**, R. Streubel, MHC-10 (Mitarbeiterworkshop für Hauptgruppenelementchemie-10), Tübingen, Germany, March 15–17, 2019 (*Oral presentation*).

2. *Synthesis and reactions of anionic 1,4-dihydro-1,4-diphosphinines*, **M. R. K. Ramachandran**, R. Streubel, 13th International Conference on Heteroatom Chemistry (ICHAC 2019), Prague, Czech Republic, June 30–July 5, 2019 (*Poster presentation*).

3. *Synthesis and reactions of anionic 1,4-dihydro-1,4-diphosphinines*, **M. R. K. Ramachandran**, R. Streubel, 17th European Workshop on Phosphorus Chemistry (EWPC 2020), Rennes, France, February 26–28, 2020 (*Poster presentation*).

4. *Synthesis and redox chemistry of anionic imidazole-2-thione-fused 1,4-dihydro-1,4-diphosphinines,* **M. R. K. Ramachandran**, R. Streubel, 18th European Workshop on Phosphorus Chemistry (EWPC 2021), conducted online as Online Workshop on Phosphorus Chemistry (OWPC), March 29–31, (*Poster presentation*).

5. *1,4-diphosphinines: Chemistry towards the development of molecular batteries*, **M. R. K. Ramachandran**, M. Majumdar, T. Sasamori, R. Streubel, 23rd International Conference on Phosphorus Chemistry (ICPC-23), July 5–9, 2021, Częstochowa, Poland (online) (*Poster presentation*).

6. *Tricyclic 1,4-heteroatom-phosphinines-small molecule activators?,* **M. R. K. Ramachandran**, R. Streubel, MHC-11 (Mitarbeiterworkshop für Hauptgruppenelementchemie-11), Bonn, Germany September 3–5, 2021 (*Oral presentation*).

7. *1,4-diphosphinines : Chemistry towards the development of molecular batteries*, **M. R. K. Ramachandran**, R. Streubel, #RSCBatteriesPoster session organized by the Twitter handle of RSC, December 7-8, 2021.

8. *How to apply imidazole-2-thiones in the synthesis of 1,4-hydro-1,4-Phosphasilines?*, **M. R. K. Ramachandran**, T. Sasamori, R. Streubel, 16th International Symposium on Inorganic Ring Systems (IRIS-16), Graz, Austria, July 24–29, 2022, (*Poster presentation*).

9. *En route to 1,4-dihydro-1,4-Phosphasilines from imidazole-2-thiones*, **M. R. K. Ramachandran**, R. Streubel, 18th European Workshop on Phosphorus Chemistry (EWPC-18), Rostock, Germany, September 14–16, 2022 (*Oral presentation*).

10. *Reactions of Functional 1,4-Dihydro-1,4-Phosphasilines*, **M. R. K. Ramachandran**, T. Sasamori, R. Streubel, 19th European Workshop on Phosphorus Chemistry (EWPC-19) and 3rd Spanish Workshop on Phosphorus Chemistry (SWPC-3), Donostia-San Sebastián, Spain, March 28–30, 2023 (*Poster presentation*).

11. *How to Access P, Ge/Si-Hetarenes?*, S. Karwasara, **M. R. K. Ramachandran**, T. Sasamori, R. Streubel, 19th European Workshop on Phosphorus Chemistry (EWPC-19), Donostia-San Sebastián, Spain, March 28–30, 2023 (*Poster presentation*).

12. *En route to mixed hetarenes from imidazole-2-thiones*, S. Karwasara, **M. R. K. Ramachandran**, T. Sasamori, R. Streubel, Canadian Chemistry Conference and Exhibition (CSC 2023), Vancouver, Canada, June 4–8, 2023 (*Poster presentation*).

Contents

1|Introduction

1.1 History and relevant chemistry of phosphanes

Phosphanes, also known as phosphines, played a major role in the development of organophosphorus chemistry. The parent compound PH_3 was discovered in 1783 by Philippe Gengembre by heating white phosphorus in an aqueous solution of potash (potassium carbonate). Once, it was mistakenly regarded as the gaseous form of the element phosphorus, but Lavoisier rectified this misinformation and recognised it as a combination of phosphorus with hydrogen. The industrial production of phosphane (PH_3) came later into the scenario and its manufacture was patented in 1961 and 1962. Industrially, by the "alkaline process" (Scheme 1.1), it can be made by the reaction of white phosphorus with sodium or potassium hydroxide, producing potassium or sodium hypophosphite as the by-product. Alternatively, by the "acid process", the acid-catalyzed disproportionation of white phosphorus yielded phosphoric acid and phosphine.[1]

$$\text{(i)} \quad 3\ MOH + P_4 + 3\ H_2O \xrightarrow{80\ °C} 3\ MH_2PO_2 + PH_3 \; ; M = K, Na$$

$$\text{(ii)} \quad 2\ P_4 + 12\ H_2O \xrightarrow{H^+,\ 280\ °C} 3\ H_3PO_4 + 5\ PH_3$$
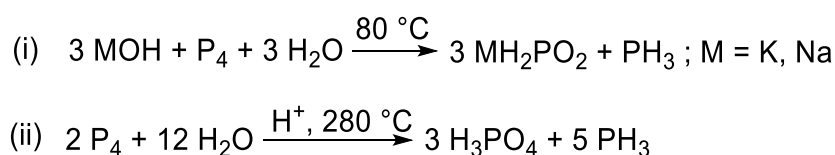
Scheme 1.1. (i) Phosphine synthesis via alkaline process; (ii) phosphane synthesis via the acid process.[1]

Phosphane is widely used in organophosphorus chemistry mainly for the synthesis of functionally substituted organic and hetero-organic phosphanes, effectively used as important auxiliary reagents, ligands for metal-complex catalysts, extractants, fire-proofing agents, etc.,[2–5] Phosphanes have shown immense application in the field of nucleophilic phosphine catalysis.[6] Among its first reports was the formation of the zwitterionic adducts **I** formed from triethylphosphane and ethylenemalononitrile (Scheme 1.2) by Horner in 1955.[7] Later, Winterfeldt reported the first hetero-bimolecular phosphine catalysis between dimethyl acetylenedicarboxylate and aldehydes to form butenolides **II**.[8]
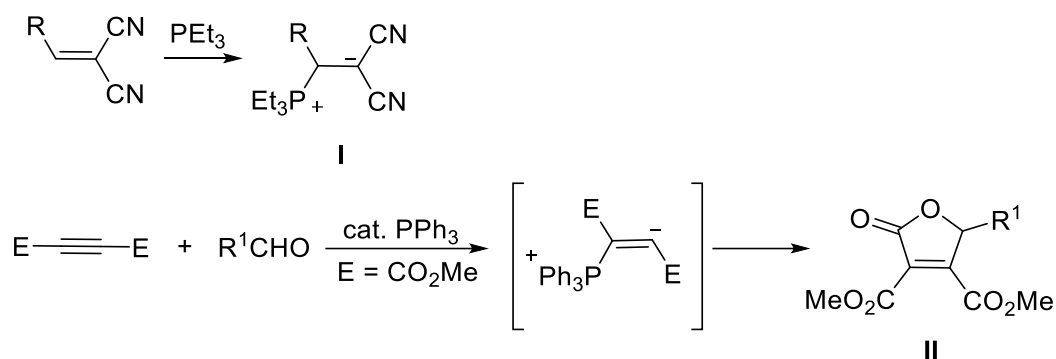
Scheme 1.2. Formation of the zwitterionic adducts **I** from triethylphosphane and ethylene malononitrile; phosphane-catalyzed reaction to form butenolides **II**.[7,8]

1.2 Chemistry of low-coordinate organophosphorus compounds

Phosphorus–carbon multiple bonds are generally formed by the overlap of p-orbitals on both atoms ($p\pi$, $p\pi$-multiple bonds). The formal CH/P substitution of respective unsaturated organic compounds could result in P,C multiple bonded compounds, owing to the same number of electrons and valence electrons for a phosphorus atom and a CH fragment, respectively. The theoretical studies by Pitzer[9] and Mulliken[10] neglected the existence of species possessing π-bonds to phosphorus or other heavy elements. But, the reports from Gier[11] and also from Dimroth and Hoffman[12] regarding the isolable low-coordinate phosphorus compounds broke down the hypothesis of Pitzer and Mulliken. Becker synthesized the first phosphorus–carbon double bonded compound with hetero-substitution by implementing kinetic stabilization, in 1976.[13] A couple of years later, Bickelhaupt reported the first stable all carbon-substituted phosphorus–carbon double bonded compound, phosphaethene (**III**), kinetically stabilized by a bulky mesityl group (Figure 1.1).[14] After a few years, Yoshifuji reported the first stable phosphorus–phosphorus double bonded compound, named diphosphene **IV**, again, kinetically stabilized by a 2,4,6-tri-*tert*-butylphenyl group (abbreviated as Mes*).[15,16] Moreover, the synthetically challenging phosphaalkyne compound **V**, was achieved by Becker by the implementation of the bulky *tert*-butyl substituent.[17] The phosphinine derivative **IX** (Figure 1.3) reported by Märkl earlier on also gave a boost to the field of P,C multiple bonded chemistry.[18]
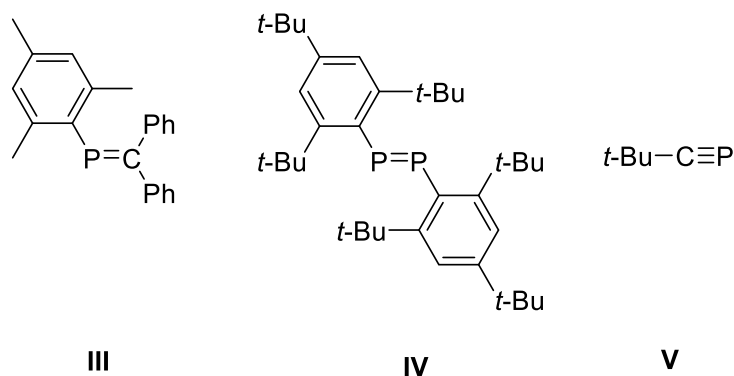
Figure 1.1. First stable phosphaethene compound **III**; first stable diphosphene compound **IV**; first stable phosphaalkyne compound **V.**[14–16]

The π-conjugated phosphorus analogs of butadienes, polyenes, and cumulenes containing one or more phosphorus atoms were synthetically explored.[19] Most importantly, their spectroscopic properties tethered with the π-conjugation were also investigated.[20,21] The π-conjugating substituents were successfully implemented to lower the LUMO energies of a number of P,C double bonded systems.[22–24] Apart from the usual phosphaalkene systems, a recent book chapter discusses the redox behavior of diphosphenes, and beyond.[25] Due to the in-sufficient overlap of the $3p$ orbitals of the P atoms, weaker π-bond, and lower lying π* orbitals result, with respect to the N=N double bond, and it is observed that the P=P double bond can be easily reduced to the corresponding anion radical species.[26–28]
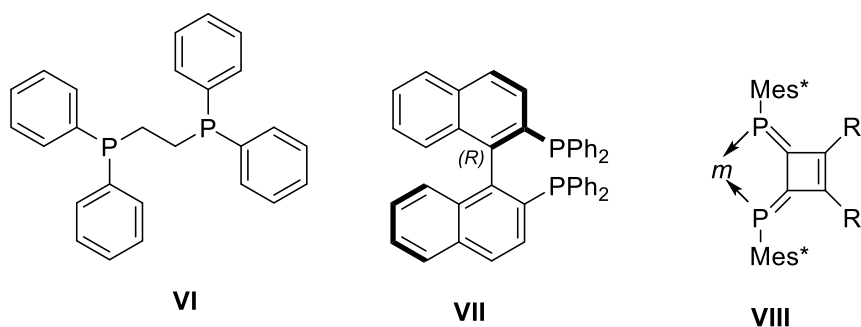
Figure 1.2. Important phosphine ligands majorly used in coordination chemistry and catalysis.[29–36]

1,2-Bis(diphenylphosphino) ethane (DPPE, **VI**) and 2,2'-bis(diphenylphosphino)-1,1'-binaphthyl (BINAP, **VII**) have been widely used in organic synthesis as well as in coordination chemistry utilizing their sp^3-hybridized P-atoms in a bidentate coordination mode (Figure 1.2).[29] Diphosphinidene-cyclobutenes[34,37] were reported to act as bidentate ligand[32,33] to

ligate transition metals to form the complexes of the form **VIII**. These complexes were generally used for cross-coupling reactions[31,35], polymerization catalysts[36] etc.

1.3   Hetarenes : Phosphinines and other group 15 analogs

Phosphinines, also known as phosphabenzenes, are the most intensively studied out of the heavier group 15 analogs of benzene.[38–42] With the synthesis of the first $\sigma^2\lambda^3$-phosphinine (σ^2 indicates two substituents attached to the P and λ^3 refers to a P with three bonding valence electrons) derivative **IX** (Figure 1.3) by Märkl, a remarkable expansion of phosphorus heterocyclic chemistry was achieved,[18] e.g., Ashe III synthesized the parent compound **X**.[43]

IX   **X**   **XI**   **XII**
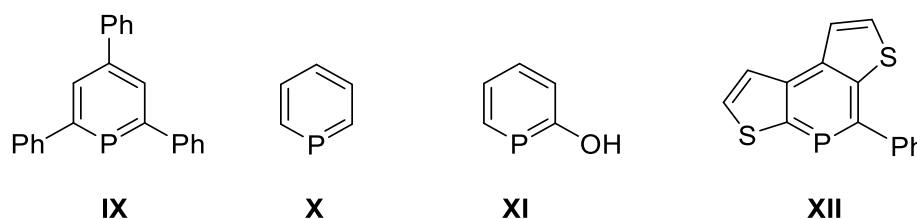
Figure 1.3. First $\sigma^2\lambda^3$-phosphinine derivative **IX**, the parent phosphinine **X** as well as some examples of functionalized phosphinines **XI**, **XII**.[18,43–49]

Due to the incorporation of the phosphorus atom in the benzene ring, the π-conjugation within the ring is perturbed and, therefore, the aromaticity is diminished to ~ 88 % of the aromaticity of benzene.[47] There is a remarkable difference in the nature of the lone pair when phosphinine is compared to pyridine considering their frontier molecular orbital situation. It was calculated that the lone pair in the parent phosphinine has little to no nucleophilic character as it resides in a less directional and more diffused HOMO^{-2} orbital being energetically very low (Figure 1.4).[40] In addition, the LUMO in phosphinine has a large coefficient on the phosphorus atom and is much lower in energy compared to that of pyridine. This is considered to be the major reason that the weaker σ-donor and much stronger π- acceptor properties are attributed to phosphinine compared to pyridine.
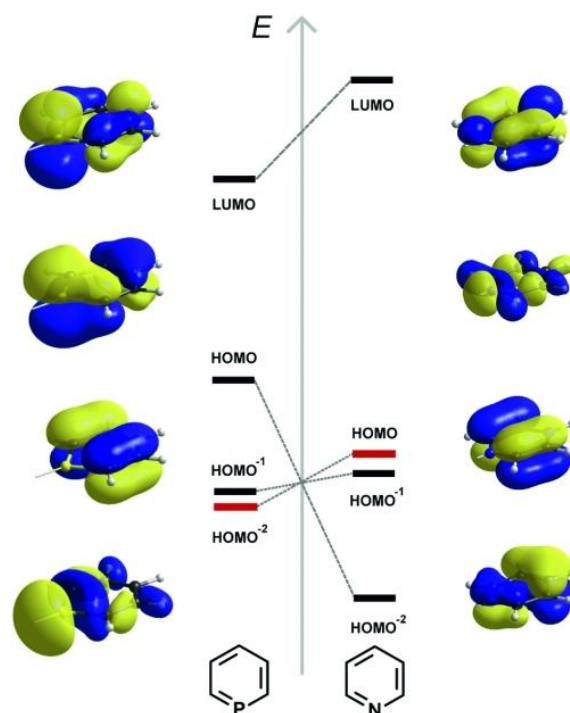
Figure 1.4. Frontier orbitals of phosphinine and pyridine (taken from the literature contribution of C. Müller).[39]

Development of different synthetic approaches for a large variety of differently substituted phosphinines, like *o*-hydroxy functionalized phosphinines **XI**[44–46], thienyl-substituted phosphinines **XII**[48,49] etc. were also reported later (Figure 1.3).

The other heavier group 15 benzene analogs, parent arsabenzene[43] and extremely labile stibabenzene[50,51] were successfully isolated by Ashe III in 1971. The very first example of bismabenzene compound was also isolated quite recently, implementing bulky substituents in the *ortho*-positions[52], thus kinetically stabilizing a highly reactive system.

1.4   Key reactivity studies on phosphinines

It has been reported that the sequential addition of nucleophiles and electrophiles to the electrophilic phosphorus center of a η^6-complex **XIII** would lead, finally, to η^5-phosphacyclohexadienyl complexes **XV** (Scheme 1.3).[53–55] The intermediately formed λ^4-phosphinine anions can be formed, e.g. from λ^3-phosphinine by the attack of MeLi which was reacted with $FeCl_2$ to form bis(1-R-2,4,6-trisubstituted phosphinine) iron complexes.[56–58]

Later on, Le Floch isolated stable λ^4-phosphinine anions **XVII** from phosphinines **XVI** with either phenyl or trimethylsilyl groups at the 2 and 6 positions.[59]
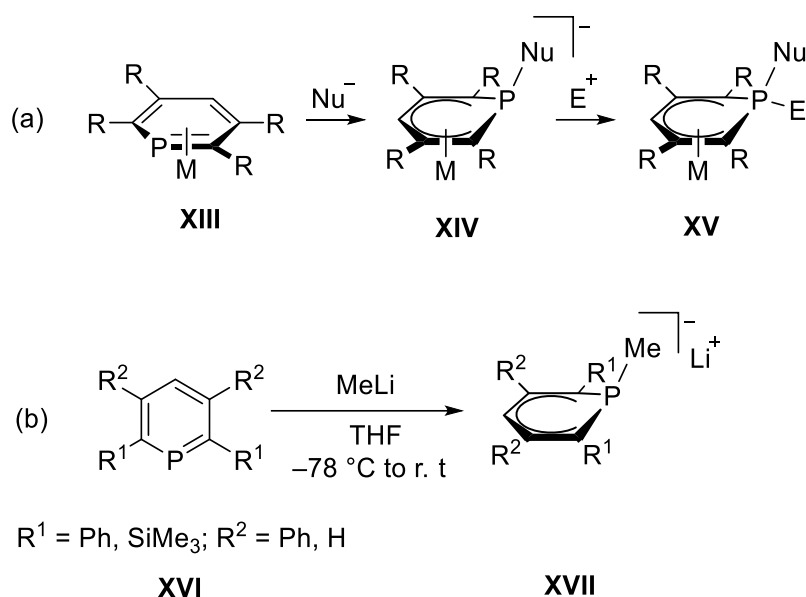
Scheme 1.3. (a) Sequential addition of nucleophiles and electrophiles to form the η^5-phosphacyclohexadienyl complexes **XV**; (b) synthesis of the first isolated stable λ^4-phosphinine anions **XVII**.[53–55,59,60]

The electrophilic nature of the P-centers was further explored by the reactions of Grignard or organolithium reagents to form λ^4-phosphinines **XVIII**[61], and this compound was then transformed into an η^6-Rh^{I} complex (Figure 1.5). The low basicity of the P-centers was confirmed by the many failures of protonation reactions, and only if super-strong Brønsted acids were used, compounds such as **XIX** could be formed.[62] In the same vein, alkylation and silylation forming **XX** using alkyl/silyl carborane reagents was discussed.[62] Phosphinium cations **XXI** were also achieved by treating a λ^4-phosphinine with hexachloroethane and, subsequently, abstracting a chloride with GaCl$_3$.[60] Another important aspect regarding the synthetic versatility of phosphinines were to undergo one electron reduction and oxidation.[63–66] The seminal report from Le Floch and Mathey described the formation of a radical monoanion from a phosphinine heterocycle and its further reduction with Na naphthalenide led to the formation of dianion **XXII**, linked by a P-P bond.[67] Here, most importantly, two phosphinine moieties adopted a phosphacyclohexadienyl structure and were linked by a P–P bond whose length (2.305(2) Å) observed to be only slightly longer than a usual P–P bond.

$CHB_{11}Me_5Cl_6$

E = Me; X = $CHB_{11}Me_5Br_6$
E = Et_3Si; X = $CHB_{11}Cl_{11}$

XVIII   **XIX**   **XX**

2 [Na(2.2.2)]$^+$

$GaCl_4^-$

XXI   **XXII**
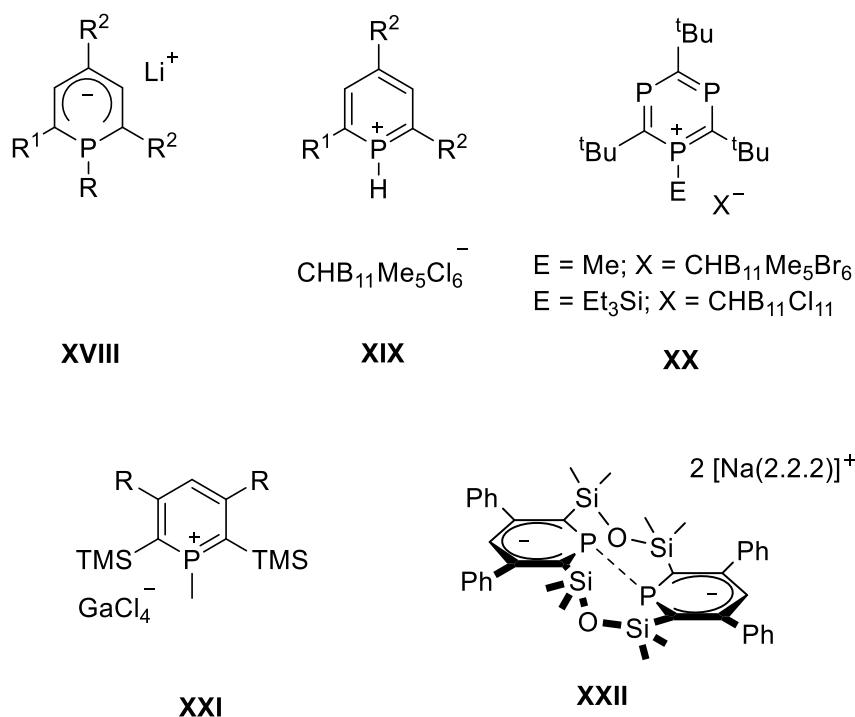
Figure 1.5. Examples of important classes of compounds accessed via σ²λ³-phosphinines.[61–66]

Phosphinines are generally considered as ambidentate ligands due to their ability to coordinate to metal centers via the lone pair on the phosphorus atom or via the aromatic π-system. Their HOMO^{-2} is suitable for σ-coordination to a metal center and, on the other hand, HOMO^{-1} and HOMO orbitals can participate in η⁶-coordination.[40] Considering these aspects, phosphinines show a rich transition metal coordination chemistry.[68–70] Most commonly observed is the η¹-coordination[71,72] via the phosphorus lone-pair and η⁶-coordination via the π-system generally occurring with early transition metals (Figure 1.6).[53,73–76] Apart from these general coordination modes, μ²-mode with phosphinines bridging two or more metal centers are also known.[77–79] A combination of η¹, μ²-coordination modes were also described in the case of an Os complex possessing bridging phosphinine ligands with an additional coordination to another metal center via the α-carbon.[80]

σ-mode; η¹   π-mode; η⁶   σ/π-mode; η¹, η⁶   σ-mode; μ²
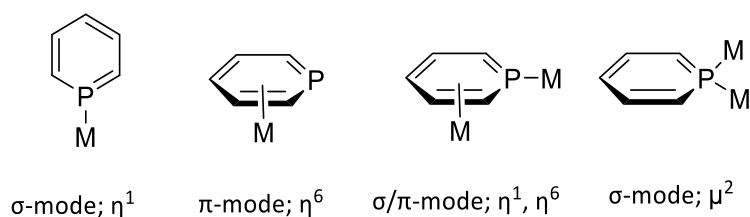
Figure 1.6. Common coordination modes of phosphinines.

The first report on phosphinine-based homogenous catalysis was reported by Zenneck in 1996[81], when an η^6-phosphinine–Iron complex was used in the catalytic [2+2+2] cyclotrimerization reactions to give phenyl and pyridine derivatives. There are a number of reports on Rhodium-catalyzed hydroformylation of terminal and internal olefins where phosphinine ligands are used.[82–84] Phosphinine-based Pd[II] complexes were used for Miyaura coupling reactions between aryl halides and pinacolborane to form boronic esters.[85] Mixtures of chiral and achiral monodentate phosphorus ligands were used in Rh-[39,86] and Ir-catalyzed[39] asymmetric hydrogenation reactions.

1.5   The synthetic history of diphosphinines

In the case of $1\lambda^5,2\lambda^3$-diphosphinines, a single report came from the group of Bickelhaupt concerning **XXIII**, but the compound was not isolated and purified (Figure 1.7).[87] Comparatively well-known $1\lambda^3,3\lambda^3$-diphosphinines were intially reported by Zenneck in 1995.[88] The first product of metal-assisted cyclotrimerization was formed as an iron complex, and the free 1,3-diphosphinine **XXIV** was released via oxidation with CCl_4 at elevated temperature.
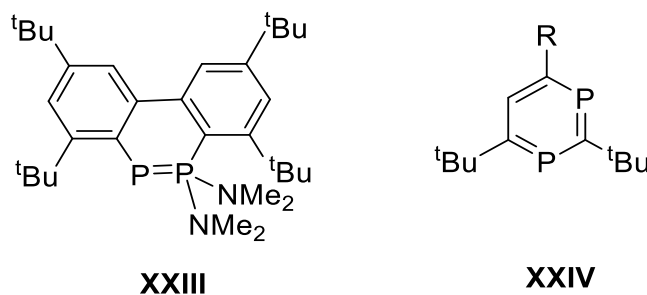
Figure 1.7. Reported $1\lambda^5,2\lambda^3$-diphosphinines **XXIII** and $1\lambda^3,3\lambda^3$-diphosphinines **XXIV**.[87,88]

The chemistry of 1,4-diphosphinines was instigated by the discovery of the very first derivative **XXV** (Figure 1.8) by Kobayashi in 1976.[89] Despite the unsuccessful isolation, the derivative was effectively used for a few *in situ* organic transformations.[89] After four decades, Streubel and coworkers isolated the first stable, tricyclic 1,4-diphosphinine derivatives with imidazole-2-thione **XXVI**[90]or thiazole-2-thione **XXVII**[91] fused to both sides.

XXV

XXVI : E = NR ; R = Me, ^{n}Bu

XXVII : E = S
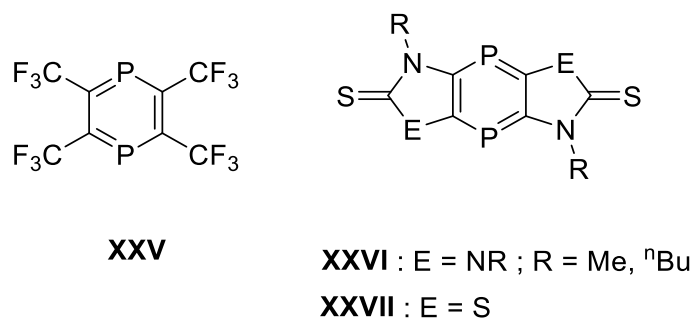
Figure 1.8. First 1,4-diphosphinines **XXV**; first synthetically isolated 1,4-diphosphinines **XXVI** and **XXVII**.[89−91]

Later on, the group of Ghadwal synthesized and isolated a series of zwitterionic or salt-like, dinuclear compounds: 1,4-digermine **XXVIII**[92], 1,4-distannine **XXIX**[93], 1,4-diarsinine **XXX**[94], 1,4-distibine **XXXI** [95], and tuned them for applications such as small molecule activation. Here, Ghadwal utilized the imadazolium unit fused tricycles with appropriate substitutions towards the target compounds (Figure 1.9).

XXVIII

XXIX

XXX
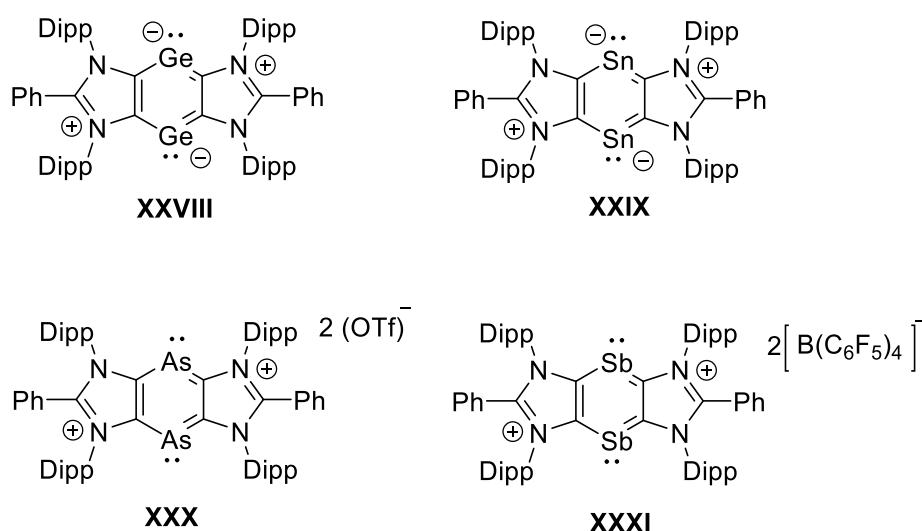
XXXI

Figure 1.9. The isolated heterodinuclear benzene analogs, 1,4-digermine **XXVIII**, 1,4-distannine **XXIX**, 1,4-diarsinine **XXX**, 1,4-distibine **XXXI**.[92−95]

1.6   P-centered reactions of 1,4-diphosphinines

1.6.1   Theoretical studies

A number of theoretical studies have explained the electrophilic nature[90,91,96] of the P-centers of stable 1,4-diphosphinines by focusing on orbital energies and, hence, helped to understand the feasibility of the formation of ionic/radical species.
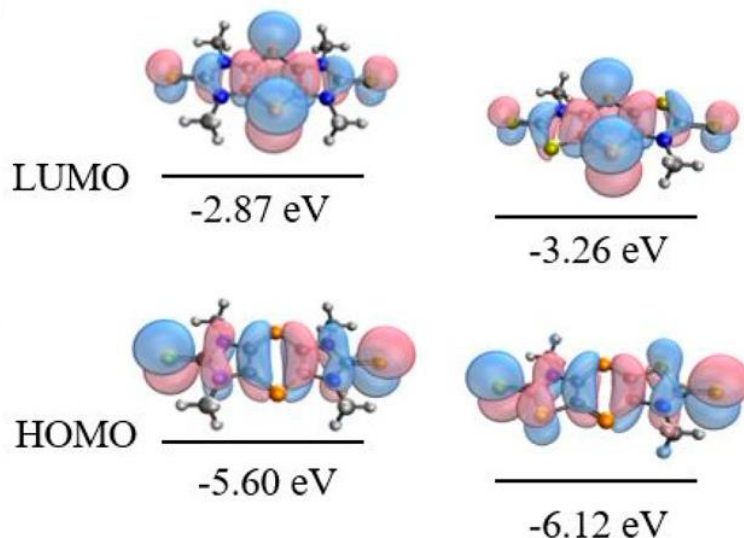
Figure 1.10. HOMO and LUMO for **XXVI** (left) and **XXVII** (right) calculated at B3LYP/cc-pVTZ//M06-2X/cc-pVTZ level of theory.[97,98]

The HOMOs consist of the anti-bonding combination contributed by the HOMOs of imidazole-2-thione (for **XXVI**) and thiazole-2-thione (for **XXVII**) with zero contribution at the phosphorus atoms (Figure 1.10). Importantly, the LUMOs were observed to have large contributions at phosphorus pointing to the good π-acceptor abilities. On the other hand, the phosphorus lone pairs are calculated to be very low in energy, represented by the HOMO^{-6} (for **XXVI**, ε = −8.40 eV) and HOMO$^{\pi}$ (for **XXVII**, ε = −8.85 eV), underlining the poor σ-donor ability of these compounds.[97]

1.6.2 Electrochemical studies

The feasibility of the formation of monoanion and dianion was investigated thoroughly via CV experiments on 1,4-diphosphinines **XXVI** and **XXVII** (Table 1.1). The theoretical calculations and the aforementioned orbital energy studies together helped to obtain an understanding on the accessibility and stability of these anions.[90,91]

Table 1.1. Oxidation and reduction peak potentials of 1,4-diphosphinines **XXVI** and **XXVII**.

Compound	E_p^a/V	E_p^c/V	Redox process reversibility
XXVI	−0.61, −0.34	−1.74, −2.59	Irreversible (oxidation), pseudo-reversible (reduction)
XXVII	−1.042, −1.343, 0.698	−1.28, −1.45	Irreversible

XXVI showed two pseudo-reversible redox waves representing a two-electron reduction and one-electron reduction and the theoretical studies confirmed the stability of the first radical anionic state.[90] Same was observed for **XXVII**, but the central reduction processes E_p^c were at significantly lower potential than in **XXVI** pointing to the easily reducible nature of **XXVII**. Also, it was found that monoanion and dianion were more stable for **XXVII** than for **XXVI** which was supported by the lower energies of LUMO and HOMO for **XXVII** compared to **XXVI** (Figure 1.10). The dianion was anti-aromatic in nature which was somewhat surprising.

1.6.3 Reactivity studies

The electrochemical and theoretical observations were validated by various reactivity studies. The Streubel group has reported the sequential addition of nucleophiles such as *n*-BuLi to 1,4-diphosphinine **XXVII** leading to the formation of the anionic derivatives **XXXII** and the subsequent reaction with *n*-BuI giving **XXXIII** (Scheme 1.4).[91]
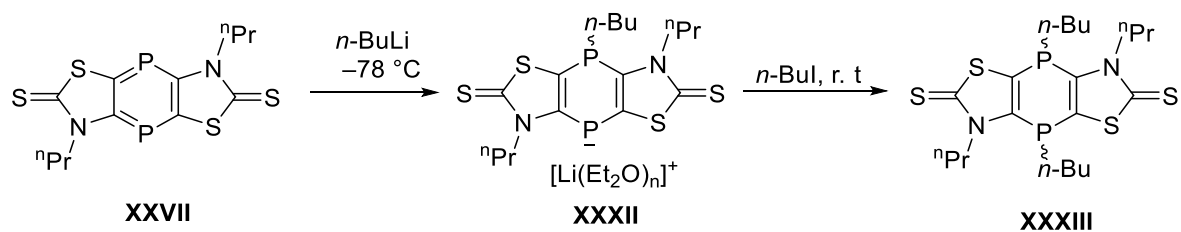
Scheme 1.4. Sequential addition of nucleophiles and electrophiles into the 1,4-diphosphinine **XXVII** to form the species **XXXIII**.[91]

In a modified protocol, the thiazole-2-thione-based 1,4-diphosphinine **XXVII** gave access to an isolable anionic tricyclic 1,4-dihydro-1,4-diphosphinine derivative **XXXIV**. Anionic derivative **XXXIV** was oxidized by I_2 to give product **XXXV** with a P-P bond via an assumed transient radical intermediate (Scheme 1.5).[91]

XXVII   **XXXIV**   **XXXV**
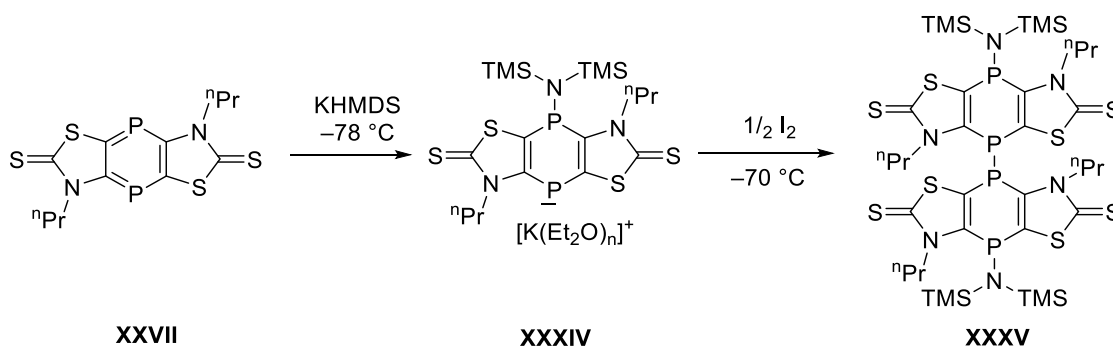
Scheme 1.5. Synthesis of **XXXIV** from 1,4-diphosphinine **XXVII** by the addition of weak nucleophile KHMDS and its subsequent oxidation to form the dimer **XXXV**.[91]

1.7   P-centered reactions of 1,4-dihydro-1,4-diphosphinines

1.7.1   Monocyclic systems

When it comes to monocyclic 1,4-dihydro-1,4-diphosphinines, only a few synthetic examples are known until now. Märkl reported the synthesis of 1,4-dihydro-1,4-diphosphinine **XXXVI** by the cyclizing addition of phenylphosphane to *tert*-butyl(diethinyl)phosphane.[99] The first example of a double phosphonium formation, starting from 1,4-dihydro-1,4-diphosphinine **XXXVI**, was provided by Märkl thus leading to the bicyclic bis-phosphonium salt **XXXVII** (Scheme 1.6).[99]
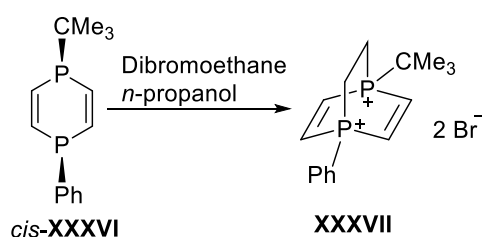
cis-**XXXVI**   **XXXVII**

Scheme 1.6. Reaction of *cis*-**XXXVI** and 1,2-dibromoethane to form the bridging bis-phosphonium salt **XXXVII**.[99]

1.7.2   Tricyclic 1,4-dihydro-1,4-diphosphinines

A seminal example of a nucleophilic substitution reaction at the P-centers was reported by Streubel,[100] *i.e.*, 1,4-dichloro-1,4-dihydro-1,4-diphosphinines **XXXVIII** reacted with organo lithium derivatives to form substitution products such as **XXXIX** (Scheme 1.7). 1,4-Dichloro-1,4-dihydro-1,4-diphosphinines **XXXVIII** were also effectively used for the synthesis of the first isolated derivative of 1,4-diphosphinines **XXVI** by the reduction using *n*-Bu$_3$P.[90]
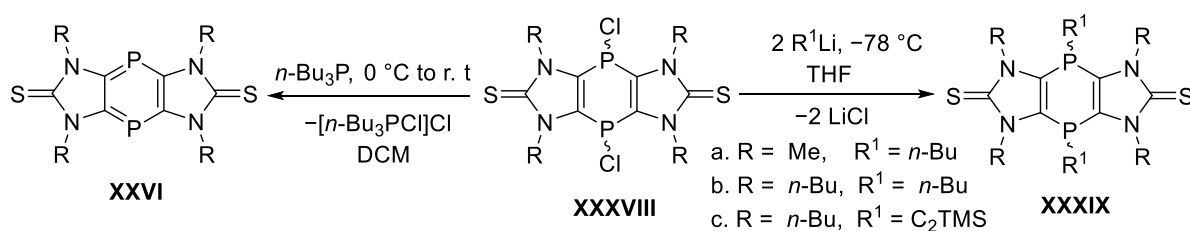
Scheme 1.7. Nucleophilic substitution reactions of the 1,4-dichloro-1,4-dihydro-1,4-diphosphinines **XXXVIII** to form the alkylated products **XXXIX;** reduction of **XXXVIII** to form the first stable 1,4-diphosphinines **XXVI**.[90]

The P-centered reduction of 1,4-dihydro-1.4-diphosphinine derivative **XL** gained prominent attention and formation of very reactive, antiaromatic P-anionic species **XLI** was observed by the addition of strong reducing agents such as potassium. Unfortunately, they could not be isolated but quenched with *n*-butyl iodide to form neutral *P*-butyl substitution products **XLII** (Scheme 1.8).[101]
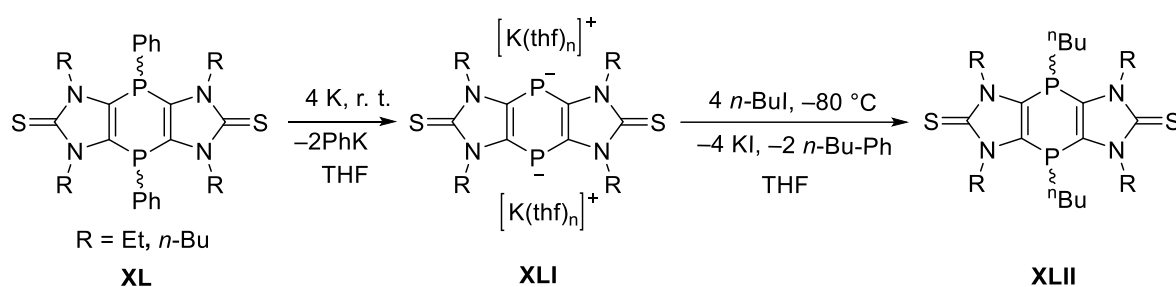
Scheme 1.8. Twofold reductive cleavage of P–Ph bonds to form tricyclic bis-phosphanides **XLI** and their quenching to form the neutral products **XLII.**[101]

In a recent report from Ghadwal[102], they synthesized a 1,4-diphosphinine-1,4-diide compound **XLIV** which was isolated and structurally characterized**,** by the reduction of the tetrachlorinated zwitterionic compound **XLIII** either by Mg or KC$_8$ (Scheme 1.9). They also

reported that the dianionic compound **XLIV** has a 8π-electron C_4P_2 system with significant anitiaromatic character. But the latter has been recognized earlier by the Streubel group.[101]
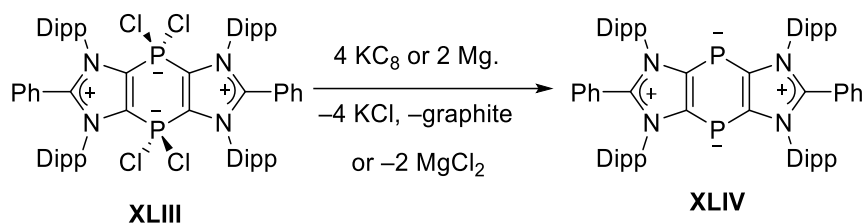
Scheme 1.9. Synthesis of 1,4-diphosphinine-1,4-diide compound **XLIV** from zwitterionic **XLIII** by reduction using KC_8 or Mg.[102]

1.8 P-containing mixed heterocyclic aromatic systems

There are only few examples of mixed systems with two different main group atoms in a benzene ring. Examples can be found with the first row main group elements, *e.g.*, 1,2-, 1,3- and 1,4-azaborines have been synthetically achieved. A lot of reports have explained their aromatic nature experimentally and computationally[103–105] On the other hand, the isolated 1,2-azaalumines adopt non-planar structures due to the absence of π- bonding between aluminum and nitrogen.[106]
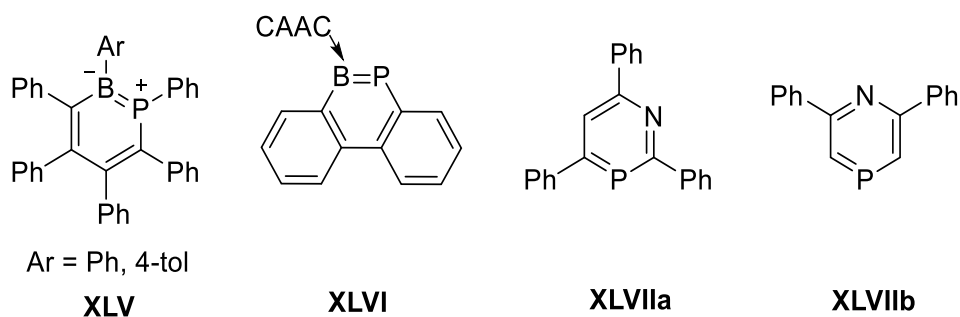
Figure 1.11. 1,2-Phosphaborines **XLV** and **XLVI**; 1,3-azaphosphinine **XLVIIa** and 1,4-azaphosphinine **XLVIIb**.[30,107–113]

Concerning mixed diatomic rings with one phosphorus atom and another main group element, there are very few examples with a non-second row element. On the other hand, the ring expansion reactions of boroles with suitable conditions led to the successful formation of 1,2-phosphaborines with highly planar C_4BP rings **XLV** (Figure 1.11).[107] Half a

decade later, Wilson and Gilliard reported the cyclic(alkyl)(amino)carbene (CAAC) stabilized BP-doped phenanthryne compound **XLVI**.[108] A number of 1,3[30,109–111] and 1,4-azaphosphinine[112,113] derivatives **XLVIIa** and **XLVIIb**, respectively, were synthesized from triazines, as reported by Mathey.

1.9   Group 13 analogs of phosphinines

The implementation of kinetic stabilization on the heteroatomic center via bulky substituents in the *o*-positions effectively blocked further reactions as well as dimerization. This enabled the successful synthesis of an array of phosphinine analogs in which the phosphorus is replaced by a group 13 element fragment ER such as in galabenzenes **XLVIII** and **XLIXa**, aluminabenzenes **XLIXb** and indabenzenes **XLIXc** in their anionic form (Figure 1.12).[114–117]
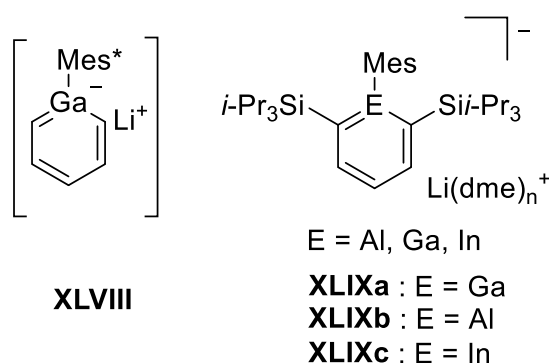
Figure 1.12. First gallatabenezene derivative **XLVIII** and first structurally confirmed derivative **XLIXa**; aluminatabenzene **XLIXb** and indatabenzene **XLIXc**.[114–117]

1.10 Group 14 analogs of phosphinines and diphosphinines

In the case of phosphinine analogs containing group 14 elements, especially Si, there were several reports where these aromatic species were (merely) observed but not isolated.[118,119]

In 1997, Tokitoh reported the first isolated and structurally determined silabenzenoid compound, 2-silanaphthalene **L** (Figure 1.13), by protecting its reactive silicon center with an extremely bulky substituent, namely the 2,4,6-tris[bis(trimethylsilyl)methyl]phenyl (abbreviated as 'Tbt').[120] Later on, they utilized the same kinetic stabilization to synthesize the stable

silabenzene compound **LI**[121] and germabenzene compounds including **LII**.[122,123] The afore-mentioned technique enabled them to synthesize room temperature stable compounds. When it comes to stannabenzenes, it was found that they are extremely reactive despite the kinetic protection provided by a Tbt or Bbt group. This elevated reactivity always led to the formation of the [4+2] dimer of stannabenzene, either irreversibly[124] or in an equilibrium[125]. But, later on, the first monomeric stannabenzene **LIII** was isolated by the group of Yamashita[126], stabilized by two bulky triisopropylsilylgroups in 2,6-position.
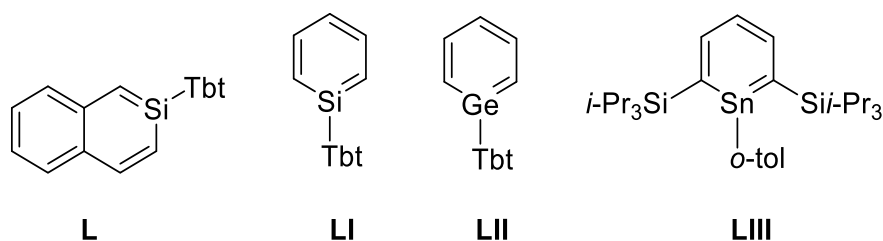
Figure 1.13. First isolated silaaromatic species **L**; first silabenzene compound **LI** and germabenzene compound **LII**; first isolated stannabenzene compound **LIII**.[120−123,126]

1,2-Disilabenzenes **LVa** with the bulky aryl group Bbt or Tbb on Si atoms were prepared by the groups of Tokitoh and Sasamori[127,128] from the reaction of acetylene or monosubstituted acetylene which showed considerable aromaticity (Scheme 1.10).
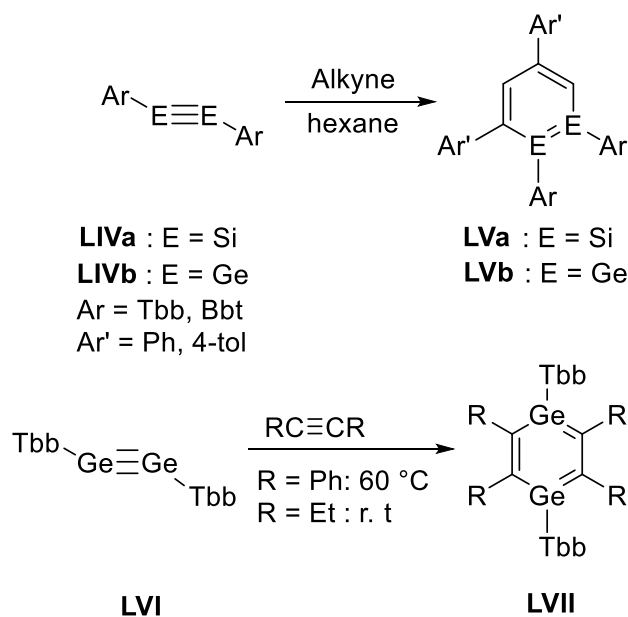
Scheme 1.10. Aromatic 1,2-disila/digermabenzene **LVa,b** from the respective disilynes and digermynes **LIVa,b**; first isolated 1,4-digermabenzenes **LVII** from respective digermynes **LVI**.[127−132]

By slightly altering the reaction parameters, they were also able to form 1,4-disilabenzene as an inseparable mixture with disilabenzvalene.[133] In the same manner, 1,2-digermabenzenes **LVb** [129,130] and 1,4-digermabenzenes **LVII** [131,132] were isolated. Following a similar synthetic strategy in the case of group 13 elements, Power could isolate 1,4-digalabenzene in 2009.[134]

2|Objectives of this PhD thesis

Based on these background studies, the aim of this thesis was to explore the P-centered as well as other heteroatom-centered reactions. In addition to that, the reduction to give novel 1,4-phosphasilines and 1,4-dihydro-1,4-phosphasiline-4-ylidenes was also studied.

The main goals of this Ph.D. thesis are :

I. Synthesis and reactivity studies of P-anionic 1,4-dihydro-1,4-diphosphinines and detailed investigation of their P-centered redox process.

II. Synthesis of novel, 1,4-dihydro-1,4-phosphasiline and -1,4-phosphagermine derivatives.

III. Detailed investigation of P-centered redox processes of 1,4-dihydro-1,4-phosphasiline derivatives.

IV. Detailed investigation of Si-centered reactions of the novel 1,4-dihydro-1,4-phosphasiline derivatives including the transformation into aromatic 1,4-phosphasiline derivatives.

3|Investigation on the redox chemistry of anionic 1,4-dihydro-1,4-diphosphinines M[2a]−M[2c]

Major share of the optoelectronic/electrochemical studies involving a P-heterocycle are mainly focused on P^V-phospholes with the redox behavior centered in the unsaturated hydrocarbon portion of the molecules rather than the P^V centers.[135,136] λ^5-Phosphinines[55,137] and P^V-phospharhodamines[138] were also electrochemically investigated for optovoltaic applications.
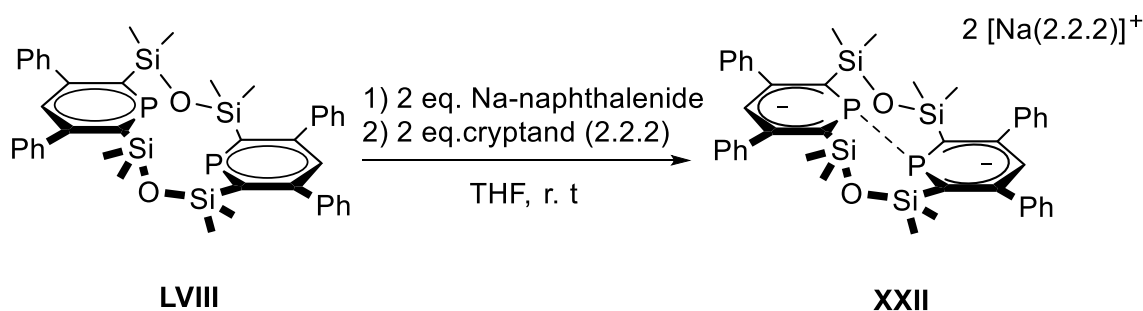
Scheme 3.1. Two-electron reduction of the macrocyclic phosphinine **LVIII** to form the dianionic dimer **XXII**.[67]

There are a lot of examples where λ^3-phosphinines are reduced by alkali metals to generate paramagnetic anion radicals and diamagnetic dianions.[139,140] A noteworthy example is the combined CV and ESR studies of trianion radicals by Märkl.[66] The seminal report from Le Floch and Mathey depicted the formation of a radical monoanion from a phosphinine heterocycle **LVIII** and its further reduction led to the formation of dianion **XXII**, linked by a P-P bond (Scheme 3.1).[67] Here, the radical monoanion couldn't be isolated or structurally characterized, but confirmed by EPR and from the first reversible reduction wave observed in the CV studies. Märkl's report on the dimerization of the phosphino radicals **LX** to give the corresponding diphosphanes **LXI** by the oxidation of 4-N,N-dimethylaminophenyl-1-phosphabutatrienes **LIX** is one of the preliminary studies involving the forming and breaking of a P-P single bond (Scheme 3.2) and their redox process is explained by a detailed redox mechanism.[141]
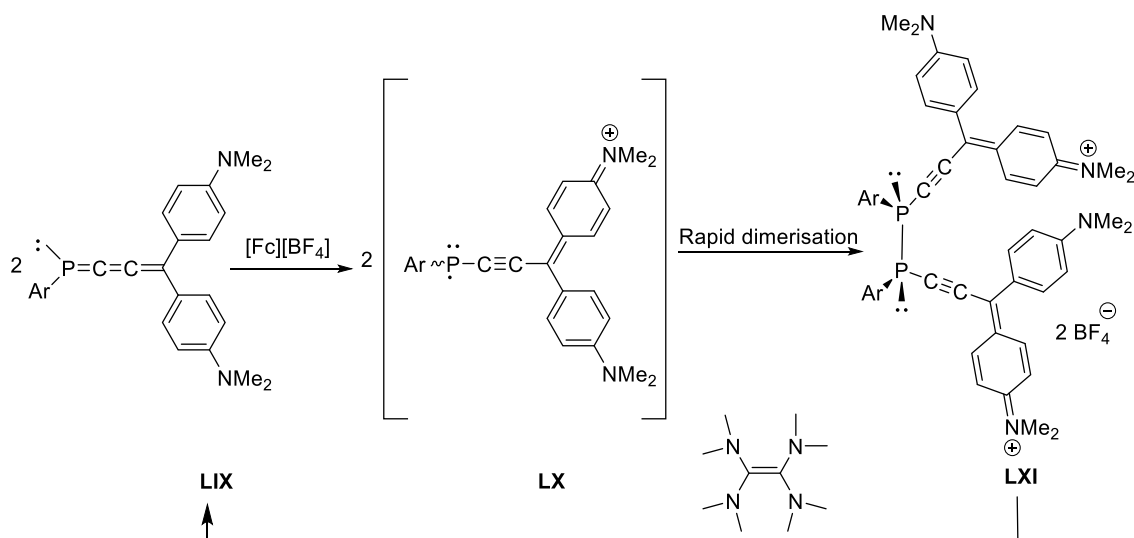
Scheme 3.2. Oxidation of **LIX** to form the phosphino radicals **LX** and their rapid dimerization to form the diphosphanes **LXI**.[141]

Other than this report, electrochemical investigations of P-P single bond formation have been reported from both anodic and cathodic processes involving reversible organometallic $\sigma^4\lambda^4$-1,2-biphosphane dication formation,[142] radical ion formation during reduction of diphospha-alkenes[24] etc. Relevant redox studies were also performed on acyclic P-systems such as substituted diphosphenes where alkali metal induced rupture of the phosphorus–phosphorus double bond to form anionic radical species was investigated. But here too, no detailed studies were focussed on the redox chemistry of this particular system.[143]

With the assumption of the disclosure of a rich electrochemistry involving the P[III] centers, it was decided to initially synthetically explore the synthesis of anionic 1,4-diphosphinines **2a-c** and their derivatives. Further on, they were quenched with methyl iodide to form the neutral products **3a-c**. Their dimeric oxidation products were successfully isolated and also subjected to extensive electrochemistry studies.

3.1 Synthesis of the anionic 1,4-dihydro-1,4-diphosphinines M[2a]−M[2c] and their reactions with methyl iodide

Imidazole-2-thione-fused 1,4-diphosphinine **1** was treated with different bases, KHMDS, LDA and KO^{t}Bu in diethyl ether at room temperature. A drastic color change from red to deep blue occurred in all cases, indicating the formation of **K[2a]**, **Li[2b]** and **K[2c]** which were isolated as blue-violet powders (Scheme 3.3).

M = K, Li
a: R = N(SiMe$_3$)$_2$
b: R = Ni-Pr$_2$
c: R = Ot-Bu
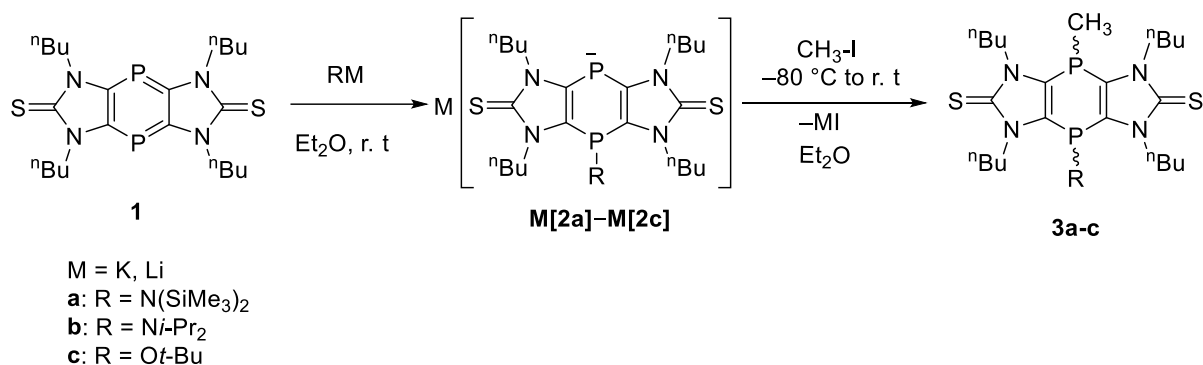
Scheme 3.3. Synthesis of **M[2a]−M[2c]** from 1,4-diphosphinine **1**; reactions of **M[2a]−M[2c]** to give *P*-methylated products **3a-c**.

The ^{31}P{^{1}H} NMR spectra of **M[2a]−M[2c]** clearly indicated two resonance signals corresponding to the anionic P-center and the P-center with the substitution without any evidence of P-P coupling across the rings (Table 3.1).

Table 3.1. ^{31}P{^{1}H} NMR data of **M[2a]−M[2c]** in Et$_2$O-d10 (with and without the presence of crown ethers), CH$_3$CN and THF (P-R and anionic P notations are in accordance with Scheme 3.3).

	δ ^{31}P / ppm							
	R-P				Anionic P			
	Et$_2$O	CH$_3$CN	THF	Et$_2$O'*	Et$_2$O	CH$_3$CN	THF	Et$_2$O'*
K[2a]	−12.1	−11.3	−28.1	−11.8	−76.1	−78.2	−72.1	−75.7
Li[2b]	−30.8	−31.8	−32.2	−30.6	−78.0	−79.4	−79.5	−77.6
K[2c]	18.1	11.6	−28	18.3	−74.1	−70.1	−72.1	−74.3

* Et$_2$O' indicates the ethereal solutions in the presence of crown ethers, 18-C-6 (**[K(18-C-6)]2a** and **[K(18-C-6)]2c**) or 12-C-4 (**[Li(12-C-4)]2b**).

The composition of **K[2a]** was confirmed by ESI-MS which retained its phosphanide form despite the presence of the reactive P-anionic center. On the other hand, the tricyclic phosphanides, **Li[2b]** and **K[2c]** had stability issues while measuring ESI-MS. However, the oxidation product obtained for **Li[2b]**, and the fragment obtained for **K[2c]** were also in accordance with the presence of the respective anion (Table 3.2).

Table 3.2 : Selected neg. ESI-MS spectrometric data of the anions of **M[2a]−M[2c]**.

Compound	m/z (%)	Ion composition
K[2a]	642.2 (22)	$[M]^+$
Li[2b]	614.2 (90)	$[M+O_2]^+$
K[2c]	499.1 (100)	$[C_{22}H_{37}N_4OP_2S_2]^+$

The $^{31}P\{^1H\}$ NMR of **M[2a]−M[2c]** were taken in a number of solvents including diethyl ether and tetrahydrofuran as well as in acetonitrile. The intense blue color of the anions remained to be same in the ethereal solvent with insignificant shifts in the $^{31}P\{^1H\}$ NMR values (Table 3.1). But, surprisingly the color of the anions were observed to be yellow in acetonitrile solutions. In order to get deeper insights into this peculiar change in color in different solvent environments, UV-Vis spectra of the anions were measured (Figure 3.1). Inferences were drawn from these spectra that the intense blue colors observed for solids and solutions of **M[2a]−M[2c]** correspond to single intense absorptions with $\lambda_{max} \sim 517$ nm in Et_2O. On the other hand, the CH_3CN solution of **K[2a]** gave the maximum absorption at $\lambda_{max} \sim 372$ nm, corresponding to yellow color. Here, only the anionic salt **K[2a]** was taken for the analysis, as the further studies will be focused on this particular compound owing to its superior stability compared to **Li[2b]** and **K[2c]**.

The TD-DFT calculations on **2a'$^-$** (maxima of the lowest excited states at 354 nm and 326 nm, Table 3.3) at B3LYP/6-311G**//M06-2X/6-311+G** level of theory performed by Nyulászi and co-workers were in good agreement with experimentally determined UV/vis absorption value in CH_3CN but not with the deep blue colors observed in ether solvents (Figure 3.1).
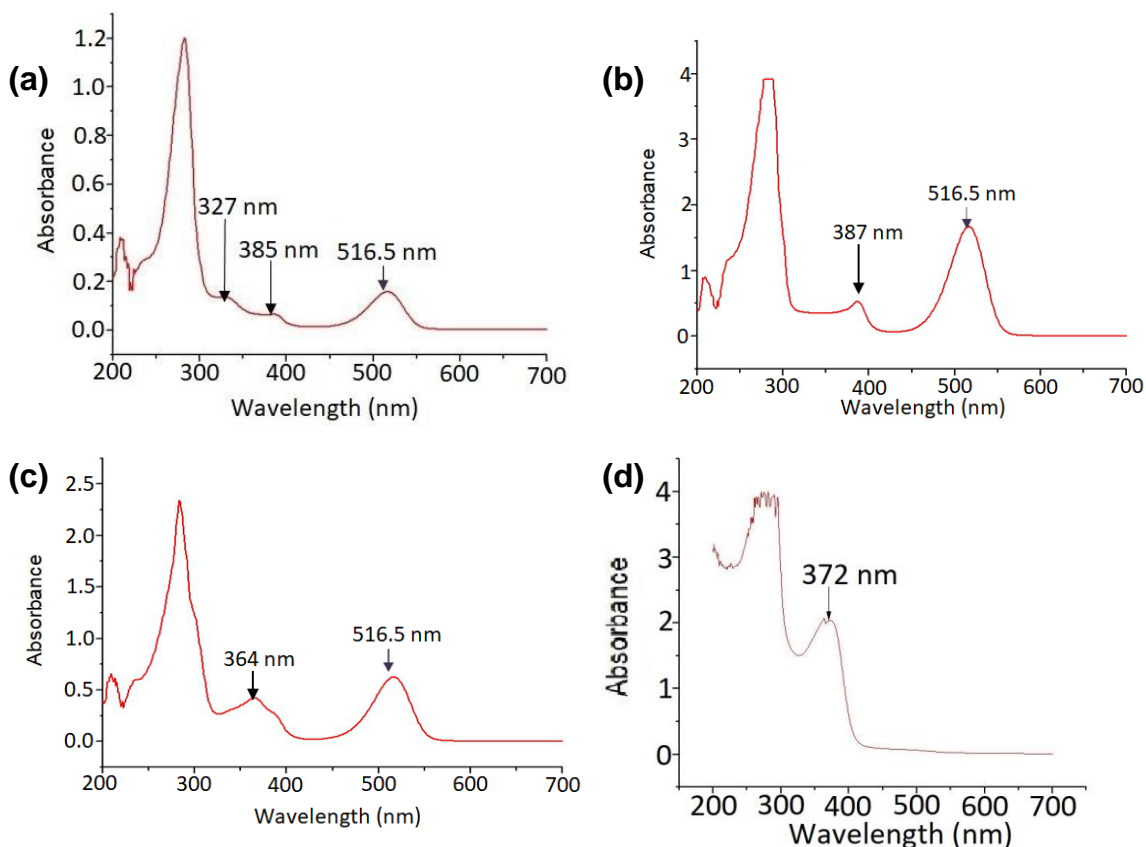
Figure 3.1. UV-Vis spectrum of (a) **K[2a]**, (b) **Li[2b]**, (c) **K[2c]** in Et$_2$O and of (d) **K[2a]** in CH$_3$CN.

Additional TD-DFT calculations at B3LYP/6-311G**//M06-2X/6-311+G** level of theory were performed by Nyulászi and co-workers, on the optimized structures of the K$^+$ salts (Table 3.3) in order to investigate the charge transfer (CT) bands associated with the formation of contact ion-pairs due to the weaker solvation of K$^+$ cation by ethers compared to CH$_3$CN. The lowest energy excitation of the calculated contact ion pair was calculated to be the (anion-centered) HOMO to (K$^+$ s-type centered) LUMO transition, indicative of a charge transfer transition. In order to corroborate these results, the K$^+$ or Li$^+$ cations were encapsulated by crown ethers (18-crown-6 and 12-crown-4). Encapsulated compounds **[K(18-C-6)]2a** and **[K(18-C-6)]2c** could be isolated from Et$_2$O as orange solids but **[Li(12-C-4)]2b** remained purple which could be resulted from improper encapsulation of Li$^+$ by the crown ether. Nevertheless, the ^{31}P{^{1}H} NMR chemical shift changes observed in cases of encapsulation and also in the cases of CH$_3$CN and Et$_2$O were rather insignificant (Table 3.1). These results could point to a small energy difference between the ether-solvated and ion-paired states which will be discussed in the context of cyclic voltammetric experiments in later parts.

Table 3.3. Important TD-DFT results at B3LYP/6-311G**//M06-2X/6-311+G** level of theory calculated for **2a'-c'⁻** and CAM-B3LYP/6-31G*//M06-2X/6-311+G** level of theory calculated for the contact ion pair **M[2a']**−**M[2c']**.

Model	Excited state	Wavelength	Oscillator strength	Transition	Contribution
2a'⁻	1	354 nm	0.1137	HOMO-LUMO	0.69524
	2	326 nm	0.1735	HOMO-1-LUMO	0.10945
				HOMO-LUMO+1	0.22399
				HOMO-LUMO+2	0.65285
K[2a']	1	523 nm	0.0171	HOMO-LUMO	0.68460
				HOMO-LUMO+3	0.13519
2b'⁻	1	366 nm	0.1501	HOMO-LUMO	0.69593
	4	319 nm	0.0774	HOMO-LUMO+3	0.69343
Li[2b']	1	393 nm	0.0231	HOMO-4-LUMO	0.15155
				HOMO-LUMO	0.68258
2c'⁻	1	354 nm	0.1235	HOMO-LUMO	0.69214
	4	294 nm	0.4978	HOMO-1-LUMO	0.65771
				HOMO-LUMO+1	0.17021
				HOMO-LUMO+2	0.12292
K[2c']	1	419 nm	0.0178	HOMO-LUMO	0.67546
				HOMO-LUMO+4	-0.14105

In order to gain deeper insight into the electronic structures of **2a−c⁻**, DFT calculations at the M06-2X/6-311+G** level of theory were performed by Nyulászi and co-workers, on models wherein the *N*-*ⁿ*Bu groups are truncated to *N*-Me (indicated by '). As expected, the middle rings of **2a'−c'⁻** exhibited lower aromatic character than in neutral **1a'** ((NICS(0) values for **2a'−c'⁻** varied between −3.4 and − 5.2, Tables 3.4), while the aromatic character of the outer ring remained high (NICS(0) varied between −8.8 and −9.4, Table 3.4).

Table 3.4. NICS(0) and NICS(1) values of the anions **2a'-c'⁻** (N-Me derivative).

		Middle ring	Outer ring
Anion **2a'⁻**	NICS(0)	−3.4	−9.4
	NICS(1)	−4.0 (−2.7)	−7.0 (−8.2)
Anion **2b'⁻**.	NICS(0)	−4.2	−8.8
	NICS(1)	−5.3 (−3.1)	−6.9 (−7.3)
Anion **2c'⁻**	NICS(0)	−5.2	−9.0
	NICS(1)	−4.4 (−6.0)	−7.1 (−7.5)

The frontier Kohn-Sham molecular orbitals calculations were performed at the M06-2X/6-311+G** level of theory for **2a-c⁻** by Nyulászi and co-workers, inorder to explain the shapes and energies of the delocalized π frontier molecular orbitals (FMO). It is evident that they were little affected by the variations of substituents (Figure 3.2).
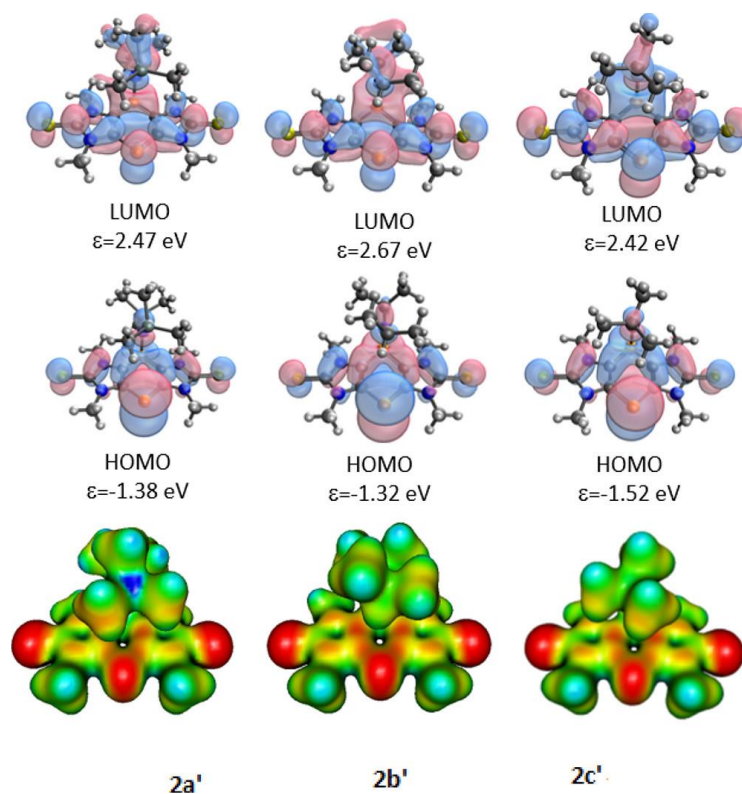
Figure 3.2. Kohn-Sham frontier orbitals, their energies (top) and electrostatic potential maps of **2a-c⁻** (bottom, color code of electrostatic potential: red <-0.1, yellow -0.1 − -0.05, green -0.05 − 0.05, light blue 0.05 −0.1, blue >1.0).

The HOMOs showed large coefficients of the unsubstituted anionic phosphorus of the 1,4-dihydro-1,4-diphosphinine central rings, while the sulfur p lone pairs showed non-negligible contributions. Electrostatic potential maps (Figure 3.2) depicted the negative charges reside mainly on the unsubstituted anionic phosphorus sites and the two sulfur atoms, in accordance with the HOMO coefficients.

P-anionic salts **M[2a]**–**M[2c]** were reacted with methyl iodide at low temperature to form the products **3a-c** (Scheme 3.3) as clearly revealed by their ^{31}P{^{1}H} NMR spectra. **3a**, **3b** and **3c** were isolated as white powders, selected data are given in Table 3.5.

While for **3b-c** mixtures of *cis/trans* isomers were obtained, in the case of **3a** (see Table 3.5; for the structure of *trans*-**3a**, see Figure 3.4) only the *trans* product was detected in NMR as well single crystal X-ray diffraction method. While it was assumed that the steric demand of the bulky bis(trimethylsilyl)amino group leads to the selective formation of *trans*-**3a**, DFT calculations at M06-2X/6-311+G** level of theory performed by Nyulászi and co-workers, revealed the energy difference between the *cis* and *trans* isomers: ΔE (*cis/trans* is 0.2, 1.1 and 0.9 kcal/mol for **3a'**, **3b'** and **3c'**, respectively). In addition to that, very high and similar inversion barriers (ΔE#) were determined at M06-2X/6-311+G** level of theory (Table 3.5). For example, the optimized structure of the transition state (TS) of one of the derivatives, **3a'**, determined at M06-2X/6-311+G** level of theory is shown in Figure 3.3.
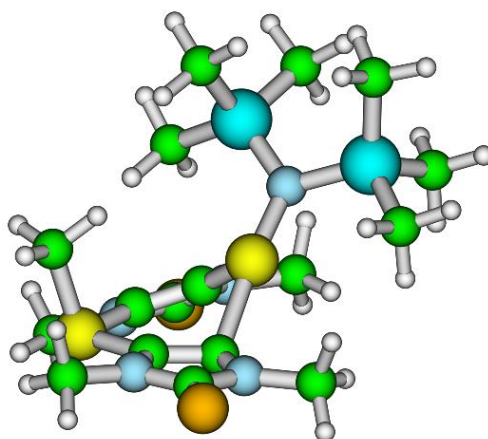
Figure 3.3. Optimized structure of TS of the >P(NSiMe$_3$)$_2$ inversion in case of **3a'.**

Table 3.5. ^{31}P{^{1}H} NMR data (C$_6$D$_6$) of **3a-c**; ΔE of *cis-trans* isomers and inversion barrier (ΔE#) for **3a', 3b', 3c'** (inversion at >P(N(SiMe$_3$)$_2$, >P(N*i*-Pr$_2$) >PO*t*-Bu, respectively) at M06-2X/6-311+G** level of theory.

	δ ^{31}P{^{1}H} (R-P)/ ppm	δ ^{31}P{^{1}H} (CH$_3$-P) / ppm	$^3J_{P,P}$ / Hz	*cis* & *trans* ratio	ΔE(cis-trans) / kcal·mol^{-1}	ΔE#/ kcal·mol^{-1}
3a	−4.7	−72.3	16.6	only *trans* isomer	0.2	88.5
3b	−17.2 & − 19.7	−75.2 & − 69.3	9.1, 11.1	1 : 3.1	1.1	46.0
3c	25.6 & 26.5	−79.6 & − 69.4	7.2, 13.4	1 : 4.1	0.9	73.1
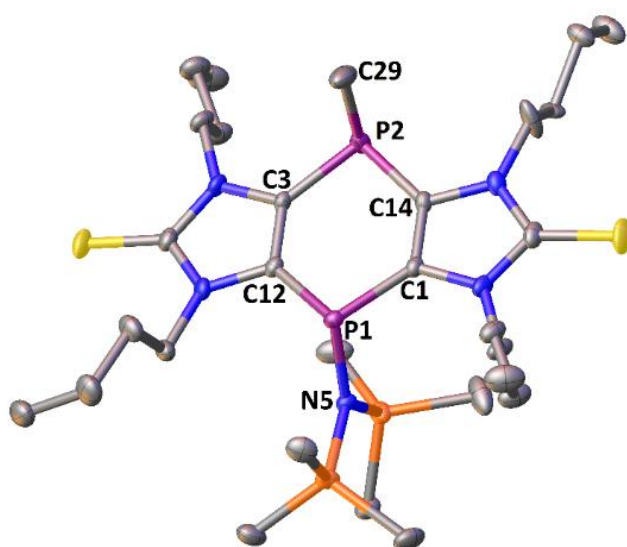
Figure 3.4. Molecular structure of *trans*-**3a**; hydrogen atoms are omitted for clarity (50 % probability level). Selected bond lengths [Å] and angles [°]: P1-N5 1.7161(16), P2-C29 1.846(3), P1-C1 1.8240(19), P1-C12 1.816(2), P2-C3 1.803(2), P2-C14 1.8033(19); C1-P1-C12 95.19(9) , C3-P2-C14 96.11(9); Σ<°P1 307.86 and Σ<°P2 297.08.

Despite the small energy difference, the selective formation of the *trans* isomer in case of **3a** could be favored by the kinetic control. Apparently, the bulky N(SiMe$_3$)$_2$ group was observed to occupy much more space below the central ring than the other two substituents, raising a kinetic barrier for the formation of the *cis* isomer. Single crystals of compound **3a**, suitable for X-ray diffraction analysis, were grown from a saturated diethyl ether solution by slow evaporation at room temperature. The analysis revealed a triclinic crystal system with the $P\bar{1}$ space group.The structure confirmed the *trans* position of the amino and methyl groups of

the central ring (Figure 3.4) having sums of angles at P1 and P2 of 307.9° and 297.1°, respectively. The endocyclic angles C1-P1-C12 of 95.19(9)° and C3-P2-C14 of 96.11(9)° were rather in the acute range.

3.2 Formation of the dimeric 1,4-dihydro-1,4-diphosphinines 4a by one electron oxidation of the anionic 1,4-dihydro-1,4-diphosphinines K[2a]

Compound **K[2a]** was then selected for further chemical redox reactions because it has shown a promising robustness under various reaction conditions. Et_2O solution of I_2 was added dropwise at − 80 °C to a freshly prepared solution of **K[2a]** in Et_2O (Scheme 3.4), gave an orange solution via a transient green color formation. The product **3a** was isolated as orange powder. The $^{31}P\{^1H\}$ NMR spectrum of **4a** ($CDCl_3$) depicted a pseudo-triplet signal at −0.4 ($^{3/4}J_{P,P}$ = 25.6 Hz, P-N(SiMe₃)₂), and −50.9 ($^{3/4}J_{P,P}$ = 25.6 Hz, P-P) ppm.
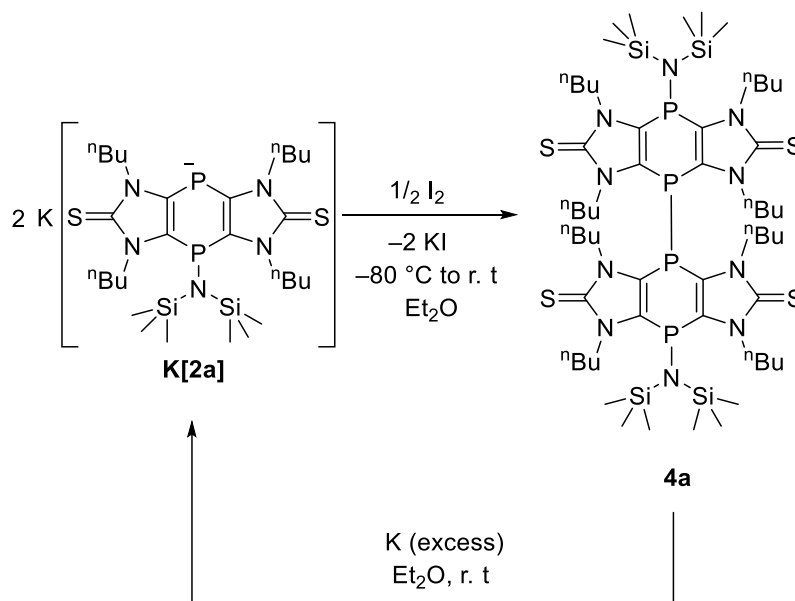
Scheme 3.4. Oxidation of **K[2a]** to **4a** and subsequent reduction.

The attribution of the transient green color to an intermediate free radical was supported by TD-DFT calculations at B3LYP/6-311G**//M06-2X/6-311+G** level of theory, performed by Nyulászi and co-workers, on **2a'** (Table 3.6, lowest transition calculated at 1005 nm). The orange color of **4a** also was in well-accordance with calculations on **4a'** (Table 3.7, computed

as 509 nm) and also consistent with the UV-Vis spectroscopy results (observed the maximum absorbance at λ_{max} = 440 nm).

Table 3.6. TD-DFT results at B3LYP/6-311G**//M06-2X/6-311+G** level of theory (first 5 excited state) of **2a'•**.

Excited state	Wavelength	Oscillator strength	Transition	Contribution
1	1005 nm	0.0871	β-HOMO-β-LUMO	0.99153
2	682 nm	0.0000	β-HOMO-3-β-LUMO	-0.13499
			β-HOMO-1-β-LUMO	0.98415
3	658 nm	0.0047	β-HOMO-3-β-LUMO	0.40247
			β-HOMO-2-β-LUMO	0.89461
			β-HOMO-1-β-LUMO	0.13453
4	656 nm	0.0042	β-HOMO-3-β-LUMO	0.90050
			β-HOMO-2-β-LUMO	-0,40329
5	453 nm	0.0125	α-HOMO-α-LUMO+1	0.20231
			β-HOMO-4-β-LUMO	0.96571

Table 3.7. TD-DFT results at B3LYP/6-311G**//M06-2X/6-311+G** level of theory (first 4 excited state) of **4a'**.

excited state	wavelength	oscillator strength	Transition	contribution
1	509 nm	0.1335	HOMO-LUMO	0.70062
2	486 nm	0.0065	HOMO-1-LUMO	0.70413
3	468 nm	0.0079	HOMO-2-LUMO	0.70107
4	421 nm	0.0124	HOMO-3-LUMO	0.69936

The formation of **4a'** from two radicals was calculated to be exergonic (298 K, 1 bar), and the rather high reaction Gibbs free energy (28.7 kcal/mol) was found to be in good agreement with the rapid color change from green to orange by Nyulászi and co-workers.

Clear orange crystals of compound **4a**, suitable for X-ray diffraction analysis, were grown from a saturated diethyl ether solution by slow evaporation method at room temperature (Figure 3.5). The analysis revealed a monoclinic crystal system with the space group *C*2/*c*. The structure indicated a twisted arrangement along the P-P single bond of length 2.303(2) Å. The C3-P2-P2'-C3' torsion angle of 96.3° between the two tricyclic units was found to be greater than the torsion angle observed previously for the sterically less demanding thiazol-2-thione-based tricycle[91]. Most probably, also in this case, dispersion forces induced orientation of the two tricyclic units helped in the aggregation and pre-organization during the formation of the P-P bond.
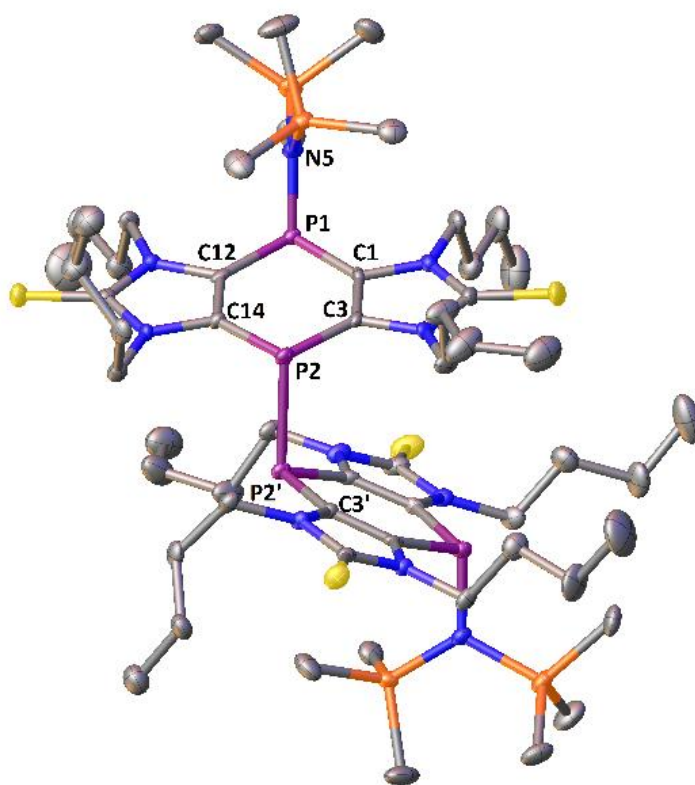
Figure 3.5. Molecular structure of compound **4a**; hydrogen atoms are omitted for clarity (50 % probability level). Selected bond lengths [Å] and angles [°]: P1-C1 1.807(4), P1-C12 1.817(4), P2-C3 1.791(4), P2-C14 1.806(4), C12-C14 1.360(5), C1-C3 1.376(5), P1-N5 1.718(3), P2-P2' 2.303(2); C1-P1-C12 94.43(18), C3-P2-C14 96.40(18), Σ<°P1 304.48 and Σ<°P2 300.79.

In order to examine if compound **4a** can be used to re-form two equivalents of **K[2a]** in a clean fashion, *i.e.* to formally reverse the oxidation with I$_2$, compound **4a** was treated with an excess of potassium in Et$_2$O at room temperature to avoid desulfurization of the thione functionality

which usually takes place at higher temperatures[144] (Scheme 3.4). After 10 minutes stirring, the color of the solution turned dark blue, indicating that the anionic species **K[2a]** was formed, which was additionally confirmed by the $^{31}P\{^1H\}$ NMR spectrum of the reaction mixture showing two singlets at −13 and −78 ppm.

The frontier Kohn-Sham molecular orbitals calculations were performed at TPSS-D3/def2-TZVP (CPCM$_{THF}$)//PW6B95-D3/def2-QZVP(CPCM$_{THF}$) level of theory by Brehm, on models wherein the N-^{n}Bu groups are truncated to N-Me (indicated by ′), indicated as **4a′** (Figure 3.6). This model helped to explain the shapes and the energies of the delocalized π frontier molecular orbitals (FMO) as in the case of **2a-c**$^-$. Most important aspect was the LUMOs which showed large coefficients on the diphosphane phosphorus atoms of the 1,4-dihydro-1,4-diphosphinine central rings with π- delocalization to the neighboring carbon atoms. This clearly established that the reduction with excess of potassium selectively cleaved the P-P single bond to from the anionic **K[2a]**.

LUMO : −2.0917 eV   **4a**

HOMO : −5.6793 eV
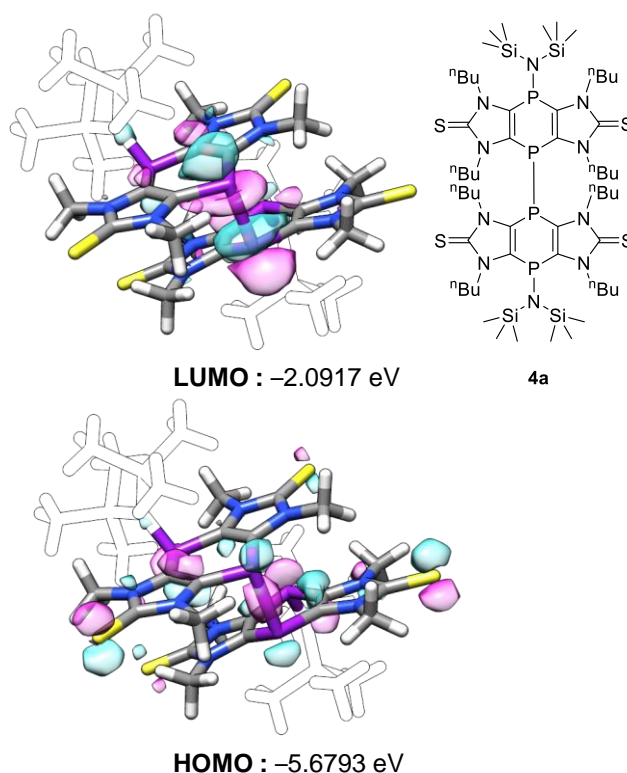
Figure 3.6. Kohn-Sham molecular orbitals of **4a′** at TPSS-D3/def2-TZVP (CPCM$_{THF}$)//PW6B95-D3/def2-QZVP(CPCM$_{THF}$) level of theory.

3.3 Investigation of the redox behavior of the anionic 1,4-dihydro-1,4-diphosphinines K[2a]

The redox chemistry of **K[2a]** and **4a** were investigated to firmly establish the oxidation of **K[2a]** to **4a** and subsequent reduction back to **K[2a]** itself.

CV on **K[2a]** in CH$_3$CN/ [n-Bu$_4$N][PF$_6$] clearly showed a chemically irreversible (IRR) oxidation process at E_p^{Ia} = − 0.90 V and a similarly chemically irreversible reduction process at E_p^{IIIc} = − 1.63 V (Figure 3.7a, black trace) vs. the ferrocene/ferrocenium redox couple (Fc$^{+/0}$). But, when the initial scan direction was cathodic, no reduction signal was observed on the first cycle (Figure 3.7a, red trace). Thus, it is inferred that the species responsible for E_p^{IIIc} peak appeared to be an electrolysis product of process corresponding to E_p^{Ia}.
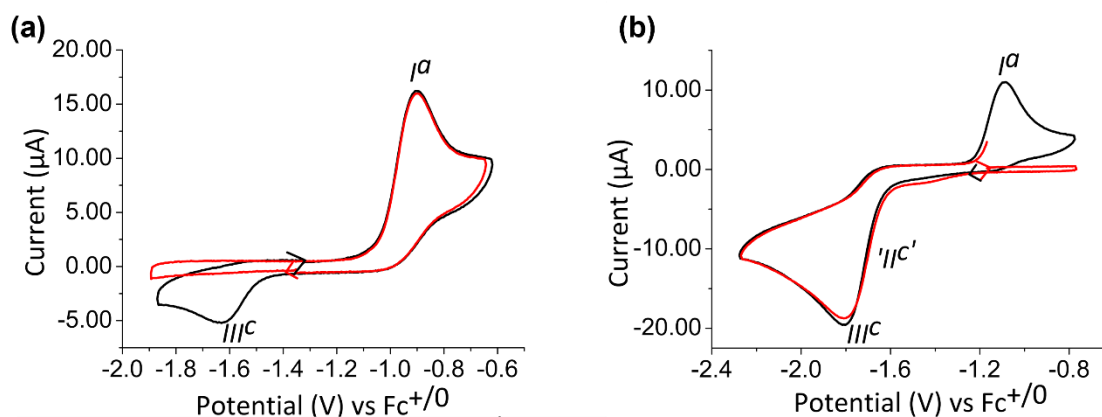
Figure 3.7. (a) Cyclic voltammograms of **K[2a]** (2.59 mM) at a Pt electrode in a 0.1 M [n-Bu$_4$N][PF$_6$]/CH$_3$CN solution; black solid line, anodic initial scan direction; red solid line, cathodic initial scan direction; scan rates = 200 mV/s. (b) Cyclic voltammograms of **4a** (2.59 mM) at a Pt electrode in a 0.1 M [n-Bu$_4$N][PF$_6$]/CH$_3$CN solution; red solid line, anodic initial scan direction; black solid line, cathodic initial scan direction; scan rates = 200 mV/s.

The repeatability of the CVs was examined by carrying out multicycle experiments. Even after 50 cycles, the oxidation peak and reduction peak positions showed no variation and hardly any attenuation in peak intensities was observed (Figure 3.8a). The scan rate dependence was examined from 0.05 V/s to 2.5 V/s with the expected current increase with scan rate and incremental increases in the potential peak positions as expected for IRR processes (Figure 3.8b and Table 3.8). The current ratios, moreover, remained quite similar over all the scan rates.

Table 3.8. Peak potentials and currents for CVs of **K[2a]** at different scan rates.[a]

Scan rate/ mV/s	E_p^{IIIc}/V	E_p^{Ia}/V	I_p^{IIIc}/µA	I_p^{Ia}/µA	$\left|I_p^{IIIc}/I_p^{Ia}\right|$
2500	−1.81	−0.92	−19.52	57.28	0.34
1000	−1.79	−0.94	−10.37	30.17	0.34
500	−1.77	−0.95	−6.65	20.46	0.32
200	−1.63	−0.90	−5.20	16.20	0.32
50	−1.62	−0.91	−1.70	6.65	0.25

[a]Potentials are in V vs. the Fc$^{+/0}$ redox couple
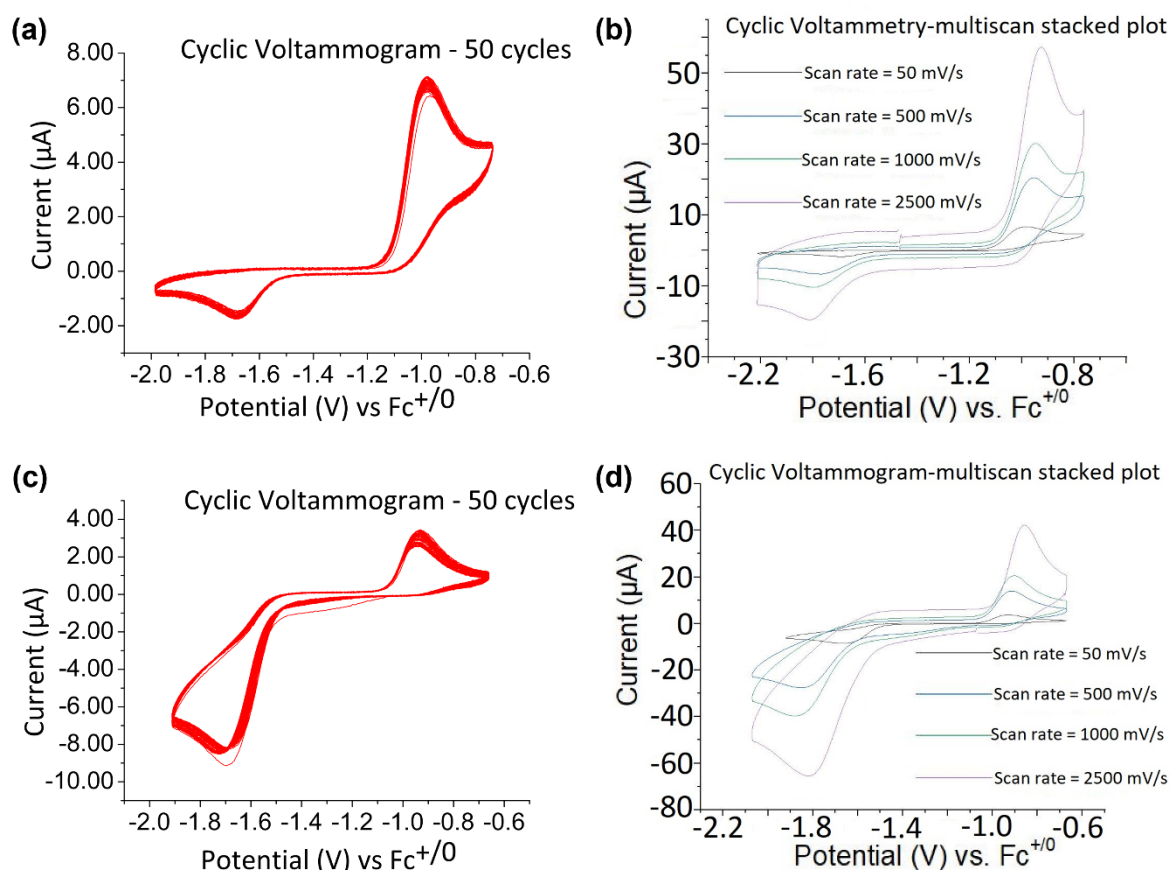
Figure 3.8. (a) Multicycle CV scans of 2.0 mM **K[2a]** (initial scan anodic; v = 50 mV/s) with 50 repeats (0.1 M [n-Bu$_4$N][PF$_6$]/CH$_3$CN). (b) Stacked plots of 2.0 mM **K[2a]** with v = 50, 500, 1000, 2500 mV/s (0.1 M [n-Bu$_4$N][PF$_6$]/CH$_3$CN). (c) Multicycle CV scans of 2.0 mM **4a** (initial scan cathodic; v = 50 mV/s) with 50 repeats (0.1 M [n-Bu$_4$N][PF$_6$]/CH$_3$CN). (d) Stacked plots of 2.0 mM **4a** with v = 50, 500, 1000, 2500 mV/s (0.1 M [n-Bu$_4$N][PF$_6$]/CH$_3$CN).

CV experiments (Figure 3.7b) were also conducted on solutions of **4a** under similar experimental conditions to **K[2a]**. The results appeared to be in an inverse fashion of the previous case shown in Figure 3.7a: a large, IRR, reduction peak labelled E_p^{IIIc} was found at -1.80 V and an equally IRR oxidation process labelled E_p^{Ia} occured at -1.08 V (Figure 3.7b, black trace), when the initial scan direction was cathodic. Scans started in the anodic direction didn't display E_p^{Ia} in the first cycle (Figure 3.7b, red trace). Notably, however, the current ratios of the two processes were observed to be distinctly different, with the relative size of I_p^{IIIc} compared to the anodic peak appeared much larger in Figure 3.7b compared to Figure 3.7a. Here too, the multicycle experiments corroborated the robust repeatability of the CV processes (Figure 3.8c), while variable scan rate experiments from 0.05 V/s to 2.5 V/s also fit expectations for increased currents with scan rates and incrementing of the potentials with faster scans (Figure 3.8d, Table 3.9).

Table 3.9. Peak potentials and currents for CVs of **4a** at different scan rates.[a]

Scan rate/mV/s	E_p^{IIIc}/V	E_p^{Ia}/V	I_p^{IIIc}/µA	I_p^{Ia}/µA	$\left|I_p^{Ia}/I_p^{IIIc}\right|$
2500	−1.82	−0.85	−65.42	42.22	0.64
1000	−1.88	−0.90	−39.71	20.50	0.51
500	−1.85	−0.91	−27.60	13.99	0.50
200	−1.80	−1.08	−19.55	10.96	0.56
50	−1.73	−0.99	−8.45	3.69	0.43

[a]Potentials are in V vs. the Fc$^{+/0}$ redox couple

These CV experiments, as voltammetric monitors, were fully consistent with the redox interconversion of **K[2a]** and **4a** already demonstrated in the chemical oxidation with I_2 and reduction by elemental potassium.

According to the standard notation, E are electrochemical and C are following rapid chemical steps. Process **I** represented the oxidation of **K[2a]** to form **4a** via dimerization of a short-lived P-centered radical species **2a•** (Scheme 3.5). The reduction of **4a** involved the cleavage of the P-P bond and was almost certainly a two-step process, denoted **II** and **III**. There was some evidence for process **II** in very fast scan rate CVs at ~ −1.6 V (Figure 3.8d), but under most CV

conditions, **II** and **III** appeared as a merged peak of double intensity, which accounted for the larger relative size of I_p^{IIIc} when **4a** was the bulk analyte at the electrode interface.

EI :　　　$2\mathbf{a}^- \overset{k_I^\circ}{\rightleftharpoons} e^- + 2\mathbf{a}^{\bullet}$　(fast)

CI :　　　$2\mathbf{a}^{\bullet} + 2\mathbf{a}^{\bullet} \underset{k_{-I}}{\overset{k_I}{\rightleftharpoons}} 4\mathbf{a}$　(strongly product favoured)

EII :　　　$4\mathbf{a} + e^- \overset{k_{II}^\circ}{\rightleftharpoons} 4\mathbf{a}^{\bullet-}$　(fast)

EIII:　　　$4\mathbf{a}^{\bullet-} + e^- \overset{k_{III}^\circ}{\rightleftharpoons} 4\mathbf{a}^{2-}$　　　(fast)

CIII:　　　$4\mathbf{a}^{2-} \underset{k_{-III}}{\overset{k_{III}}{\rightleftharpoons}} 2\mathbf{a}^- + 2\mathbf{a}^-$　(strongly product favoured)
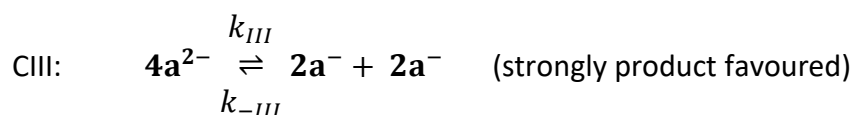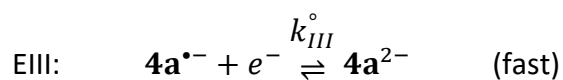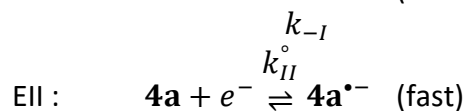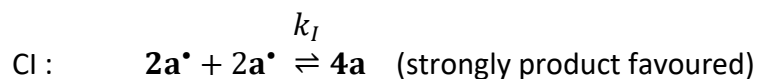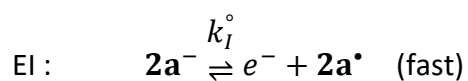
Scheme 3.5. Plausible mechanism for the electrochemical processes based on the CV results for the **K[2a]/4a** interconversion.

4|Synthesis of Si-/Ge-bridged imidazole-2-thiones 9a,b and 10a,b

P^{III}-bridged bis(imidazole-2-thione-4-yl)phosphanes such as **LXIIIa,b** have been widely explored concerning P- as well as thione C-centered reactions.[145] Selective access was obtained by lithiation of **LXIIa,b** and *in situ* reaction with dichlorophosphanes at low temperature (Scheme 4.1).
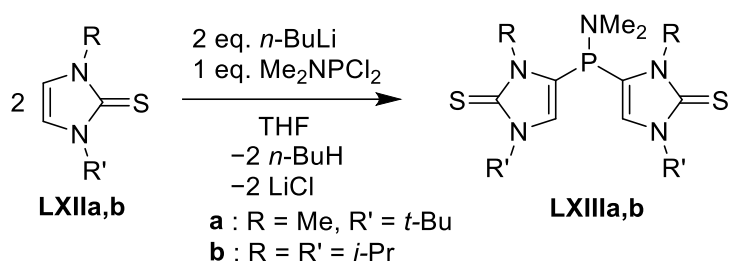
Scheme 4.1. Synthesis of bis(imidazole-2-thione-4-yl)phosphanes **LXIIIa,b** from imidazole-2-thiones **LXIIa,b**.[145]

Another report from the group of Streubel described the formation of tricyclic 1,4-dihydro-1,4-diphosphinines **LXIVc,d** as minor products when imidazole-2-thiones **LXIIc,d** with primary alkyl groups on the N-atoms were used (Scheme 4.2),[100] but the use of these precursors in the synthesis of tricyclic compounds weren't successful as it was shown later.
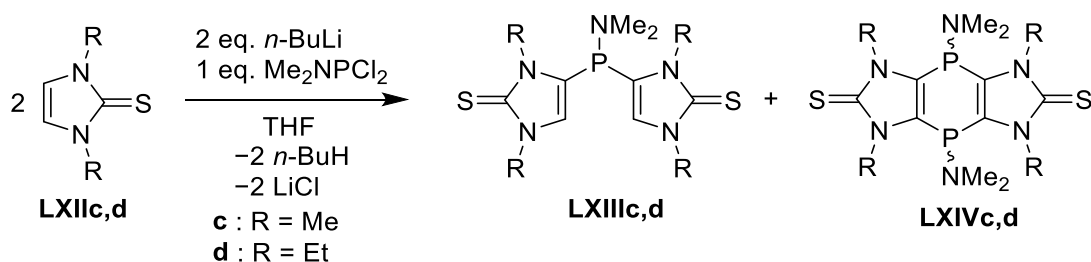
Scheme 4.2. 1,4-Dihydro-1,4-diphosphinines **LXIVc,d** formed as by-products.[100]

The chemistry of **LXIII**-related tricyclic, functionalizable Si-or Ge-bridged systems was almost unexplored when this PhD project was started. Radius reported the serendipitous formation of the backbone-tethered bis(imidazolium) salt [(H*i*-Pr$_2$Im)$_2$SiPh$_2$]$^{2+}$ 2 Cl$^-$ obtained from the

reaction of *i*-Pr₂Im and Ph₂SiCl₂ (Scheme 4.3).[146] Apart from this example, no dialkylsilanyl backbone-tethered bis(imidazolium) salt/imidazole-2-thione compounds were reported.
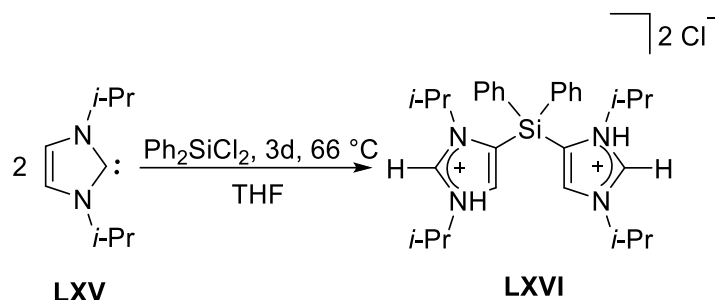
Scheme 4.3. Synthesis of [(H*i*-Pr₂Im)₂SiPh₂]²⁺ 2 Cl⁻ **LXVI** from **LXV**.[146]

Baumgartner used 2,3-dibromothiophene **LXVII** and dichlorodimethylsilane for the synthesis of the dimethyl(dithien-2-yl)silane **LXVIII** (Scheme 4.4). The *ortho*-directing effect of the S-atom played a major role in favoring the selective lithiation at the 2-position as well as the selective formation of **LXVIII**.[147]
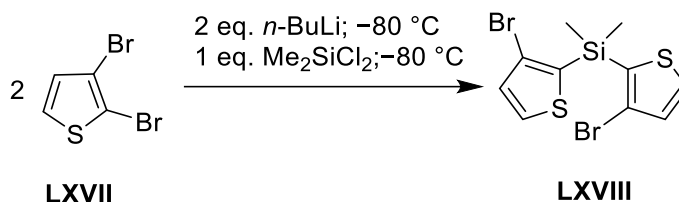
Scheme 4.4. Synthesis of dimethyl(dithienyl)silane **LXVIII** from 2,3-dibromothiophene **LXVII**.[147]

As imidazole-2-thiones (**LXII**) are very different to thioles in terms of reactivity, backbone lithiation was performed at low temperature, followed by the addition of different disubstituted dichlorosilanes. The first step was hence to adjust reaction parameters thus allowing for the synthesis of bis(diorganoamino)silanyl-substituted imidazole-2-thiones; transfer and implementation of these results should furnish access later to related germanium derivatives.

4.1 Optimization of the reaction parameters

Formerly reported protocols by the group of Streubel concerning the P-functionalization of imidazole-2-thione **5b** were then slightly modified to access group 14 heteroatom-bridged systems. Initially, backbone lithiation of the imidazole-2-thione was performed with *n*-BuLi at

−80 °C (Scheme 4.5), followed by the addition of dichlorodimethyl- or diethoxysilanes at − 80 °C. Reaction monitoring by ^{29}Si{^{1}H} dept20 NMR spectroscopy revealed an unselective reaction forming derivatives **6b** in the case of dichlorodimethylsilane addition, although a resonance was observed at δ = −27.2 ppm (content 47% from the mixture) tentatively attributed to the targeted product **6b**. The major signals found at δ = −10.8 and −8.9 ppm could be assigned to silanediols formed by the hydrolysis.[148] This is further corroborated by comparison with the ^{29}Si{^{1}H} dept20 NMR spectroscopic data of the reported compound **LXVI** with a chemical shift of δ = −33 ppm,[146] but, unfortunately, no ^{29}Si{^{1}H} dept20 NMR spectroscopic data was reported for the structurally close analogue **LXVIII**.
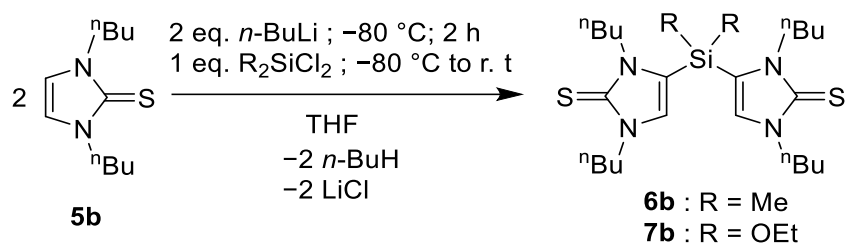
Scheme 4.5. First attempts to get Si-bridged products, **6b** and **7b** from **5b**.

When dichloro(diethoxy)silane was used to target **7b**, the selectivity improved compared to the previous case (Scheme 4.5). Signals that might correspond to hydrolysis products were not observed in this case. The unreacted starting material was observed at δ = −52 ppm along with a new signal at δ = −49 ppm which could be attributed to **7b** (82% of the mixture). The initial protocol parameters were then changed, *i.e.*, after the addition of *n*-BuLi to **5a** at −80 °C, dichlorodimethylsilane was added at a higher temperature (−50 °C).
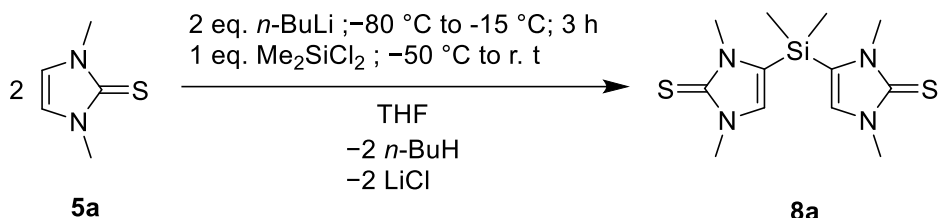
Scheme 4.6. Synthesis of Si-bridged product **8a** from **5a**.

Reaction monitoring by ^{29}Si{^{1}H} dept20 NMR spectroscopy revealed a selective conversion to **8a** (89% of the mixture, δ = −25.1 ppm) without the formation of hydrolysis products (Figure

4.1); the product was isolated as white powder and its constitution confirmed by NMR and EI-MS experiments (Table 4.1).
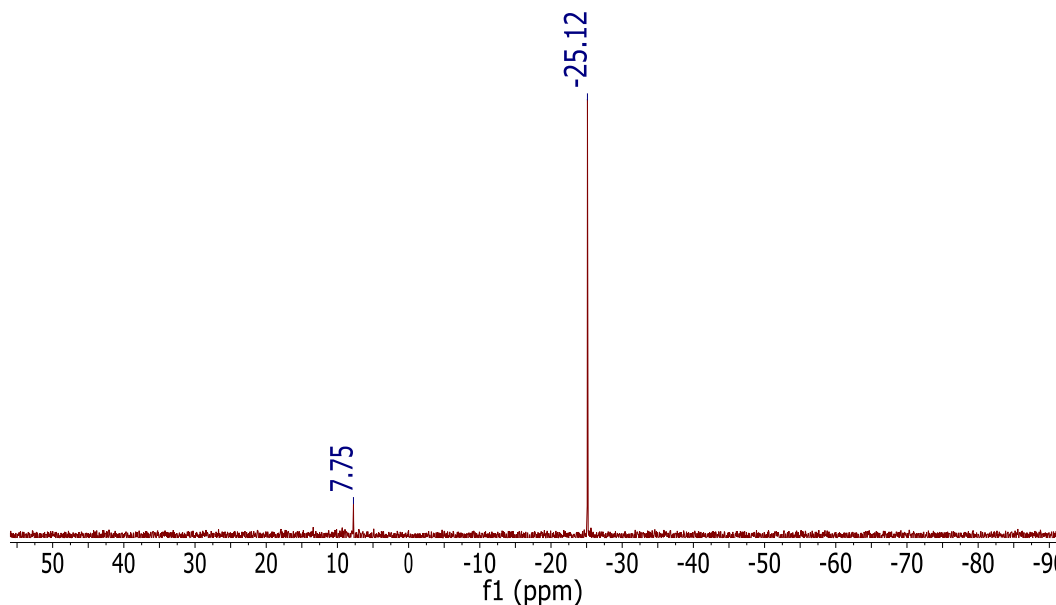
Figure 4.1. $^{29}Si\{^{1}H\}$ dept20 NMR spectrum of the reaction mixture of **8a**.

Since, the aforementioned protocol worked well for the synthesis of **8a**, we confirmed its credibility for the Si(OEt)$_2$ derivatives **7a/7b** too; so we didn't target them.

4.2 Synthesis of 4-bis(diorganoamino)silanyl- 9a,b and 4-bis(diorganoamino)germanyl-substituted imidazole-2-thiones 10a,b

To access derivatives with greater functional opportunities, it was decided to test the applicability of the synthetic protocol for the dimethylsilyl-bridged imidazole-2-thione **8a** in the synthesis of derivatives with bis(diorganoamino)silyl bridges; the latter should enable selective access to SiCl$_2$-bridged derivatives, later on.

Therefore, bis(diethylamino)dichlorosilane **LXIX,** a well-established derivative was chosen as the starting point.[149] Backbone-lithiation of imidazole-2-thiones **5a,b** using *n*-BuLi, followed by the addition of bis(diethylamino)dichlorosilane at low temperatures (−50 °C) resulted in

the selective formation of the products **9a,b** (Scheme 4.7) as confirmed by ^{29}Si{^{1}H} dept 20 NMR spectroscopy. Both derivatives were successfully isolated via extraction with toluene and obtained as white powders; their constitutions were confirmed by NMR experiments (Table 4.1).
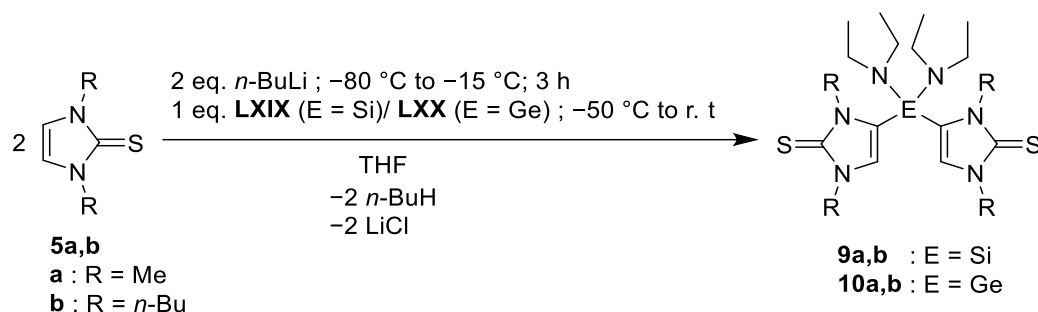
Scheme 4.7. Conversion of **5a,b** to give heteroatom-bridged products **9a,b** and **10a,b.**

Table 4.1. ^{29}Si{^{1}H} dept20, ^{1}H NMR (CDCl$_3$),^{13}C{^{1}H} NMR (CDCl$_3$) and MS data of **9a,b** and **10a,b**.

| Compound	NMR/ppm			EI-MS/m/z	Yield/%
	δ ^{29}Si{^{1}H} dept20	δ ^{1}H (amino-bound group)	δ ^{13}C{^{1}H} (amino-bound group)		
8a	−24.9	0.5 (s, 6H, *Si-(CH$_3$)$_2$*)	−0.8 (s, *Si-(CH$_3$)$_2$*).	312.0 [M]$^+$	97
9a*	−38.8	1.0 (t, 12H, $^3J_{H,H}$ = 7.0 Hz, *Si-(N-CH$_2$-CH$_3$)$_2$*), 2.9 (q, 8H, $^3J_{H,H}$ = 7.0 Hz, *Si-(N-CH$_2$-CH$_3$)$_2$*)	13.8 (s, *Si-(N-CH$_2$-CH$_3$)$_2$*), 35.1 (s, *Si-(N-CH$_2$-CH$_3$)$_2$*), 35.9 (s, *Si-(N-CH$_2$-CH$_3$)$_2$*),	427.2 [M+H]$^+$	94
9b	−37.8	1.0 (t, 12H, $^3J_{H,H}$ = 7.0 Hz, *Si-(N-CH$_2$-CH$_3$)$_2$*), 2.9 (q, 8H, $^3J_{H,H}$ = 7.0 Hz, *Si-(N-CH$_2$-CH$_3$)$_2$*)	13.6 (d, ^3J = 6.4 Hz, *Si-(N-CH$_2$-CH$_3$)$_2$*), 38.2 (s, *Si-(N-CH$_2$-CH$_3$)$_2$*),	594.4 [M]$^+$	45
10a	---	0.9 (*br*.t, 12H, *Ge-(N-CH$_2$-CH$_3$)$_2$*), 2.9 (*br*.q, 8H, *Ge-(N-CH$_2$-CH$_3$)$_2$*)	15.1 (s, *Ge-(N-CH$_2$-CH$_3$)$_2$*), 35.4 (s, *Ge-(N-CH$_2$-CH$_3$)$_2$*), 35.9 (s, *Ge-(N-CH$_2$-CH$_3$)$_2$*),	472.1 [M]$^+$	82
10b	---	1.0 (t, 12H, $^3J_{H,H}$ = 7.0 Hz, *Ge-(N-CH$_2$-CH$_3$)$_2$*), 2.9 (q, 8H, $^3J_{H,H}$ = 7.0 Hz, *Ge-(N-CH$_2$-CH$_3$)$_2$*)	13.8 (s, *Ge-(N-CH$_2$-CH$_3$)$_2$*), 41.4 (s, *Ge-(N-CH$_2$-CH$_3$)$_2$*)	640.1 [M]$^+$	53

*FTMS+pos-ESI technique was used for mass spectrometrical analysis.

Single crystals of compounds **9a,b** suitable for X-ray diffraction analysis, were grown from saturated diethyl ether solutions at room temperature (Figure 4.2). The analysis revealed a monoclinic crystal system and $P2_1/c$ space group for **9a**; orthorhombic crystal system and *Pbca* space group for **9b**. Both structures showed the typical tetrahedral environment of the Si atom.
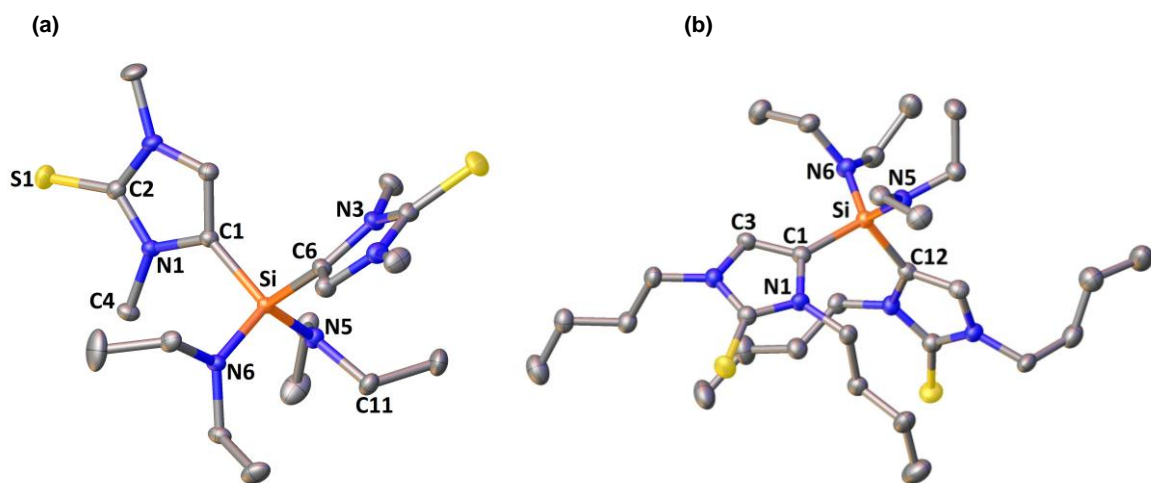
Figure 4.2. Molecular structure of compounds **9a** (a)**;** hydrogen atoms are omitted for clarity (50 % probability level). Selected bond lengths [Å] and angles [°]: Si-C1 1.8602(10) , Si-N6 1.7043(9), C1-N1 1.4095(13), C1-C3 1.3612(14); C1-Si-C6 108.64(5), N5-Si-C6 109.02(5), N5-Si-N6 113.75(4), N6-Si-C1 106.79(4).Molecular structure of compounds **9b** (b)**;** hydrogen atoms are omitted for clarity (50 % probability level). Selected bond lengths [Å] and angles [°]: Si-C1 1.864(3), Si-N5 1.703(3), C1-N1 1.411(4), C1-C3 1.354(5); C1-Si-C12 108.04(15), N5-Si-C12 109.40(15), N5-Si-N6 116.35(14), N6-Si-C1 107.48(14).

The synthesis of imidazole-2-thione species with aminogermyl bridging **10a,b** was achieved by the same protocol applied for the synthesis of their Si analogues **9a,b**.

Following the same protocol discussed beforehand, bis(diethylamino)dichlorogermane **LXX**[150] was added to backbone-lithiated imidazole-2-thiones **5a,b** at -50 °C to afford selectively Ge-bridged derivatives **10a,b** (Scheme 4.7) which were isolated in good yields and confirmed by various NMR spectroscopic means (Table 4.1).

Single crystals of **10a,** suitable for X-ray diffraction analysis, was grown from saturated diethyl ether solutions at −20 °C (Figure 4.3). The analysis revealed a triclinic crystal system and $P\bar{1}$ space group for **10a.** The molecular structure of **10a** shows the typical tetrahedral environment of the Ge atom, as expected.
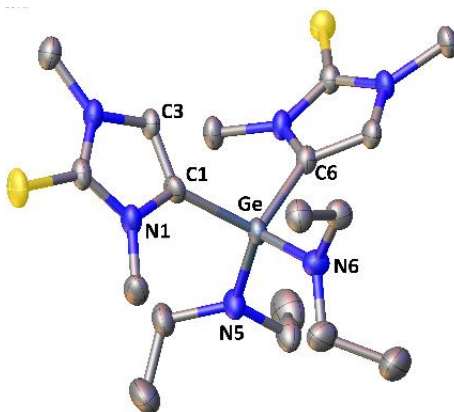
Figure 4.3. Molecular structure of compound **10a** (50 % probability level)**:** hydrogen atoms are omitted for clarity. Selected bond lengths [Å] and angles [°]: Ge-C1 1.936(4) , Ge-N6 1.823(3), C1-N1 1.404(5), C1-C3 1.352(6) ; C1-Ge-C6 107.38(16), N5-Ge-C6 111.58(16), N5-Ge-N6 107.68(16), N6-Ge-C1 110.96(15).

5|Investigations on the synthesis of tricyclic 1,4-dihydro-1,4-phosphasilines and -1,4-phosphagermines

The report from the group of Streubel described the formation of the 1,4-dihydro-1,4-diphosphinines **LXIVa,b** from the phosphanylated imidazole-2-thiones **LXXIa,b** in a selective manner (Scheme 5.1).[90]

a : R = Me
b : R = *n*-Bu
LXXIa,b
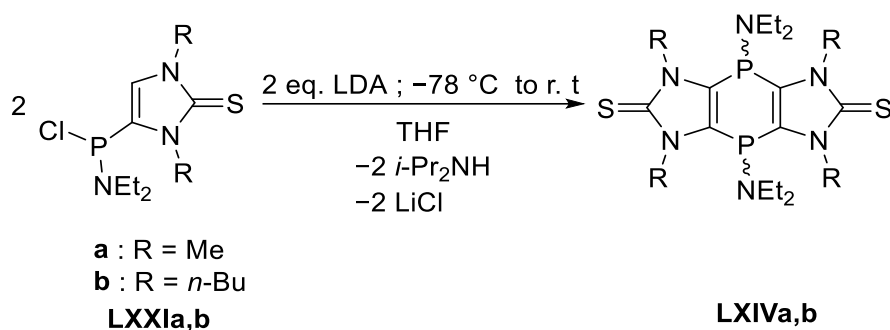
LXIVa,b

Scheme 5.1. Synthesis of 1,4-dihydro-1,4-diphosphinines **LXIVa,b** from the phosphanylated imidazole-2-thiones **LXXIa,b**.[90]

It was intriguing to see that the sole report discussing the synthesis of 1,4-dihydro-1,4-phosphasilines, reported by Baumgartner in 2009, has had no further impact (Scheme 5.2).[147] Maybe, even more surprising was that, apart from studies of the photophysical properties, no reactivity studies were performed on these compounds **LXXII** such as targeting/functionalizing P and Si centers.

LXVII   **LXVIII**   **LXXII**
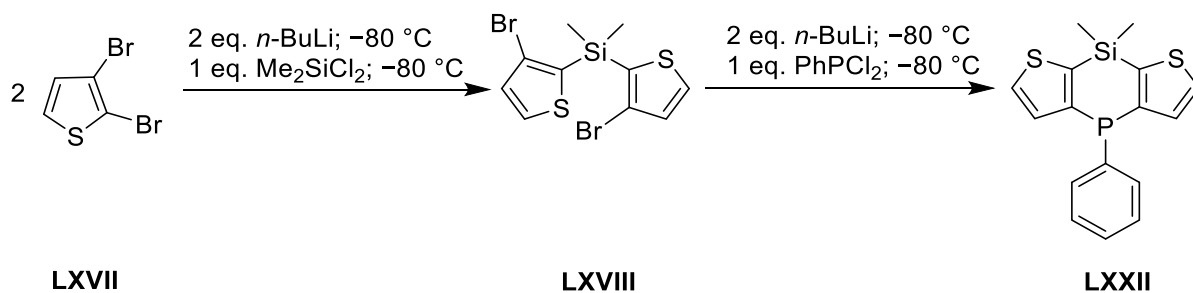
Scheme 5.2. Synthesis of the dithienophosphasiline **LXXII** from **LXVIII**.[147]

Apart from the synthesis of a novel class of 1,4-dihydro-1,4-phosphasilines, it's an intriguing aspect that, the synthesis of 1,4-dihydro-1,4-phosphagermines is synthetically unexplored till this date. Bearing these two targets in mind, we proceeded, initially, with the investigations regarding the ring closing reactions with the Si-bridged compounds **9a,b**.

5.1 Optimization of the ring formation reaction

5.1.1 Initial investigations based on the past reports on ring closing protocols

Following the previous report shown in scheme 5.1[90], we targeted the diamino(chloro)silanyl-substituted imidazole-2-thiones **9a,b'** from imidazole-2-thione derivatives **5a,b**. Here, 1:1 ratio of both **5a,b** and **LXIX** were taken and same protocol was followed that was used for the synthesis of **9a,b** (Scheme 5.3). The ^{29}Si{^{1}H} dept20 NMR spectra of the reaction mixtures apparently showed intense signals for unreacted starting material, **LXIX** (δ = −30.8 ppm; 89.2 % of the mixture) and the disubstituted products **9a** (δ = −38.4 ppm; 10.7 % of the mixture) (Figure 5.1) and **9b** (δ = −37.6 ppm; 26 % of the mixture) (Figure 5.2).
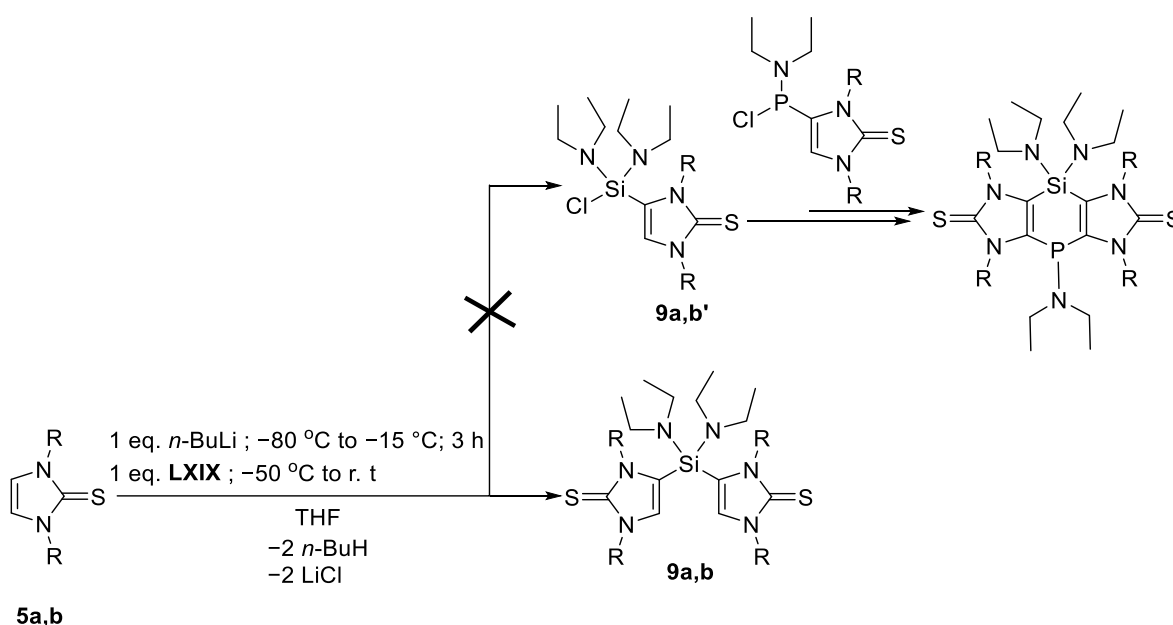
Scheme 5.3. Attempts towards the synthesis of diamino(chloro)silanyl-substituted imidazole-2-thiones **9a,b'** from **5a,b.**
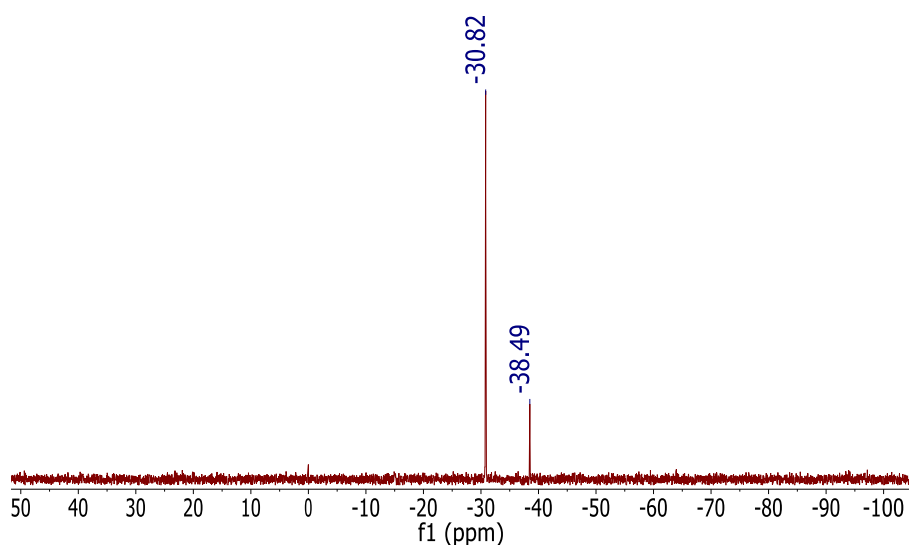
Figure 5.1. $^{29}Si\{^1H\}$ dept20 NMR spectrum of the reaction mixture for **9a'**.
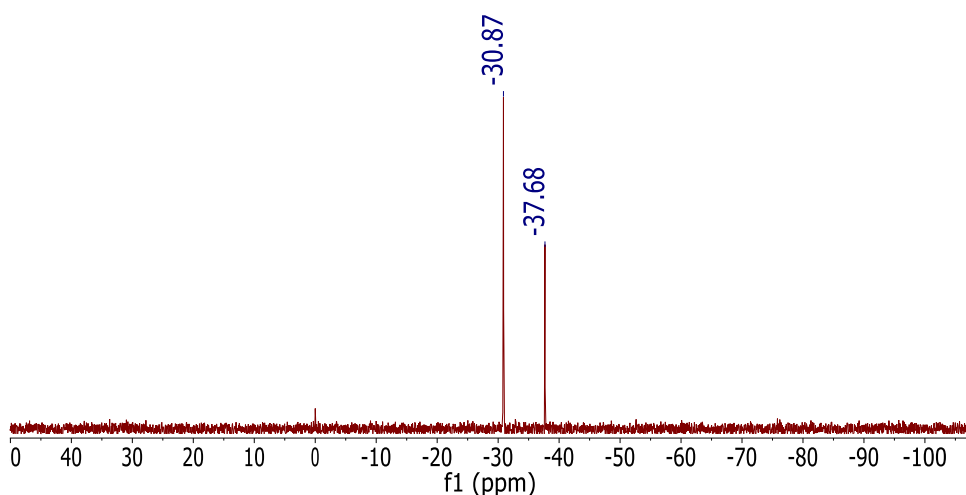
Figure 5.2. $^{29}Si\{^1H\}$ dept20 NMR spectrum of the reaction mixture for **9b'**.

Inference was made that the only way to perform the ring closing reaction is either via the Si-bridged **9a,b** or the acyclic bis(imidazole-2-thione-4-yl)phosphane **LXIII** by stepwise deprotonation at their backbones and a cyclizing phosphanylation or silanylation. But this was already discussed in chapter 4: the formation of the tricyclic 1,4-dihydro-1,4-diphosphinines **LXIVc,d** as a minor product with very little yield when imidazole-2-thiones **LXIIc,d** with primary alkyl groups on the N-atoms were used (Scheme 4.2).[100] Apart from that, the stepwise deprotonation at the backbone of the acyclic bis(imidazole-2-thione-4-yl)phosphane **LXIII** and a cyclizing phosphanylation wasn't an effective choice towards the ring closing reaction.[96]

5.1.2 Searching for the most suitable reaction parameters

As an initial test reaction, Si-bridged compound **9a** was taken and dissolved in THF to obtain a clear yellow solution. Then, it was cooled down to − 80 °C and bases such as *n*-BuLi and Li- TMP were added dropwise. Then they were warmed to −10 °C and stirred for almost 3 hours (Scheme 5.4); but no color change was observed. The reactions were monitored *in situ* via ^{1}H NMR spectroscopy. It was observed from the spectra that the backbone proton at δ = 6.9 ppm from the imidazole-2-thione moiety **9a** was not removed in both cases. Even after warming them up to room temperature and stirring for overnight, no changes were observed.
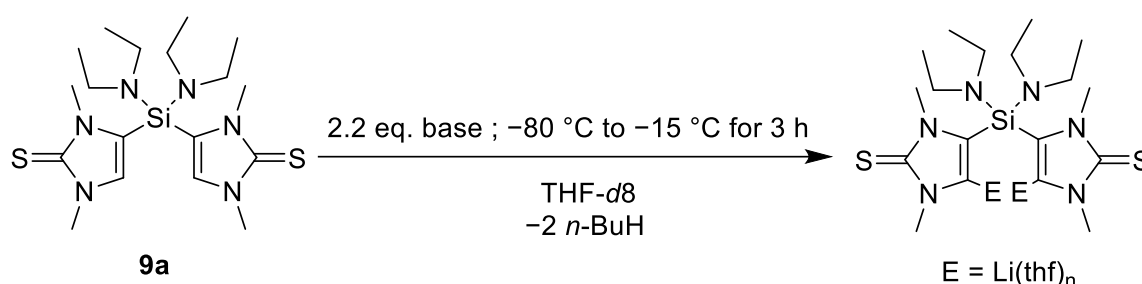
Scheme 5.4. Attempts towards the lithiation of the Si-bridged species **9a**.

Since milder conditions failed to provide any promising results, harsher methods were implemented and tested to look into better deprotonation outcomes. In this case, instead of adding *n*-BuLi at low temperature, it was added at room temperature into the THF solution of Si-bridged compound **9a.**
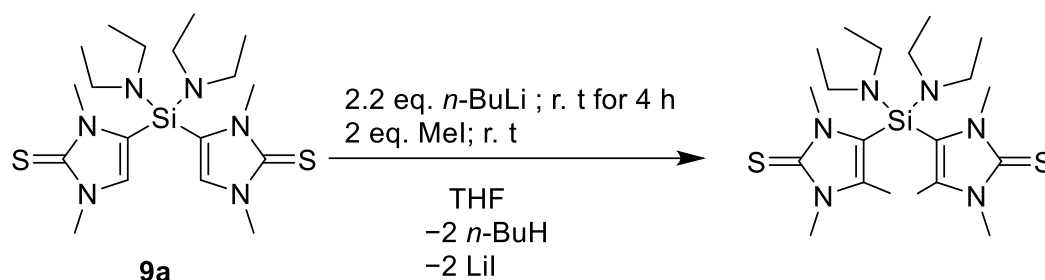
Scheme 5.5. *In situ* lithiation and methylation of the Si-bridged species **9a**.

Even though the color change wasn't evident, the intermediate formation of the lithiated species was checked by a subsequent methylation reaction by the addition of MeI after 4 hours (Scheme 5.5). The formation of the methylated species was confirmed by the formation

of salt precipitate and the reaction was kept for overnight stirring for the completion of the reaction. The solvent was removed *in vacuo* and ^{1}H NMR spectroscopy of the residue was measured in CDCl$_3$. The spectrum revealed the removal of the backbone protons at δ = 6.9 ppm (residual THF signals were observed at δ = 1.8 and 3.7 ppm) and the singlet signals at δ = 2.6 and 2.4 ppm signifying the methyl protons corresponding to the backbone methylated group (Figure 5.3).
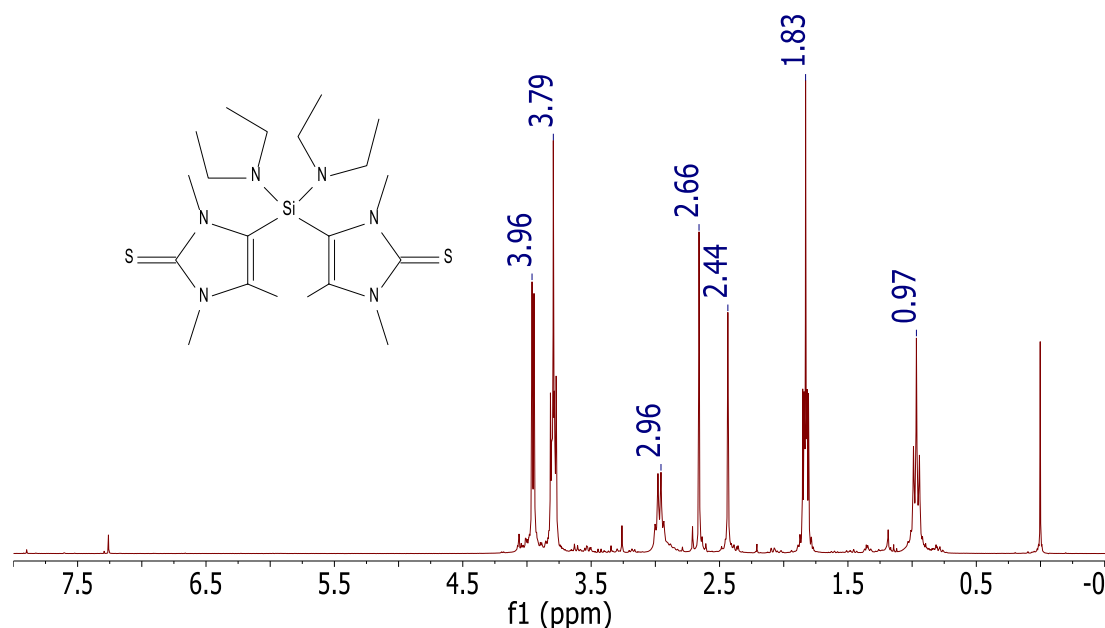
Figure 5.3. ^{1}H NMR spectrum of the methylated compound formed by the MeI addition to **9a.**

Employing this effective and selective method, we confirmed that the backbone deprotonation can be achieved and can be used to achieve ring closing to form the 1,4-dihydro-1,4-phosphasilines.

5.2 Synthesis of the tricyclic 1,4-dihydro-1,4-phosphailines 11a,b and -1,4-phosphagermines 12a and 13a

Initially, the new 1,4-dihydro-1,4-phosphasilines were tried to access utilizing the protocol depicted in scheme 5.5**.** Backbone-lithiation of **9a,b** using *n*-BuLi at room temperature, followed by the addition of diethylamino(dichloro)phosphine at low temperatures (−80 °C) resulted in the selective formation of the products **11a,b** (Scheme 5.6) as confirmed by

^{29}Si{^{1}H} dept20 NMR and ^{31}P{^{1}H} NMR spectroscopies. The products were extracted with toluene and obtained as white powders. Their constitutions were initially confirmed by NMR experiments (Table 5.1) The ^{31}P{^{1}H} and ^{29}Si{^{1}H} dept20 NMR spectroscopic data showed phosphorus resonances in the range of δ = −10 to −20 ppm. Besides, ^{31}P{^{1}H} and ^{29}Si{^{1}H} dept20 NMR shifts observed for the reported 1,4-dihydro-1,4-phosphasiline derivative **LXXII** are at δ = −20.7 ppm and δ = −17.7 ppm, respectively.[147]
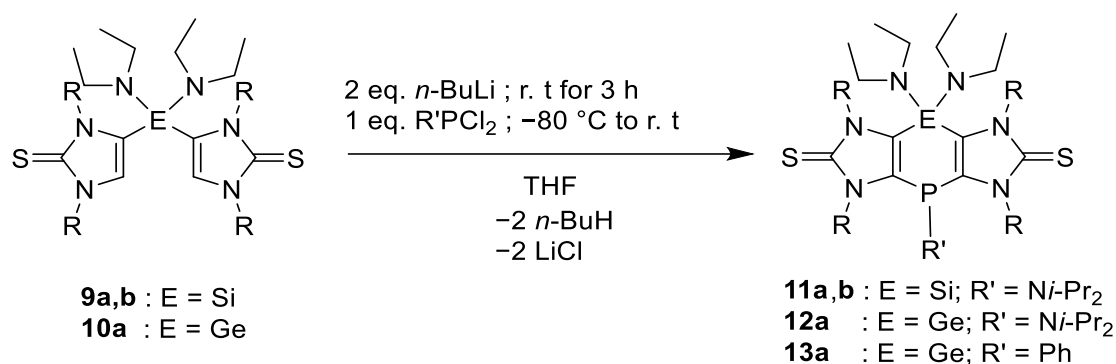

Scheme 5.6. Conversion of **9a,b** and **10a** to give the tricyclic products **11a,b**, **12a** and **13a**.

Table 5.1. ^{29}Si{^{1}H} dept20 and ^{31}P{^{1}H} NMR data (CDCl$_3$), MS data and yields of **11a,b**, **12a** and **13a**.

Compound	NMR/ppm		EI-MS/m/z	Yield/%
	δ ^{29}Si{^{1}H} dept20	δ ^{31}P{^{1}H}		
11a	−42.1	−17.0	553.3 [M]$^+$	40
11b	−42.4	−12.2	724.4 [M]$^+$	52
12a	---	−17.5	601.2 [M]$^+$	48
13a	---	−55.6	578.1 [M]$^+$	67

Colorless crystals of compounds **11a,b** suitable for X-ray diffraction analysis, were grown from saturated diethyl ether solutions, at room temperature (Figure 5.4). The analysis revealed monoclinic crystal system with the space group $P2_1/n$ for both **11a** and **11b**. The P-C bond lengths of both middle rings of both **11a** and **11b** and the C-P-C' angles were found to be similar as in previously reported tricyclic 1,4-dihydro-1,4-diphosphinines (**LXIVa,b**; Scheme 5.1).[90] Here, too, the middle rings were not planar.

The systematic synthetic protocol of the 1,4-dihydro-1,4-phosphasilines paved the path towards the achievement of first 1,4-dihydro-1,4-phosphagermine systems.
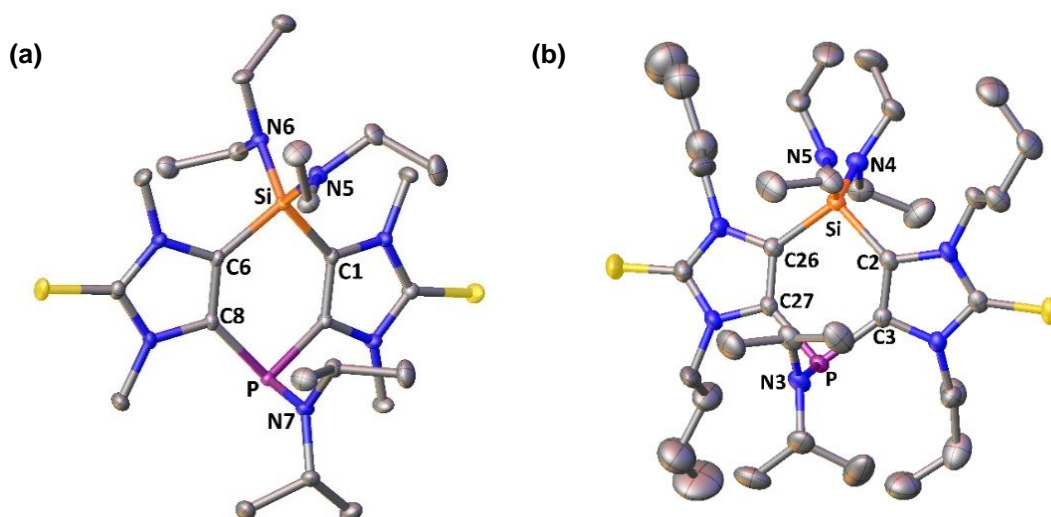
Figure 5.4. Molecular structure of compounds **11a** (a)**;** hydrogen atoms are omitted for clarity (50 % probability level). Selected bond lengths [Å] and angles [°] : Si-N5 1.7097(18), P-N7 1.6824(17), P-C8 1.826(2), Si-C1 1.862(7), C6-C8 1.378(3); Σ<°P 305.1, C1-Si-C6 99.46(9), N5-Si-C6 109.71(9), N5-Si-N6 109.42(8), N6-Si-C1 107.13(9). Molecular structure of compounds **11b** (b)**;** hydrogen atoms are omitted for clarity (50 % probability level). Selected bond lengths [Å] and angles [°] : Si-N5 1.708(2), P-N3 1.690(2), Si-C26 1.882(2), C26-C27 1.364(3); Σ<°P 304.46, C2-Si-C26 99.31(10), N5-Si-C2 112.17(10), N4-Si-N5 109.27(10), N5-Si-C26 107.93(10).

Following the protocol of 1,4-dihydro-1,4-phosphasilines, here too, backbone-lithiation of **10a** using *n*-BuLi at room temperature, followed by the addition of diethylamino-dichlorophosphane and dichlorophenylphosphane at low temperatures (−80 °C) resulted in the selective formation of the products **12a** and **13a,** respectively, (Scheme 5.6) as initially confirmed by ^{31}P{^{1}H} NMR spectra. The products **12a** and **13a** were extracted with toluene and obtained as white powders. The ^{31}P{^{1}H} NMR spectra showed phosphorus resonances in the range of −10 to −20 ppm, but no data regarding the ^{73}Ge NMR spectrum was obtained since extreme low sensitivity of ^{73}Ge nucleus is already known (Table 5.1). Unfortuntely, this protocol did not allow to achieve the synthesis of the N-*n*-Bu derivative of **12a**; the reaction was too unselective.

On the contrary to silicon analogues **11a,b**, colorless crystals of compounds **12a** and **13a** suitable for X-ray diffraction analysis, were grown from saturated diethyl ether solutions at – 20 °C rather than at room temperature(Figure 5.5). Crystallization processes whether it be via the slow evaporation method or vapor diffusion method couldn't achieve any suitable crystal formation at room temperature. The analysis revealed a triclinic crystal system with the space group $P\bar{1}$ for **12a** and a monoclinic crystal system with the space group $C2/c$ for **13a.** The structure of **12a** was similar to the silicon analogues **11a,** except the fact that the Ge-N and Ge-C bond lengths were observed to be elongated compared to **11a**. Despite the different substitution on P, **13a** showed similar parameters and structural conformation as **12a**.
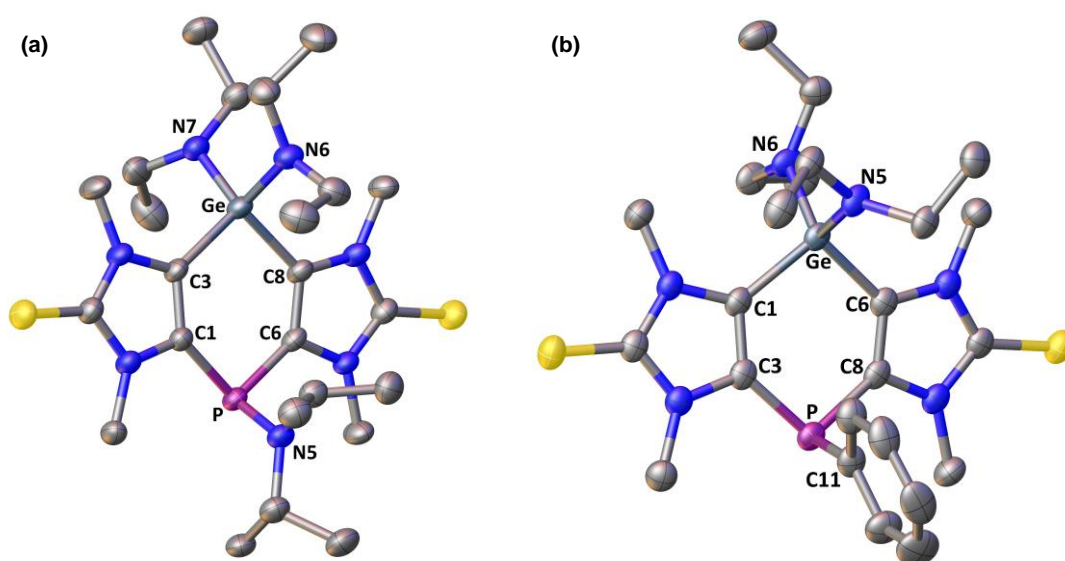

Figure 5.5. Molecular structure of **12a** (a)**;** hydrogen atoms are omitted for clarity (50 % probability level). Selected bond lengths [Å] and angles [°]: Ge-N6 1.810(3), P-N5 1.689(3), P-C1 1.835(4), Ge-C3 1.936(4), C1-C3 1.376(5); Σ<°P 306.83, C3-Ge-C8 98.39(15), N6-Ge-C3 118.23(16), N6-Ge-N7 105.19(15), N6-Ge-C8 107.45(15). Molecular structure of **13a** (a)**;** hydrogen atoms are omitted for clarity (50 % probability level). Selected bond lengths [Å] and angles [°]: Ge-N5 1.8092(18), P-C11 1.847(2), P-C8 1.818(2), Ge-C1 1.939(2), C6-C8 1.361(3); Σ<°P 302.1, C1-Ge-C6 98.42(10), N5-Ge-C6 109(9), N5-Ge-N6 107.6(9), N6-Si-C1 108.6(9).

6|Investigations on the selective P-centered reactions of the tricyclic 1,4-dihydro-1,4-phosphasiline 11b

The sole report of a reaction involving the P-center of 1,4-dihydro-1,4-phosphasilines was described in the report by Baumgartner.[147] They have performed modifications of the P-center of **LXXII** by converting it into its corresponding phosphane oxide **LXXIIIa** and P-coordinated gold(I) complex **LXXIIIb**, respectively (Scheme 6.1).


LXXII   **LXXIIIa,b**

                             a : E = O
                             b : E = AuCl
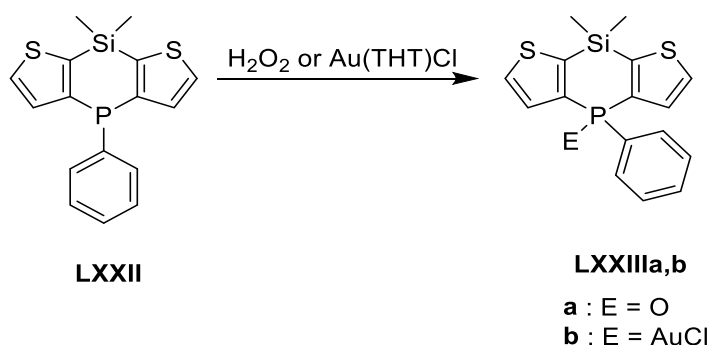
Scheme 6.1. Chemical modifications at P-center of dithieno-1,4-phosphasiline **LXXII** to form **LXXIIIa,b**.[147]

A possible P-selective P-N bond cleavage reduction was forecasted by the studies based on calculated FMOs. The P-centered anionic derivative **K[14b]** was synthetically established via reduction using an excess of KC_8. Furthermore, a redox cycle was established starting with the oxidation to give the P-P coupled product **15b** which could be chemically reduced by KC_8 to yield **K[14b]**, again. In chapter 3, the redox processes involving anionic 1,4-dihydro-1,4-diphosphinine **K[2a]** and its dimeric counterpart **4a** was explained in great detail. Based on these firm studies, efforts were made for the present case, too, to establish the redox chemistry and its plausible mechanism. Even though the CV studies may show negligible deviations from the former studies (see chapter 3), FMO studies, were performed, too, to affirm this negligible deviation.

6.1 Selective reduction at the P-center of the tricyclic 1,4-dihydro-1,4-phosphasilines 11b

### 6.1.1 Theoretical study on a selective cleavage of the P-N bond

Detailed theoretical studies on the 1,4-dihydro-1,4-phosphasiline **11a,b** precursors were performed by Brehm on models of **11a** (designated by ', with the P-Ni-Pr$_2$ group replaced by P-NEt$_2$). We were intrigued by the FMO situation at P and Si centers of the model compound **11a**. The Figure 6.1 showed that the LUMO was calculated to be at an energy level of – 0.91 eV and observed a large p-π contributions from the P and Si atoms with further delocalization over the neighboring carbon atoms. Most notable aspect is that the LUMO is observed to have some P–N σ* character, suggesting the possibility of P–N bond dissociation upon chemical reduction whereas Si–N σ* character was not observed. On the other hand, HOMO was calculated to be at an energy level of – 5.76 eV and no orbital contributions on the P and Si centers were apparently observed. This aspect instigated us to take up the reduction chemistry targeting both Si and P centers and profit from unlocking the heteroatom centered reactivity studies.

HOMO: –5.76   **LUMO** :–0.91
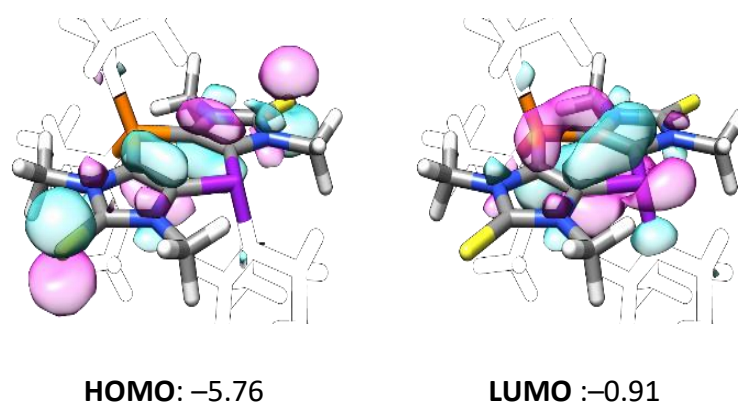
Figure 6.1. HOMO and LUMO of the model compound **11a** (NEt$_2$ groups given as silhouettes for clarity) with absolute molecular orbital energies ε in eV.

6.1.2 Selective cleavage of the P-N bond of 11b

Here, the addition of 3 equivalents or more amount of KC_8 to **11b** instantly accessed the anionic 1,4-dihydro-1,4-phosphasiline salt **K[14b]** (Scheme 6.2) without cleaving off the NEt_2 groups at the Si center. In this case, the highly soluble N-*n*-Bu derivative was used since it's very well soluble in Et_2O. The initial confirmation of the product formation was done via $^{31}P\{^1H\}$ and $^{29}Si\{^1H\}$ dept20 NMR spectroscopies which confirmed the phosphinide center and Si center unaffected by the reduction (Table 6.1). From the clear orange-brown diethyl ether solution **K[14b]** was isolated as light-yellow powder. This observation showcased a deviation compared to the anionic 1,4-dihydro-1,4-diphosphinine case where the anionic analogues gave stark deep blue colored solutions in Et_2O. The explanation for different colors in different solvent systems are well-explained there both experimentally and theoretically.
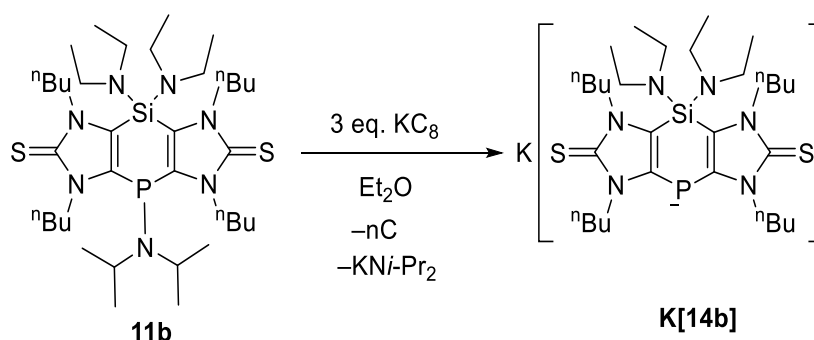
Scheme 6.2. Reductive cleavage of the P-N bond of **11b** to form **K[14b]**.

Single colorless crystals of compound **K[14b]** suitable for X-ray diffraction analysis, were grown from saturated diethyl ether solutions at room temperature. As a simplified concept, **K[14b]** exist as a coordination polymer with each potassium ion coordinated by five donors via their S centers in the solid state (Figure 6.2(top)). The chemical formula determined by the SC-XRD model, $C_{64}H_{123}KN_{12}OP_2S_4Si_2$, for this polymeric structure (Figure 6.2(bottom)) in $P\bar{1}$ with Z = 2 (including one equivalent of uncoordinated diethyl ether as solvent of crystallization) and inspection of Fourier maps suggests ED consistent with about *half* an H atom at each P, suggesting that the crystallisation has trapped a "phosphane hemi-hydride" as a side product. The formulation of free radical at one of the two independent anions in the polymer was observed to be incompatible with crystal color or with the chemical and

electrochemical evidence for rapid dimerization to form P–P bonds from presumed radical intermediates.
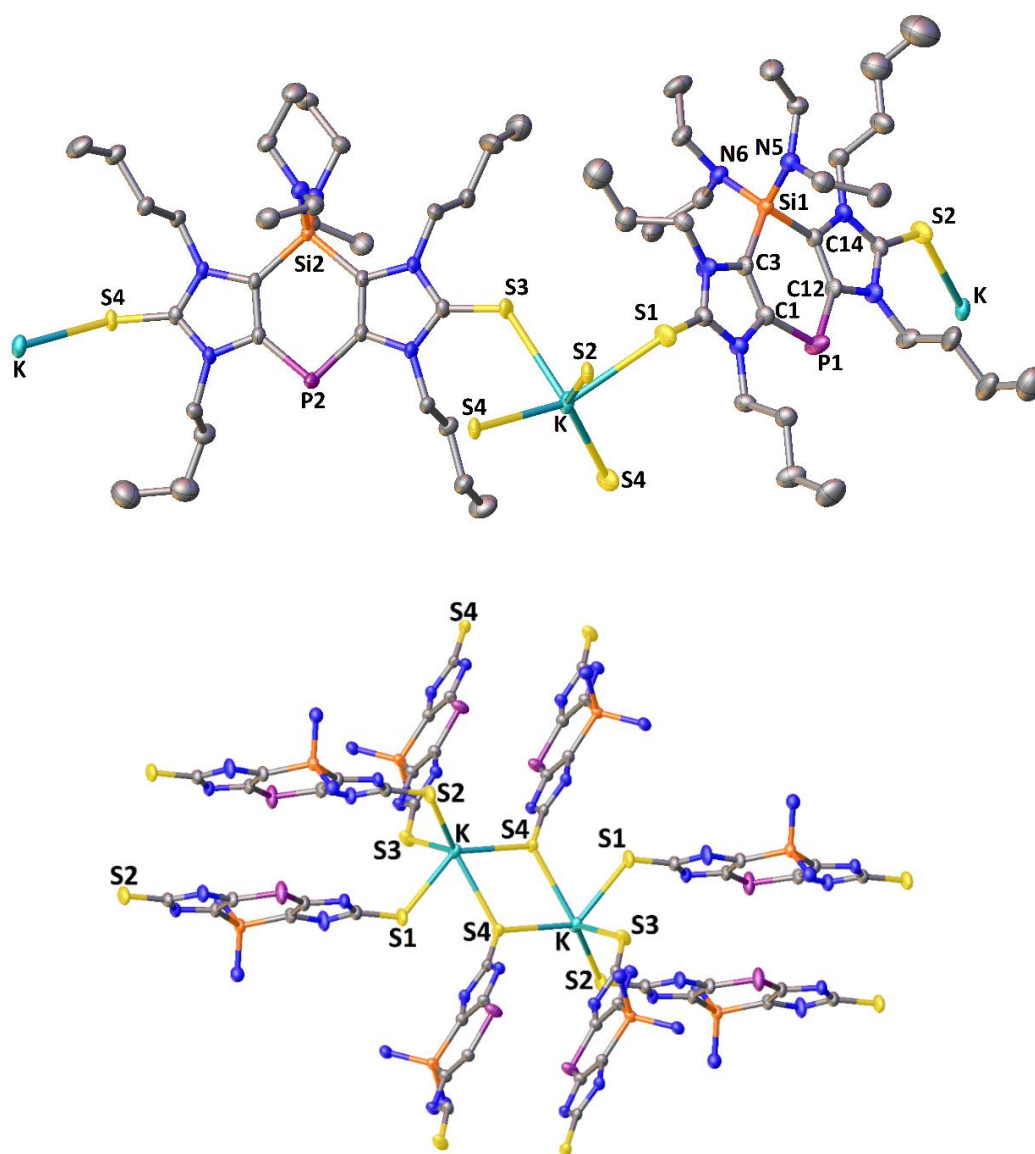
Figure 6.2. Cut-out of the polymeric structure; displacement ellipsoids (50 % probability) plot showing the two crystallographically inequivalent **K[14b]** anions and three of the equivalent K⁺ ions, with additional S atoms to show the full coordination environment at the central K⁺ (top); (hydrogen atoms are omitted for clarity). Selected bond lengths in Å and angles in °: Si-N5 1.720(2), P1-C1 1.796(2), Si-C3 1.856(2), C12-C14 1.372(3), S1-K 3.0425(8), S3-K 3.1093(7); C3-Si1-C14 99.45(10), N5-Si1-C14 116.01(10), N5-Si-N6 107.46(9), N5-Si1-C3 107.27(10). Alternate depiction of the structure of **K[14b]** emphasizing the coordination around a pair of centrosymetrically related K⁺ ions (bottom); hydrogen atoms and whole butyl and ethyl groups attached at N and Si, respectively, are omitted for clarity (50% probability displacement ellipsoids). There are in all four unique S atoms and one potassium atom in the asymmetric unit. Selected bond lengths [Å] and angles [°]: K_{left}-$S1_{left}$ 3.0422(6), K_{left}-$S2_{left}$ 3.1356(7), K_{left}-$S3_{left}$ 3.1092(7), K_{left}-$S4_{top}$ 3.1086(4), K_{left}-$S4_{bottom}$ 3.1600(4), K-K 5.2768(4); S3-K_{left}-S1 90.18(2), S1-K_{left}-S2 96.93(2), S1-K_{left}-S4 70.49(1), S4-K_{left}-S3 106.50(2), S4-K_{left}-S2 140.40(2), S4-K_{left}-S4 65.35(1), S4-K_{right}-S1 134.55(2), S4-K_{right}-S2 123.94(2), S4-K_{right}-S3 92.30(1).

However, the attentive comparison of ^{31}P and ^{31}P{^{1}H} NMR investigation showed no evidence of "phosphane hydrides" in bulk samples of **K[14b]**.

The existence of this kind of 'phosphane-hydrides' were also observed in the crystal structure for the phosphanide compound **XXXIV**[91] discussed in chapter 1. ***In this case,*** each potassium cation was observed to be coordinated to the thione sulfur centers of two neighboring molecules and three diethyl ether molecules and exist as sulfur-coordinated K$^+$ polymer (Figure 6.3).
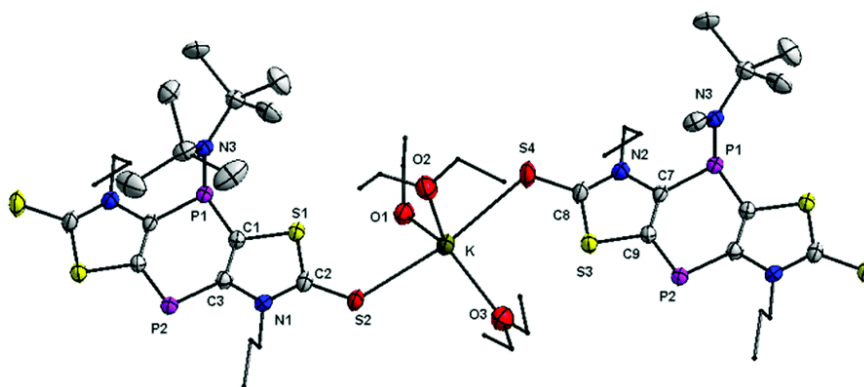
Figure 6.3. Cut-out of the polymeric structure of **XXXIV** (50 % probability level); hydrogen atoms are omitted for clarity.[91]

6.2 Formation of the dimeric 1,4-dihydro-1,4-phosphasilines 15b by one electron oxidation of the anionic fused 1,4-dihydro-1,4-phosphasiliines K[14b]

Based on the previous studies on redox reactions of anionic 1,4-dihydro-1,4-diphosphinines **K[2a]** and **XXXIV**[91,151], a freshly prepared Et$_2$O solution of **K[14b]** was treated dropwise with an Et$_2$O solution of I$_2$ at –80 °C. The formation of a pale greenish-yellow solution was observed containing product **15b** having a P-P bond (Scheme 6.3). Compound **15b** was isolated as yellow powder by extraction with Et$_2$O. The formal reversion of the reaction 2 x **K[14b]** -> **15b** + 2KI was then examined by using compound **15b** and an excess of KC$_8$ in Et$_2$O at ambient temperature (Scheme 6.3); the latter condition was specifically chosen to avoid desulfurization of the C=S bonds[152]. Immediately, the color of the solution turned from yellow

to orange-brown, consistent with re-formation of **K[14b]**. Formation of the latter was then confirmed by the ^{31}P{^{1}H} NMR spectrum of the reaction mixture showing a singlet at – 87.9 ppm (Table 6.2).
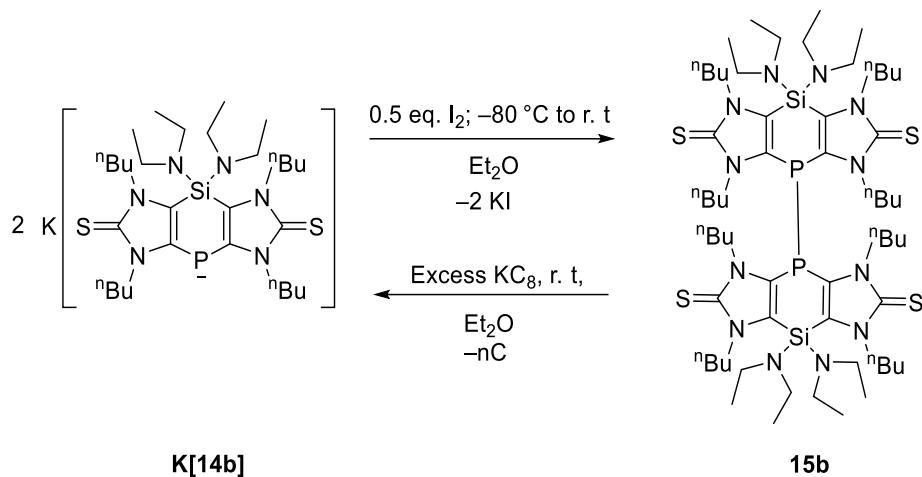

Scheme 6.3. Oxidation of **K[14b]** to give **15b** and the subsequent reduction.

Table 6.2. ^{29}Si{^{1}H} dept20, ^{31}P{^{1}H} NMR chemical shifts (CDCl$_3$), MS data and yields of **K[14b]** and **15b**.

Compound	NMR/ppm		MS/m/z	Yield/%
	δ ^{29}Si{^{1}H} dept20	δ ^{31}P{^{1}H}		
K[14b]^a	−36.2	−87.9	623.3 [M]$^-$ (neg-ESI)	70
15b	−42.2	−49.5	1247.7 [M+H]$^+$ (FTMS+pos-APCI-MS)	63

^{a} In THF-d$_8$ solution.

The single crystals for the X-ray diffraction analysis were obtained from Et$_2$O solutions by slow evaporation of the solvent at room temperature (Figure 6.4a). The structure revealed a monoclinic crystal system with the space group $P2_1/c$. The structure evidently showed the two middle rings in an antarafacial conformation at the P-P bond (bond length = 2.270(2) Å) with no torsion angle. The truncated structure (Figure 6.4b) was in good agreement with this observation. This was in contrast to the twisted conformations occurring in the structures of related tricyclic 1,4-diphosphinine derivatives **4a** and **XXXV**[91,151], most possibly reflecting the steric effects of the additional alkyl chains at the Si-bound N centers.
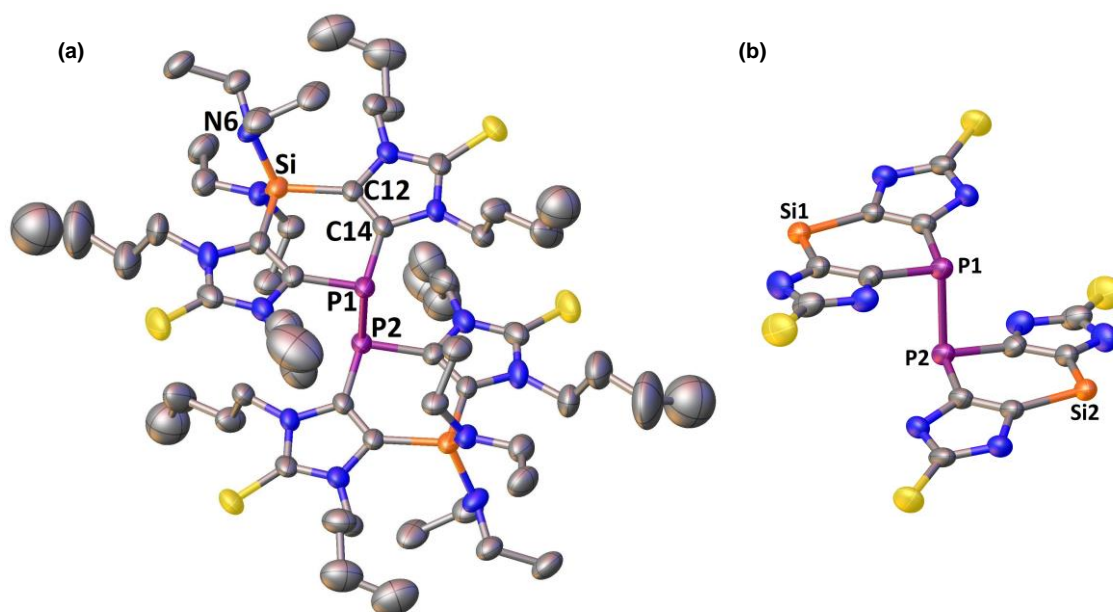
Figure 6.4. Molecular structure of **15b** (a); hydrogen atoms are omitted for clarity (50% probability level); right side: truncated molecular structure of compound **15b** (b); hydrogen atoms and N- and Si-substituents are omitted for visualizing the parallel arrangement of the central rings (50% probability level). Selected bond lengths [Å] and angles [°]: Si-N6 1.696(4), P1-C14 1.822(4), Si-C12 1.889(5), C12-C14 1.362(6), P1-P2, 2.270(2); Σ<°P 293.87.

6.3 Investigation of the redox behavior of the anionic 1,4-dihydro-1,4-phosphasilines K[14b]

The protocol for effectively performing the cyclic voltammetry studies under inert conditions was analogous to the studies performed/described in Chapter 3. Nevertheless, minor alterations in the electrolyte solution systems and electrodes were made here, according to the solubility and the reactive nature of the respective analytes.

CV scans starting in the anodic direction from the open circuit potential (OCP) conducted on **K[14b]** in CH_3CN/[n-Bu_4N][PF_6] solutions showed a chemically irreversible (IRR) oxidation process with E_p^{Ia} = −0.96 V and a similarly IRR reduction process with E_p^{IIIc} = −1.85 V *vs*. the ferrocene/ferrocenium redox couple ($Fc^{+/0}$) (Figure 6.5a)**.**
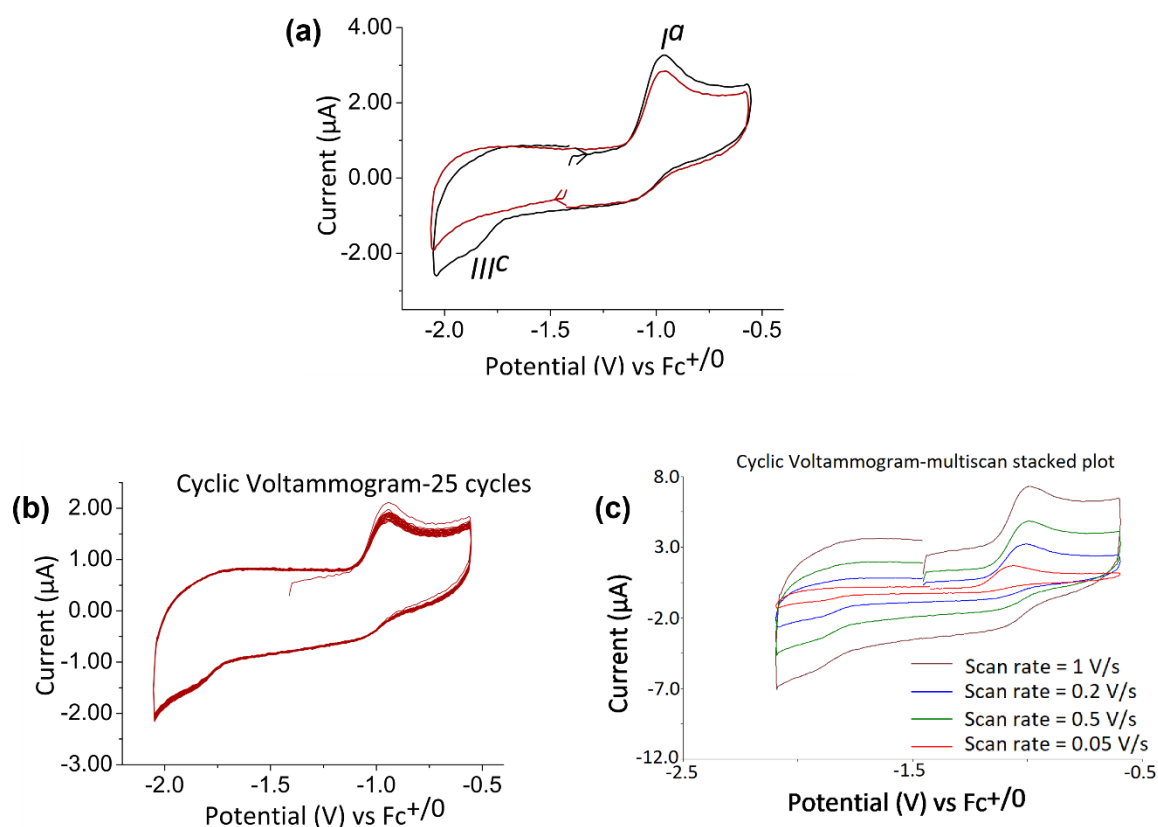
Figure 6.5. Cyclic Voltammograms of **K[14b]** (1.32 mM) at a Pt electrode in a 0.1 M [n-Bu$_4$N][PF$_6$]/CH$_3$CN solution; black solid line, anodic initial scan direction; red solid line, cathodic initial scan direction; scan rates = 200 mV/s. (c) Multicycle CV scans (0.1 M [n-Bu$_4$N][PF$_6$]/CH$_3$CN) of **K[14b]** (1.32 mM) (initial scan anodic ; v = 0.2 V/s) with 25 repeats. (d) Stacked plots (0.1 M [n-Bu$_4$N][PF$_6$]/CH$_3$CN) of **K[14b]** (1 mM) with v = 0.05, 0.2, 0.5, 1 V/s.

But when the initial scan direction was cathodic, the E_p^{IIIc} signal didn't appear on the first cycle. Thus, the species responsible for E_p^{IIIc} appeared to be an electrolysis product of process E_p^{Ia}. The repeatability of the processes was examined by carrying out multicycle CVs. Even after 25 cycles, the oxidation peak and reduction peak positions showed no variation and hardly any attenuation in peak intensities was observed (Figure 6.5b). The scan rate dependence was examined from 50 to 1000 mV/s which showed the expected current increase with scan rate, slight incremental increases in the reduction peak potentials, but essentially invariant oxidation peak potentials (Table 6.3 and Figure 6.5c). In fact, all these experiments showed same behavior as we have seen for the 1,4-dihydro-1,4-diphosphinine systems in chapter 3, indicating the same redox phenomenon happening in both systems.

Table 6.3. Peak potentials and currents for cyclic voltammograms of **K[14b]** at different scan rates[a].

Scan rate/ mV/s	E_p^{IIIc}/V	E_p^{Ia}/V	I_p^{IIIc}/µA	I_p^{Ia}/µA	$\left| I_p^{IIIc}/I_p^{Ia} \right|$
1000	−1.87	−0.95	−5.58	7.34	0.76
500	−1.85	−0.95	−3.38	4.89	0.69
200	−1.85	−0.96	−1.85	3.26	0.57
50	−1.84	−1.02	−0.71	1.74	0.41

[a]Potentials are in V vs. the $Fc^{+/0}$ redox couple
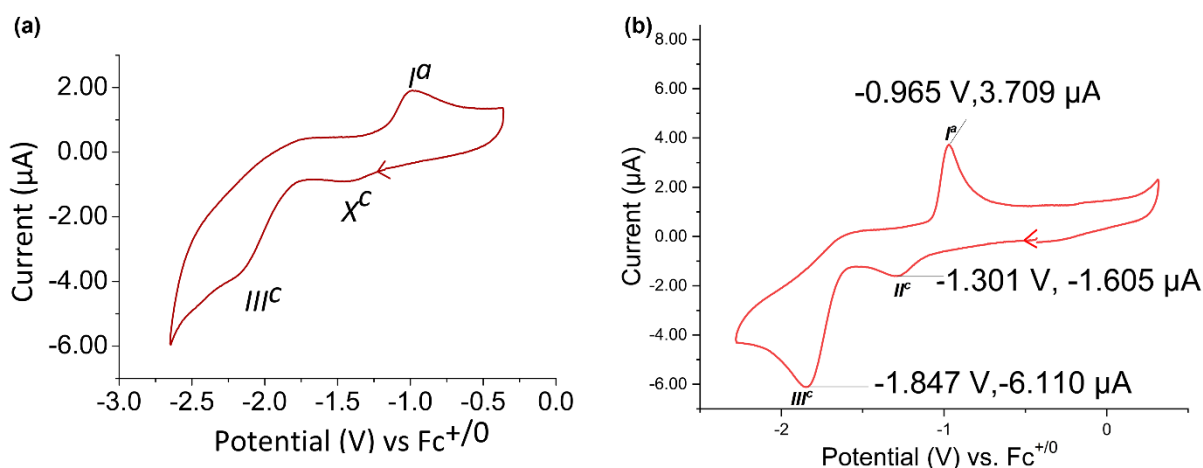
Figure 6.7: (a) Cyclic voltammogram of **15b** (1 mM) at a Pt electrode in a 0.2 M n-[n-Bu₄N][PF₆]/THF solution, starting in the cathodic direction from OCP and showing the second cycle; scan rate = 200 mV/s. (b) Cyclic voltammograms of **4a** (2 mM) at a Pt electrode in a 0.2 M n-Bu₄NPF₆/THF solution in the cathodic initial scan direction; scan rates = 200 mV/s.

Following the studies performed in chapter 3, here too, CV experiments were also conducted on the dimeric compound **15b** in [n-Bu₄N][PF₆]/THF to electrochemically investigate its reduction to yield back the anionic **K[14b]**. In this case, a large, IRR reduction peak labelled E_p^{IIIc} was found at −2.27 V and an IRR re-oxidation process labelled E_p^{Ia} occurs at −0.9 V (Figure.6.7a), when the initial scan direction was cathodic.

Scans starting from OCP in the anodic direction didn't showcase E_p^{Ia} in the first cycle (Figure. 6.8d). As previously observed in CVs of diphosphinine analogue **4a**, the behavior in THF is less ideal than in CH₃CN because **15b** proved to be insufficiently soluble to conduct CV studies in CH₃CN. The behavior of both P-P bonded dimers (in THF, but not in CH₃CN for **4a**) showed a large initial wave (Figure 6.7a,b) which didn't persist in multicycle experimental studies (Figure 6.8a,b). A small residue (labelled X[c] in Figure 6.7a) was still visible in the second scan but completely vanished thereafter. The peak potentials of **4a** and **15b** could be compared as the investigations were also performed in in THF.
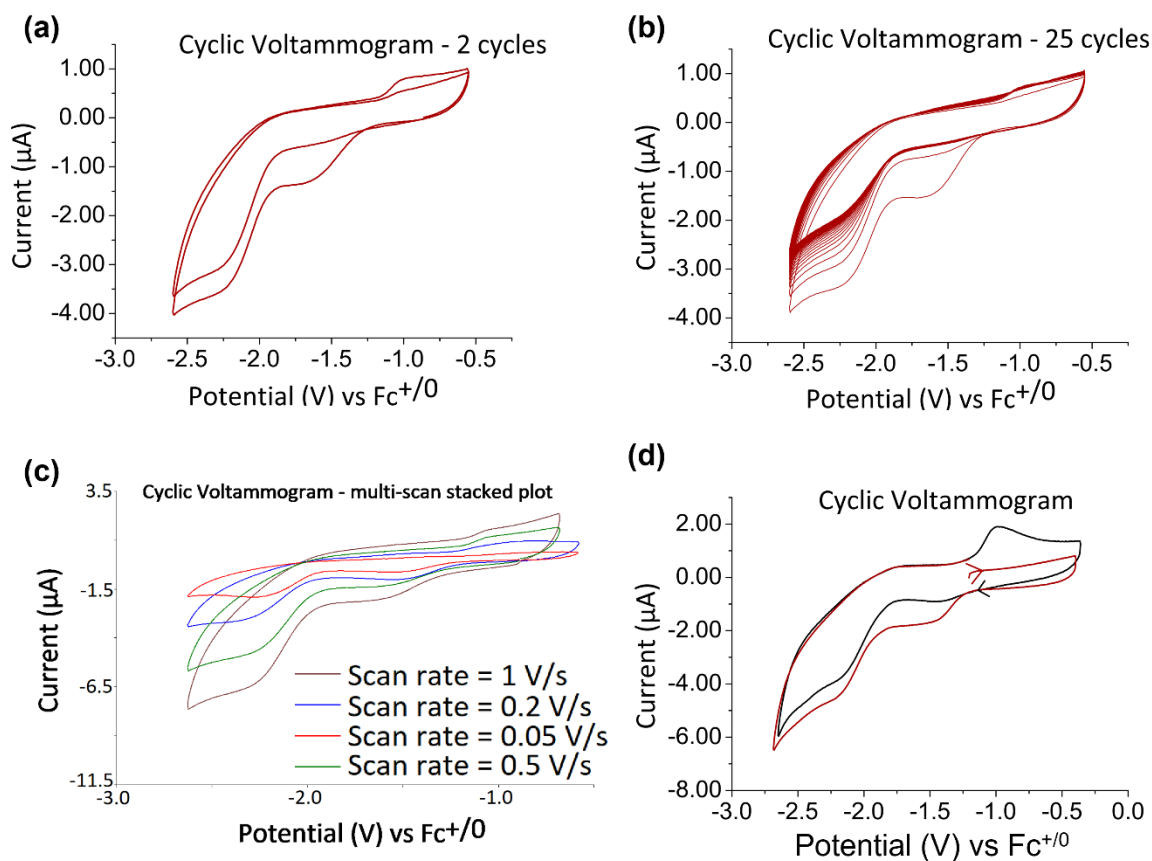
Figure 6.8: (a) Multicycle CV scans (0.2 M [*n*-Bu₄N][PF₆]/THF) of **15b** (1 mM) (initial scan cathodic; v = 0.2 V/s) with 2 repeats. (b) Multicycle CV scans (0.2 M [*n*-Bu₄N][PF₆]/ THF) of **15b** (1 mM) (initial scan cathodic; v = 0.2 V/s) with 25 repeats (c) Stacked plots (0.2 M [*n*-Bu₄N][PF₆]/ THF) of **15b** (1 mM) with v = 0.05, 0.2, 0.5, 1 V/s (d) 3-repeat CV scans (0.2 M [*n*-Bu₄N][PF₆]/ THF) of **15b** (1 mM) in the cathodic direction stacked with the first scan in the anodic direction with no repeat (initial scan cathodic; v = 0.2 V/s).

The variable scan rate experiments from 200 to 1000 mV/s matched the expectations for increased currents with scan rates (Figure 6.8c). The reduction peak potentials and the current ratios remained almost constant and the oxidation peak potentials showed a small increment as the scan rate was increased (Table 6.4 and Figure 6.8c).

Table 6.4. Peak potentials and currents for cyclic voltammograms of **15b** at different scan rates[a].

Scan rate/ mV/s	E_p^{IIIc}/V	E_p^{Ia}/V	I_p^{IIIc}/µA	I_p^{Ia}/µA	$\left\|I_p^{IIIc}/I_p^{Ia}\right\|$
1000	-2.25	-1.01	-6.38	1.60	0.25
500	-2.25	-1.01	-4.70	1.18	0.25
200	-2.27	-0.90	-2.96	0.94	0.31
50	-2.25	-0.80	-1.88	0.41	0.22

[a]Potentials are in V vs. the Fc$^{+/0}$ redox couple

These CV experiments proved to be consistent with the redox interconversions of **K[14b]** and **15b** established in the chemical oxidation with I$_2$ and reduction by KC$_8$. Moreover, we could also see the analogy with those of the diphosphinine analogues **K[2a]/4a** described in chapter 3. However, in the former case, both the monomer salt and the P-P bonded dimer could be studied in CH$_3$CN due to the enhanced solubility and a detailed mechanistic study supported by digital simulation was possible.

EI : $\quad$ **14b**$^-$ $\overset{k_I^\circ}{\rightleftharpoons}$ $\boldsymbol{e}^-$ + **14b**$^{\bullet}$ $\qquad$ (fast)

CI : $\quad$ **14b**$^{\bullet}$ + **14b**$^{\bullet}$ $\underset{k_{-I}}{\overset{k_I}{\rightleftharpoons}}$ **15b** $\qquad$ (strongly product favoured)

EII : $\quad$ **15b** + $\boldsymbol{e}^-$ $\overset{k_{II}^\circ}{\rightleftharpoons}$ **15b**$^{\bullet-}$

EIII: $\quad$ **15b**$^{\bullet-}$ + $\boldsymbol{e}^-$ $\overset{k_{III}^\circ}{\rightleftharpoons}$ **15b**$^{2-}$ $\qquad$ (fast)

CIII: $\quad$ **15b**$^{2-}$ $\underset{k_{-III}}{\overset{k_{III}}{\rightleftharpoons}}$ **14b**$^-$ + **14b**$^-$ $\quad$ (strongly product favoured)
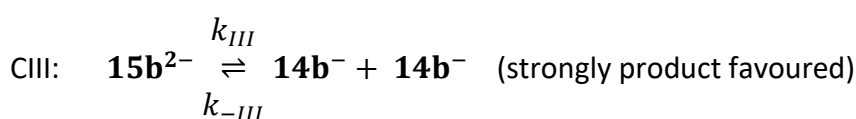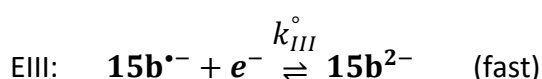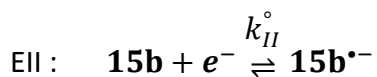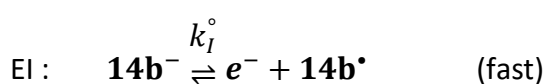
Scheme 6.4. Equations for the CV mechanism proposed for the **K[14b]/15b** interconversion.

That mechanism involved an EC/EEC sequence, *i.e.* a one-electron oxidation of the monomeric anion (**14b⁻,2a⁻**) followed by a fast chemical step (dimerization at P). This dimer (**15b**, **4a**) was reduced in two steps, with the first forming (**15b⁻•/4a⁻•**) as the rate limiting step followed by a second oxidation either at the same potential or marginally more negative (visible only at high scan rates) leading to the chemical step of P-P bond cleavage and hence reforming **14b⁻** or **2a⁻** (Scheme 6.4). Evidently, all these observations pointed to the same mechanism to be operative for the **K[14b]/15b** interconversion. The peak separations for both the processes were observed to be 3.17 V for **15b** and 2.81 V for **4a**. The deviations in the peak separations for both the P,P-system and P,Si-system were found to be similar (0.28 V for the P,P-system; 0.36 V for the P,Si-system). This concluded that the extent to which the peak potentials shift in the anion-dimer redox process was similar regardless of the heteroatomic system as well as the substitution on the heteroatom.

In order to provide insights into electronic and thermodynamic aspects of the redox processes in this 1,4-dihydro-1,4-phosphasiline derivative, and to enable comparison to those of the 1,4-dihydro-1,4-diphosphinine already investigated, DFT calculations were performed by Brehm, on models **14b** and **15b** at at TPSS-D3/def2-TZVP (CPCM_THF)//PW6B95-D3/def2-QZVP(CPCM_THF) level of theory . The energies and topologies of the Redox Molecular Orbitals (RMOs) relevant to the two systems obtained from the fully geometry optimized DFT calculations are shown in Figure 6.9. The HOMO of **14b** was observed to be dominated by a *p*-orbital contribution of the unsubstituted phosphorus of the middle ring, and indeed very similar to the HOMO calculated for anionic species **2a'**. Similarly, a huge contribution from the σ* orbital of the P-P bond was observed for the LUMO of **15b** as well as **4a'**.

Table 6.5. Peak potentials for cyclic voltammograms of **K[2a]**, **4a**, **K[14b]** and **15b** at scan rate = 200 mV/s[a].

Compound	E_p^{IIIc}/V	E_p^{Ia}/V
K[2a]	−1.63	−0.90
K[14b]	−1.85	−0.96
3a	−1.85	−0.96
15b	−2.27	−0.90

[a]Potentials are in V vs. the Fc⁺/⁰ redox couple.

Satisfyingly, the computed RMO energies were in excellent match to the experimental voltammetry data. Comparative peak potential values for both the system of compounds are provided in Table 6.5. All these values were found to be consistent with the slightly lower RMO energy calculated for both **K[2a]** and **4a** compared to their 1,4-phosphasiline counterparts **K[14b]** and **15b** (Figure 6.9).

LUMO: −2.06   **LUMO**:−2.09

HOMO: −4.05   **HOMO**: −4.08
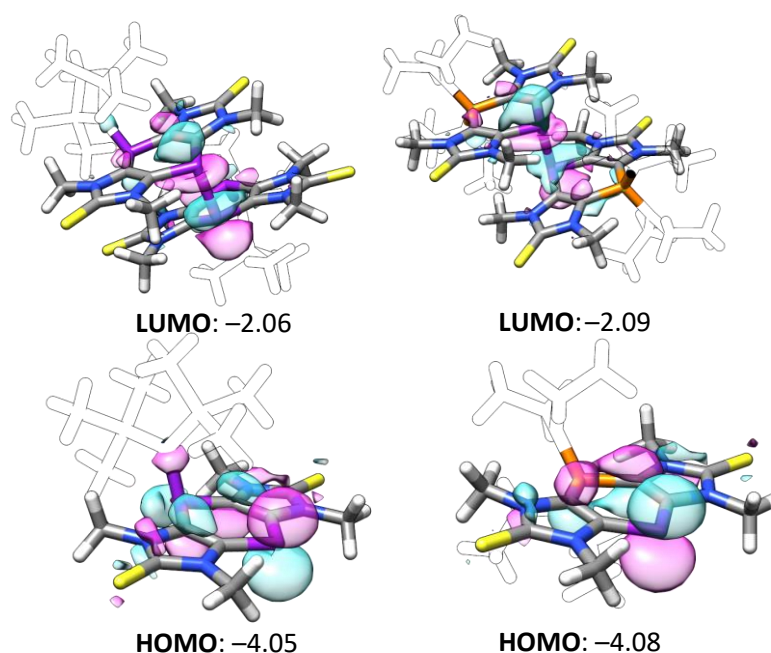
Figure 6.9. Calculated redox molecular orbitals of **14b** (bottom right) and **2a'** (bottom left), and of **15b** (top right) and **4a'** (top left) with absolute molecular orbital energies ε in eV. (Large substituents given as silhouettes for clarity).

In addition to that, the dimerization energies for the formation of the dimeric species **4a'** and **15b** from the respective P-centered radical species were calculated to be similar, at −26.6 kcal/mol and −25.7 kcal/mol, respectively.

7|Reactivity studies of 1,4-dihydro-1,4-phosphasiline 11b focussed on the Si center

In 1915, Bygden synthesized the first authentic cyclic organosilicon compounds, 1,2-dihydro-1,1'-dichlorosilines as well as its dimethyl and diethyl derivatives.[153] This was the very first credible example where cyclic dichlorosilanes were effectively used for the synthesis of differently functionalized cyclic silanes.
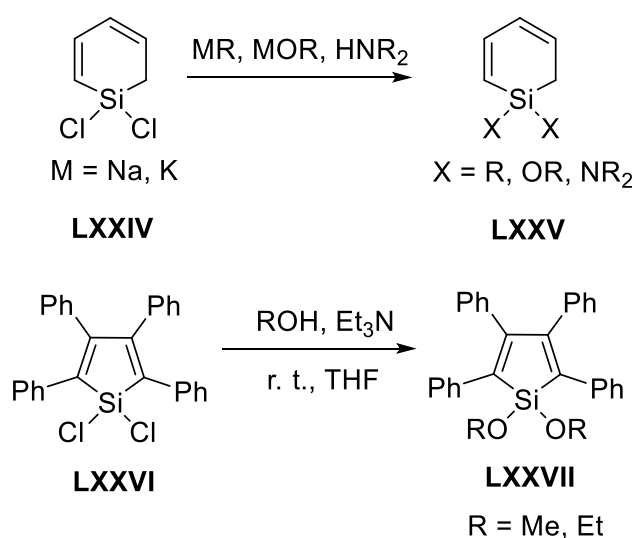
Scheme 7.1. Si-derivatization of 1,2-dihydro-1,1'-dichlorosilines **LXXIV**[154]; synthesis of 1,2-dihydro-1,1'-dialkoxy-2,3,4,5-tetraphenylsiloles **LXXVII** from 1,2-dihydro-1,1'-dichloro-2,3,4,5-tetraphenylsilole **LXXVI**.[155]

Later on, in 1954, West developed a strategy by improving Bygden's protocol to synthesize five-, six- and seven-membered silicon-containing rings from different difunctional Grignard reagents of varying alkyl chain length. By this method, a number of ring compounds with varying functionalities at the silicon atom were prepared.[156] There are a number of reports regarding difunctionalization of the Si centers in unsaturated Si-heterocycles such as the functionalized 1,2-dihydro-1-silines **LXXIV** and **LXXV** (Scheme 7.1). In this report from Maier, 1,2-dihydro-1,1'-dichlorosilines **LXXIV** was effectively used for Si-derivatization to form alkyl, alkoxy, aryloxy, amino, etc. substituted 1,2-dihydro-silines **LXXV**[154] via addition of nucleophilic

reagents at low temperature. In another report, a series of 1,1'-disubstituted-3,4-dimethyl-2,5-bis(trimethylsilyl)siloles were synthesized from their 1,2-dihydro-1,1'-dimethoxy derivative,[157] where the addition of the reagents were performed at low temperatures. In a recent report, West synthesized the 1,2-dihydro-1,1'-dialkoxy-2,3,4,5-tetraphenylsiloles **LXXVII** from 1,2-dihydro-1,1'-dichloro-2,3,4,5-tetraphenylsilole **LXXVI** by the direct addition of alcohols at room temperature (Scheme 7.1).[155]

7.1 Conversion of 1,4-dihydro-1,4-phosphasiline K[14b] into Si(NR$_2$)$_2$ and SiCl$_2$ derivatives 16b, 17b

The 1,4-dihydro-1,4-phosphasiline salt **K[14b]** was treated with triphenylmethyl chloride to form the alkylated derivative **16b** (Scheme 7.2) in a clean fashion. The pure product was isolated as yellow powder via extraction with *n*-pentane and filtration to remove lithium chloride as well as traces of the "pseudo-dimeric" product **15b**. Significant ^{29}Si{^{1}H} dept20 and ^{31}P{^{1}H} NMR signals are collected in table 7.1.
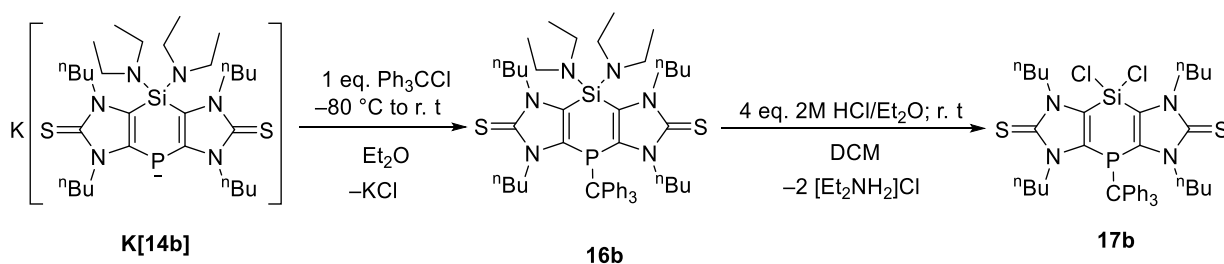
Scheme 7.2. Reaction of **K[14b]** to form the *P*-trityl derivative **16b** and subsequent conversion of **16b** to form the Si-dichloro compound **17b**.

After having introduced the trityl group to the P-center, the Si-bound amino groups of **16b** were replaced with chloro groups using a HCl-ether solution to form the derivative **17b** (Scheme 7.2); yields and selected MS and NMR data are shown in table 7.1.

Reaction of **16b** with 3 eq. of KC$_8$ at lower temperatures didn't cleave the P-C bond but also not the Si-N bond. In fact, the KC$_8$ addition at lower temperature just gave back the starting material **16b** itself without any reaction. On the other hand, reaction of **16b** with 3 eq. of KC$_8$ at room temperature resulted in the formation of the anionic **K[14b]**, without effecting the Si-Cl functions, but only with the NMR conversion of 25% owing to the bulky trityl group.

Table 7.1. $^{29}Si\{^1H\}$ dept20 and $^{31}P\{^1H\}$ NMR data (CDCl$_3$), MS data and yields of **16b**, **17b**, **18b**, **19b**, **20b** and **21b**.
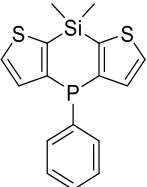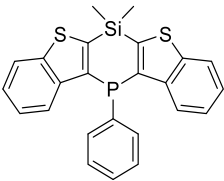
Compound	NMR/ppm		MS/m/z	Yield/%
	δ $^{29}Si\{^1H\}$ dept20	δ $^{31}P\{^1H\}$		
16b	−42.1	−57.2	866.5 [M]$^+$ (MALDI TOF-MS)	90
17b		−55.8	793.2 [M]$^+$ (FTMS + pos-APCI-MS)	85
18b	−25.6	−56.7	753.3 [M+H]$^+$ (FTMS + pos-APCI-MS)	96
19b	−47.5	−56.8	785.3 [M+H]$^+$ (FTMS + pos-APCI-MS)	83
20b		−58.0	776.4 [M]$^+$ (EI-MS)	80
21b		12.9	723.5 (15) [C$_{36}$H$_{70}$N$_7$PS$_2$Si]$^+$, 586.6 (5) [M+H$_2$]$^+$, 514.2 (12) [M-Cl$_2$]$^+$ (EI-MS)	80

7.2 Si-Derivatization of 17b using methyllithium and methanol

As mentioned beforehand, acyclic and/or cyclic compounds having Si-bound chlorides can be successfully exchanged by alkyl and alkoxy groups, thus leading to a wide variety of derivatives. Using compound **17b** and methyllithium or methanol as nucleophiles led to clean substitution reactions at the Si center and the formation of derivatives **18b** and **19b** (Scheme 7.3). All products were isolated as white powders, and NMR and MS data as well as yields are shown in table 7.1. The comparison of **18b** with the dithienophosphasiline **LXXII** with P-phenyl and Si-Me$_2$ functionalities, reported by Baumgartner gave a rather low field shifted NMR peaks. (Table 7.2) The benzo-extension of the dithienophosphasiline (compound **LXXVIII**) led to high field shifted $^{31}P\{^1H\}$ NMR resonance and low field shifted $^{29}Si\{^1H\}$ NMR resonance compared to **LXXII** and overall low field shifted hetero nuclear NMR resonances compared to **18b.**

Table 7.2. $^{29}Si\{^1H\}$ and $^{31}P\{^1H\}$ NMR data (CDCl$_3$) of **V**, **VI** and **18b**.[147]

Compound	NMR/ppm	
	δ $^{29}Si\{^1H\}$ dept 20	δ $^{31}P\{^1H\}$
LXXII	−17.7	−20.7
LXXVIII	−16.9	−36.5
18b	−25.6	−56.7

The reported dialkoxy compounds **LXXVII**[155] also showed low field shifted $^{29}Si\{^1H\}$ NMR resonance to δ = −20.7 ppm compared to **19b** (Table 7.1).
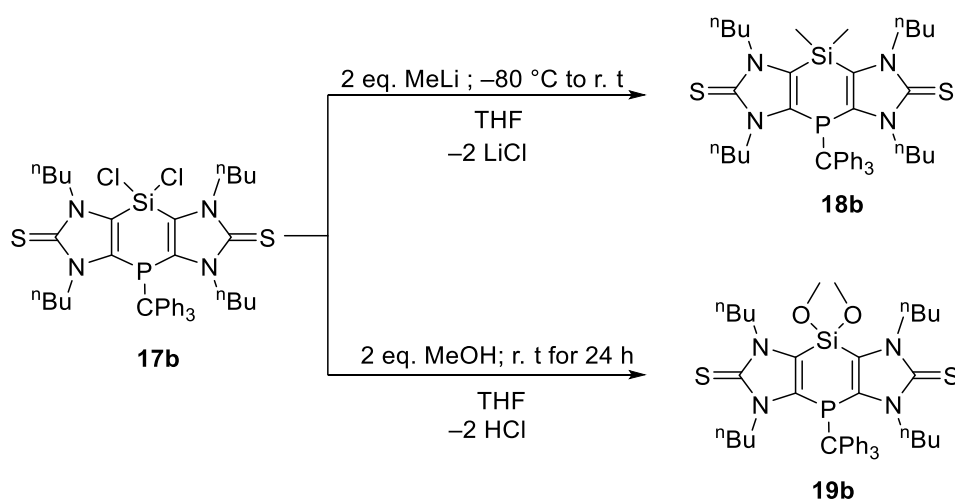
Scheme 7.3. Substitution reactions of **17b** to form **18b** with methyl lithium and **19b** with methanol.

7.3 Studies on the Si-centered reduction of 17b

In the past three decades, silylene chemistry has flourished worldwide, a development that was initiated by the ground breaking discovery by West in 1994, *i.e.*, the synthesis of the first isolable N-heterocyclic silylene **LXXIX** from its $SiCl_2$ precursor (Figure 7.1).[158] Apart from these well-explored 5- membered silylene ring systems, six-membered *N*-heterocyclic low-valent silicon species were also explored, instigated by the discovery of the neutral silylenes **LXXX** by Driess.[159] In all these examples, the strong interactions between the empty *p*π-orbital at the Si center and filled π-type orbitals of nitrogen played a huge rule in stabilizing such low-coordinate species. On the other hand, the first isolable dialkylsilylene **LXXXI**[160,161] was synthesized, effectively utilizing the steric protection towards dimerization; the latter also represent examples having electronically least perturbed divalent silicon, unlike in **LXXIX** and **LXXX**. In these examples, both **LXXX** and **LXXXI** were synthesized from their $SiBr_2$ precursors and using KC_8 as the reducing agent. Transient silylenes, thermally formed from silanorbornadienes were effectively trapped using dimethylbutadiene to form the silole derivatives **LXXXII** via 1,4-addition reaction (Figure 7.1).[162,163]
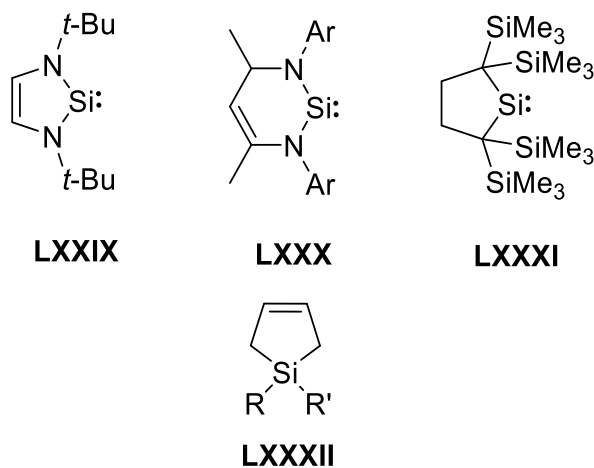
Figure 7.1. Different types of isolated heterocyclic[158,159] and cyclic silylenes[160,161]; product **LXXXII** of the trapping of transient silylenes.[162,163]

7.3.1 Theoretical studies

To gain deeper insight into the redox properties at Si as well as P-centers of **17b**, DFT calculations were performed by Brehm at the TPSS-D3/def2-TZVP (CPCM$_{THF}$)//PW6B95-D3/def2-QZVP(CPCM$_{THF}$) level of theory. Here, models were used where the N-^{n}Bu groups were truncated to N-Me, and indicated by ' and trityl groups were omitted from the FMO calculations (Figure 7.2).

LUMO : –1.9244 eV

HOMO : –6.0080 eV
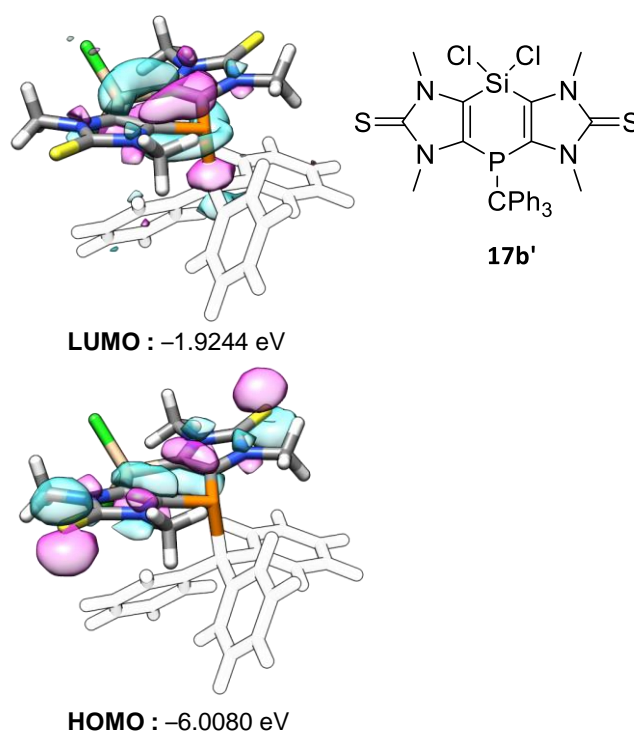
Figure 7.2. Calculated frontier molecular orbitals of the model compounds **17b'**.

The LUMO showed large coefficients at the P and Si centers, with slight delocalization to the neighboring carbon atoms and also included P–C σ*-orbital, suggesting the possible cleavage of the P–C bond upon reduction. On the other hand, the LUMO didn't include any Si-Cl σ*-orbitals, thus suggesting a relative inertness of the Si-Cl bond towards reductive conditions.

In addition, theoretical calculations were performed by Brehm at the TPSS-D3/def2-TZVP (CPCM$_{THF}$)//PW6B95-D3/def2-QZVP(CPCM$_{THF}$) level of theory, to investigate the Si-centered reduction and ease of silylene formation. Here, models were used where the N-^{n}Bu groups

were truncated to *N*-Me, and trityl groups were truncated to Me (denoted by '') for the ease of calculations.
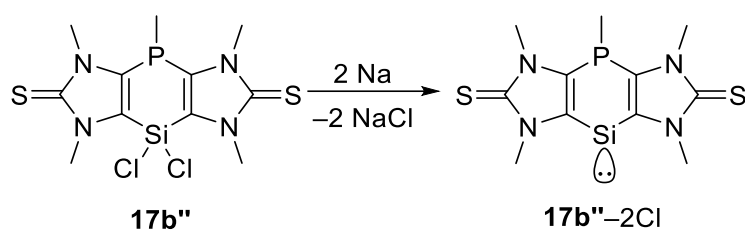
Scheme 7.4. Theoretical depiction of the reduction of **17b''** to form the silylene **17b''–2Cl**.

The calculations revealed that the reduction reaction (Scheme 7.4) to form the corresponding Si(II) species, with 2 eq. of Na accompanied by the elimination of Sodium Chloride (2 eq.) was an exergonic process with a significant reaction Gibbs free energy of 19 kcal/mol (with no lattice energy involved).

(a)

17b''–2Cl

LUMO : –2.6851 eV

HOMO : –5.8773 eV

HOMO^{-4} : –6.8234 eV

(b)
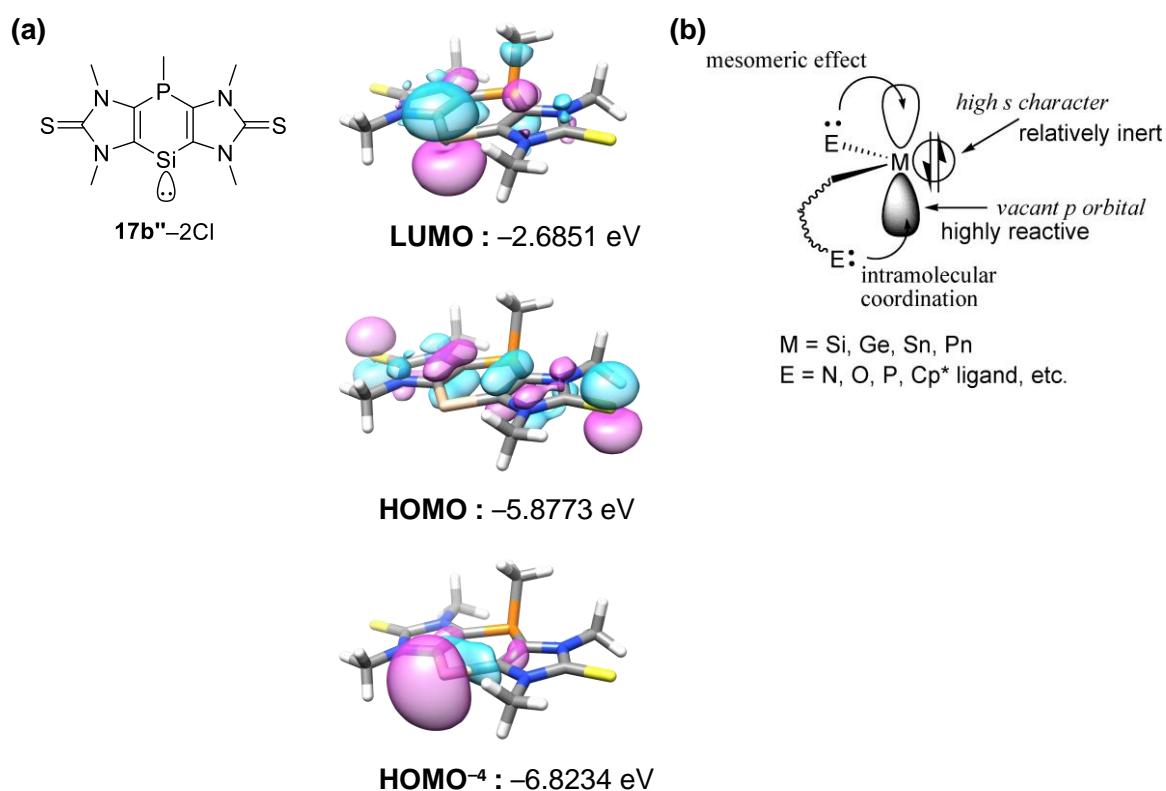
Figure 7.3. (a) Calculated FOMO of the model compounds **17b''–2Cl**; (b) thermodynamic stabilization of silylenes and other metallylenes[164,165].

The FOMO (Floating Occupation Molecular Orbital)[166] calculations on the model, **17b''**–2Cl (singlet state was calculated) showed that the energetically lower HOMO^{-4} with a high *s*-character has a huge contribution from the in-plane non-bonding lone pair of electrons at silicon (Figure 7.3a). The LUMO was observed to be dominated by a *p*-orbital contribution of the Si(II) center which is expected for silylenes with a singlet ground state (Figure 7.3b). The high reactivity of the silylene derivative **17b''**–2Cl was also expected, too, owing to the presence of this vacant *p*-orbital.[164,165]

7.3.2 Experimental studies

Having a bulky trityl group at the P center and two chlorides on the Si center, the possibility of a (selective) reduction at the Si center was investigated for **17b**. These attempts were made initially at room temperature and included strong reducing agents such as KC_8 as well as bare metals (Mg, K) (Scheme 7.5). But the P-C bond was easily cleaved off, always, thus allowing for further reactions to occur.
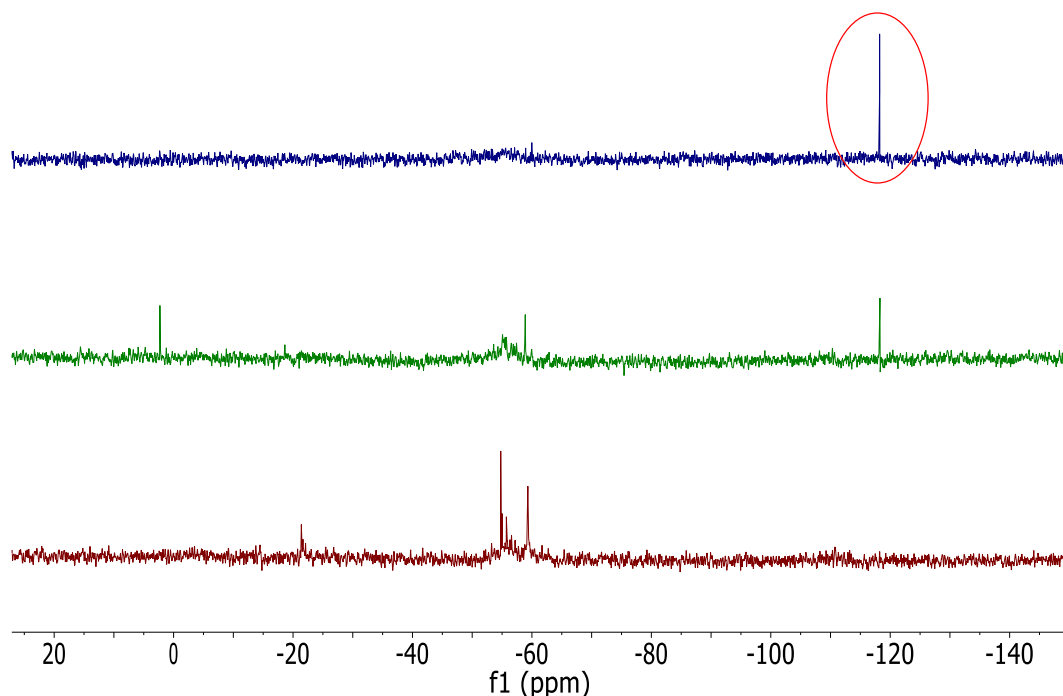
Figure 7.4. Stacked plots of the time-dependent $^{31}P\{^{1}H\}$ NMR spectra of the reaction of **17b** with KC_8; (bottom) immediately after the addition of KC_8; (middle) after 15 minutes and (top) after 2 days.

This development was monitored for the reaction of **17b** with KC_8 by $^{31}P\{^1H\}$ NMR spectroscopy (starting material: δ = −55 ppm, in toluene-d8). After 2 days, a selective signal was observed at δ = −118 ppm ($^1J_{P,H}$ = 237 Hz) which couldn't be attributed to any known compound, unfortunately (Figure 7.4).

On the other hand, when the reduction was targeted at − 80 °C it didn't result in the P-C bond cleavage. In case of the addition of 2 eq. of KC_8, the reaction mixture was kept stirring overnight, and the formed graphite was removed by filtration and the solution was concentrated to dryness. The residue was dissolved in toluene-d8 for NMR spectroscopic studies, but the $^{31}P\{^1H\}$ spectrum revealed hardly any change of the chemical shift compared to **17b** (Figure 7.5).
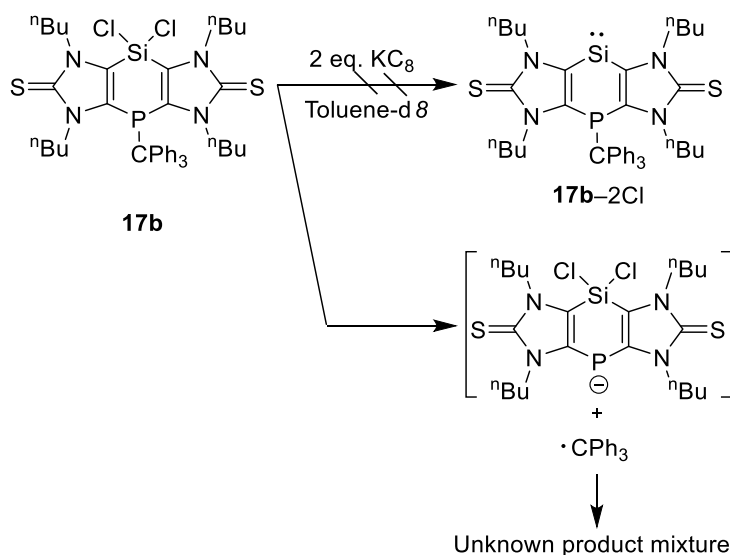
Scheme 7.5. Reduction of compound **17b**.

On the other hand, in the ^1H NMR spectrum (Figure 7.6) signals became much broader and appeared slightly high-field shifted. The latter might point at a C-H activation of the long N-alkyl chains by the transiently formed silylene but, unfortunately, the products could not be separated and studied by other analytical means to prove or disprove this assumption. The outcome of the reaction did not change if 4.eq of KC_8 was used, leading to the same observation.
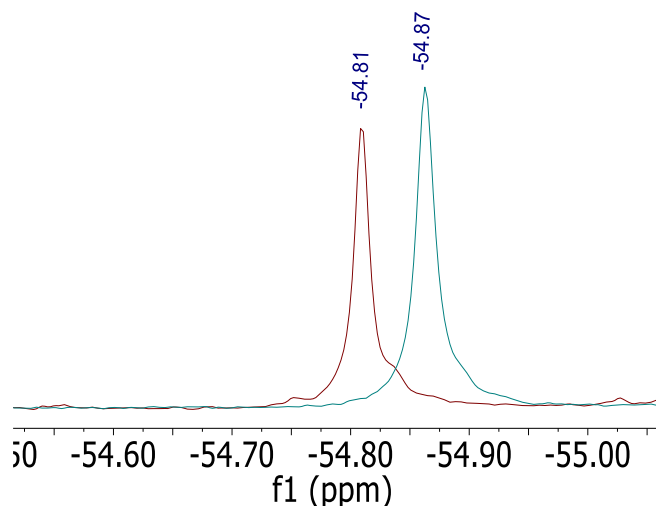
Figure 7.5. Superimposed and zoomed-in ^{31}P{^{1}H} NMR spectrum of the dried filtrate of **17b** reduction reaction (maroon signal) and **17b** (cyan signal) measured in toluene-d8.
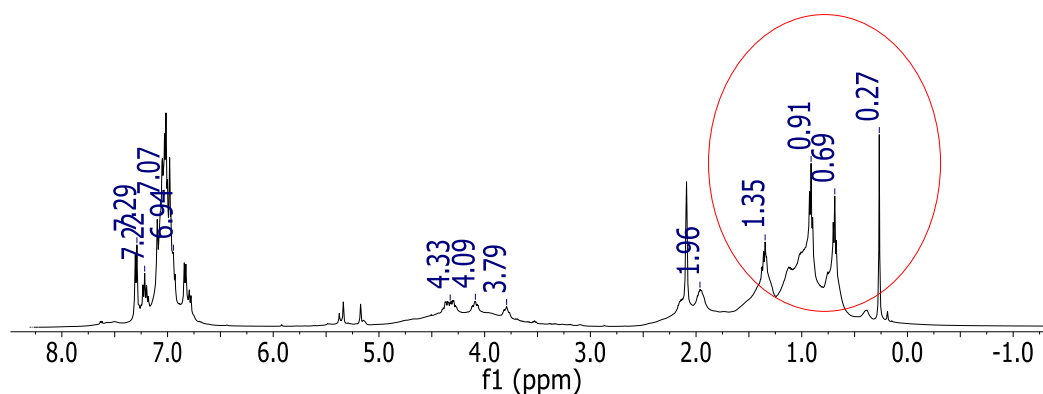
Figure 7.6. ^{1}H NMR spectrum of the dried filtrate of **17b** reduction reaction measured in toluene-d8 (significantly broader peaks are marked with a red-circle).

Trapping reactions to capture a transiently formed silylenes by using, *e.g.*, 1,3-butadiene very well established.[162,163] Therefore and to test this idea for the present case, an excess of KC$_8$ and 1,3-butadiene were added to a clear yellow solution of **17b** at – 80 °C and warmed up to room temperature (Scheme 7.6). The reaction mixture was filtered to remove graphite and KCl and the residue dried to get a cream-colored powder. The product **20b** was characterized by ^{31}P{^{1}H}, ^{1}H NMR spectroscopies and EI-MS spectrometry. All analytical data indicate clearly the presence of the silole compound **20b** and the ^{31}P{^{1}H} NMR spectra showed a slight high-field shift compared to the parent compound **17b** (Table 7.1) indicating the replacement of the -Cl group on the Si-center; other unknown decompositions products were observed, too.

The product was isolated as a white powder by washing the dried residue mixture with a 3:1 solvent mixture of *n*-Pentane and diethyl ether. Apart from the NMR spectral analysis, EI-MS spectrum showed strong evidence for the molecular ion peak at m/z = 776.4 (20 %) (Figure 7.7). The compound was additionally characterized by the HRMS experiment, i.e., for $C_{45}H_{57}N_4PS_2Si$. theor./exp. 776.3531/776.3526.
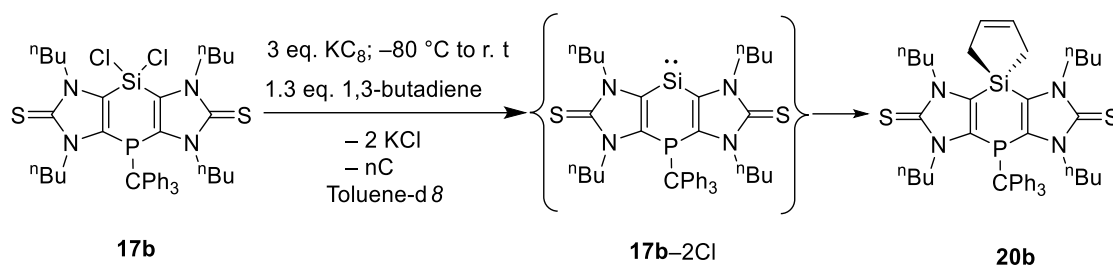
Scheme 7.6. Reduction of compound **17b** and trapping reaction of silylenes **17b–2Cl** to form the silole derivative **20b**.
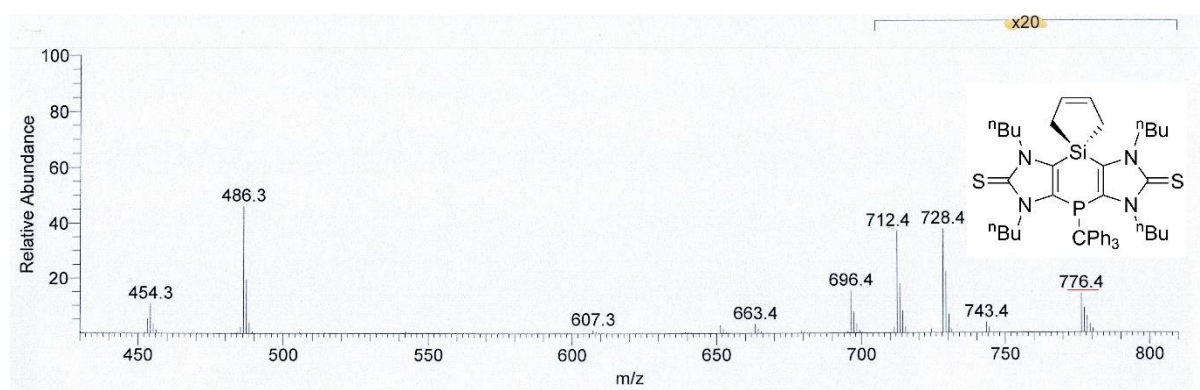
Figure 7.7. EI-MS spectrum of **20b** depicting the molecular ion peak (the relative abundances corresponding to the fragments are underlined in red).

8|Reactivity studies involving both Si and P centers of 1,4-dihydro-1,4-phosphasiline 11b

The group of Streubel has reported on the synthesis of tricyclic *P*–Cl substituted derivatives **LXXXIV** and **LXXXIV'** using the imidazole-2-thione and thiazole-2-thione fused 1,4-dihydro-1,4-diphosphinine derivatives **LXXXIII** and **LXXXIII'**, respectively and 2 eq. of PCl$_3$. These *P*-Cl heterocyclic derivatives were subjected to reduction with tri-*n*-butylphosphane to form selectively the (aromatic) 1,4-diphosphinine derivatives **XXVI**[90] and **XXVII**[91] (Scheme 8.1).

LXXXIII : E = NR ; R = Me, *n*-Bu
LXXXIII' : E = S

LXXXIV : E = NR ; R = Me, *n*-Bu
LXXXIV' : E = S

XXVI : E = NR ; R = Me, *n*-Bu
XXVII : E = S
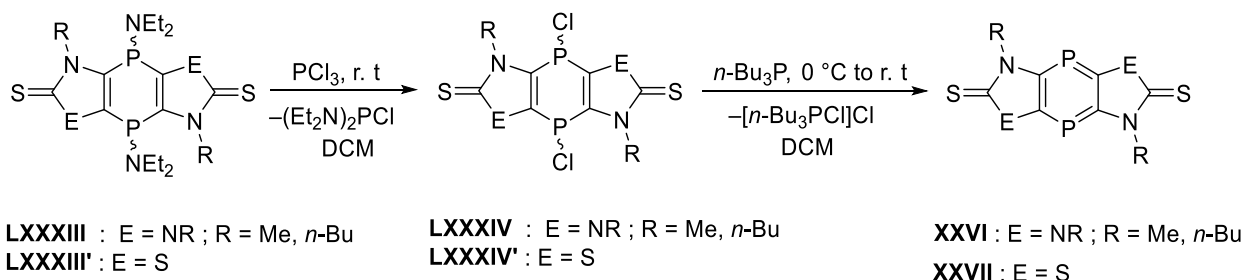
Scheme 8.1. Synthesis of the P–Cl-functional tricyclic compounds **LXXXIV**, **LXXXIV'** and of the 1,4-diphosphinines **XXVI**, **XXVII**.[90,91]

8.1 Synthesis of the 1,4,4'-trichlorinated 1,4-dihydro-1,4-phosphasiline 21b

To enable a broader exploitation of 1,4-dihydro-1,4-phosphasiline **11b**, the latter was treated with 6 eq. of HCl (in Et$_2$O) in dichloromethane to synthesize *P*-Cl and *Si*-Cl substituted derivative **21b** (Scheme 8.2). Compound **21b** was formed with a content of 100% in the product mixture according to the ^{31}P NMR spectroscopy; the product was extracted using diethyl ether and dried to obtain in moderate to good yields (80 %). The ^{31}P{^{1}H} NMR showed a singlet at δ = 12.9 ppm where the previously reported 1,4-dihydro-1,4-diphosphinine **LXXXIV**[90] showed two singlets at δ = 2.6 (*cis*), 10.9 (*trans*) ppm with an isomer ratio of 1.8:1 in the ^{31}P{^{1}H} NMR spectrum; the ^{31}P{^{1}H} NMR and MS data of **21b** are given in Table 7.1. The

molecular ion peak at m/z = 514.2 (12%) was observed under EI-MS conditions which corresponds to the mass of either the aromatic derivative **22b** or the de-dichlorinated derivative **21b**–2Cl having the silylene center (Table 7.1 and Figure 8.1). Based on the theoretical calculations (Figure 8.2), we expected **22b** to be the more probable fragment than **21b**–2Cl due to the labile nature of P-Cl bond on reduction conditions than the Si-Cl bond.
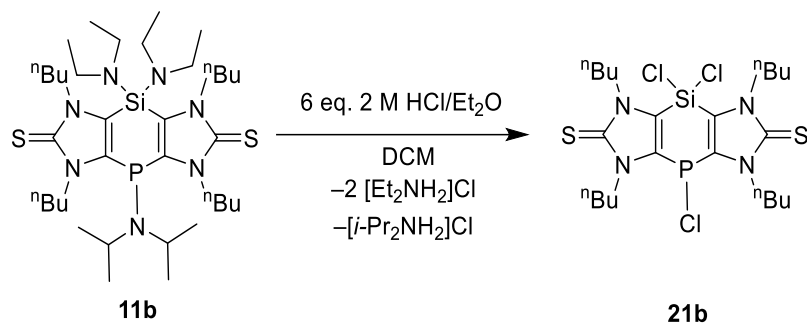
Scheme 8.2. Synthesis of P-Cl and Si-Cl functionalized tricyclic compound **21b**.
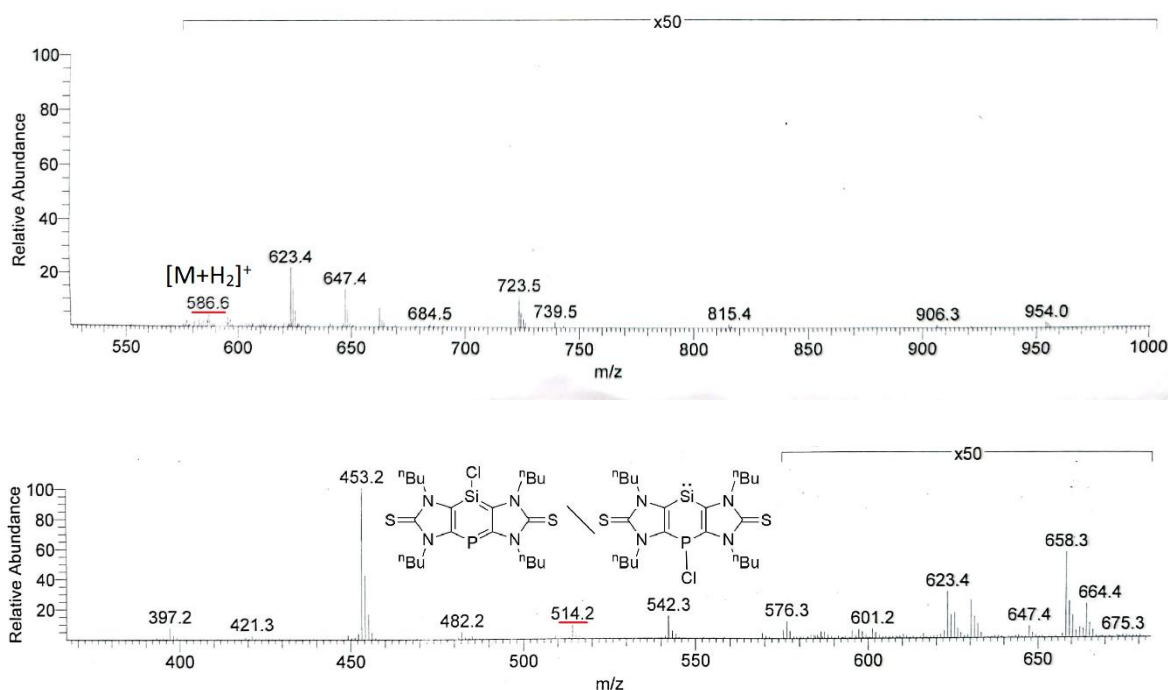
Figure 8.1. EI-MS spectrum of **21b** showing the molecular ion peaks of different fragments (the relative abundances corresponding to the fragments are underlined in red).

8.2 Theoretical studies on 21b and its aromatic counterpart 22b and their reactivity studies

To get further theoretical insight into the bonding and relative energies, NICS(1) calculations were performed by Brehm at the TPSS-D3/def2-TZVP (CPCM$_{THF}$)//B3LYP-D3/def2-TZVPPD level of theory on models wherein the N-^{n}Bu groups are truncated to N-Me (indicated by '). They NICS(1) value of the middle ring of **22b'**, was calculated to be − 9.223 ppm, comparable with that of benzene (− 9.896 ppm) pointing to a very similar aromaticity (Table 8.1). Due to this calculated high aromaticity of **22b** a strong driving force was expected, thus facilitating the reduction of the trichlorinated compound **21b'**. The calculations revealed an elevated aromaticity for the middle ring of **22b'** compared to the reported 1,4-diphosphinine system **XXVI'** with NICS(1) = − 8.146 ppm. Another interesting result was the relative decrease of the NICS(1) value of the hypothetical, monocyclic 1,4-phosphasiline **23**, thus revealing the importance of the two tethered imidazole-2-thiones for the aromatic behavior of this 1,4-phosphasiline.

Table 8.1. NICS(1) values of various benzene analogs calculated at the TPSS-D3/def2-TZVP (CPCM$_{THF}$)//B3LYP-D3/def2-TZVPPD level of theory.

	21b'	22b'	XXVI'		23
NICS(1)	− 0.090	− 9.223	− 8.146	− 9.896	− 7.045

To get a first estimate about reactivity options of **21b**, DFT calculations were performed by Brehm at the TPSS-D3/def2-TZVP (CPCM$_{THF}$)//PW6B95-D3/def2-QZVP(CPCM$_{THF}$) level of theory using the same truncated N-Me model as before. Figure 8.2 signified that the LUMO showed large coefficients at the P and Si centers, and were observed to be slightly delocalized to the neighboring carbon atoms. To be noted is that the LUMO of **21b'** included P–Cl σ* (antibonding) orbital, thus pointing to the possible cleavage of the P– Cl bond upon reduction. On the other hand, the LUMO didn't include any antibonding Si-Cl bond orbitals, pointing to

the uneasiness of reduction conditions involving the Si-Cl bond cleavage. The FMO calculations on **22b'** revealed that both the LUMO and HOMO showed large coefficients at the P and Si centers, without any delocalization on to the neighboring carbon atoms. Interestingly, this pointed to the good π-acceptor as well as donor abilities attributed to these phosphasiline derivatives. Surprisingly, these results showed deviation from the FMO situation of 1,4-diphosphinines **XXVI** and **XXVII** where the HOMOs showed zero contribution at the phosphorus atoms.

LUMO: – 2.3977 eV   LUMO: – 2.0205 eV

HOMO: – 6.1389 eV   HOMO: – 5.9703 eV

21b'   **22b'**
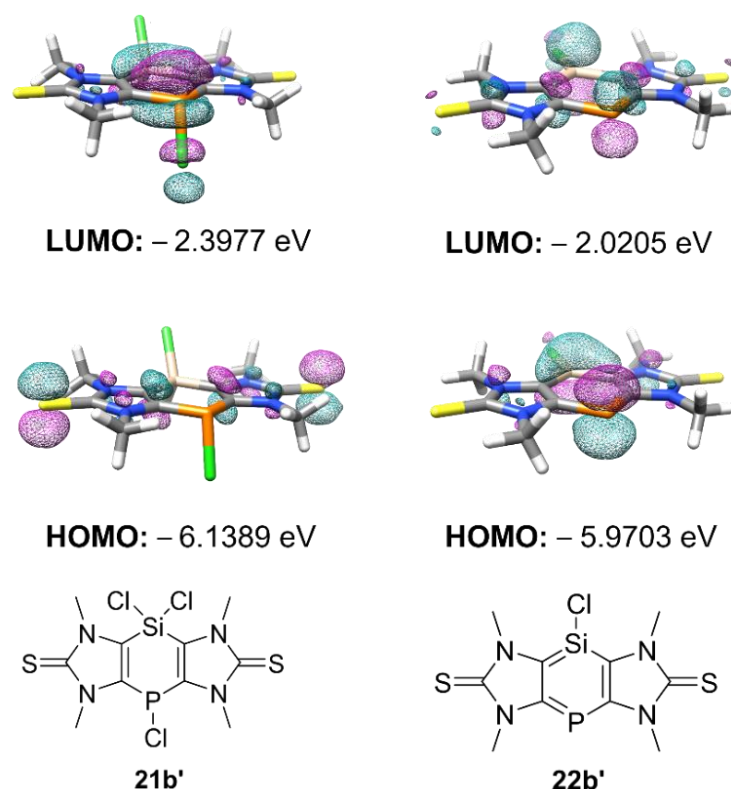
Figure 8.2. Calculated frontier molecular orbitals of the model compounds **21b'** and **22b'**.

Based on the hypothesis of an increased aromaticity to be the driving force for the formation of the 1,4-phosphasiline, initial trials to achieve the selective reduction at Si- and P-centers of **21b** were performed, using stoichiometric amounts of n-Bu$_3$P (Scheme 8.3). Unfortunately, the "pseudo-dimeric" product was formed, resulting from the reductive coupling of two P- centers, but keeping the Si-Cl bonds intact; the latter is corroborated by the FMO data. Figure 8.3 depicts the ^{31}P{^{1}H} NMR spectrum of the reduction reaction of **21b** by n-Bu$_3$P, and the signal at – 53.2 ppm (22%) was assigned to the corresponding "pseudo-dimeric" product

24b. We have seen that the dimeric 1,4-dihydro-1,4-diphosphinine derivative **4a** and the dimeric 1,4-dihydro-1,4-phosphasiline derivative **15b** gave the chemical shifts at $\delta = -50.9$ ppm (in $CDCl_3$) and $\delta = -49.5$ ppm (in $CDCl_3$), respectively, corresponding to their P-P bonds. The products exhibiting signals at $\delta = 52.0$ ppm and $\delta = 46.9$ ppm remained unknown. Surprisingly, no signal corresponding to the chlorophosphonium chloride by-product [n-Bu_3PCl]Cl was observed in the $^{31}P\{^1H\}$ NMR spectrum even when the reaction was performed in DCM. Later on, as a reference, the compound **24b** was generated by the addition of 8 eq. of HCl (in Et_2O) in dichloromethane and extracted via filtration using diethyl ether. The formation of **24b** was supported by ^{31}P and ^1H NMR spectroscopies (Figure 8.4 and 8.5).
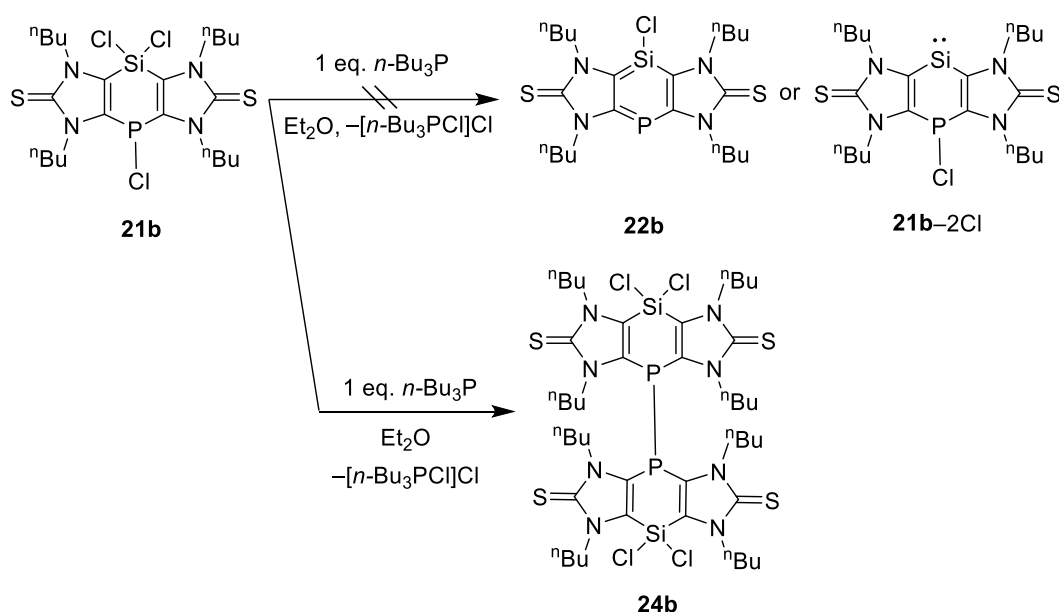
Scheme 8.3. Reduction of **21b** targeting 1,4-phosphasiline **22b** and the outcome, the P-P coupled product **24b**.
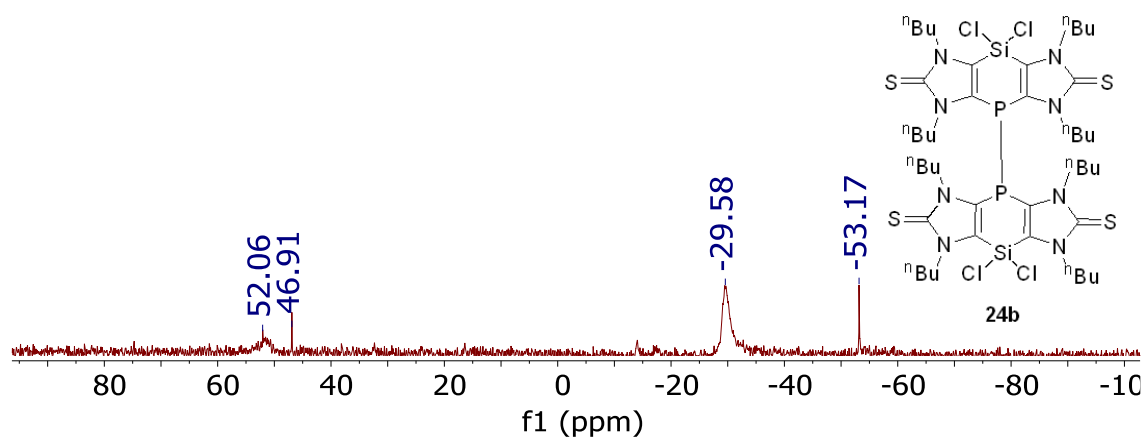
Figure 8.3. $^{31}P\{^1H\}$ NMR spectrum of the reaction mixture of the reduction trial of **21b**.
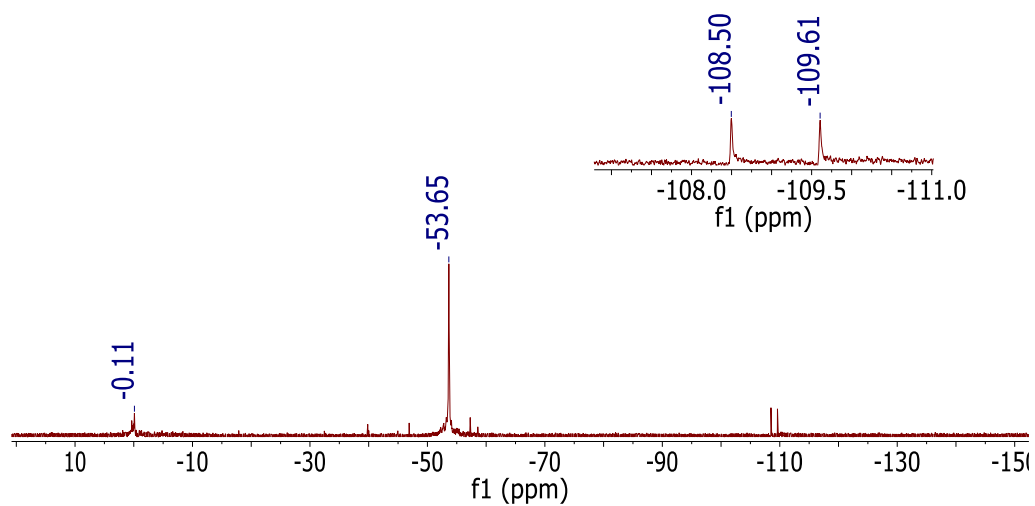
Figure 8.4 . ^{31}P NMR spectrum of the dried filtrate of **24b** in THF-d*8.*
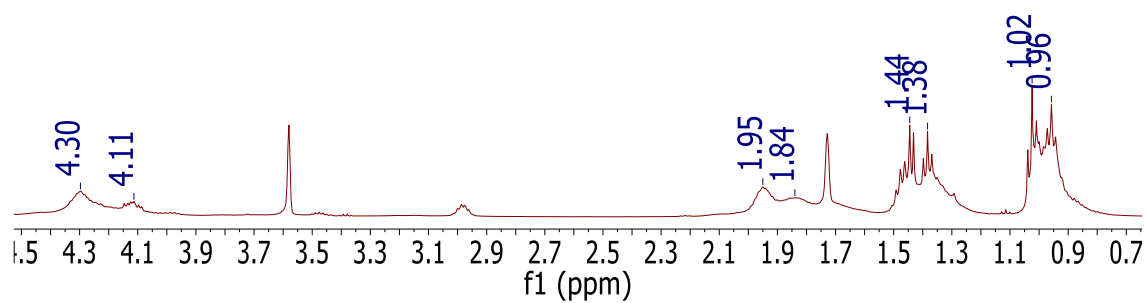
Figure 8.5. ^{1}H NMR spectrum of the dried filtrate of **24b** in THF-d*8.*

9|Summary

In this Ph.D. thesis, investigations on the chemistry of tricyclic, P-anionic 1,4-dihydro-1,4-diphosphinines were carried out, having a special focus on P-centered redox processes which includes detailed voltammetry experiments and simulations as well as theoretical calculations. In addition, first investigations on the synthesis of novel tricyclic 1,4-dihydro-1,4-phosphasiline and -1,4-phosphagermine derivatives and their use in the synthesis of the corresponding aromatic heterocycles were performed. This was accompanied by detailed P- and Si-centered redox chemistry studies, again, being supported by theoretical calculations.

Chapter 3.1 describes the synthesis of the anionic imidazole-2-thione-fused 1,4-dihydro-1,4-diphosphinines **M[2a]–M[2c]** from 1,4-diphosphinine **1** which were isolated as deep blue powders (Scheme 9.1). DFT calculations revealed that the middle rings of **2a'–c'⁻** exhibited lower aromatic character than in neutral 1,4-diphosphinine model, while the aromatic character of the outer rings were calculated to be high. The FMO calculations revealed that the HOMOs showed large coefficients of the anionic phosphorus of the 1,4-dihydro-1,4-diphosphinine central rings, pointing to its nucleophilic character. But only the anionic salt **K[2a]** was taken for the further reactivity studies, due to its superior stability and better solubility compared to **Li[2b]** and **K[2c]**.

M = K, Li
a: R = N(SiMe$_3$)$_2$
b: R = Ni-Pr$_2$
c: R = Ot-Bu
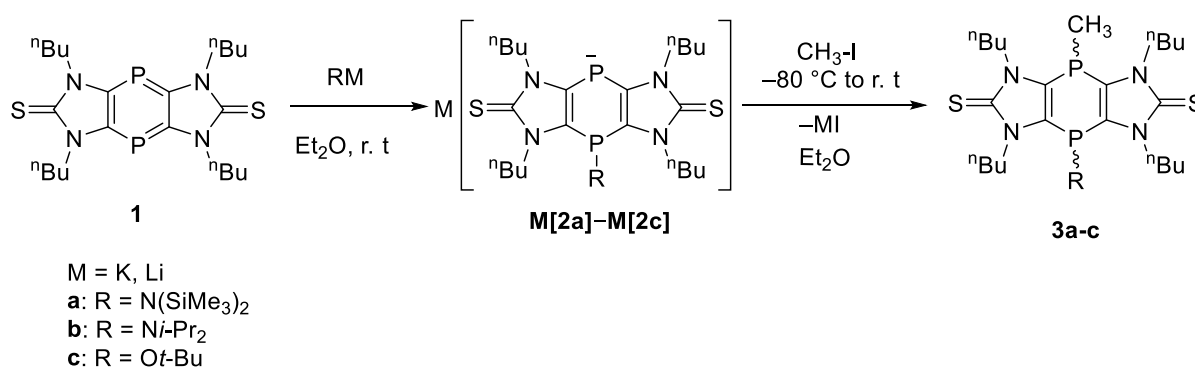
Scheme 9.1. Synthesis of **M[2a]–M[2c]** from 1,4-diphosphinine **1**; reactions of **M[2a]–M[2c]** to give P–methylated products **3a-c**.

The intense blue color of these anions in ethereal solvents and yellow color in acetonitrile were investigated by UV-Vis spectroscopy and TD-DFT calculations. The TD-DFT calculations were in good agreement with UV/vis experiments in CH_3CN but not with the deep blue colors observed in ether solvents which supported the charge transfer bands associated with the formation of contact ion-pairs due to the weaker solvation of K^+ cation by ethers compared to CH_3CN. The small energy difference between the ether-solvated and ion-paired states were additionally supported by the insignificant $^{31}P\{^1H\}$ NMR chemical shifts of crown ether encapsulated anions.

In addition, the synthesis and isolation of the methylated products **3a-c** from the P–anionic salts **M[2a]**–**M[2c]** was described (Scheme 9.1). For **3b-c** mixtures of *cis/trans* isomers were obtained, but for **3a** only the *trans* product was detected in the ^{31}P NMR spectrum; a single crystal X-ray diffraction study confirmed the proposed structure. Despite the small energy difference calculated between the *cis* and *trans* isomers, the selective formation of the *trans* isomer in case of **3a** could have been favored through kinetic control.

In chapter 3.2, the P–P "pseudo-dimeric" compound **4a** was synthesized by one-electron oxidation of **K[2a]** using I_2 in Et_2O, and the product was isolated as orange powder (Scheme 9.2).
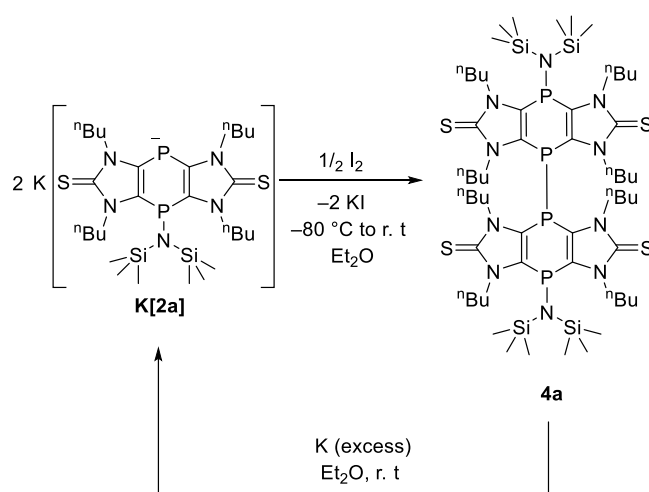
Scheme 9.2. Oxidation of **K[2a]** to **4a** and subsequent reduction.

The transiently formed green color upon I_2 addition was attributed to a short-lived, intermediate radical, supported by TD-DFT calculations, which homocouples in an exergonic

reaction. This is associated with a rapid color change from green to orange. The crystal structure of **4a** revealed a twisted arrangement of the tricyclic parts along the P–P single bond.

In addition, **4a** could be reduced to re-form two equivalents of **K[2a]** in a clean fashion by using potassium. This process was further supported by the FMO calculation which revealed that the LUMOs showed large coefficients on the diphosphane-type phosphorus atoms, thus leading to a P-centered reduction and P-P bond cleavage, finally.

Chapter 3.3 describes the investigation of the redox behavior of the anionic **K[2a]** and its dimeric counterpart **4a**. CV on **K[2a]** clearly showed a chemically irreversible (IRR) oxidation process at E_p^{Ia} = –0.90 V and a similarly chemically irreversible reduction process at E_p^{IIIc} = – 1.63 V (Figure 9.1a, black trace). But, when the initial scan direction was cathodic, no reduction signal was observed on the first cycle (Figure 9.1a, red trace). Thus, it is inferred that the species responsible for E_p^{IIIc} peak appeared to be an electrolysis product of process corresponding to E_p^{Ia}. On the other hand, **4a** showed a large, IRR, reduction peak labelled E_p^{IIIc} was found at –1.80 V and an equally IRR oxidation process labelled E_p^{Ia} occurred at – 1.08 V (Figure 9.1b, black trace), when the initial scan direction was cathodic. Scans started in the anodic direction didn't display E_p^{Ia} in the first cycle (Figure 9.1b, red trace). The repeatability of the CVs was examined by carrying out multicycle experiments and the scan rate dependence study was also carried out for both **K[2a]** and **4a**.
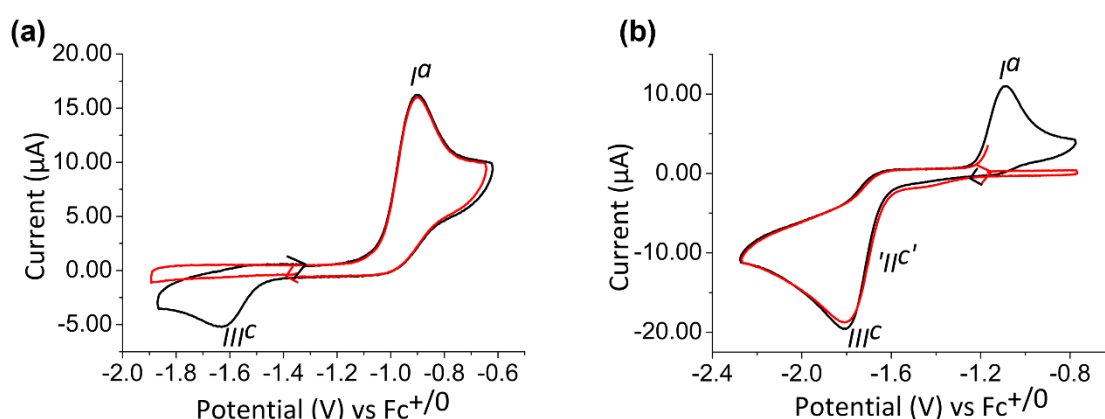
Figure 9.1 (a) Cyclic voltammograms of **K[2a]**; black solid line, anodic initial scan direction; red solid line, cathodic initial scan direction; (b) cyclic voltammograms of **4a**; red solid line, anodic initial scan direction; black solid line, cathodic initial scan direction; (0.1 M [n-Bu$_4$N][PF$_6$]/CH$_3$CN, 200 mV/s).

A plausible mechanism for the electrochemical processes based on the CV results was derived as (E -> Electrochemical step, C -> Chemical step; standard notations)shown in Scheme 9.3.

EI : $2a^- \rightleftharpoons e^- + 2a^{\bullet}$ (fast) k_I°

CI : $2a^{\bullet} + 2a^{\bullet} \underset{k_{-I}}{\overset{k_I}{\rightleftharpoons}} 4a$ (strongly product favoured)

EII : $4a + e^- \rightleftharpoons 4a^{\bullet -}$ (fast) k_{II}°

EIII: $4a^{\bullet -} + e^- \rightleftharpoons 4a^{2-}$ (fast) k_{III}°

CIII: $4a^{2-} \underset{k_{-III}}{\overset{k_{III}}{\rightleftharpoons}} 2a^- + 2a^-$ (strongly product favoured)
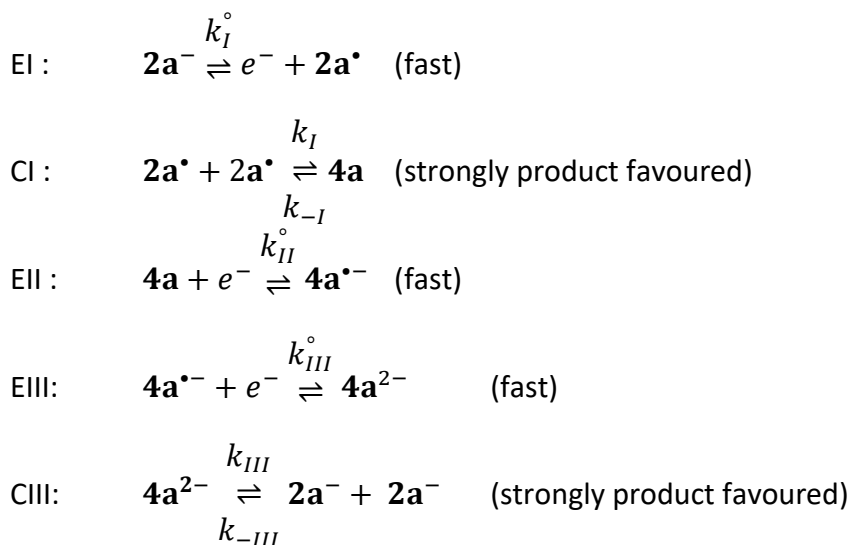
Scheme 9.3. Equations for the CV mechanism proposed for the redox processes.

Process **I** represented the oxidation of **K[2a]** to form **4a** via dimerization of a short-lived P– centered radical species **2a•**. Processes **II** and **III** denoted the reduction of **4a** involving the P– P bond cleavage.

Chapter 4 discusses the synthesis of 4-bis(diorganoamino)silanyl- **9a,b** and 4-bis(diorgano-amino)germanyl-substituted imidazole-2-thiones **10a,b** (Scheme 9.4). These new compounds were successfully isolated and obtained as white powders. The crystal structures of **9a,b** and **10a** showed the typical tetrahedral environments of the Si and Ge atom.
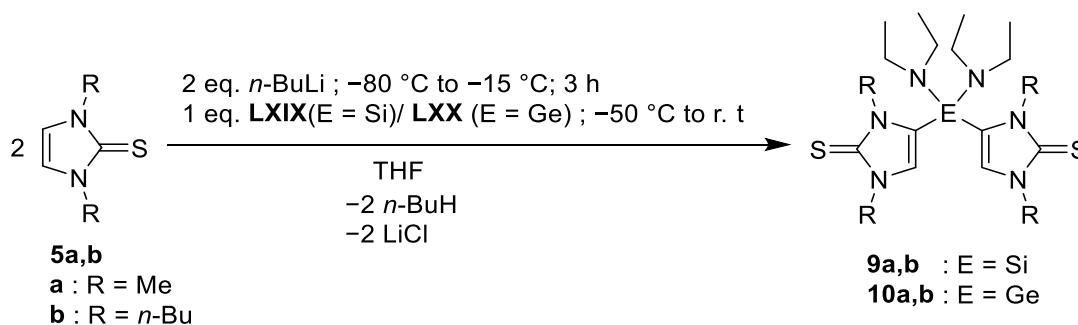
Scheme 9.4. Conversion of **5a,b** to give heteroatom-bridged products **9a,b** and **10a,b.**

In chapter 5, synthesis of the tricyclic 1,4-dihydro-1,4-phosphailines **11a,b** and -phospha-germines **12a** and **13a** were achieved by the backbone-lithiation of **9a,b** and **10a,** respectively,

followed by the addition of different dichlorophosphanes (Scheme 9.5). The products were extracted with toluene and obtained as white powders.
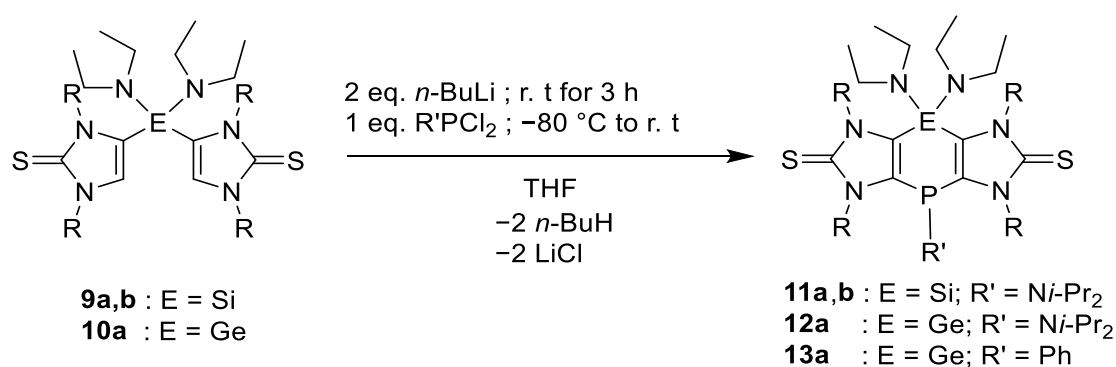
Scheme 9.5. Conversion of **9a,b** to give the tricyclic products **11a,b, 12a** and **13a.**

Crystal structures of **11a,b**, **12a**, and **13a** revealed non-planar middle rings in all cases and the Ge–N and Ge–C bond lengths of **12a** were observed to be elongated compared to **11a,b** (Figure 9.2).
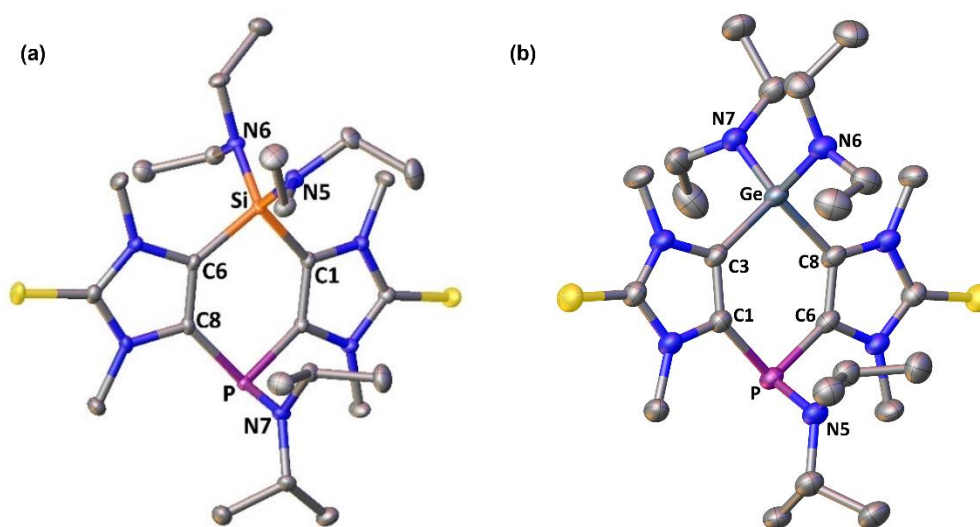
Figure 9.2. Molecular structure of compounds **11a** (a) and **12a** (b); hydrogen atoms are omitted for clarity (50 % probability level).

Chapter 6.1 discusses the selective reduction at the P–center of the tricyclic 1,4-dihydro-1,4-phosphasilines **11b** (Scheme 9.6). The FMO calculations on the model compound **11a'** showed that the LUMO has some P–N σ* character, suggesting the possibility of P–N bond cleavage upon chemical reduction.
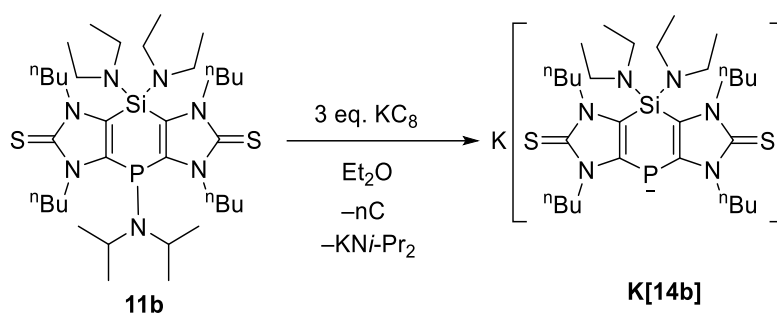
Scheme 9.6. Reductive cleavage of the P–N bond of **11b** to form **K[14b]**.

Accordingly, the P–N bond of **11b** was reductively cleaved in a selective manner using 3 eq. of KC_8, and the formed P-anionic 1,4-dihydro-1,4-phosphasiline salt **K[14b]** was isolated as light-yellow powder. The crystal structure of **K[14b]** revealed its structure as a coordination polymer with each K^+ ion coordinated by five donors via their S centers in the solid state (Figure 9.3).
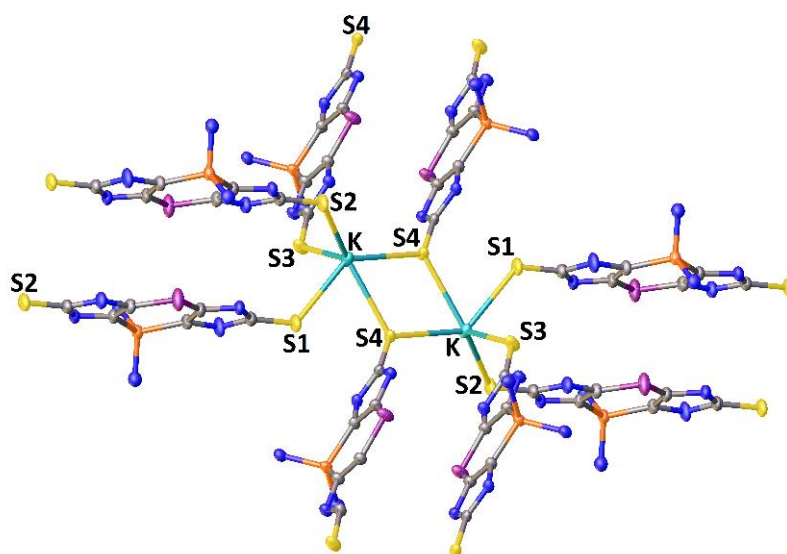
Figure 9.3. Depiction of a cut-out of the polymeric structure, focussing on the full coordination environment at the central K^+ of **K[14b]**; hydrogen atoms are omitted for clarity (50% probability level).

In chapter 6.2, the P–P "pseudo-dimeric" compound **15b** was synthesized via oxidation of **K[14b]** using I_2 in Et_2O and isolated as yellow powder (Scheme 9.7). Here, **15b** could be reduced to form two equivalents of **K[14b]** in a clean fashion with KC_8, similar to **4a.** FMO calculations revealed that the LUMOs showed large coefficients on the diphosphane phosphorus atoms attributing to the reductive cleavage of the P-P bond, again just like in **4a.**
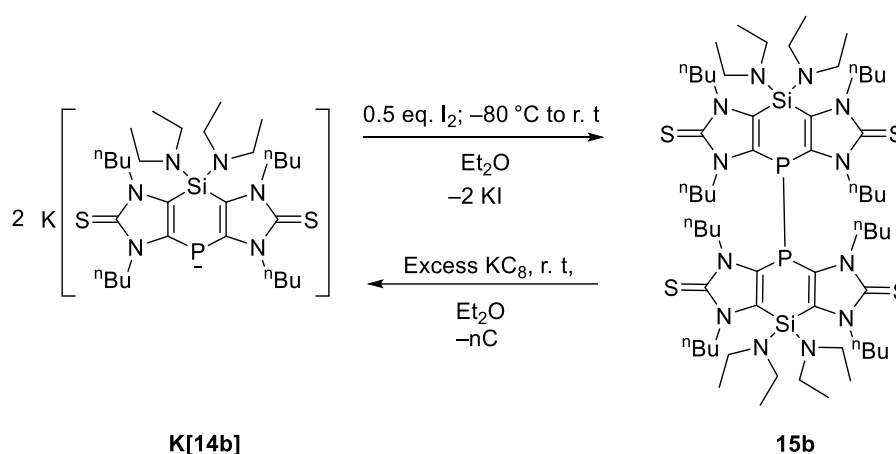
Scheme 9.7. Oxidation of **K[14b]** to give **15b** and the subsequent reduction.

In chapter 6.3, investigation of the redox behavior of both the anionic **K[14b]** and "pseudo-dimeric" **15b** was discussed. CV scans on **K[14b]** showed a chemically irreversible (IRR) oxidation process with E_p^{Ia} = −0.96 V and a similarly IRR reduction process with E_p^{IIIc} = − 1.85 V. But when the initial scan direction was cathodic, the E_p^{IIIc} signal didn't appear on the first cycle (Figure 9.4a). Thus, the species responsible for E_p^{IIIc} appeared to be an electrolysis product of process E_p^{Ia}. When CV scans were performed on **15b**, a large, IRR reduction peak labelled E_p^{IIIc} was found at −2.27 V and an IRR re-oxidation process labelled E_p^{Ia} occurs at −0.9 V (Figure.9.4b), when the initial scan direction was cathodic.
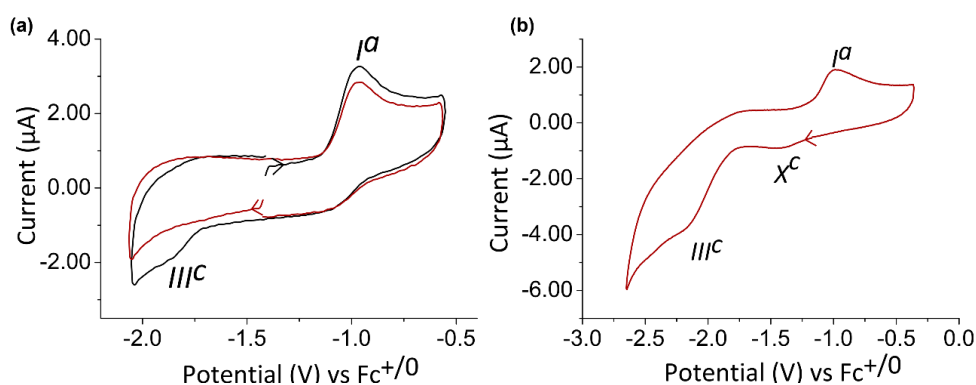
Figure 9.4: (a) Cyclic voltammograms of **K[14b]**; black solid line, anodic initial scan direction; red solid line, cathodic initial scan direction; (0.1 M [n-Bu₄N][PF₆]/CH₃CN, 200 mV/s); (b) cyclic voltammogram of **15b**, starting in the cathodic direction from OCP and showing the second cycle; (0.2 M [n-Bu₄N][PF₆]/THF, 200 mV/s).

The repeatability of the CVs was examined by carrying out multicycle experiments and the scan rate dependence study was also carried out for both **K[14b]** and **15b**. In the case of **15b**,

a small residual signal (labelled X^c in Figure 9.4b) was still visible in the second scan but completely vanished thereafter. Apart from the CV studies, the **K[14b]/15b** interconversion was further proved to be similar to the **K[2a]/4a** interconversion via FMO calculations, including a plausible mechanism.

Chapter 7.1 discusses the conversion of **K[14b]** into its $Si(NR_2)_2$ derivative **16b** by the addition of triphenylmethyl chloride and, subsequently, into its $SiCl_2$-containing derivative **17b** by the addition of an HCl ether solution (Scheme 9.8).
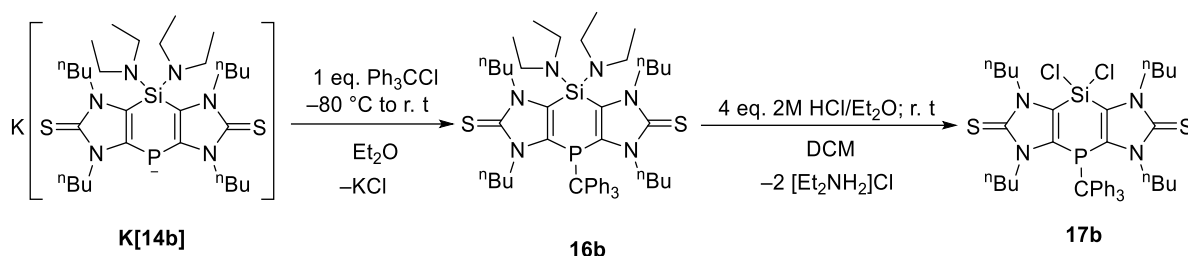
Scheme 9.8. Reaction of **K[14b]** to form the P –trityl derivative **16b** and subsequent conversion of **16b** to form the Si–dichloro compound **17b**.

In chapter 7.2, compound **17b** was reacted with methyllithium and methanol as nucleophiles to form the Si-centered derivatives **18b** and **19b**, respectively (Scheme 9.9).
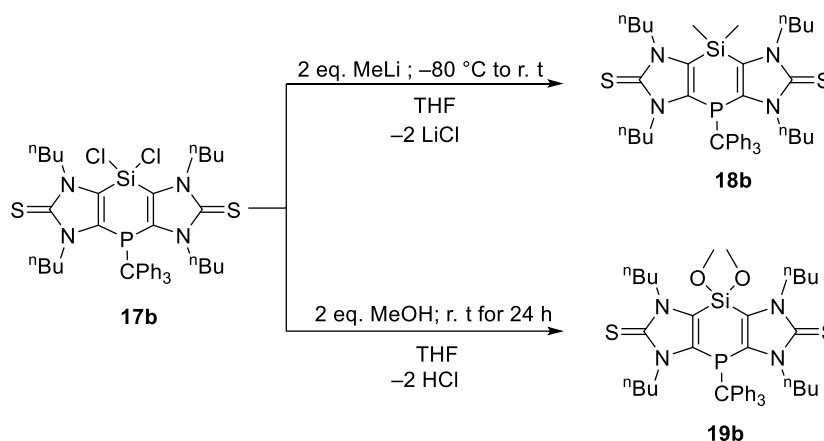
Scheme 9.9. Substitution reactions of **17b** to form **18b** with methyl lithium and **19b** with methanol.

Chapter 7.3 discusses the studies on Si-centered reduction of **17b** which was initially corroborated by the theoretical models in which the LUMO showed a strong contribution of the P–C σ*-orbital, thus suggesting the possible cleavage of the P–C bond upon reduction. On the other hand, the LUMO didn't include any Si–Cl σ*-orbital participation, thus suggesting a relative inertness of the Si– Cl bond towards reductive conditions. Reduction of **17b** with KC_8

at room temperature cleaved the P–C bond and led to the formation of other products (Scheme 9.10). But if the reduction was carried out at lower temperatures, it didn't result in the P–C bond cleavage. Instead, the outcome pointed to a probable C–H activation of the long N–alkyl chains by a transiently formed silylene.
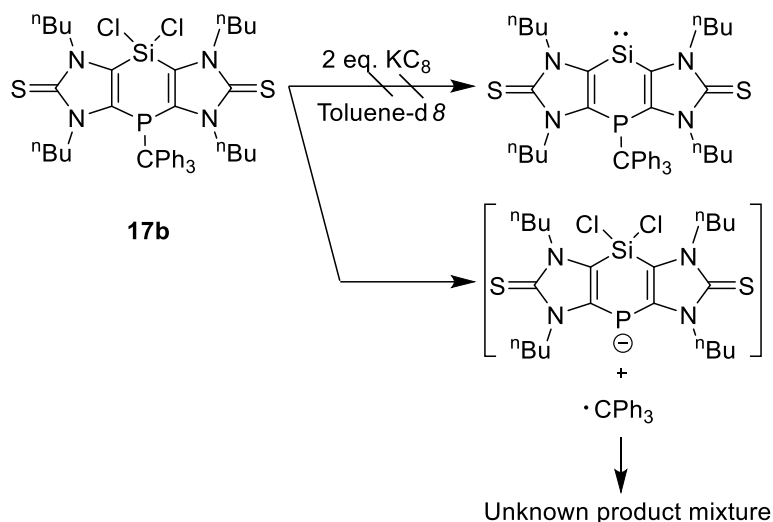
Scheme 9.10. Reduction of compound **17b.**

Trapping reactions of the transient silylene species with 1,3-butadiene led to the formation of the silole compound **20b** (Scheme 9.11) which was mainly characterized by NMR and EI-MS techniques.
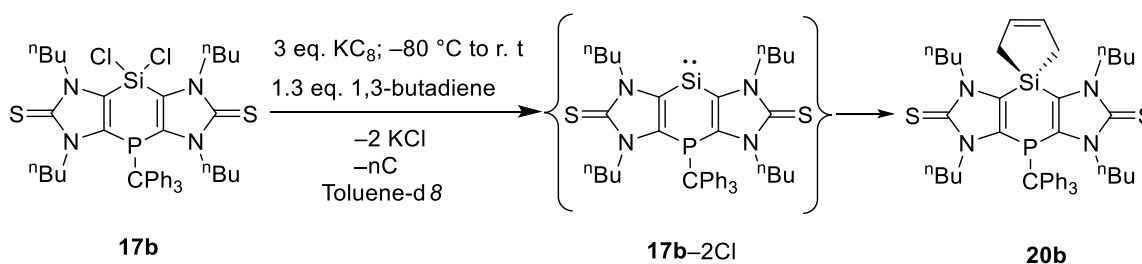
Scheme 9.11. Reduction of compound **17b** and trapping reaction of silylenes **17b**–2Cl to form the silole derivative **20b.**

Chapter 8 discusses the synthesis of the 1,4,4'-trichloro substituted 1,4-dihydro-1,4-phosphasiline **21b** from **11b.** The initial attempts to synthesize the first example of an aromatic 1,4-phosphasiline derivative **22b** from **21b** were met with limited success as the final product could not be isolated (Scheme 9.12). But the molecular ion peak of **22b** was detected under EI-MS conditions (Figure 9.5).
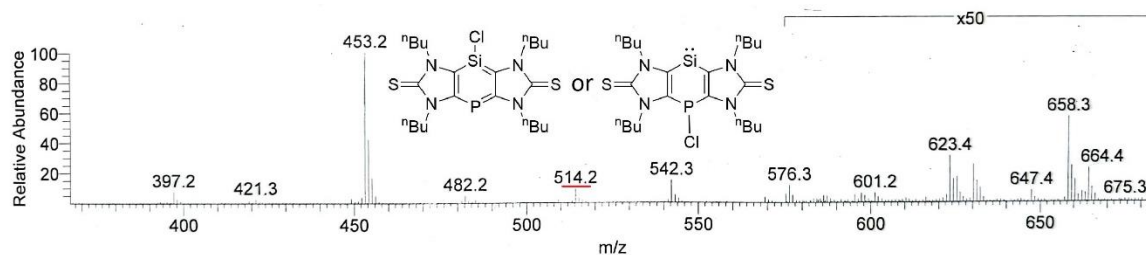
Figure 9.5. EI-MS spectrum of **21b** showing the molecular ion peaks of different fragments (the relative abundances corresponding to the fragments are underlined in red).
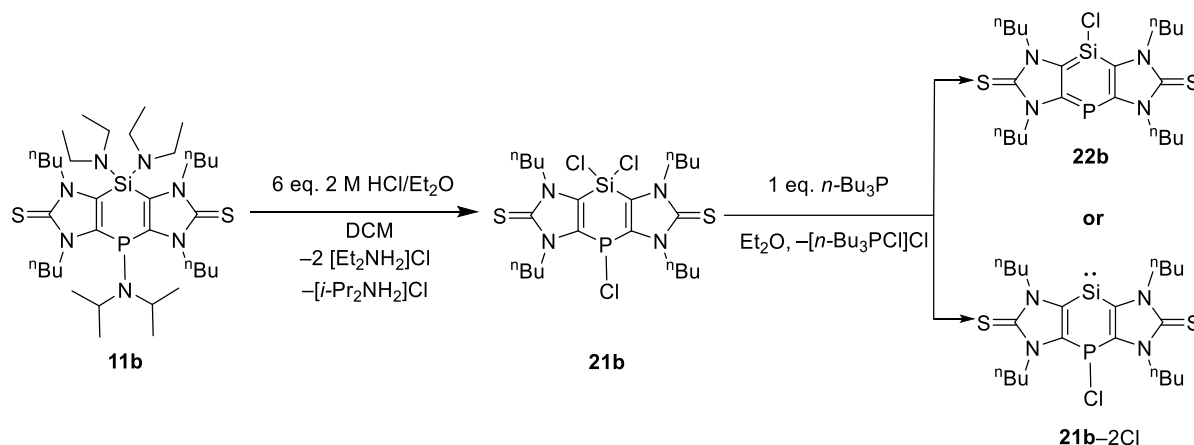
Scheme 9.12. Synthesis of P–Cl and Si–Cl functionalized tricyclic compound **21b** and its reduction attempts.

Theoretical calculations on model compound **21b'** (bearing N-Me groups only) pointed to a possible cleavage of the P–Cl bond upon reduction without affecting the Si–Cl bond supporting the assumption of the formation of a P-P dimer. The NICS(1) calculation of **22b'** pointed to its highly aromatic character as compared to benzene. The FMO calculations on **22b'** revealed that both the LUMO and HOMO showed large coefficients at the P and Si centers, pointing to good π-acceptor as well as donor abilities, thus being in contrast to the FMO situation of tricyclic 1,4-diphosphinines **XXVI** and **XXVII.**

10|Experimental Section

10.1. General techniques

All reactions and manipulations of air and moisture sensitive compounds were carried out under inert gas (argon) atmosphere using standard Schlenk line technique or glovebox. The argon gas was deoxygenated using pre-heated BTS catalyst (BASF PuriStar® R3-15S) at 100–130 °C and dried using phosphorus pentoxide desiccant with indicator (Sicapent®), calcium chloride and silica gel. All air and/or moisture sensitive chemicals were stored in either Schlenk flasks/tubes or J Young® tubes/flasks or handled in the glovebox. Prior to use these Schlenk flasks/tubes or J Young® tubes/flasks were heated with a heat gun (up to 550 °C) under active vacuum (<0.02 mbar) and filled with argon, according to the usage. Solvents were dried and distilled according to standard procedures[167] and were used freshly from distills under argon pressure. In addition, diethyl ether and toluene were dried using a Mbraun SPS-800 solvent purification system. All the glass joints were lubricated with OKS grease type 1112. High-temperature reactions were carried out in an oil bath. In the case of low-temperature reactions, the mixture of ethanol and liquid nitrogen was employed as coolant. For removing the salts formed as reaction by-products in the reaction mixture, common 3G frits having two Schlenk joints, along with an oven-dried (at 100 °C–120 °C) silica gel bed (Merck 60–200) were used. Cannulas with Whatman® glass microfiber filters (GF/B, Ø = 25 mm) connected to one end bound with Teflon band which were dried in oven at 75 °C, were used for filtrations, washings and extractions with pressure gradient of the argon gas. For transferring solvents or clear solutions, stainless steel double-ended cannulas (Ø = 1 mm and 2 mm) were used, which were pre-heated and dried in the oven at 75 °C. Whatman® filter papers were used for filtration purposes under air. All the used glassware was soaked overnight in a KOH/isopropanol bath and then dipped into an HCl-water bath for neutralization purpose After that, cleaned glassware was rinsed with de-ionized water and acetone simultaneously before drying at 110 °C in the oven overnight. The chemical waste

disposal was performed on the basis of the latest "Gefahrstoffverordnung". Organic and inorganic wastes were separated from each other and collected in the designed container before disposing. Other dry chemical wastes along with dried column chromatography wastes were collected together and disposed. All the dangerous and reactive reagent leftovers were destroyed according to the reported protocols.[168] All the waste were submitted to the Department 4.2 "Arbeits- und Umweltschutz" of the University of Bonn for further processing.

10.2. Characterization methods and devices used

10.2.1 Melting point determination

The melting points (or decomposition temperatures) were recorded either on a Büchi 535 Type S melting point apparatus or an SRS DigiMelt device. The samples were placed inside within both-sided closed glass capillary tubes and heated quickly (ca. 5 K/min) for a rough determination of the melting point or decomposition temperature. Then, the heating rates were slowed down to ca. 1 K/min or 2 K/min until the sample is melted or decomposed. Here, no internal or external temperature corrections were performed.

10.2.2. Elemental analysis

The samples for the elemental analyses were prepared in a tin or silver (for halogen containing compounds) boat inside a clean glove box. Elemental analyses were performed using an elementary vario EL analytical gas chromatograph. The mean values of three or four independent measurements are given in each case.

10.2.3. NMR spectroscopy

NMR spectra of all the compounds were recorded on Bruker Avance DMX-300, DPX-300, DPX-400 or DMX-500 spectrometers. The used deuterated solvents were purified via distillation over proper desiccants ($CDCl_3$ and CD_2Cl_2 over CaH_2, and C_6D_6, toluene-$d8$, Et_2O-$d10$ and THF-$d8$ over a potassium mirror). The purified solvents were stored over 3 Å or 4 Å molecular

sieves. The calibration of the ^{1}H and ^{13}C NMR spectra were done according to the solvent residual signals relative to tetramethylsilane (<1 % in CDCl$_3$). ^{31}P NMR spectra were measured relative to 85 % H$_3$PO$_4$ in water as external reference. For ^{29}Si NMR spectra were measured relative to tetraamethylsilane as external reference. The chemical shifts are expressed in parts per million, ppm. Coupling constants are abbreviated as $^nJ_{X,Y}$, where X and Y denote the coupling nuclei (ordered by decreasing atomic number) and n is the number of bonds that separate X and Y. The following abbreviations were used for expression of the multiplicities of the resonance signals: *s* = singlet, *d* = doublet, *t* = triplet, *q* = quartet, *quin* = quintet, *sept* = septet, *m* = multiplet and *br* = broad signal. All the measurements were recorded at 298K unless some specific temperature is given. HSQC, HMBC and DEPT experiments were used for purpose of assigning the ^{1}H NMR, ^{13}C NMR and ^{29}Si NMR signals of all the compounds. All the spectra were analyzed by the program *Mestrenova 14.2.*

10.2.4. Mass spectrometry

Electron ionization mass spectra (70 eV). were recorded on a *Thermo Finnigan* MAT 90 or a *Thermo Finnigan* MAT 95 XL spectrometer. Electrospray Ionization (ESI +/-) mass spectra were recorded in a Thermo Fisher Scientific Orbitrap XL Mass spectrometer .MALDI mass spectra were recorded in a Bruker Daltonik ultrafleXtreme TOF/TOF time-of-flight spectrometer. The peaks were given in mass-to-charge ratio (m/z) while only the isotopomer with the highest relative abundance was depicted/reported. Additionally, the relative intensities of the peaks are given in parentheses and the proposed molecule fragments in square brackets. Only selected data are given for the detected ions (mass to charge ratio, relative intensity in percent).

10.2.5. Single crystal X-ray diffraction studies

Single crystals were grown by evaporation of saturated solutions of the compounds or by diffusion technique. After growing the crystals in sufficient dimensions, the single crystals were separated from the supernatant solution and were covered with Fomblin for avoiding further decomposition. A suitable single crystal was selected under the microscope and

loaded onto the diffractometer. The crystallographic data were collected on Brucker D8-Venture diffractometer, Bruker X8-Kappa Apex II or STOE IPDS 2T diffractometer equipped with a low-temperature device at 100.0 K or 123.0 K using graphite monochromated Mo Kα radiation (λ = 0.71073 Å) or Cu-Kα radiation (λ = 1.54178 Å). The structure was solved with ShelXT 2014/5[169] solution program using iterative methods or ShelXS 97 solution program using direct methods and by using Olex2 1.5-dev[170] as the graphical interface. The model was refined with olex2.refine 1.5-dev[171] or with ShelXL 2018/3[169] using full matrix least squares minimisation on F^2. All non-hydrogen atoms were refined anisotropically, the hydrogen atoms were included isotropically using the riding model on the bound carbon atoms.

10.2.6. UV/vis spectroscopy

UV/vis spectra were obtained from a Shimadzu UV-1650PC spectrometer ($λ_{max}$ range = 200–800 nm) using diethyl ether as the solvent and quartz glass cells (Hellma precision cells 110-QS with dimension 46 mm × 12.5 mm × 12.5 mm, made of Suprasil® quartz, Heraeus, with two polished windows) of optical path 1 cm at room temperature.

10.2.7. Infrared spectroscopy

IR-spectra were recorded from the pure solids on a Nicolet 380 (FT-IR) spectrometer or on a Bruker Alpha Diamond ATR FTIR spectrometer at room temperature inside the glovebox. The following abbreviations were used for expression of the intensities of the absorption bands: *vs* = very strong, *s* = strong, *m* = medium, *w* = weak. All analyses were performed using the programs *EZ OMNIC 7.3* of *Fisher Scientific*, *OPUS* of *Bruker* and *LabSolutions IR 2.26* of *Shimadzu*.

10.2.8. Cyclic Voltammetry

All solution and sample preparations were undertaken in the glove box. Electrolyte solutions for voltammetry were 0.2 M [*n*-Bu₄N][PF₆] in THF and 0.1 M [*n*-Bu₄N][PF₆] in CH₃CN (purchased from Aldrich and dried by heating for 24h at 80°C in *vacuo* ($2.1×10^{-2}$ mbar)).
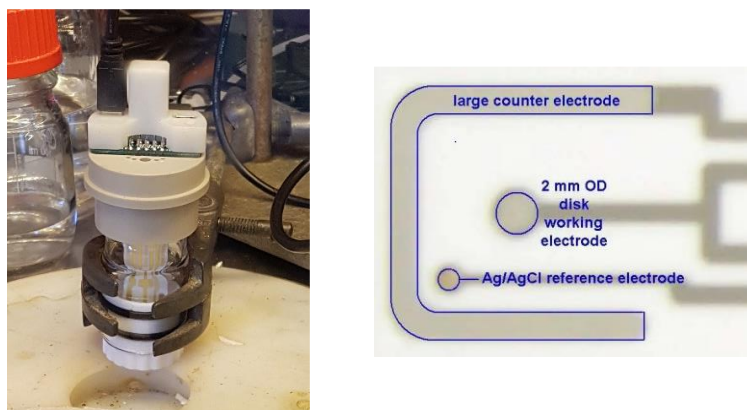
Figure 10.2. (a) Pine microcell with Teflon insert and the electrode connector ready for cable attachment with the attached electrode from Pine Research; (b) Ceramic Patterned Electrodes (CPE). Copyright 2023 Pine Research Instrumentation.

After all measurements were completed, ferrocene ($C_{10}H_{10}Fe$, hereafter designated as Fc) was added to a concentration of 2.0 mM and served as an internal reference using the ferrocene/ferrocenium ($Fc^{+/0}$) redox couple, set to 0 V according to IUPAC recommendations.[172] Voltammograms were obtained using a Pine Instruments, Inc., WaveNano potentiostat/galvanostat connected to platinum (Pt) or gold (Au) screen-printed electrodes on rugged ceramic substrates (Figure 10.2b). The patterned electrodes formed an inner working disk and outer auxiliary ring separated by an Ag/AgCl spot (for further information, consult the website at https://www.pineresearch.com/shop/products/electrodes/screen-printed-electrodes/ceramic/). Experiments were controlled and data were processed using AfterMath software (https://pineresearch.com/shop/kb/knowledge-category/downloads/).

The solvent tetrahydrofuran (THF) was first distilled and further purified by recondensation over potassium mirror, and subsequently stored under argon (Ar) in a controlled-atmosphere glove box. Acetonitrile (CH_3CN) for voltammetry was double-distilled, initially, over CaH_2 and then over P_2O_5 and then, degassed. This was subsequently stored under argon (Ar) in a controlled-atmosphere glove box.

10.2.9. Chemicals used

All the chemicals used during the experiments are listed below with supplier names (Table 10.2.1). All chlorophosphanes, chlorosilanes and chlorogermanes that were commercially purchased, were subjected to further purification by means of fractional distillation.

Table 10.2.1. List of commercially obtained chemicals and their suppliers.

Chemicals	Suppliers
Acetonitrile	Fisher Scientific
Aluminum oxide 90 active neutral (70–230 mesh ASTM)	Merck
Benzene-*d*6	Aldrich
1,3-Butadiene	TCI
n-Butyllithium	Acros
t-butyllithium, 1.6 M in *n*-pentane	Aldrich
t-butyllithium, 1.7 M in *n*-pentane	Aldrich
Chloroform-d	Eurisotop
12-Crown-4	Thermo Scientific
18-Crown-6	Aldrich
Dichlorodimethylsilane	Alfa, Acros
Dichlorodiethoxysilane	Flourchem
Dichloromethane	VWR
Dichlorophenylphosphine	TCI
Diethylamine	Alfa Aesar
Diethylether	VWR
Diethylether-*d*10	Sigma-Aldrich
Diisopropylamine	Acros
Ethanol	Hofmann
Germanium tetrachloride	Alfa Aesar

Hydrogen Chloride solution in diethyl ether	Acros
Iodine	Grüssing
Iodomethane	Merck
Isopropylamine	Sigma Aldrich
Isopropanol	Biesterfeld
Methanol	Sigma-Aldrich
Methyllithium	Sigma-Aldrich
Molecular sieves, 3 Å, 1.7–2.4 mm	Carl Roth
Molecular sieves, 4 Å, 1–2 mm	Alfa Aesar
Potassium metal ()	Riedel de Haen
Potassium bis(trimethylsilyl)amide	Aldrich
Potassium *tert*-butoxide	Alfa Aesar
n-Pentane	VWR
Petrol ether 40/60	Biesterfeld
Phosphorus trichloride	Acros
Silicon tetrachloride	Acros
Silica gel 60 (63–200 mesh)	Merck
Sodium Metal	Riedel de Haen
Sodium hydroxide	Sigma-Aldrich
Sulfur	Acros
Tetrahydrofuran	Fisher Scientific
THF-*d*8	Eurisotop
Tri-*n*-butyl-phosphane	Acros
Triethylamine	Sigma-Aldrich
Triphenylmethyl chloride	Aldrich

Toluene	Fisher Scientific
Toluene-*d*8	Eurisotop

Table 10.2.2. Synthesis/distillation of the starting materials according to literature-described procedures.

Compound	Experimentalist
Bis(diethylamino)chlorophosphane[173]	M.Ram
Dichloro(diethylamino)phosphane[174,175]	M.Ram
Dichloro(diisopropylamino)phosphane[174,175]	M.Ram
Dichlorobis(diethylamino)silane[149]	M.Ram
Dichlorobis(diethylamino)germane[150]	M.Ram
Dichlorodimethylsilane*	R.Kunzmann
Dichlorodiethoxysilane*	R.Kunzmann
1,4-diphosphinine[90]	M.Ram, N. R. Naz
Lithium diisopropylamide[176]	M.Ram
Lithium tetramethylpiperidide[177]	M.Ram
1,3-dibutylimidazole-2-thione[178]	M.Ram
1,3-dimethylimidazole-2-thione[178]	A.Koner
Potassium Graphite[179]	P.Brehm

*Only the distillation of the purchased compound was performed by the corresponding experimentalist.

10.3 General synthetic method for M[2a]–M[2c]

To 1,4-diphosphinine **1** (100 mg, 0. 206 mmol) the nucleophile (each 0.206 mmol) was added (in a Schlenk tube) followed by the addition of 3mL of dry Et_2O under ambient conditions. A rapid color change was observed from red to blueish-violet. The reaction mixture was then stirred for an additional hour at room, the solvent then removed under reduced pressure (3.8 x 10^{-2} mbar) to obtain blue-violet powders. The raw products **M[2a]–M[2c]** were washed with *n*-pentane (3 x 2 mL) to remove other impurities and then dried under reduced pressure for an hour (3.8 x 10^{-2} mbar).

10.3.1 Potassium [1,3,5,7-tetra-*n*-butyl-[2,3-d:5,6-d']bisimidazole-2,6-dithione-4-bis(trimethylsilyl)amino-8-phosphane-1-ide] (K[2a])
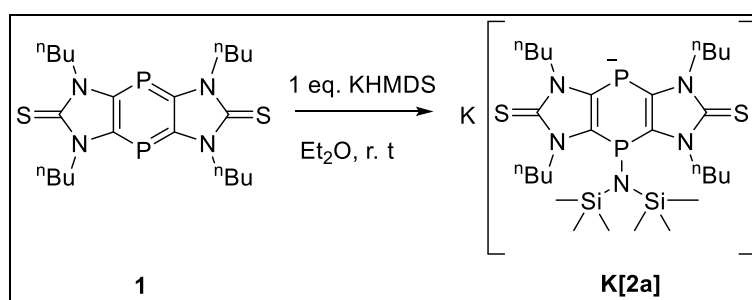
Lab Journal Code (LJC): MR-KHMDS.

NMR Code : MR-KHMDSPHC (13c5a025.19.fid).

Yield : (without coordinated solvent): 78 mg (0.11 mmol, 53 %)   **Appearance :** deep-blue powder

EA (%) (without coordinated solvent, expected chemical formula: $C_{28}H_{54}N_5P_2S_2Si_2K$) exp. C 48.01, H 7.72, N 9.53, S 9.42; Calc. C 49.30, H 7.97, N 10.26, S 9.40.

Neg. ESI-MS : m/z (%) = 499.1 (100) $[C_{22}H_{38}N_5P_2S_2]^+$, 642.2 (15) $[M]^+$.

HRMS : for $C_{28}H_{54}N_5P_2S_2Si_2$ theor./exp. 642.2838/642.2840.

IR: ṽ (cm^{-1}) = 2960 (*w*), 2929 (*w*), 2864 (*w*), 1400 (*w*), 1380 (*s*), 1250 (*m*), 1210 (*m*), 870 (br. *s*).

**^{1}H NMR (300 MHz, Et$_2$O-d10): δ =** −0.3–0.5 (m, 18H, N-Si$\underline{CH_3}$), 0.9–1.0 (m, 1H, $^3J_{H,H}$ = 7.3 Hz, NCH$_2$CH$_2$CH$_2$$\underline{CH_3}$), 1.3–1.5 (m, 8H, NCH$_2CH_2$$\underline{CH_2}$Me), 1.8–1.9 (m, 8H, NCH$_2$$\underline{CH_2}CH_2$Me), 3.7–3.9 (m, 2H, N$\underline{CH_2}CH_2CH_2$Me), 4.0–4.1 (m, 2H, N$\underline{CH_2}CH_2CH_2$Me), 4.2–4.4 (m, 2H, N$\underline{CH_2}CH_2CH_2$Me), 4.5–4.7 (m, 2H, N$\underline{CH_2}CH_2CH_2$Me).

**^{13}C{^{1}H} NMR (75 MHz, Et$_2$O-d10): δ =** 0.3 (br s, N-Si$\underline{CH_3}$), 1.6 (br s, N-Si$\underline{CH_3}$), 20.0 (s, NCH$_2$CH$_2$CH$_2$$\underline{CH_3}$), 20.1 (s, NCH$_2CH_2CH_2$$\underline{CH_3}$), 29.6 (s, NCH$_2CH_2$$\underline{CH_2}$Me), 31.3 (s, NCH$_2CH_2$$\underline{CH_2}$Me), 30.6 (br, NCH$_2$$\underline{CH_2}CH_2$Me), 45.0 (d, $^3J_{P,C}$ = 15.0 Hz, N$\underline{CH_2}$CH$_2$CH$_2$Me), 45.6 (d, $^3J_{P,C}$ = 9.6 Hz, N$\underline{CH_2}$CH$_2$CH$_2$Me), 117.2 (broad s, P-C of the middle ring), 160.9 (s, C=S).

^{31}P{^{1}H} NMR (121.5 Hz, Et$_2$O-d10): δ = −12.1 (s, P-N(SiMe$_3$)$_2$), −77.9 (s, anionic P).

UV/Vis (Et$_2$O): λ$_{max}$ in nm (ε in Lmol^{-1}cm^{-1}) = 517 (ε = 1580), 385 (ε = 650), 327 (ε = 1370).

10.3.2 Lithium [1,3,5,7-tetra-n-butyl-[2,3-d:5,6-d']bisimidazole-2,6-dithione-4-diisopropylamino-8-phosphane-1-ide] (Li[2b])
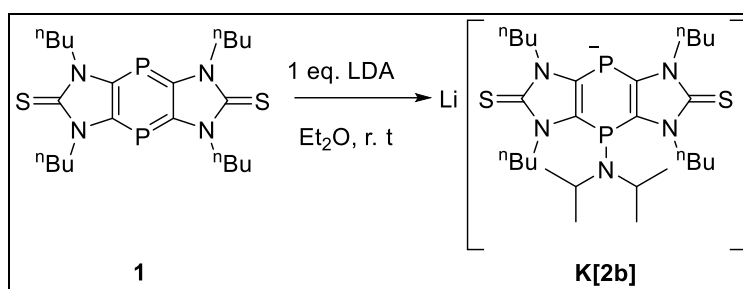
LJC : MR-103ET.

NMR Code : MR- ME103ET (12c5c003.19.11.fid).

Yield : (without coordinated solvent) :   **Appearance :** deep-blue powder 75 mg (0.13 mmol, 63 %)

EA (%) (without coordinated solvent, expected chemical formula : C$_{28}$H$_{50}$N$_5$P$_2$S$_2$Li$_4$): exp. C 54.63, H 7.72, N 10.78, S 10.87; Calc. C 55.08, H 8.25, N 11.47, S 10.50.

Neg-ESI-MS: m/z (%) = 614.287 (90), [M+O$_2$]$^+$, 563.167 (100), [C$_{27}$H$_{43}$N$_5$P$_2$S$_2$]$^+$.

IR: ṽ (cm^{-1}) = 2960 (*w*), 2929 (*w*), 2864 (*w*), 1442 (*m*), 1408 (*s*), 1363 (*m*), 1217 (*s*), 1172 (*w*), 1150 (*w*), 879 (*s*), 770 (*m*), 666 (*w*).

^{1}H NMR (300 MHz, Et$_2$O-d10): δ = 0.9 (t, 12H, $^2J_{H,H}$ = 7.4 Hz, NCH$_2$CH$_2$CH$_2$C$\underline{H_3}$), 1.0 (d, 12H, $^2J_{H,H}$ = 6.1 Hz, N-^iPr, N-CH-(($\underline{CH_3})_2$)), 1.9–2.1 (m, 8H, NCH$_2$CH$_2$C$\underline{H_2}$Me), 2.9–3.1 (m, 2H, N-^iPr, N-C$\underline{H_2}$-Me$_2$), 3.1–3.3 (m, 4H, NCH$_2$C$\underline{H_2}$CH$_2$Me), 3.5–3.7 (m, 4H, NCH$_2$C$\underline{H_2}$CH$_2$Me), 4.1–4.2 (m, 2H, NC$\underline{H_2}$CH$_2$CH$_2$Me), 3.8–4.0 (m, 2H, NC$\underline{H_2}$CH$_2$CH$_2$Me), 4.1–4.4 (m, 2H, NC$\underline{H_2}$CH$_2$CH$_2$Me), 4.6–5.0 (m, 2H, NC$\underline{H_2}$CH$_2$CH$_2$Me).

**^{13}C{^{1}H} NMR (75 MHz, Et$_2$O-d10): δ =** 17.6 (s, NCH$_2$CH$_2$CH$_2$C$\underline{H_3}$), 20.6 (s, N-^iPr, N-CH-(($\underline{CH_3})_2$)), 27.5 (s, NCH$_2$CH$_2$C$\underline{H_2}$Me), 29.0 (s, NCH$_2$C$\underline{H_2}$CH$_2$Me), 42.6 (s, NC$\underline{H_2}$CH$_2$CH$_2$Me), 43.0 (m, N-^iPr, N-C$\underline{H_2}$-Me$_2$), 115.7 (br s, P-C of the middle ring), 156.8 (s, C=S).

^{31}P{^{1}H} NMR (121.5 MHz, Et$_2$O-d10): δ = −30.8 (s, P-Ni-Pr), −78.0 (s, anionic P).

UV/Vis (Et$_2$O): λ$_{max}$ in nm (ε in Lmol^{-1}cm^{-1}) = 517 (ε = 16690), 387 (ε = 5280), 350 (ε = 3540).

10.3.3 Potassium [1,3,5,7-tetra-n-butyl-[2,3-d:5,6-d']bisimidazole-2,6-dithione-4-*tert*-butoxy-8-phosphane-1-ide] (K[2c])
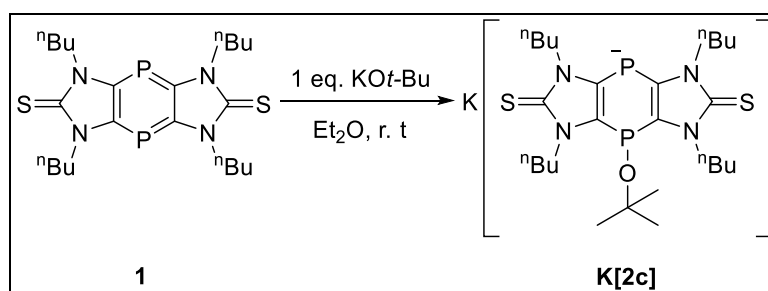
LJC : MR-104.

NMR Code : MR- ME104Et (12c5b042.19.11.fid).

Yield (without coordinated solvent): 78 mg (0.13 mmol, 63 %)　　　　**Appearance :** deep-blue powder

EA (%) (without coordinated solvent, expected chemical formula : C$_{26}$H$_{45}$N$_4$OP$_2$S$_2$K$_2$): exp. C 49.19, H 7.28, N 9.1, S 10.54; Calc. C 49.26, H 7.15, N 8.84, S 10.12.

Neg-ESI-MS: m/z (%) = 500.192 (26), [C$_{22}$H$_{38}$N$_4$OP$_2$S$_2$]$^+$, 499.189 (100), [C$_{22}$H$_{37}$N$_4$OP$_2$S$_2$]$^+$.

IR: ṽ (cm^{-1}) = 2963 (*w*), 2934 (*w*), 2870 (*w*), 1441 (*m*), 1402 (*s*), 1363(*m*), 1291(*w*), 1258 (*w*), 1217 (*m*), 1170 (*w*), 1150 (*w*), 773 (*m*), 669 (*m*), 628 (*w*).

^{1}H NMR(300 MHz, Et$_2$O-*d*10): δ = 1.0 (t, 12H, $^3J_{H,H}$ = 7.4 Hz, NCH$_2$CH$_2$CH$_2$C*H$_3$*), 1.1 (s, 9H, O-C(C*H$_3$*)), 1.3–1.5 (m, 8H, NCH$_2$CH$_2$C*H$_2$*Me), 1.7–1.9 (m, 8H, NCH$_2$C*H$_2$*CH$_2$Me), 4.0–4.2 (m, 4H, NC*H$_2$*CH$_2$CH$_2$Me), 4.2–4.3 (m, 2H, NC*H$_2$*CH$_2$CH$_2$Me), 4.6–4.7 (m, 2H, NC*H$_2$*CH$_2$CH$_2$Me).

^{13}C{^{1}H} NMR (75 MHz, Et$_2$O-*d*10): δ = 20.6 (s, NCH$_2$CH$_2$CH$_2$C*H$_3$*), 20.8 (s, NCH$_2$CH$_2$CH$_2$C*H$_3$*), 29.8 (d, $J_{P,C}$ = 4.1Hz, NCH$_2$CH$_2$C*H$_2$*Me), 30.8 (d, $J_{P,C}$ = 6.8 Hz, NCH$_2$C*H$_2$*CH$_2$Me), 31.5 (m, NCH$_2$C*H$_2$*CH$_2$Me), 46.0 (d, $^3J_{P,C}$ = 10.6 Hz, NC*H$_2$*CH$_2$CH$_2$Me), 46.4 (d, $^3J_{P,C}$ = 14.3 Hz, NC*H$_2$*CH$_2$CH$_2$Me), 74.8 (s, O-*C*(CH$_3$)$_3$), 120.5 (d, $J_{P,C}$ = 4.8 Hz, P-*C* of the middle ring), 120.4 (d, $J_{P,C}$ = 4.6 Hz, P-*C* of the middle ring), 164.2 (br, *C*=S).

^{31}P{^{1}H} NMR (Et$_2$O-*d*10): δ = 18.3 (s, *P*-O-C(CH$_3$)$_3$), −74.1 (s, anionic *P*).

UV/Vis (Et$_2$O): λ$_{max}$ in nm (ε in Lmol^{-1}cm^{-1}) = 517 (ε = 6260), 364 (ε = 4240).

10.4 General synthetic method for 3a–c

1,4-Diphosphinine **1** (100 mg, 0.206 mmol) was taken in a Schlenk tube and the base (KHMDS for **3a**, LDA for **3b** and KO*t*-Bu for **3c**) (0.206 mmol) was added into it followed by the addition of 3mL dry Et$_2$O. A rapid color change was observed from red to bluish violet. Then, the reaction mixture was stirred for an hour at room temperature. Then, the reaction mixture was brought to −80 °C by keeping it in Dewar bath. Then, methyl iodide (13µL, 0.206 mmol) was added into the reaction mixture, dropwise using a micro-syringe. After an hour, color change was observed from blueish violet to bright orange. The color became paler when it was kept for further 4 hours more. After stirring the reaction mixture for overnight at room temperature obtained white turbid solutions, in all the cases from **3a**–**c**. The reaction mixture was filtered through a silica bed to remove the KI/LiI salt and concentrated under reduced pressure (6.3 x 10^{-2}) to get the compound **3a**–**3c** as white powders.

10.4.1 4-Bis(trimethylsilyl)amino-8-methyl-1,3,5,7-tetra-*n*-butyl-4,8-dihydro[1,4]diphosphinine[2,3-d:5,6-d']bisimidazole-2,6-dithione (3a)
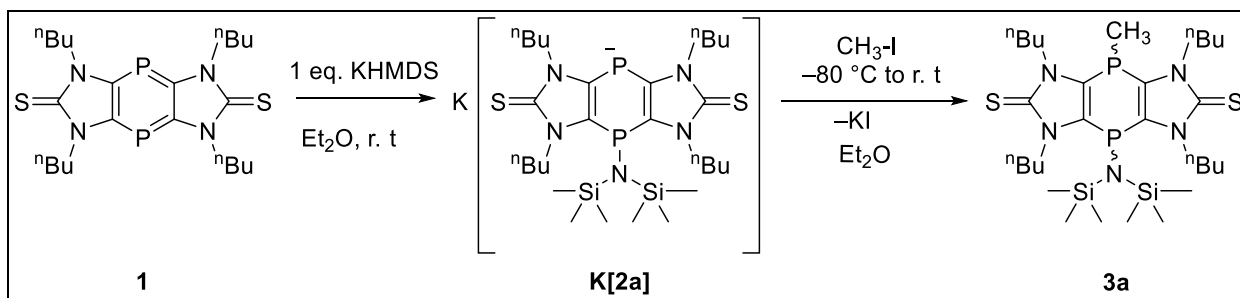
LJC : MR-100.

NMR Code : MR- ME100PH (09t4a020.19.11.fid).

Crystal Structure Identification Code (CSIC) **:** GSTR773, GXray5985f.

Yield : 47.4 mg (0.07 mmol, 35 %)   **Appearance :** white powder   **M.p. :** 139 °C

EA (%): exp. C 52.71, H 8.70, N 10.58, S 9.45. Calc. C 52.93, H 8.73, N 10.64, S 9.74.

EI-MS (70 eV): m/z (%) = 657.0 (25), $[M]^+$,147 (100), $[C_5H_{17}NSi_2]^+$.

HRMS: for $C_{29}H_{57}N_5P_2S_2Si_2$ theor./exp. 657.3069/657.3069.

IR : ṽ (cm^{-1}) = 2956 (*w*), 2929 (*w*), 2861 (*w*), 1437 (*m*), 1402 (*s*), 1253 (*m*), 1217 (*m*), 887 (*s*), 871(*s*), 842 (*s*).

^{1}H NMR(300 MHz, C_6D_6) : δ = −0.2 (s, 9H, N-SiC*H₃*), 0.3 (t, 9H, $^4J_{P,H}$ = 2.7 Hz, N-SiC*H₃*), 0.7 (d, $^3J_{H,H}$ = 5.1 Hz, P-C*H₃*), 0.8 (t, 6H, $^3J_{H,H}$ = 7.3 Hz, NCH₂CH₂CH₂C*H₃*), 0.9 (t, 6H, $^3J_{H,H}$ = 7.5 Hz, NCH₂CH₂CH₂C*H₃*), 1.2–1.4 (m, 8H, NCH₂CH₂C*H₂*Me), 1.8–2.2 (m, 8H, NCH₂C*H₂*CH₂Me), 3.5–3.6 (m, 2H, NC*H₂*CH₂CH₂Me), 3.9–4.0 (m, 2H, NC*H₂*CH₂CH₂Me), 4.6–4.7 (m, 2H, NC*H₂*CH₂CH₂Me), 4.9–5.0 (m, 2H, NC*H₂*CH₂CH₂Me).

^{13}C{^{1}H} NMR (75 MHz, C_6D_6) : δ = 2.9 (s, N-SiC*H₃*), 4.6 (d, $^2J_{P,C}$ = 14.7 Hz, N-SiC*H₃*), 13.4, 13.6 (s, NCH₂CH₂CH₂C*H₃*), 16.3 (dd, $J_{P,C}$ = 18.2 Hz, $J_{P,C}$ = 12.2 Hz, P-C*H₃*), 19.9, 20.2 (s, NCH₂CH₂C*H₂*Me), 30.6 (br, NCH₂C*H₂*CH₂Me), 46.9 (d, $^3J_{P,C}$ = 5.7 Hz, NC*H₂*CH₂CH₂Me), 47.3 (d, $^3J_{P,C}$ = 8.6 Hz, NC*H₂*CH₂CH₂Me), 126.5 (d, $J_{P,C}$ = 1.5 Hz, P-*C* of the middle ring), 128.6 (dd, $J_{P,C}$ = 16.8 Hz , $J_{P,C}$ = 2.8 Hz, P-*C* of the middle ring), 168.5 (br, *C*=S).

^{31}P{^{1}H} NMR (121.5 Hz, C_6D_6) : δ = −4.7 (d, $^3J_{P,P}$ = 16.6 Hz, *P*-N(SiMe₃)₂), −72.3 (d, $^3J_{P,P}$ = 16.6 Hz, *P*-Me).

10.4.2   4-Diisopropylamino-8-methyl-1,3,5,7-tetra-*n*-butyl-4,8-dihydro[1,4] diphosphinine[2,3-d:5,6-d']bisimidazole-2,6-dithione (3b)
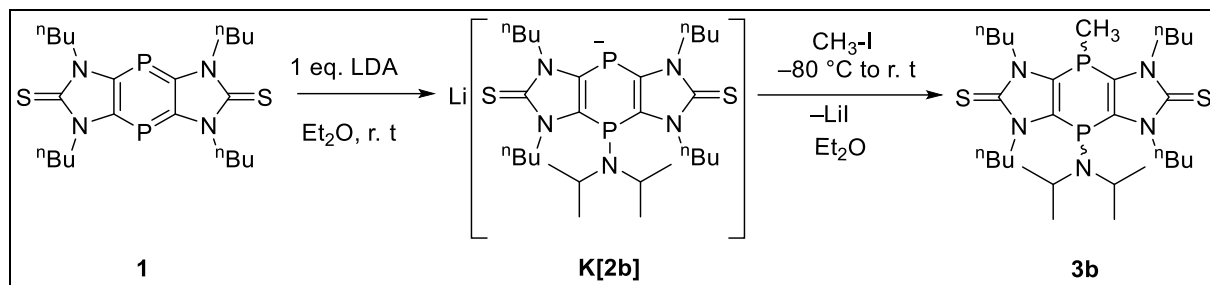
LJC : MR-137.

NMR Code : MR- ME137HCP2 (19m3b001.19.11.fid).

Yield : 49.26 mg (0.08 mmol, 40 %)   **Appearance :** white powder   **M.p. :** 115 °C

EA (%) : exp. C 45.44, H 7.72, N 8.15, S 8.68; Calc. C 58.26, H 8.93, N 11.71, S 10.72.

EI-MS (70 eV): m/z (%) = 597.2 (22), $[M]^+$, 497.1 (100), $[C_{23}H_{39}N_4P_2S_2]^+$.

HRMS: for $C_{27}H_{48}N_4OP_2S_2$ theor./exp. 597.3217/597.3216.

^{1}H NMR(300 MHz, C_6D_6) : δ = 0.8 (m, 12H, NCH$_2$CH$_2$CH$_2$C$\underline{H}_3$), 1.2–1.4 (m, 12H, *N-^{i}Pr*, N-CH-((C$\underline{H}_3$)$_2$), 1.6 (d, $^3J_{H,H}$ = 14.6 Hz, P-C$\underline{H}_3$), 1.7–1.8 (m, 4H, NCH$_2$CH$_2$C$\underline{H}_2$Me), 1.9–2.1 (m, 4H, NCH$_2$CH$_2$C$\underline{H}_2$Me), 3.2–3.3 (m, 2H, *N-^{i}Pr*, N-C$\underline{H}_2$-Me$_2$), 3.9–4.1 (m, 4H, NCH$_2$C$\underline{H}_2$CH$_2$Me), 4.1–4.3 (m, 4H, NCH$_2$C$\underline{H}_2$CH$_2$Me), 4.3–4.4 (m, 4H, NC$\underline{H}_2$CH$_2$CH$_2$Me), 4.6–4.9 (m, 4H, NC$\underline{H}_2$CH$_2$CH$_2$Me).

^{13}C{^{1}H} NMR (75 MHz, C_6D_6) : δ = 13.9 (s, NCH$_2$CH$_2$CH$_2$C$\underline{H}_3$), 14.0 (s, NCH$_2$CH$_2$CH$_2$C$\underline{H}_3$), 20.4 (d, $J_{P,C}$ = 3.1 Hz, *N-^{i}Pr*, N-CH-((C$\underline{H}_3$)$_2$), 30.8 (d, $J_{P,C}$ = 2.2 Hz, NCH$_2$C$\underline{H}_2$CH$_2$Me), 31.0 (s, $J_{P,C}$ = 3.2 Hz, NCH$_2$C$\underline{H}_2$CH$_2$Me), 46.0, 46.1 (s, NC$\underline{H}_2$CH$_2$CH$_2$Me), 46.4 (d, $J_{P,C}$ = 10.2 Hz, *N-^{i}Pr*, N-C$\underline{H}_2$-Me$_2$), 126.8 (d, $J_{P,C}$ = 10.3 Hz, P-*C* of the middle ring), 168.1 (br, *C*=S).

^{31}P{^{1}H} NMR (121.5 Hz, C_6D_6) : δ = −16.8 (d, $^3J_{P,P}$ = 9.1 Hz, *P*- N-^{i}Pr) & −75.9 (d, $^3J_{P,P}$ = 9.1 Hz, *P*-Me) and −19.6 (d, $^3J_{P,P}$ = 11.1 Hz, *P*- N-^{i}Pr) and −69.4 (d, $^3J_{P,P}$ = 11.1 Hz, *P*-Me) *cis* & *trans* isomers (1:3.1).

10.4.3 4-*Tert*-butoxy-8-methyl-1,3,5,7-tetra-*n*-butyl-4,8-dihydro[1,4] diphosphinine-[2,3-d:5,6-d']bisimidazole-2,6-dithione (3c)
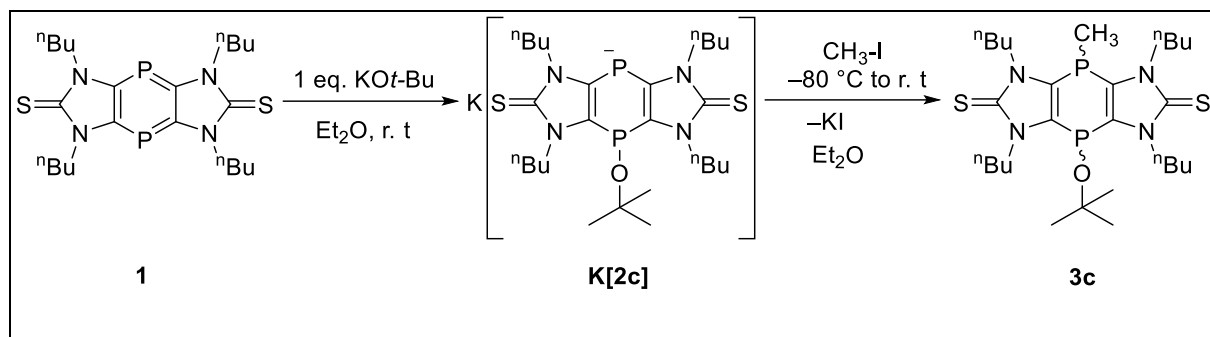
LJC : MR-102.

NMR Code : MR- ME102PHC (09p5a001.19.11.fid).

 Yield : 83.3 mg (0.146 mmol, 71.2 %)   **Appearance :** white powder   **M.p. :** 118 °C

EA (%) : exp. C 56.01, H 8.56, N 9.19, S 10.68; Calc. C 56.81, H 8.47, N 9.81, S 11.23.

EI-MS (70 eV): m/z (%) = 570.2 (82), $[M]^+$, 514.1 (100), $[C_{23}H_{40}N_4OP_2S_2]^+$.

HRMS: for $C_{27}H_{48}N_4OP_2S_2$ theor./exp. 570.2744/570.2745.

IR : ṽ (cm^{-1}) = 2960 (*w*), 2934 (*w*), 2870 (*w*), 1434 (*w*), 1402 (*s*), 1363(*m*), 1253 (*m*), 1217 (*m*), 1160 (*m*), 903 (*s*), 860 (*m*), 800 (*m*).

^{1}H NMR(300 MHz, C$_6$D$_6$) : δ = 0.8–0.9 (m, 12H, NCH$_2$CH$_2$CH$_2$C*H$_3$*), 1.0 (s, 9H, O-C*(CH$_3$)$_3$*), 1.2–1.3 (m, 8H, NCH$_2$CH$_2$C*H$_2*$Me), 1.5 (d, 3H, $^3J_{H,H}$ = 4.9 Hz, P-C*H$_3$*), 1.6–1.7 (m, 2H, NCH$_2$C*H$_2$*CH$_2$Me), 1.8–1.9 (m, 2H, NCH$_2$C*H$_2$*CH$_2$Me), 1.8–1.9 s(m, 4H, NCH$_2$C*H$_2$*CH$_2$Me), 4.1–4.2 (m, 2H, NC*H$_2$*CH$_2$CH$_2$Me), 4.1–4.2 (m, 2H, NC*H$_2$*CH$_2$CH$_2$Me), 4.2–4.3 (m, 2H, NC*H$_2$*CH$_2$CH$_2$Me), 4.7–4.8 (m, 2H, NC*H$_2$*CH$_2$CH$_2$Me).

^{13}C{^{1}H} NMR (75 MHz, C$_6$D$_6$) : δ = 13.9, 14 (s, NCH$_2$CH$_2$CH$_2$C*H$_3$*), 18.2 (dd, $J_{P,C}$ = 11.8 Hz, $J_{P,C}$ = 3.3 Hz, P-C*H$_3$*), 20.3, 20.3 (s, NCH$_2$CH$_2$C*H$_2$*Me), 30.3 (d, $J_{P,C}$ = 7.8 Hz, NCH$_2$C*H$_2$*CH$_2$Me), 31.6 (d, $J_{P,C}$ = 11.3 Hz, NCH$_2$C*H$_2$*CH$_2$Me), 46.7 (t, $^3J_{P,C}$ = 10.2 Hz, NC*H$_2$*CH$_2$CH$_2$Me), 77.6 (d, $J_{P,C}$ = 10.9 Hz, O-*C*(CH$_3$)$_3$), 132.3 (d, $J_{P,C}$ = 5.25 Hz, P-*C* of the middle ring), 133.2 (d, $J_{P,C}$ = 4.0 Hz, P-*C* of the middle ring), 167.2 (br, *C*=S).

^{31}P{^{1}H} NMR (121.5 MHz, C$_6$D$_6$) : δ = 25.6 (d, $^3J_{P,P}$ = 7.2 Hz, *P*-O-^{t}Bu) and −79.6 (d, $^3J_{P,P}$ = 7.2 Hz, *P*-Me) and 26.5 (d, $^3J_{P,P}$ = 13.4 Hz, *P*-O-^{t}Bu) & −69.4 (d, $^3J_{P,P}$ = 13.4 Hz, *P*-Me) *cis* & *trans* isomers (1:4.1).

10.5 P-P coupled product 4a

1,4-Diphosphinine **1** (100 mg, 0.206 mmol) was taken in a Schlenk tube and KHMDS (42 mg, 0.206 mmol) was added into it followed by the addition of 10 mL dry Et$_2$O. A rapid color change was observed from red to bluish violet. Then, the reaction mixture was stirred for an hour at room temperature. The reaction mixture was brought to −90 °C by keeping it in Dewar bath. I$_2$ (25.5 mg, 0.103 mmol) was dissolved in 2.5 mL diethyl ether and added drop wise into the reaction mixture. A transient deep green coloration was formed which gradually turned to reddish brown. After stirring for 1 hour, the reaction mixture turned bright orange and the solvent was removed *in vacuo* (3.8 x 10^{-2}). The residue was re-dissolved in n-pentane and filtered out via a cannula to remove the potassium iodide salt formed in course of the reaction. Solvent was removed *in vacuo* (5.3 x 10^{-2}) to obtain a bright orange powder **4a**.
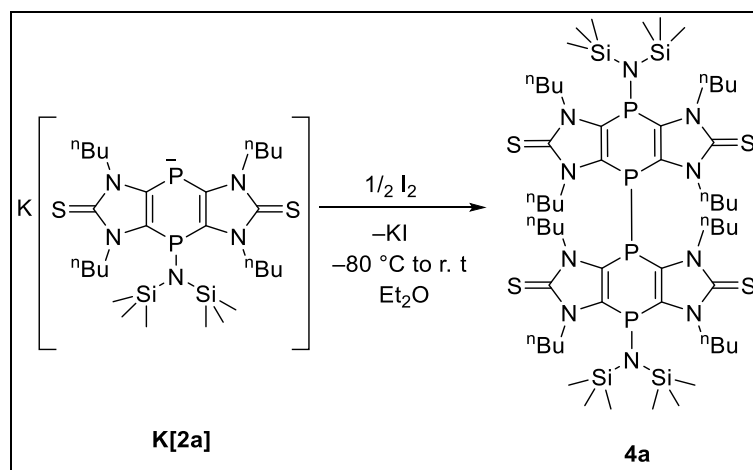
LJC : MR-501P3.

NMR Code : MR- 501P3-B (16m3b012.21.10.fid).

CSIC : GSTR684, GXray6128f.

Yield : 111 mg (0.0863 mmol, 42 %)   **Appearance :** orange powder   **M.p. :** 165 °C

EA (%) : exp. C 51.02, H 8.29, N 9.74, S 9.26; Calc. C 52.30, H 8.46, N 10.89, S 9.97.

EI-MS (70 eV): m/z (%) = 1284.2 (40) $[M]^+$, 642.1 (100) $[C_{28}H_{55}N_5P_2S_2Si_2]^+$, 482.1 (40) $[C_{22}H_{36}N_4P_2S_2]^+$.

IR : ṽ (cm^{-1}) = 2956 (*w*), 2930 (*w*), 2861 (*w*), 1436 (*m*), 1397 (*s*), 1257 (*m*), 1216 (*m*), 796 (*w*), 680 (*w*).

^{1}H NMR(300MHz, CDCl$_3$) : δ = −0.3 (s, 18H, N(Si(C*H$_3$*)$_3$)$_2$), 0.4 (d, 18H, $^4J_{P,H}$ = 2.1 Hz, N(Si(C*H$_3$*)$_3$)$_2$), 0.9 (d, 12H, $^3J_{H,H}$ = 21 Hz, NCH$_2$CH$_2$CH$_2$C*H$_3$*), 1.1 (t, 12H, $^3J_{H,H}$ = 21 Hz, NCH$_2$CH$_2$CH$_2$*CH$_3$*), 1.2–1.4 (m, 8H, NCH$_2$CH$_2$C*H$_2$*Me), 1.4–1.5 (m, 8H, NCH$_2$CH$_2$*CH$_2$*Me), 1.7–1.8 (m, 8H, NCH$_2$*CH$_2$*CH$_2$Me), 1.9–2.1 (m, 8H, NCH$_2$C*H$_2$*CH$_2$Me), 3.0–3.1 (m, 4H, NC*H$_2$*CH$_2$CH$_2$Me), 3.8–4.0 (m, 4H, NC*H$_2$*CH$_2$CH$_2$Me), 4.3–4.5 (m, 8H, NC*H$_2$*CH$_2$CH$_2$Me).

^{13}C{^{1}H} NMR (75MHz, CDCl$_3$) : δ = 3.4 (s, N-Si*CH$_3$*), 4.7 (d, $^2J_{P,C}$ = 15.7 Hz, N-Si*CH$_3$*), 13.8 (s, NCH$_2$CH$_2$CH$_2$*CH$_3$*), 13.9 (s, NCH$_2$CH$_2$CH$_2$*CH$_3$*), 20.2 (s, NCH$_2$CH$_2$*CH$_2$*Me), 20.5 (s, NCH$_2$CH$_2$*CH$_2$*Me), 30.6 (s, NCH$_2$*CH$_2$*CH$_2$Me), 30.7 (s, NCH$_2$*CH$_2$*CH$_2$Me), 47.3 (t, $^3J_{P,C}$ = 4.8 Hz, N*CH$_2$*CH$_2$CH$_2$Me), 47.7 (*br*. t, N*CH$_2$*CH$_2$CH$_2$Me), 134.8 (*br*. s, P-*C* of the middle ring), 135.2 (br.s, P-*C* of the middle ring), 167.7 (s, *C*=S).

^{31}P{^{1}H} NMR (121.5 MHz, CDCl$_3$) : δ = −0.3 (t, $^3J_{P,P}$ = 25.6 Hz, *P*-N(TMS)$_2$), −50.9 (d, $^3J_{P,P}$ = 25.6 Hz, *P*-P).

UV/Vis (Et$_2$O): λ$_{max}$ in nm (ε in Lmol^{-1}cm^{-1}) = 440 (ε = 9210).

10.6 General synthetic method for 9a,b and 10a,b

In 50 mL Schlenk flasks imidazole-2-thiones **5a** (100 mg, 0. 78 mmol) and **5b** (100 mg, 0. 47 mmol) were dissolved in 2 mL THF, cooled to −80 °C and then *n*-BuLi (0.532 mL, 0.86 mmol for **5a** & 0.324 mL, 0.518 mmol for **5b**) added while stirring. The reaction mixtures were slowly warmed to −15 °C and kept stirring for 3 h at this temperature. The reaction mixtures were again cooled to −50 °C and dichloro(dimethyl)silane (0.05 mL, 0.39 mmol for **5a**), bis(diethyl-amino)dichlorosilane (0.092 mL, 0.39 mmol for **5a** & 0.055 mL, 0.235 mmol for **5b**)/ bis(diethylamino)dichlorogermane (0.11 mL, 0.39 mmol for **5a** & 0.065 mL, 0.235 mmol for

5b) was added dropwise and the reaction mixtures then stirred for 12 hours while warming to ambient temperature. The solvent was then removed under reduced pressure (2.5×10^{-2} mbar), the residues re-dissolved in toluene and then filtered using a filter cannula to remove the lithium chloride salt. The filtrates were collected and the solvent removed under reduced pressure (3.8×10^{-3} mbar). The raw products **8a**, **9a,b** and **10a,b** were washed with *n*-pentane (3 x 5 mL) to remove other impurities and then dried under reduced pressure for an hour (1.2×10^{-2} mbar) to obtain white powders.

10.6.1 Bis(1,3-dimethylimidazole-2-thione-4-yl)dimethylsilane (8a)
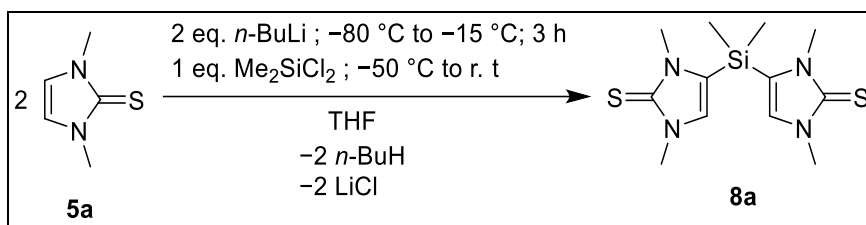
LJC : MR-155.

NMR Code : MR-155HSi (22m3b008.19.10.fid).

Yield : 78.2 mg (0.18 mmol, 47 %)   **Appearance :** white powder

EI-MS (70 eV): m/z (%) = 312.0 (100), $[M]^+$.

^{1}H NMR (300 MHz, CDCl$_3$): δ = 0.5 (s, 6H, *Si*-(*CH$_3$*)$_2$), 3.5 and 3.6 (s, 12H, *N*-*CH$_3$*), 6.7 (s, 2H, C^5-*H*).

^{13}C{^{1}H} NMR (75 MHz, CDCl$_3$): δ = −0.8 (s, Si-(*CH$_3$*)$_2$), 35.3 (s, *N*-*CH$_3$*), 117.6 (s, C^5), 124.3, 127.6 (s, C^4), 166.7 (s, *C*=S).

^{29}Si{^{1}H} dept20 NMR (60 Hz, CDCl$_3$): δ = −24.9 (s, *Si*-(CH$_3$)$_2$).

10.6.2 Bis(1,3-dimethylimidazole-2-thione-4-yl)bis(diethylamino)silane (9a)
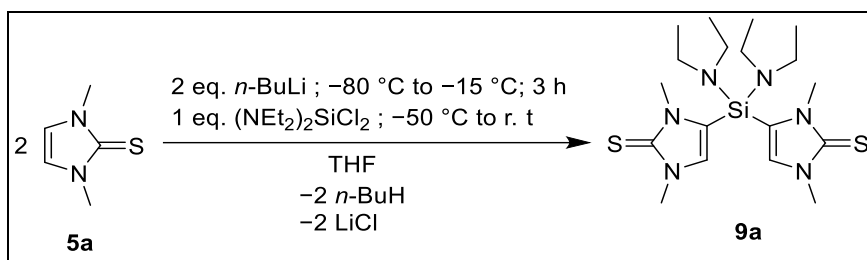
LJC : MR-301.

NMR Code : MR-301HC (04m3a027.20.10.fid).

CSIC : GSTR702, GXray6356.

Yield : 156.4 mg (0.36 mmol, 94 %)   **Appearance :** white powder   **M.p. :** 190 °C

EA (%): exp. C 48.78, H 7.02, N 19.81, S 18.81. Calc. C 50.66, H 8.03, N 19.69, S 15.03.

FTMS+pos-ESI : m/z (%) = 427.214 (100), [M+H]$^+$, 395.242 (45), [C$_{18}$H$_{35}$N$_6$SSi]$^+$.

HRMS: for C$_{18}$H$_{35}$N$_6$S$_2$Si theor./exp. 427.2133/427.2128.

IR: ṽ (cm^{-1}) = 2973 (*w*), 2480 (*w*), 1467 (*m*), 1389 (*s*), 1159 (*s*), 1024 (*s*), 791 (*s*), 732 (*s*), 662 (*s*).

^{1}H NMR (300 MHz, CDCl$_3$): δ = 1.0 (t, 12H, $^3J_{H,H}$ = 7.0 Hz, *Si-(*N-CH$_2$-*CH$_3$*)$_2$), 2.9 (q, 8H, $^3J_{H,H}$ = 7.0 Hz, *Si-(*N-*CH$_2$*-CH$_3$)$_2$), 3.6 (s, 12H, *N*-*CH$_3$*), 6.6 (s, 2H, C^5-*H*).

^{13}C{^{1}H} NMR (75 MHz, CDCl$_3$): δ = 13.8 (s, Si-(N-CH$_2$-*CH$_3$*)$_2$), 35.1 (s, Si-(N-*CH$_2$*-CH$_3$)$_2$), 35.9 (s, Si-(N-*CH$_2$*-CH$_3$)$_2$), 38.2 (s, *N*-*CH$_3$*), 117.2 (s, *C^5*), 124.7, 128.4 (s, *C^4*), 165.9 (s, *C*=S).

^{29}Si{^{1}H} dept20 NMR (60 Hz, CDCl$_3$) : δ = −38.8 (s, *Si-(*N-CH$_2$-CH$_3$)$_2$)).

10.6.3 Bis(1,3-di-*n*-butylimidazole-2-thione-4-yl)bis(diethylamino)silane (9b)
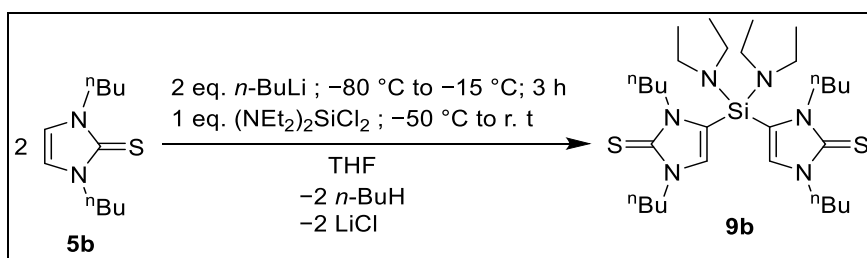
LJC : MR-575.

NMR Code: MR-575 (10s7a023.22.10.fid).

CSIC: GSTR699, GXray6332_matrixa.

Yield : 62.7 mg (0.105 mmol, 45 %)   **Appearance :** white powder   **M.p. :** 132 °C

EA (%): exp. C 58.05, H 9.71, N 13.23, S 9.97. Calc. C 60.55, H 9.82, N 14.12, S 10.78.

EI-MS (70 eV): m/z (%) = 594.4 (5) $[M]^+$, 456.4 (92) $[C_{23}H_{50}N_5SSi]^+$, 427.3 (76) $[C_{21}H_{45}N_5SSi]^+$.

HRMS: for $C_{30}H_{58}N_6S_2Si$ theor./exp. 594.3933/594.3944.

IR: ṽ (cm^{-1}) = 2945 (*m*), 1545 (*w*), 1448 (*m*), 1410 (*m*), 1321 (*m*), 1202 (*s*), 1167 (*s*), 1108 (*s*), 1027 (*s*), 940 (*m*), 797 (*m*), 697 (*m*).

^{1}H NMR (300 MHz, CDCl₃): δ = 0.8 (t, 6H, $^3J_{H,H}$ = 7.5 Hz, NCH₂CH₂CH₂C*H₃*), 0.9 (t, 6H, $^3J_{H,H}$ = 7.3 Hz, NCH₂CH₂CH₂C*H₃*), 1.0 (t, 12H, $^3J_{H,H}$ = 7.0 Hz, Si-*(N-CH₂-C*H₃*)₂*), 1.1–1.2 (m, 4H, NCH₂CH₂C*H₂*Me), 1.3–1.4 (m, 4H, NCH₂CH₂C*H₂*Me), 1.5–1.6 (m, 4H, NCH₂C*H₂*CH₂Me), 1.7–1.8 (m, 4H, NCH₂C*H₂*CH₂Me), 2.9 (q, 8H, $^3J_{H,H}$ = 7.0 Hz, Si-*(N-C*H₂*-CH₃)₂*), 3.8 (t, 4H, $^3J_{H,H}$ = 8.1 Hz , NC*H₂*CH₂CH₂Me), 4.1 (t, 4H, $^3J_{H,H}$ = 7.5 Hz , NC*H₂*CH₂CH₂Me), 6.8 (s, 2H, C^5-*H*).

^{13}C{^{1}H} NMR (75 MHz, CDCl₃) : δ = 13.6 (d, ^3J = 6.4 Hz*,* Si-*(*N-CH₂-C*H₃*)₂), 13.8 (s, NCH₂CH₂CH₂*Me*), 19.9 (s, NCH₂CH₂C*H₂*Me), 20.2 (s, NCH₂CH₂C*H₂*Me), 29.6 (s, NCH₂C*H₂*CH₂Me), 30.9 (s, NCH₂C*H₂*CH₂Me), 38.2 (s, Si-*(N-C*H₂*-CH₃)₂*), 47.6 (s, NC*H₂*CH₂CH₂Me), 48.7 (s, NC*H₂*CH₂CH₂Me), 116.5 (s, C^5), 124.4, 126.9 (s, C^4), 165.0 (s, *C=S*).

^{29}Si{^{1}H} dept20 NMR (60 Hz, CDCl₃) : δ = −37.8 (s, *Si-(*N-CH₂-CH₃)₂)).

10.6.4 Bis(1,3-dimethylimidazole-2-thione-4-yl)bis(diethylamino)germane (10a)
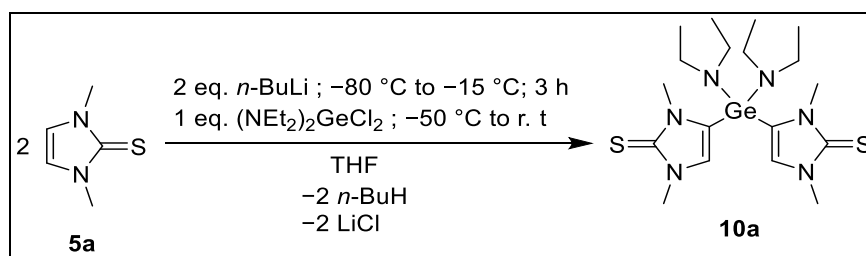
LJC : MR-391.

NMR Code : MR-391-full (MRI230117p5a022.10.fid).

CSIC : GSTR799, GXray7148.

Yield : 150.5 mg (0.32 mmol, 82 %)   **Appearance :** white powder   **M.p. :** 124 °C

EA (%): exp. C 45.13, H 6.66, N 17.55, S 14.04. Calc. C 45.88, H 7.27, N 17.83, S 13.61.

EI-MS (70 eV): m/z (%) = 472.1 (90), [M]$^+$, 400.1 (90), [C$_{14}$H$_{24}$N$_5$S$_2$Ge]$^+$, 328.0 (100), [C$_{10}$H$_{14}$N$_4$S$_2$Ge]$^+$.

HRMS: for C$_{18}$H$_{34}$GeN$_6$S$_2$ theor./exp. 468.1529/468.1524.

IR: ṽ (cm^{-1}) = 2965 (*w*), 1442 (*m*), 1383 (*s*), 1182 (*s*), 1155 (*s*), 898 (*m*), 779 (*s*), 622 (*s*).

^{1}H NMR(500 MHz, CDCl$_3$): δ = 0.9 (*br*.t, 12H, Ge-*(N-CH$_2$-CH$_3$)$_2$), 2.9 (*br*.q, 8H, Ge-*(N-CH$_2$-CH$_3$)$_2$), 3.55 (*br*.d, 12H, N-CH$_3$), 6.7 (*br*.s, 2H, C^5-H).

^{13}C{^{1}H} NMR (125 MHz, CDCl$_3$): δ = 15.1 (s, Ge-(N-CH$_2$-CH$_3$)$_2$), 35.4 (s, Ge-(N-CH$_2$-CH$_3$)$_2$), 35.9 (s, Ge-(N-CH$_2$-CH$_3$)$_2$), 41.1 (s, N-CH$_3$), 117.5 (s, C^5), 123.8, 126.8 (s, C^4), 166.1 (s, C=S).

10.6.5 Bis(1,3-di-*n*-butylimidazole-2-thione-4-yl)bis(diethylamino)germane (10b)
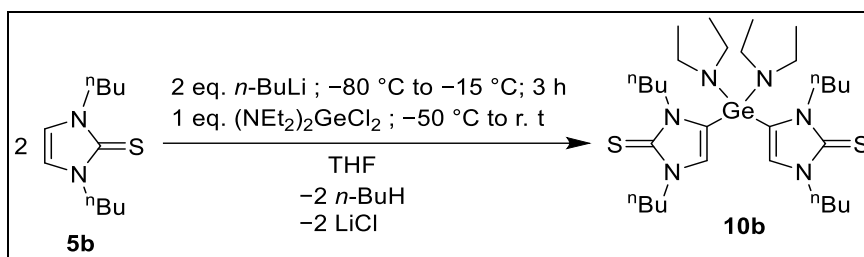
LJC : MR-384.

NMR Code : MR-384HC (28p5a018.20.10.fid).

Yield : 80 mg (0.124 mmol, 53 %)   **Appearance :** white powder   **M.p. :** 148 °C

EI-MS (70 eV): m/z (%) = 640.1 (20), [M]$^+$, 568.1 (30), [C$_{26}$H$_{48}$GeN$_5$S$_2$]$^+$, 496.2 (30), [C$_{22}$H$_{38}$GeN$_4$S$_2$]$^+$.

HRMS: for C$_{30}$H$_{58}$GeN$_6$S$_2$ theor./exp. 636.3407/636.3402.

IR : ṽ (cm^{-1}) = 2961 (*w*), 1417 (*w*), 1262 (*s*), 1091 (*s*), 1016 (*s*), 799 (*s*).

¹H NMR (500 MHz, CDCl₃): δ = 0.8 (t, 6H, $^3J_{H,H}$ = 7.5 Hz, NCH₂CH₂CH₂C*H₃*), 0.9 (t, 6H, $^3J_{H,H}$ = 7.3 Hz, NCH₂CH₂CH₂C*H₃*), 1.0 (t, 12H, $^3J_{H,H}$ = 7.0 Hz, Ge-*(*N-CH₂-C*H₃*)₂), 1.1–1.2 (m, 4H, NCH₂CH₂C*H₂*Me), 1.3–1.4 (m, 4H, NCH₂CH₂C*H₂*Me), 1.4–1.5 (m, 4H, NCH₂C*H₂*CH₂Me), 1.7–1.8 (m, 4H, NCH₂C*H₂*CH₂Me), 2.9 (q, 8H, $^3J_{H,H}$ = 7.0 Hz, Ge-*(*N-C*H₂*-CH₃)₂), 3.9 (t, 4H, $^3J_{H,H}$ = 8.1 Hz , NC*H₂*CH₂CH₂Me), 4.0 (t, 4H, $^3J_{H,H}$ = 7.5 Hz , NC*H₂*CH₂CH₂Me), 6.8 (s, 2H, C⁵-*H*).

¹³C{¹H} NMR (125 MHz, CDCl₃): δ = 13.8 (s, Ge-*(*N-CH₂-C*H₃*)₂), 15.2 (s, NCH₂CH₂CH₂C*H₃*), 20.0 (s, NCH₂CH₂C*H₂*Me), 20.2 (s, NCH₂CH₂C*H₂*Me), 30.2 (s, NCH₂C*H₂*CH₂Me), 31.0 (s, NCH₂C*H₂*CH₂Me), 41.4 (s, Ge-(N-C*H₂*-CH₃)₂), 47.9 (s, NC*H₂*CH₂CH₂Me), 48.6 (s, NC*H₂*CH₂CH₂Me), 123.1 (s, *C*⁵), 125.5 (s, *C*⁴), 165.2 (s, *C*=S).

10.7 General synthetic method for 11a,b, 12a and 13a

Si-bridged derivatives **9a** (100 mg, 0. 234 mmol), **9b** (100 mg, 0. 168 mmol) and Ge-bridged derivative **10a** (100 mg, 0. 212 mmol) were taken in 50 mL Schlenk flasks, each dissolved in THF, and *n*-BuLi (0.32 mL, 0.516 mmol for **9a,** 0.23 mL, 0.37 mmol for **9b** and 0.29 mL, 0.466 mmol for **10a**) was added on stirring at room temperature. The reaction mixtures were stirred for 4 h at this temperature. The reaction mixtures were cooled down to −80 °C and phosphanes (diisopropyl(dichloro)phosphane : 0.04 mL, 0.234 mmol for **9a** , 0.03 mL, 0.168 mmol for **9b** and diisopropyl(dichloro)phosphane : 0.038 mL, 0.212 mmol for **10a**, dichloro(phenyl)phosphane : 0.028 mL, 0.212 mmol for **10a**) were added dropwise into the reaction mixture. The reaction mixture was then stirred for 12 hours while warming to ambient temperatures. The solvent was then removed under reduced pressure (1.7 x 10⁻² mbar) , residue were re-dissolved in toluene and filtered using a filter cannula to remove the lithium chloride salt. The filtrates were collected and the solvent removed under reduced pressure (1.4 x 10⁻² mbar). The raw products **11a,b, 12a** and **13a** were washed with *n*-pentane (3 x 5 mL) to remove other impurities and then dried under reduced pressure for an hour (1.5 x 10⁻² mbar) to obtain white powders.

10.7.1   4-Bis(diisopropylamino)-8-diethylylamino-1,3,5,7-tetramethyl-4,8-hydro[1,4]phosphasiline[2,3 -d:5,6-d']bisimidazole-2,6-dithione (11a)
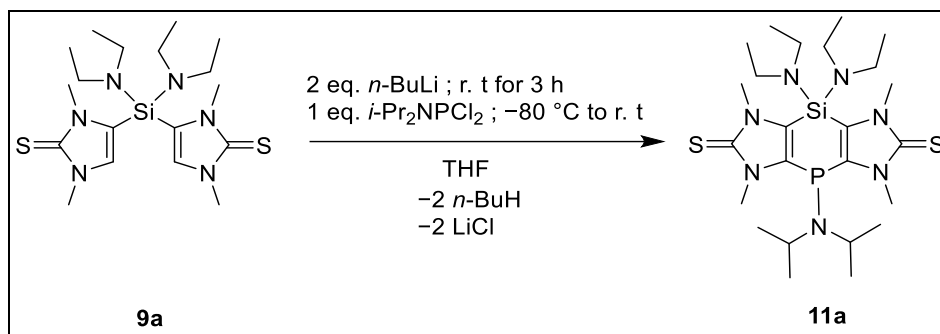
LJC : MR-424.

NMR Code : MR-424F3 (35m3a016.20.fid).

CSIC : GSTR706, GXray6417f.

Yield : 52 mg (0.093 mmol, 40 %)   **Appearance :** white powder   **M.p. :** 195 °C

EA(%) : exp. C 51.24, H 8.06, N 16.21, S 10.28. Calc. C 51.86, H 8.34, N 17.64, S 11.54

EI-MS (70 eV): m/z (%) = 555.3 (54) [M]$^+$, 455.2 (64) [C$_{18}$H$_{32}$N$_6$PS$_2$Si]$^+$, 384.1 (100)[C$_{14}$H$_{23}$N$_5$PS$_2$Si]$^{+\bullet}$.

HRMS: for C$_{24}$H$_{46}$N$_7$PS$_2$Si theor./exp. 555.2763/555.2757.

IR : ṽ (cm^{-1}) = 2973 (*w*), 1423 (*w*), 1378 (*s*), 1159 (*s*), 1024 (*s*), 837 (*s*).

^{1}H NMR(300 MHz, CDCl$_3$) : δ = 0.9 (t, 6H, $^3J_{H,H}$ = 7.0 Hz, *Si-*(N-CH$_2$-<u>CH$_3$</u>)$_2$), 1.0 (t, 6H, $^3J_{H,H}$ = 7.0 Hz, *Si-*(N-CH$_2$-<u>CH$_3$</u>)$_2$), 1.1-1.2 (m, 12H, *N-^{i}Pr,* N-CH-(<u>(CH$_3$)$_2$</u>), 2.8 (q, 4H, $^3J_{H,H}$ = 7.0 Hz, Si-(N-<u>CH$_2$</u>-CH$_3$)$_2$), 2.9 (q, 4H, $^3J_{H,H}$ = 7.0 Hz, Si-*(*N-<u>CH$_2$</u>-CH$_3$)$_2$), 3.3–3.5 (m, 2H, *N-^{i}Pr,* N-<u>CH$_2$</u>-Me$_2$), 3.7 (s, 6H, *N-*<u>CH$_3$</u>), 3.8 (s, 6H, *N-*<u>CH$_3$</u>).

^{13}C{^{1}H} NMR (75 MHz, CDCl$_3$) : δ = 13.3 (s, *Si-*(N-CH$_2$-<u>CH$_3$</u>)$_2$), 13.7 (s, *Si-(*N-CH$_2$-<u>CH$_3$</u>)$_2$), 34.7 (s, *N-^{i}Pr,* N-CH-(<u>(CH$_3$)$_2$</u>), 34.8 (s, *N-^{i}Pr,* N-CH-(<u>(CH$_3$)$_2$</u>), 35.5 (s, *Si-*(N-<u>CH$_2$</u>-CH$_3$)$_2$), 37.2 (s, *N-^{i}Pr,* N-<u>CH</u>-Me$_2$), 37.4 (s, *N-*<u>CH$_3$</u>), 38.4 (s, *N-*<u>CH$_3$</u>), 131.0 (s, C^5), 134.3 (s, C^4), 167.2 (s, *C*=S).

^{31}P{^{1}H} NMR (121.5 Hz, CDCl$_3$) : δ = −17.0.

^{29}Si{^{1}H} dept20 NMR (60 Hz, CDCl$_3$) : δ = −42.1 (s, <u>*Si*</u>-(N-CH$_2$-CH$_3$)$_2$)).

10.7.2   4-Bis(diisopropylamino)-8-diethylylamino-1,3,5,7-tetra-*n*-butyl-4,8-hydro[1,4]phosphasiline[2,3 -d:5,6-d']bisimidazole-2,6-dithione (11b)
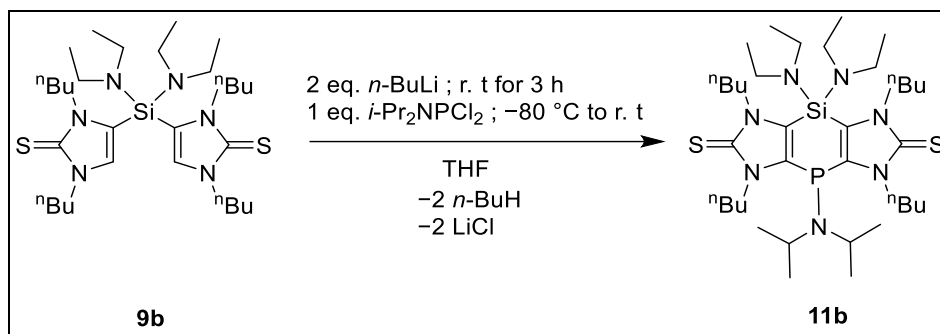
LJC : MR-422-P4.

NMR Code : MR-422-P4-F (41t4b038.21.10.fid).

CSIC : GSTR733, GXray6695.

Yield : 63.2 mg (0.08 mmol, 52 %)   **Appearance :** white powder   **M.p. :** 175 °C

EA(%): exp. C 57.99, H 9.34, N 13.02, S 8.71. Calc. C 59.71, H 9.74, N 13.54, S 8.86.

EI-MS (70 eV): m/z (%) = 724.4 (100) $[M]^+$, 595.4 (46) $[C_{28}H_{52}N_6PS_2Si]^{+\bullet}$.

HRMS: for $C_{36}H_{70}N_7PS_2Si$ theor./exp. 723.4641/723.4633.

IR : ṽ (cm^{-1}) = 3016 (*m*), 2930 (*w*), 1729 (*m*), 1694 (*m*), 943 (*m*), 835 (*s*), 794 (*s*), 842 (*s*), 703 (*s*), 651 (*s*).

^{1}H NMR (300 MHz, CDCl₃) : δ = 0.8 (t, 6H, $^3J_{H,H}$ = 6.9 Hz, NCH₂CH₂CH₂C*H₃*), 0.9 (t, 6H, $^3J_{H,H}$ = 7.4 Hz, NCH₂CH₂CH₂C*H₃*), 0.9 (t, 12H, $^3J_{H,H}$ = 7.3 Hz, *Si*-(N-CH₂-C*H₃*)₂), 1.0 (t, 6H, $^3J_{H,H}$ = 7.0 Hz, Si-*(*N-CH₂-C*H₃*)₂), 1.1 (d, 12H, $^3J_{H,H}$ = 6.8 Hz, N-^{i}*Pr*, N-CH-((C*H₃*)₂), 1.3 (m, 8H, NCH₂CH₂C*H₂*Me), 1.7 (m, 2H, NCH₂C*H₂*CH₂Me), 1.8 (m, 4H, NCH₂C*H₂*CH₂Me), 1.9 (m, 2H, NCH₂C*H₂*CH₂Me), 2.7 (q, 8H, $^3J_{H,H}$ = 7.0 Hz, Si-*(*N-C*H₂*-CH₃)₂), 3.0 (q, 8H, $^3J_{H,H}$ = 7.0 Hz, Si-*(*N-C*H₂*-CH₃)₂), 3.5 (m, N-^{i}*Pr*, N-C*H*-Me₂), 4.0 (m, 6H, NC*H₂*CH₂CH₂Me), 4.1 (m, 6H, NC*H₂*CH₂CH₂Me), 4.5 (m, 2H, NC*H₂*CH₂CH₂Me).

^{13}C{^{1}H} NMR (75 MHz, CDCl₃) : δ = 13.3 (d, ^3J = 3.7 Hz, *Si*-(N-CH₂-C*H₃*)₂), 13.9 (d, ^3J = 3.0 Hz, NCH₂CH₂CH₂C*H₃*), 20.0 (s, NCH₂CH₂C*H₂*Me), 20.4 (s, NCH₂CH₂C*H₂*Me), 30.2 (s, N-^{i}*Pr*, N-CH-((C*H₃*)₂), 30.6 (d, ^3J = 3.5 Hz, NCH₂C*H₂*CH₂Me), 37.5 (s, *Si*-(N-C*H₂*-CH₃)₂), 38.1 (s, *Si*-(N-C*H₂*-CH₃)₂), 46.2 (d, ^3J = 9.7 Hz, *N*-^{i}*Pr*, N-C*H*-Me₂), 48.8 (s, NC*H₂*CH₂CH₂Me), 130.2 (s, C^5), 134.4 (s, C^4), 166.3 (s, *C*=S).

^{31}P{^{1}H} NMR (121.5 Hz, CDCl$_3$) : δ = −12.2.

^{29}Si{^{1}H} dept20 NMR (60 Hz, CDCl$_3$) : δ = −42.4 (s, $\underline{Si}$-(N-CH$_2$-CH$_3$)$_2$)).

10.7.3 4-Bis(diisopropylamino)-8-diethylylamino-1,3,5,7-tetramethyl-4,8-hydro[1,4]phosphagermine [2,3 -d:5,6-d']bisimidazole-2,6-dithione (12a)
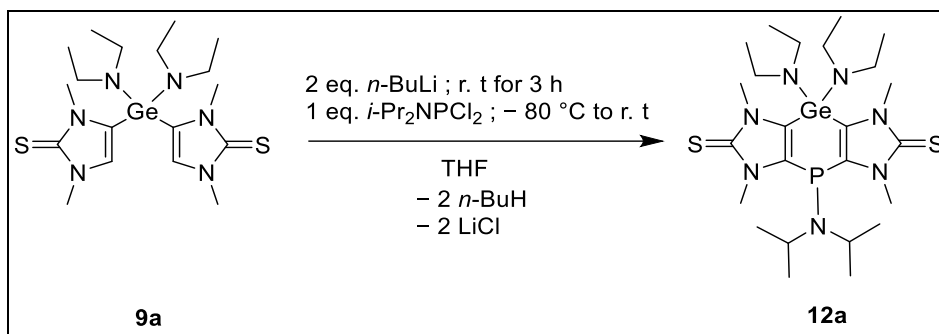
LJC : MR-425.

NMR Code : MR-425-full (41p5a024.22.12.fid).

CSIC : GSTR800, GXray7152.

Yield : 60 mg (0.1 mmol, 48 %) **Appearance :** white powder **M.p. :** 143 °C

EA(%) : exp. C 45.98, H 7.21, N 14.65, S 9.43. Calc. C 48.01, H 7.72, N 16.33, S 10.68.

EI-MS (70 eV): m/z (%) = 601.2 (100) [M]$^+$, 430.1 (90) [C$_{15}$H$_{28}$GeN$_6$S$_2$]$^+$.

HRMS: for C$_{24}$H$_{46}$GeN$_7$PS$_2$ theor./exp. 601.2205/601.2213.

IR : ṽ (cm^{-1}) = 2965 (*w*), 1430 (*w*), 1376 (*s*), 1160 (*s*), 1018 (*s*), 968 (*s*), 830 (*s*).

^{1}H NMR (300 MHz, CDCl$_3$) : δ = 0.9 (t, 6H, $^3J_{H,H}$ = 7.1 Hz, *Ge*-(N-CH$_2$-$\underline{CH_3}$)$_2$), 1.1 (t, 6H, $^3J_{H,H}$ = 7.0 Hz, Ge-*(N*-CH$_2$-$\underline{CH_3}$)$_2$), 1.1-1.2 (m, 12H, N-*^{i}Pr,* N-CH-($\underline{(CH_3)_2}$), 2.8 (q, 4H, $^3J_{H,H}$ = 7.1 Hz, Ge-*(N*-$\underline{CH_2}$-CH$_3$)$_2$), 3.0 (q, 4H, $^3J_{H,H}$ = 7.1 Hz, Ge-*(N*-$\underline{CH_2}$-CH$_3$)$_2$), 3.3-3.5 (m, 2H, N-*^{i}Pr,* N-$\underline{CH}$-Me$_2$), 3.7 (s, 6H, *N*-$\underline{CH_3}$), 3.8 (s, 6H, *N*-$\underline{CH_3}$).

^{13}C{^{1}H} NMR (75 MHz, CDCl$_3$) : δ = 14.6 (s, Ge-*(N*-CH$_2$-$\underline{CH_3}$)$_2$), 14.7 (s, Ge-*(N*-CH$_2$-$\underline{CH_3}$)$_2$), 34.7 (s, N-*^{i}Pr,* N-CH-($\underline{(CH_3)_2}$), 34.8 (s, N-*^{i}Pr,* N-CH-($\underline{(CH_3)_2}$), 35.7 (s, Ge-*(N*-$\underline{CH_2}$-CH$_3$)$_2$), 35.8 (s, N-*^{i}Pr,* N-$\underline{CH_2}$-Me$_2$), 39.6 (s, *N*-$\underline{CH_3}$), 40.8 (s, *N*-$\underline{CH_3}$), 130.6 (s, C^5), 133.3 (s, C^4), 167.3 (s, *C*=S).

^{31}P{^{1}H} NMR (121.5 Hz, CDCl$_3$) : δ = −17.5.

10.7.4 4-Phenyl-8-diethylylamino-1,3,5,7-tetramethyl-4,8-hydro[1,4]phospha-germine[2,3 -d:5,6-d']bisimidazole-2,6-dithione (13a)
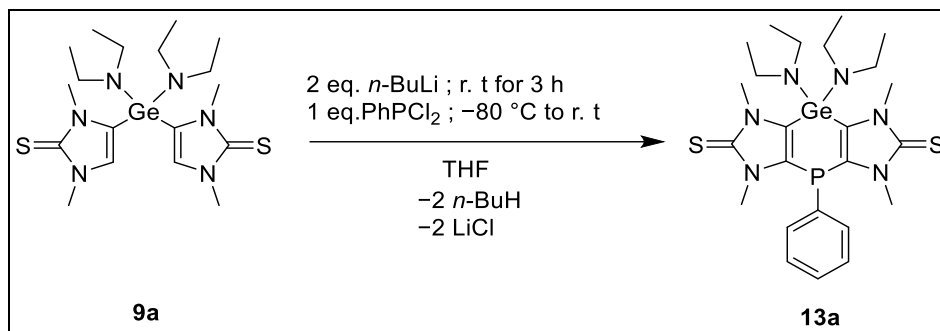
LJC : MR-446.

NMR Code : MR-446-full (MRI230117p5a023.10.fid).

CSIC : GSTR798, GXray7147.

Yield : 82 mg (0.142 mmol, 67 %)   **Appearance :** white powder   **M.p. :** 145 °C

EA(%) : exp. C 50.45, H 6.12, N 12.52, S 10.19. Calc. C 49.93, H 6.46, N 14.56, S 11.11.

EI-MS (70 eV): m/z (%) = 578.1 (40) [M]$^+$, 434.0 (60) [C$_{16}$H$_{17}$GeN$_4$PS$_2$]$^{+\bullet}$

HRMS: for C$_{24}$H$_{37}$GeN$_6$PS$_2$ theor./exp. 578.1470/578.1467.

IR : ṽ (cm^{-1}) = 2970 (*w*), 1437 (*m*), 1378 (*s*), 1337 (*w*) 1161 (*s*), 1061 (*s*), 1016 (*w*), 834 (*s*), 695 (*s*).

^{1}H NMR (500 MHz, CDCl$_3$) : δ = 0.9 (*br*. t, 6H, Ge-*(*N-CH$_2$-C*H$_3$*)$_2$), 1.0 (*br*. t, 6H, Ge-*(*N-CH$_2$-C*H$_3$*)$_2$), 2.8 (*br*. q, 4H, Ge-*(*N-C*H$_2$*-CH$_3$)$_2$), 3.0 (*br*. q, 4H, Ge-*(*N-C*H$_2$*-CH$_3$)$_2$), 3.4 (s, 6H, *N*-C*H$_3$*), 3.7 (s, 6H, *N*-C*H$_3$*), 7.3 (*br*. m, 2H, P-*Ph* protons), 7.4 (*br*. m, 3H, P-*Ph* protons).

^{13}C{^{1}H} NMR (125 MHz, CDCl$_3$) : δ = 14.4 (s, Ge-(N-CH$_2$-C*H$_3$*)$_2$), 14.6 (s, Ge-*(*N-CH$_2$-C*H$_3$*)$_2$), 33.7 (s, Ge-*(*N-C*H$_2$*-CH$_3$)$_2$), 33.8 (s, Ge-*(*N-C*H$_2$*-CH$_3$)$_2$), 39.8 (s, *N*-C*H$_3$*), 40.0 (s, *N*-C*H$_3$*), 130.1 (d, P-*Ph*), 130.3 1(d, P-*Ph*), 130.4 (d, P-*Ph*), 131.4 (s, *C*^{5}), 134.0 (s, *C*^{4}), 134.2 (s, *C*^{4}), 167.7 (s, *C*=S).

^{31}P{^{1}H} NMR (200 Hz, CDCl$_3$) : δ = −55.6.

10.8 General synthetic method for compound K[14b]

To **11b** (100 mg, 0. 138 mmol) KC$_8$ (56 mg, 0.414 mmol) was added in a 50 mL Schlenk tube, followed by the addition of 3mL of dry Et$_2$O under ambient conditions. Upon addition of the solvent, the color rapidly changed to light yellow along with carbon precipitation. The reaction mixture was then stirred for a couple of hours at room temperature and the reaction mixture was filtered to remove the carbon precipitate, to obtain a light yellow solution. The solvent was then removed under reduced pressure (2 x 10^{-2} mbar) to obtain **K[14b]** as a light yellow powder.

10.8.1 Potassium [1,3,5,7-tetra-*n*-butyl-[2,3-d:5,6-d']bisimidazole-2,6-dithione-4-bis(diethylamino)-8-sila-phosphane-1-ide] (K[14b])
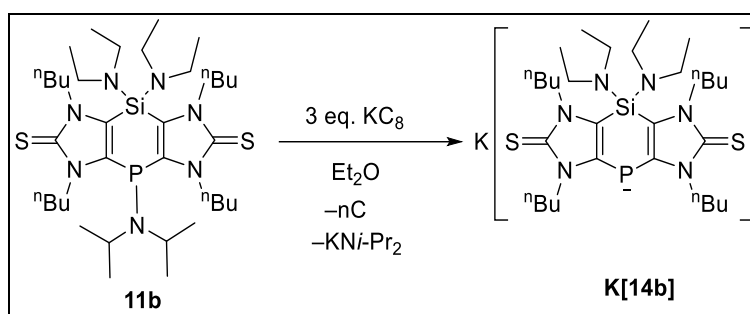
LJC : MR-614.

NMR Code : MR-614B (07m3a046.22.10.fid).

CSIC : GSTR747, GXraycu_6813f.

Yield : 62 mg (0.096 mmol, 70 %)   **Appearance :** Yellow powder   **M.p. :** 175 °C

EA (for C$_{30}$H$_{56}$K$_2$N$_6$PS$_2$Si) (%) : exp. C 52.63, H 8.27, N 11.80, S 8.29. Calc. C 51.31, H 8.04, N 11.97, S 9.13.

Neg-ESI-MS: m/z (%) = 655.341 (100) [C$_{30}$H$_{56}$N$_6$PS$_2$SiO$_2$]$^-$, 623.353 (30) [C$_{30}$H$_{56}$N$_6$PS$_2$Si]$^-$.

HRMS: for C$_{30}$H$_{56}$N$_6$PS$_2$Si theor./exp. 623.3527/623.3520.

IR : ṽ (cm⁻¹) = 2968 (*s*), 2864 (*w*), 1451 (*s*), 1413 (*m*), 1372 (*m*), 1335 (*w*), 1286 (*w*), 1200 (*s*), 1167 (*s*), 1056 (*w*), 1019 (*s*), 924 (*m*), 856 (*m*), 797 (*m*), 686 (*m*), 651 (*m*).

¹H NMR (300 MHz, THF-*d*8) : δ = 0.8 (t, 6H, $^3J_{H,H}$ = 6.9 Hz, NCH$_2$CH$_2$CH$_2$$\underline{C}$$H_3$), 0.9 (t, 12H, $^3J_{H,H}$ = 7.37 Hz, Si-(N-CH$_2$-$\underline{C}$$H_3$)$_2$), 0.9 (t, 12H, $^3J_{H,H}$ = 7.37 Hz, Si-*(*N-CH$_2$-$\underline{C}$$H_3$)$_2$), 1.3–1.4 (m, 8H, NCH$_2CH_2$$\underline{C}$$H_2$Me), 1.8–1.9 (m, 8H, NCH$_2$$\underline{C}$$H_2CH_2$Me), 1.7–1.9 (m, 8H, NCH$_2$$\underline{C}$$H_2CH_2$Me), 2.9 (q, 8H, $^3J_{H,H}$ = 7.0 Hz, Si-(N-$\underline{C}$$H_2$-CH$_3$)$_2$),), 4.0–4.1 (m, 8H, N$\underline{C}$$H_2CH_2CH_2$Me).

¹³C{¹H} NMR (75 MHz, THF-*d*8): δ = 14.1 (s, Si-(N-CH$_2$-$\underline{C}$$H_3$)$_2$), 13.6 (d, ^3J = 3.5 Hz, NCH$_2$CH$_2$CH$_2$$\underline{C}$$H_3$), 21.3 (s, NCH$_2CH_2$$\underline{C}$$H_2$Me), 21.5 (s, NCH$_2CH_2$$\underline{C}$$H_2$Me), 30.5 (d, ^3J = 4.94 Hz, NCH$_2$$\underline{C}$$H_2CH_2$Me), 39.5 (s, Si-*(*N-$\underline{C}$$H_2$-CH$_3$)$_2$), 48.4 (s, N$\underline{C}$$H_2CH_2CH_2$Me), 46.3 (s, N$\underline{C}$$H_2CH_2CH_2$Me), 46.2 (s, N$\underline{C}$$H_2CH_2CH_2$Me), 116.5 (d, ^3J = 11.17 Hz, C^5), 153.9 (s, C^4), 154.3 (s, C^4), 163.4 (s, *C*=S).

³¹P{¹H} NMR (121.5 Hz, THF-*d*8): δ = −87.9.

²⁹Si{¹H} dept20 NMR (60 Hz, THF-*d*8) : δ = −36.2 (s, $\underline{Si}$-*(*N-CH$_2$-CH$_3$)$_2$)).

10.9 Synthesis of the P-P coupled product 15b (P,Si-dimer)

The anionic 1,4-dihydro-1,4-phosphasiline derivative **K[14b]** (150 mg, 0.234 mmol) was dissolved in Et$_2$O to obtain a yellow solution in a 50 mL Schlenk tube. The reaction mixture was cooled to −90 °C by keeping it in Dewar bath. I$_2$ (30.5 mg, 0.117 mmol) was dissolved in 2.5 mL diethyl ether and added dropwise into the reaction mixture. The reaction became turbid orange which gradually turned to turbid light yellow. After overnight stirring, the solvent was removed *in vacuo* (1.8 x 10⁻² mbar). The residue was redissolved in toluene and filtered out via a cannula to remove the potassium iodide salt formed in course of the reaction. Solvent was removed *in vacuo* (1.8 x 10⁻² mbar) to obtain **15b** as yellow powder.
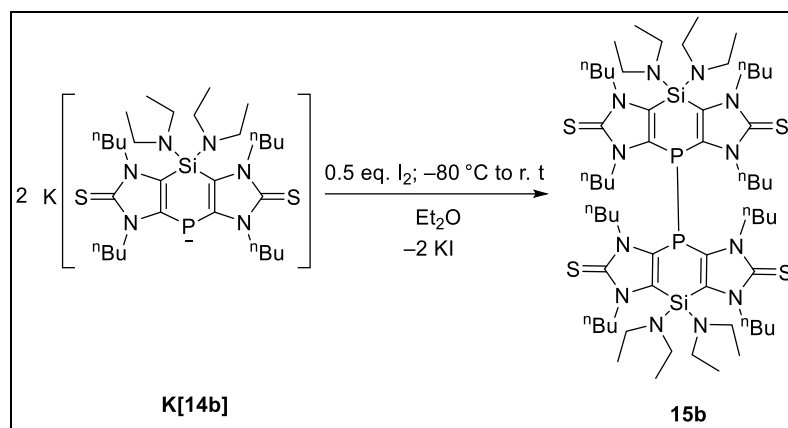
LJC : MR-dimer.

NMR Code : MR-dimer-full (41t4e022.22.10.fid).

CSIC : GXray6812.

Yield : 184 mg (0.147 mmol, 63 %)   **Appearance :** Yellow powder   **M.p. :** 235 °C

EA (%) : exp. C 55.14, H 8.57, N 12.66, S 8.80. Calc. C 57.75, H 9.05, N 13.47, S 10.28.

FTMS + pos-APCI-MS: m/z (%) = 1247.710 (10) $[M+H]^+$, 595.400 (100) $[C_{30}H_{60}N_6PSSi]^+$.

HRMS: for $C_{60}H_{113}N_{12}P_2S_4Si_2$ theor./exp. 1247.710/1247.710.

IR : ṽ (cm^{-1}) = 2962 (*w*), 2870 (*w*), 1437 (*w*), 1402 (*s*), 1205 (*m*), 1162 (*m*), 1021 (*s*), 937 (*w*), 851 (*w*), 654 (*w*).

^{1}H NMR (300 MHz, CDCl$_3$): δ = 0.7 (t, 12H, $^3J_{H,H}$ = 6.8 Hz, NCH$_2$CH$_2$CH$_2$*CH$_3$*), 0.8 (t, 12H, $^3J_{H,H}$ = 6.89 Hz, NCH$_2$CH$_2$CH$_2$*CH$_3$*), 1.0 (t, 12H, $^3J_{H,H}$ = 7.3 Hz, Si-*(*N-CH$_2$-*CH$_3$*)$_2$), 1.1 (t, 12H, $^3J_{H,H}$ = 6.8 Hz, Si-*(*N-CH$_2$-*CH$_3$*)$_2$), 1.4-1.5 (m, 16H, NCH$_2$CH$_2$*CH$_2$*Me), 1.7-1.9 (m, 8H, NCH$_2$*CH$_2$*CH$_2$Me), 2.0-2.1 (m, 4H, NCH$_2$*CH$_2$*CH$_2$Me), 2.5-2.6 (m, 4H, NCH$_2$*CH$_2$*CH$_2$Me), 2.7 (q, 8H, $^3J_{H,H}$ = 7.0 Hz, Si-(N-*CH$_2$*-CH$_3$)$_2$), 3.1 (q, 8H, $^3J_{H,H}$ = 7.0 Hz, Si-(N-*CH$_2$*-CH$_3$)$_2$), 3.9-4.0 (m, 6H, N*CH$_2$*CH$_2$CH$_2$Me), 4.1-4.2 (m, 4H, N*CH$_2$*CH$_2$CH$_2$Me), 4.2-4.3 (m, 4H, N*CH$_2$*CH$_2$CH$_2$Me).

^{13}C{^{1}H} NMR (75 MHz, CDCl$_3$) : δ = 13.4 (s, Si-(N-CH$_2$-*CH$_3$*)$_2$), 13.9 (d, ^3J = 1.5 Hz, NCH$_2$CH$_2$CH$_2$*CH$_3$*), 19.8 (s, NCH$_2$CH$_2$*CH$_2$*Me), 20.4 (s, NCH$_2$CH$_2$*CH$_2$*Me), 30.3 (s, NCH$_2$*CH$_2$*CH$_2$Me), 30.6 (s, NCH$_2$*CH$_2$*CH$_2$Me), 37.9 (s, Si-(N-*CH$_2$*-CH$_3$)$_2$), 38.4 (s, Si-(N-*CH$_2$*-CH$_3$)$_2$), 45.8 (s, N*CH$_2$*CH$_2$CH$_2$Me), 48.8 (s, N*CH$_2$*CH$_2$CH$_2$Me), 127.6 (s, *C^5*), 132.8 (s, *C^4*), 167.8 (s, *C*=S).

²⁹Si{¹H} dept20 NMR (60 Hz, CDCl₃) : δ = −42.2 (s, *Si-(*N-CH₂-CH₃)₂)).

³¹P{¹H} NMR (121.5 Hz, CDCl₃): δ = −49.5.

10.10 Conversion of 1,4-dihydro-1,4-phosphasiline K[14b] into Si(NR₂)₂ derivative 16b

Potassium 1,4-dihydro-1,4-phosphasilin-1-ide **K[14b]** (150 mg, 0.234 mmol) was dissolved in 2 mL of Et₂O at ambient temperature to obtain a yellow solution. The clear solution was cooled to −80 °C and the temperature was kept the same with a Dewar. Triphenylmethyl chloride (65.2 mg, 0.234 mmol) was dissolved in 2.5 mL of Et₂O and added dropwise into the clear solution. The reaction rapidly became turbid orange upon addition, which gradually turned to turbid light yellow. After overnight stirring, the solvent was removed *in vacuo* (2.4 x 10⁻² mbar). The residue was re-dissolved in *n*-pentane and filtered via a cannula to remove the potassium chloride salt. Then the solvent was removed *in vacuo* (1.6 x 10⁻² mbar) to obtain **16b** as a yellow powder.

10.10.1 4-Triphenylmethyl-8-diethylamino-1,3,5,7-tetra-*n*-butyl-4,8-hydro[1,4]phosphasiline[2,3-d:5,6-d']bisimidazole-2,6-dithione (16b)
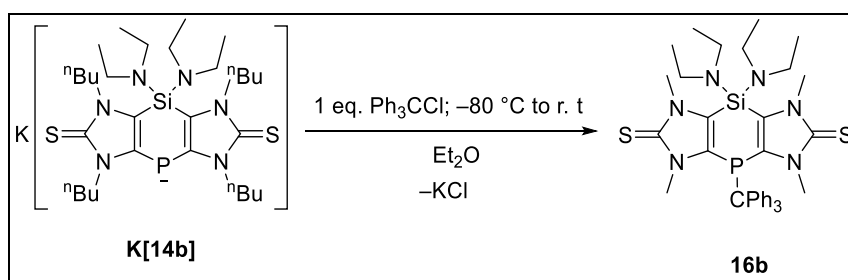
LJC : MR-785.

NMR Code : MR-785-fil (50p5a049.12.fid).

 Yield : 183 mg (0.211 mmol, 90 %)   **M.p. :** 100 °C

EA (%) : exp. C 67.90, H 8.04, N 9.03, S 6.22. Calc. C 67.86, H 8.25, N 9.69, S 7.39.

MALDI TOF-MS: m/z (intensity in a. u.) = 866.5 (9800) [M]$^+$, 835.5 (4000) [C$_{49}$H$_{72}$N$_6$PSSi] $^{+\bullet}$.

HRMS: for C$_{49}$H$_{71}$N$_6$PS$_2$Si theor./exp. 866.4683/866.4683.

IR: ṽ (cm^{-1}) =2965 (*w*), 1403 (*s*), 1098 (*w*), 1025 (*s*), 799 (*s*), 699 (*s*).

^{1}H NMR (300 MHz, CDCl$_3$) : δ = 0.7 (t, 6H, $^3J_{H,H}$ = 7.3 Hz, NCH$_2$CH$_2$CH$_2$C*H$_3$*), 0.9 (t, 6H, $^3J_{H,H}$ = 6.9 Hz, NCH$_2$CH$_2$CH$_2$C*H$_3$*), 0.9 (t, 6H, $^3J_{H,H}$ = 7.3 Hz, Si-*(N-CH$_2$-C*H$_3$*)$_2$*), 1.0 (t, 6H, $^3J_{H,H}$ = 6.9 Hz, Si-*(N-CH$_2$-C*H$_3$*)$_2$*), 1.1–1.3, 1.3–1.5 (m, 8H, NCH$_2$CH$_2$C*H$_2$*CH$_3$), 1.6-2.0 (m, 8H, NCH$_2$C*H$_2$*CH$_2$CH$_3$), 2.8 (q, 4H, $^3J_{H,H}$ = 6.9 Hz, Si-(N-C*H$_2$*-CH$_3$)$_2$), 2.9 (q, 1H, $^3J_{H,H}$ = 6.8 Hz, Si-*(N-C*H$_2$*-CH$_3$)$_2$*), 3.0 (q, 3H, $^3J_{H,H}$ = 7.0 Hz, Si-(N-C*H$_2$*-CH$_3$)$_2$), 3.8–3.9 (m, 2H, NC*H$_2$*CH$_2$CH$_2$CH$_3$), 4.0–4.1 (m, 5H, NC*H$_2$*CH$_2$CH$_2$CH$_3$), 4.2–4.4 (m, 1H, NC*H$_2$*CH$_2$CH$_2$CH$_3$), 7.0 (d, 3H, $^3J_{H,H}$ = 7.2 Hz, trityl phenyl protons), 7.1 (t, 3H, $^3J_{H,H}$ = 8.2 Hz, trityl phenyl protons), 7.2 (t, 4H, $^3J_{H,H}$ = 7.2 Hz, trityl phenyl protons), 7.3 (q, 4H, $^3J_{H,H}$ = 7.2 Hz, trityl phenyl protons), 7.4 (t, 1H, $^3J_{H,H}$ = 8.3 Hz, trityl phenyl protons).

^{13}C{^{1}H} NMR (75 MHz, CDCl$_3$) : δ = 13.4 (s, Si-*(N-CH$_2$-C*H$_3$*)$_2$*), 13.6 (s, Si-*(N-CH$_2$-C*H$_3$*)$_2$*), 13.7 (s, NCH$_2$CH$_2$CH$_2$C*H$_3$*), 13.9 (s, NCH$_2$CH$_2$CH$_2$C*H$_3$*), 20.1 (s, NCH$_2$CH$_2$C*H$_2$*CH$_3$), 20.4 (s, NCH$_2$CH$_2$C*H$_2$*CH$_3$), 29.3 (s, NCH$_2$C*H$_2$*CH$_2$CH$_3$), 30.1 (s, NCH$_2$C*H$_2$*CH$_2$CH$_3$), 37.5 ((s, Si-(N-C*H$_2$*-CH$_3$)$_2$)), 38.2 ((s, Si-(N-C*H$_2$*-CH$_3$)$_2$)), 48.7 (s, NC*H$_2$*CH$_2$CH$_2$Me), 56.7 (trityl phenyl protons), 125.9–129.4 (trityl phenyl protons), 131.2 (s, C^5), 134.3 (s, C^4), 134.5 (s, C^4), 142.8 (trityl phenyl protons), 166.6 (s, *C*=S).

^{31}P{^{1}H} NMR (121.5 Hz, CDCl$_3$): δ = –57.2.

^{29}Si{^{1}H} dept20 (60 Hz, CDCl$_3$): δ = – 42.1 (d, ^3J = 3.8 Hz, *Si*-(N-CH$_2$-CH$_3$)$_2$)).

10.11 Synthesis of SiCl$_2$ derivative 17b from 16b

The 1,4-dihydro-1,4-phosphasiline derivative **16b** (150 mg, 0.17 mmol) was dissolved in 2 mL of DCM to obtain a yellow solution. A 2M solution of hydrogen chloride in diethyl ether (0.38mL, 0.76 mmol) was added dropwise into the clear solution at room temperature but no color change was observed. After stirring for an hour, the solvent was removed *in vacuo* (2.1 x 10^{-2} mbar). The residue was re-dissolved in toluene and filtered via a cannula to remove the

ammonium chloride salt formed. The solvent was then removed *in vacuo* (1.8 x 10^{-2} mbar) to obtain **17b** as yellow powder.

10.11.1 4-Triphenylmethyl-8-dichloro-1,3,5,7- tetra-*n*-butyl-4,8-hydro[1,4]phos-phasiline[2,3-d:5,6-d']bisimidazole-2,6-dithione (17b)
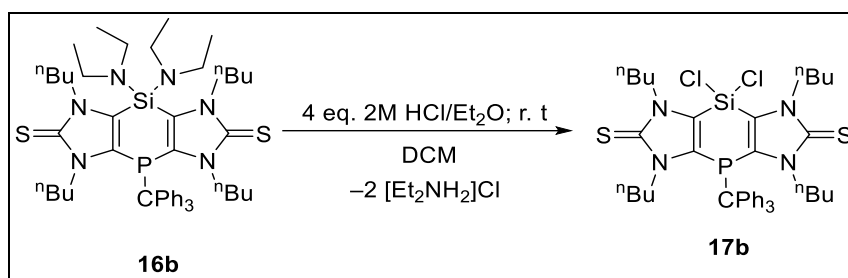
LJC : MR-792-full.

NMR Code : MR-792-full (51m3a053.22.fid).

Yield : 115 mg (0.145 mmol, 85 %)   **M.p. :** 159 °C

EA (%): exp. C 61.92, H 6.70, N 6.89, S 7.26. Calc. C 62.02, H 6.47, N 7.06, S 8.08.

FTMS + p-APCI: m/z (%) = 793.2 (45) $[M]^+$, 757.3 (40) $[M-Cl]^+$, 697.3 (100) $[C_{41}H_{55}ClN_4PSi]^{\bullet+}$.

HRMS: for $C_{41}H_{51}Cl_2N_4PS_2Si$ theor/exp. 793.2512/793.2509.

IR: ṽ (cm^{-1}) = 2947 (*w*), 1494 (*m*), 1448 (*m*), 1407 (*s*), 756 (*m*), 701 (*s*).

^{1}H NMR (300 MHz, CDCl$_3$): δ = 0.8 (t, 6H, $^3J_{H,H}$ = 7.3 Hz, NCH$_2$CH$_2$CH$_2$C$\underline{H}_3$), 1.0 (t, 6H, $^3J_{H,H}$ = 7.3 Hz, NCH$_2$CH$_2$CH$_2$C$\underline{H}_3$), 1.2–1.3 (m, 8H, NCH$_2$CH$_2$C$\underline{H}_2$CH$_3$) , 1.4–1.5 (m, 8H, NCH$_2$CH$_2$C$\underline{H}_2$CH$_3$), 1.7–2.0 (m, 8H, NCH$_2$C$\underline{H}_2$CH$_2$CH$_3$), 3.8–3.9 (m, 2H, NC$\underline{H}_2$CH$_2$CH$_2$CH$_3$), 4.0–4.1 (m, 2H, NC$\underline{H}_2$CH$_2$CH$_2$CH$_3$), 4.2–4.3 (m, 4H, NC$\underline{H}_2$CH$_2$CH$_2$CH$_3$), 7.0 (d, 3H, $^3J_{H,H}$ = 7.3 Hz, trityl phenyl protons), 7.1 (t, 2H, $^3J_{H,H}$ = 8.3 Hz, trityl phenyl protons), 7.2 (t, 6H, $^3J_{H,H}$ = 7.3 Hz, trityl phenyl protons), 7.3 (q, 3H, $^3J_{H,H}$ = 7.3Hz, trityl phenyl protons), 7.4 (t, 1H, $^3J_{H,H}$ = 8.3 Hz, trityl phenyl protons).

^{13}C{^{1}H} NMR (75 MHz, CDCl$_3$): δ = 13.7 (d, ^3J = 5.4 Hz, NCH$_2$CH$_2$CH$_2$*CH$_3$*), 20.1 (d, ^3J = 5.1 Hz, NCH$_2$CH$_2$*CH$_2$*CH$_3$), 29.3 (s, NCH$_2$*CH$_2$*CH$_2$CH$_3$), 30.1 (s, NCH$_2$*CH$_2$*CH$_2$CH$_3$), 49.2 (s, N*CH$_2$*CH$_2$CH$_2$CH$_3$), 56.8 (trityl phenyl protons), 125.9–129.4 (trityl phenyl protons) , 131.2 (s, C^5), 134.1 (s, C^4), 134.5–134.7 (trityl phenyl protons), 142.5 (trityl phenyl protons), 168.2 (s, C=S).

^{31}P{^{1}H} NMR (121.5 Hz, CDCl$_3$): δ = − 55.8.

10.12 Si-methylation of 17b

The 1,4-dihydro-1,4-phosphasiline **17b** (150 mg, 0.18 mmol) was dissolved in 2mL of THF to obtain a yellow solution, and a solution (1.6 M in diethyl ether) of methyllithium (0.23 mL, 0.37 mmol) was added dropwise into the clear solution at − 80 °C. The color rapidly changed from yellow to deep red, then to deep wine red. After overnight stirring, the color turned to deep brown-orange and the solvent was removed *in vacuo* (2.3 x 10^{-2} mbar). The residue was re-dissolved in toluene and filtered via a cannula to remove the lithium chloride salt formed. The solvent was then removed *in vacuo* (3.7 x 10^{-2} mbar), washed with *n*-pentane thoroughly and dried *in vacuo* (4.2 x 10^{-2} mbar) to obtain **18b** as yellow powder.

10.12.1 4-Triphenylmethyl-8-dimethyl-1,3,5,7-tetra-*n*-butyl-4,8-hydro[1,4]phospha-siline[2,3 -d:5,6-d']bis(imidazole-2,6-dithione) (18b)
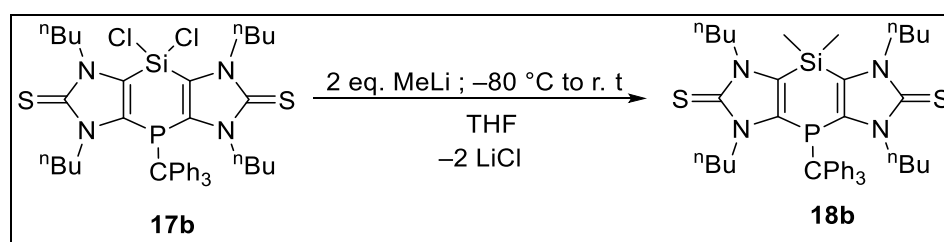
LJC : MR-788-full.

NMR Code : MR-788-full (50p5b025.fid).

Yield : 134 mg (0.17 mmol,96 %)   **M.p. :** 155 °C

EA (%): exp. C 64.61, H 7.18, N 6.70, S 7.34. Calc. C 68.58, H 7.63, N 7.44, S 8.51.

FTMS + p-APCI: m/z (%) = 753.3 (50) [M+H] $^+$, 469.2 (75) [$C_{20}H_{34}N_4OPS_2Si$] $^{+\bullet}$.

HRMS: for C$_{43}$H$_{58}$N$_4$PS$_2$Si theor./exp. 753.3604/753.3602.

IR: ṽ (cm^{-1}) = 2965 (*w*), 1437 (*m*), 1403 (*s*), 1218 (*s*), 1091 (*s*), 806 (*s*), 699 (*s*).

^{1}H NMR (300 MHz, CDCl$_3$) : δ = 0.6 (d, 6H, $^3J_{H,H}$ = 12.5 Hz, Si-C*H$_3$*), 0.8 (t, 6H, $^3J_{H,H}$ = 7.3 Hz, NCH$_2$CH$_2$CH$_2$C*H$_3$*), 1.0 (t, 6H, $^3J_{H,H}$ = 7.3 Hz, NCH$_2$CH$_2$CH$_2$C*H$_3$*), 1.2–1.3 (m, 8H, NCH$_2$CH$_2$C*H$_2$*Me), 1.4–1.5 (m, 8H, NCH$_2$CH$_2$C*H$_2$*Me), 1.7–1.9 (m, 8H, NCH$_2$C*H$_2$*CH$_2$Me), 3.8–3.9 (m, 2H, NC*H$_2$*CH$_2$CH$_2$Me), 4.0–4.1 (m, 6H, NC*H$_2$*CH$_2$CH$_2$Me), 7.0 (d, 3H, $^3J_{H,H}$ = 7.3 Hz, trityl phenyl protons), 7.1 (d, 3H, $^3J_{H,H}$ = 8.4 Hz, trityl phenyl protons), 7.2 (*br*. t, 3H, trityl phenyl protons), 7.2-7.3 (m, 5H, trityl phenyl protons)7.3 (t, 1H, $^3J_{H,H}$ = 8.4 Hz, trityl phenyl protons).

^{13}C{^{1}H} NMR (75 MHz, CDCl$_3$): δ = 0.3 (s, Si-C*H$_3$*), 13.7 (d, ^3J = 5.4 Hz, s, NCH$_2$CH$_2$CH$_2$C*H$_3$*), 20.1 (s, NCH$_2$CH$_2$C*H$_2$*Me), 20.3 (s, NCH$_2$CH$_2$C*H$_2$*Me), 29.6 (s, NCH$_2$C*H$_2$*CH$_2$Me), 30.7 (s, NCH$_2$C*H$_2$*CH$_2$Me), 49.1 (s, NC*H$_2$*CH$_2$CH$_2$Me), 56.7 (trityl phenyl protons), 125.9–129.4 (trityl phenyl protons), 131.2 (s, C^5), 134.2 (s, C^4), 134.4 (s, C^4), 142.8 (trityl phenyl protons), 166.7 (s, *C*=S).

^{31}P{^{1}H} NMR (121.5 Hz, CDCl$_3$): δ = −56.7.

^{29}Si{^{1}H} dept20 NMR (60 Hz, CDCl$_3$): δ = −25.6 (s, *Si*-(CH$_3$)$_2$)).

10.13 Si-methoxylation of 17b to form 19b

The 1,4-dihydro-1,4-phosphasiline derivative **17b** (150 mg, 0.18 mmol) was dissolved in 2 mL of THF to obtain a clear yellow solution. Excess of methanol was added drop wise into the clear solution at room temperature. After overnight stirring, the solvent was removed *in vacuo* (2.1 x 10^{-2} mbar). The residue was washed with *n*-pentane thoroughly and dried *in vacuo* (5.6 x 10^{-2} mbar) to obtain **19b** as a white powder.

10.13.1   4-Triphenylmethyl-8-dimethoxy-1,3,5,7-tetra-*n*-butyl-4,8-hydro[1,4]phosphasiline[2,3-d:5,6-d']bisimidazole-2,6-dithione (19b)
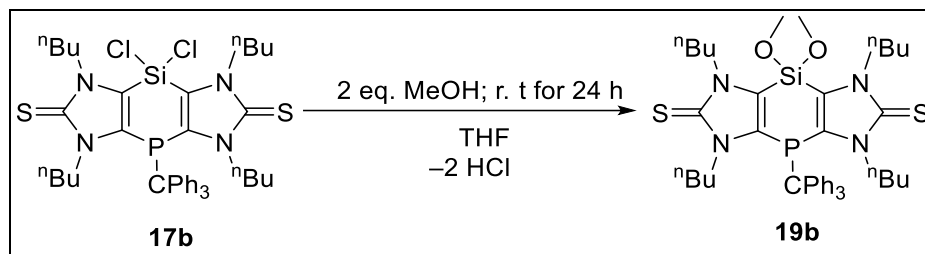
LJC : MR-789-full.

NMR Code : MR-789-full (50p5b024.fid).

Yield : 69 mg (0.08 mmol, 49 %)   **M.p. :** 188 °C

FTMS + pos-APCI: m/z (%) = 785.3 (25) [M+H]$^+$, 243.1 (25) [$C_{19}H_{15}$]$^{+•}$, 213.1 (100) [$C_{11}H_{21}N_2S$]$^+$.

HRMS: for $C_{43}H_{57}N_4O_2PS_2Si$ theor./exp. 785.3503/785.3503.

IR: ṽ (cm^{-1}) = 3403 (*w*), 2947 (*w*), 1637 (*m*), 1407 (*s*), 1241 (*s*), 1152 (*m*), 984 (*s*).

^{1}H NMR (300 MHz, CDCl$_3$): δ = 0.80 (t, 6H, $^3J_{H,H}$ = 7.3 Hz, NCH$_2$CH$_2$CH$_2$C*H$_3$*), 0.9 (t, 6H, $^3J_{H,H}$ = 7.3 Hz, NCH$_2$CH$_2$CH$_2$C*H$_3$*), 1.1–1.3 (m, 8H, NCH$_2$CH$_2$C*H$_2$*Me), 1.4–1.5 (m, 8H, NCH$_2$CH$_2$C*H$_2$*Me), 1.7–2.0 (m, 8H, NCH$_2$C*H$_2$*CH$_2$Me), 3.5 (s, 3H, P-(O-C*H$_3$*)$_2$), 3.6 (s, 3H, P-(O-C*H$_3$*)$_2$), 3.8–3.9 (m, 2H, NC*H$_2$*CH$_2$CH$_2$Me), 4.0–4.2 (m, 6H, NC*H$_2$*CH$_2$CH$_2$Me), 7.0 (*br*. d, 3H, trityl phenyl protons), 7.1 (t, 5H, $^3J_{H,H}$ = 8.2 Hz, trityl phenyl protons), 7.2 (t, 5H, $^3J_{H,H}$ = 7.2 Hz, trityl phenyl protons), 7.3 (q, 1H, $^3J_{H,H}$ = 7.2 Hz, trityl phenyl protons), 7.4 (t, 1H, $^3J_{H,H}$ = 8.3 Hz, trityl phenyl protons).

^{13}C{^{1}H} NMR (75 MHz, CDCl$_3$) : δ = 13.7 (s, NCH$_2$CH$_2$CH$_2$C*H$_3$*), 13.9 (s, NCH$_2$CH$_2$CH$_2$C*H$_3$*), 20.1 (s, NCH$_2$CH$_2$C*H$_2$*Me), 20.2 (s, NCH$_2$CH$_2$C*H$_2$*Me), 29.3 (s, NCH$_2$CH$_2$C*H$_2$*Me), 30.7 (s, NCH$_2$C*H$_2$*CH$_2$Me), 49.1 (s, NC*H$_2$*CH$_2$CH$_2$Me), 51.1 (s, P-(O-C*H$_3$*)$_2$), 51.4 (s, P-(O-C*H$_3$*)$_2$), 56.7 (trityl phenyl protons), 125.9–129.4 (trityl phenyl protons) , 131.2 (s, *C^5*), 134.2–134.4 (trityl phenyl protons), 134.7 (s, *C^4*), 142.7 (trityl phenyl protons), 167.2 (s, *C*=S).

^{31}P{^{1}H} NMR (121.5 Hz, CDCl$_3$): δ = −56.8.

^{29}Si{^{1}H} dept20 NMR (60 Hz, CDCl$_3$): δ = –47.5 (s, <u>Si</u>-(CH$_3$)$_2$)).

10.14 Si-centered reduction reactions of 17b

<u>Room temperature reactions</u> : 1,4-dihydro-1,4-Phosphasiline derivative **17b** (50 mg, 0.06 mmol) was dissolved in 0.5 mL of toluene-*d*8 in a J Young® NMR tube to obtain a clear yellow solution, inside the glovebox. The reducing agents were weighed within the glovebox and added into the NMR tube, directly in solid form. Then, the added components were mixed well by keeping the NMR tube on a Vortex shaker for 1 minute.

<u>Low-temperature reactions</u> : 1,4-dihydro-1,4-Phosphasiline derivative **17b** (50 mg, 0.06 mmol) was dissolved in 0.5 mL of toluene-*d*8 in a Schlenk tube to obtain a clear yellow solution. The reducing agents were weighed inside the glovebox in a Schlenk tube and taken out after mixing with 0.5 mL of toluene-*d*8 . Then, both the flasks were cooled down to – 80 °C and the reducing agents were transferred either by using a stainless steel cannula or using a bent-tube. Then, they were stirred well and warmed up to room temperature.

Table 10.14.1. Reduction conditions of **17b**.

Reaction Code	Reducing agent used (Amount, mmol)	Conditions
MR-740	Magnesium (3 mg, 0.12 mmol)	Room temperature
MR-741	KC$_8$ (16.2 mg, 0.12 mmol)	Room temperature
MR-818	KC$_8$ (20.2 mg, 0.15 mmol)	– 80 °C

10.15 Silylene trapping reaction to form 20b

The 1,4-dihydro-1,4-phosphasiline **17b** (150 mg, 0.18 mmol) was taken in a 10 mL Schlenk tube along with KC$_8$ (72.9 mg, 0.54 mmol). Then, the Schlenk tube was cooled down to –80 °C and 1,3-Butadiene (15 wt% in hexane) (0.08 mL, 0.23 mmol) was added along the walls. After that, 1.5 mL of toluene was cooled down to – 80 °C in another Schlenk tube and was transferred by using a stainless steel cannula/bent-tube. After overnight stirring, the

consumption of added KC$_8$ was observed, indicated by the formation of graphite precipitate. The solvent was removed *in vacuo* (3.1 x 10^{-2} mbar). The residue was re-dissolved in diethyl ether and filtered via a cannula to remove the potassium chloride salt and graphite formed. The solvent was then removed *in vacuo* (3.9 x 10^{-2} mbar), washed with a 3:1 mixture of *n*-pentane and diethyl ether thoroughly and dried *in vacuo* (5.6 x 10^{-2} mbar) to obtain **20b** as white powder.

10.15.1   4-Triphenylmethyl-1,3,5,7-tetra-*n*-butyl-4,8-hydro[1,4]phosphasiline[2,3 - d:5,6-d']bisimidazole-2,6-dithione-8-(1,2-dihydro-silole) (20b)
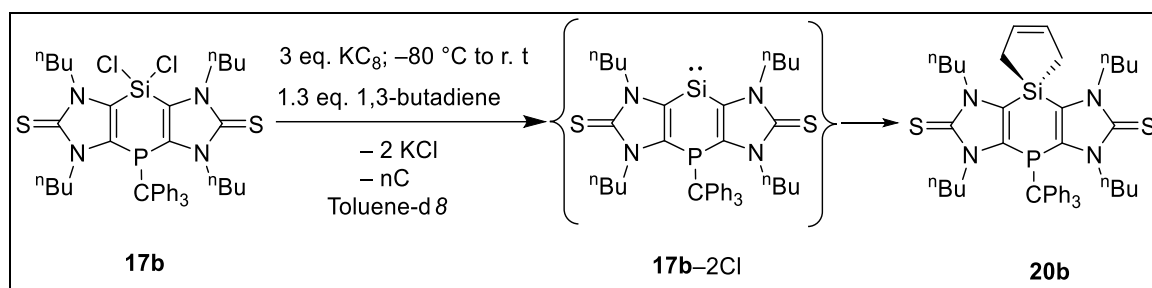
LJC : MR-835

NMR Code : MR-835-F1-B (RAM230616p5a013.fid).

Yield : 99 mg (0.168 mmol, 80 %)   **M.p. :** 161 °C

EI-MS (70 eV): m/z (%) = 776.4 (20) [M]$^+$, 743.4 (5) [M–S]$^+$, 728.4 (40) [C$_{45}$H$_{57}$N$_4$OPSi]$^+$, 712.4 (40) [M–2S]$^+$.

HRMS: for C$_{45}$H$_{57}$N$_4$PS$_2$Si theor./exp. 776.3531/776.3526.

IR: ṽ (cm^{-1}) = 2961 (*w*), 1407 (*w*), 1262 (*s*), 1089 (*s*), 1016 (*s*), 797 (*s*).

^{1}H NMR (300 MHz, CD$_2$Cl$_2$): δ = 0.5–0.7 (*br*. m, 4H, Si-(C*H$_2$*)-CH-), 0.8–1.0 (*br*. m, 12H, NCH$_2$CH$_2$CH$_2$C*H$_3$*), 1.2–1.5 (*br*. m, 8H, NCH$_2$CH$_2$C*H$_2$*Me), 1.6–2.2 (*br*.m, 8H, NCH$_2$C*H$_2$*CH$_2$Me), 3.7–4.3 (*br*. m, 8H, NC*H$_2$*CH$_2$CH$_2$Me), 4.9–5.2 (*br*. m, 1H, Si-(CH$_2$)-C*H*-), 5.3–5.4 (*br*. m, 1H, Si-(CH$_2$)-C*H*-), 6.9–7.1 (*br*. m, 6H, trityl phenyl protons), 7.1–7.2 (*br*. m, 3H, trityl phenyl protons), 7.2–7.3 (*br*. m, 4H, trityl phenyl protons), 7.4–7.5 (*br*. m, 2H, trityl phenyl protons).

^{13}C{^{1}H} NMR (75 MHz, CD$_2$Cl$_2$): δ = 13.8 (s, Si-(_CH$_2$_)-CH-), 14.2 (s, NCH$_2$CH$_2$CH$_2$_CH$_3$_), 20.1 (s, NCH$_2$CH$_2$_CH$_2$_Me), 20.3 (s, NCH$_2$_CH$_2$_CH$_2$Me), 29.8 (s, NCH$_2$_CH$_2$_CH$_2$Me), 47.1 (s, Si-(CH$_2$)-_CH_-), 49.1 (s, N_CH$_2$_CH$_2$CH$_2$Me), 56.6 (trityl phenyl protons), 56.8 (trityl phenyl protons), 126.0–129.6 (trityl phenyl protons) , 131.3 (s, _C^5_), 134.6 (s, _C^4_), 146.9 (trityl phenyl protons), 166.1 (s, _C_=S).

^{31}P{^{1}H} NMR (121.5 Hz, CD$_2$Cl$_2$): δ = −58.0.

10.16 HCl-induced P-N and Si-N cleavage of 11b to form 21b

The 1,4-dihydro-1,4-phosphasiline derivative **11b** (150 mg,0.21 mmol) was dissolved in 2 mL of DCM to obtain a yellow clear solution. 2M solution hydrogen chloride in diethyl ether (0.62 mL, 1.242 mmol) was added drop wise into the solution at −80 °C and warmed to room temperature. Then the solvent was removed _in vacuo_ (3.4 x 10^{-2} mbar). The residue was re-dissolved in diethyl ether and filtered out via a cannula to remove the chlorophosphonium chloride salt formed in course of the reaction. Solvent was removed _in vacuo_ (4.9 x 10^{-2} mbar) and dried _in vacuo_ (3.2 x 10^{-2} mbar) after washing with 3 x 2 mL of _n_-pentane to obtain a yellow powder **21b**.

10.16.1 4-Chloro-8-dichloro-1,3,5,7- tetra-_n_-butyl-4,8-hydro[1,4]phosphasiline[2,3-d:5,6-d']bis(imidazole-2,6-dithione) (21b)

11b **21b**
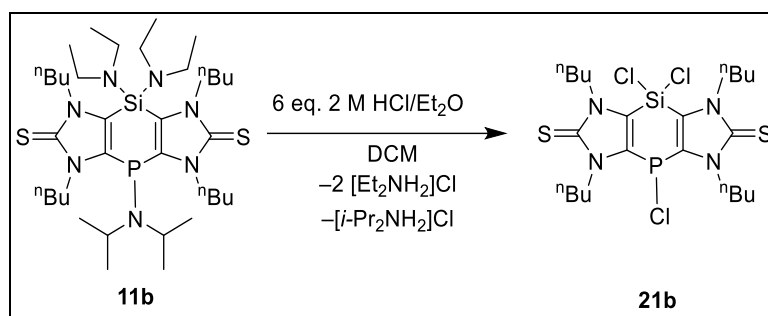
LJC : MR-793-full.

NMR Code : MR-793-full (RAM230119p5a044.fid).

Yield : 99 mg (0.168 mmol, 80 %)   **M.p. :** 172 °C

EA (%): exp. C 46.01, H 6.87, N 8.31, S 8.50. Calc. C 45.09, H 6.19, N 9.56, S 8.08

EI-MS (70 eV) : m/z (%) = 723.5 (15) $[C_{36}H_{70}N_7PS_2Si]^+$, 586.6 (5) $[M+H_2]^+$.

IR: $\tilde{v}$ (cm^{-1}) = 2965 (w), 1442 (w), 1403 (s), 1218 (s), 1082 (s), 799 (s).

^{1}H NMR (300 MHz, CD$_2$Cl$_2$): δ = 0.8–1.0 (*br*. m, 12H, NCH$_2$CH$_2$CH$_2$C*H$_3$*), 1.2–1.5 (*br*. m, 8H, NCH$_2$CH$_2$C*H$_2$*Me), 1.6–2.0 (*br*.m, 8H, NCH$_2$C*H$_2$*CH$_2$Me), 3.6–3.8 (*br*. m, 2H, NC*H$_2$*CH$_2$CH$_2$Me), 3.9–4.4 (*br*. m, 6H, NC*H$_2$*CH$_2$CH$_2$Me).

^{13}C{^{1}H} NMR (75 MHz, CD$_2$Cl$_2$): δ = 13.8 (*br*. d, NCH$_2$CH$_2$CH$_2$C*H$_3$*), 20.4 (*br*. d, NCH$_2$CH$_2$C*H$_2$*CH$_3$), 31.2 (*br*. s, NCH$_2$C*H$_2$*CH$_2$CH$_3$), 47.4 (*br*. s, NC*H$_2$*CH$_2$CH$_2$CH$_3$), 49.6 (*br*. s, NC*H$_2$*CH$_2$CH$_2$CH$_3$), 131.2 (*br*. s, *C^5*), 133.0 (*br*. s, *C^4*), 169.6 (s, *C*=S).

^{31}P{^{1}H} NMR (121.5 Hz, CD$_2$Cl$_2$): δ = −12.9.

10.17 Si- and P-centered reduction reactions of 21b

<u>Room temperature reactions</u> : 1,4-dihydro-1,4-phosphasiline derivative **21b** (50 mg, 0.08 mmol) was dissolved in 0.5 mL of the solvent in a Schlenk tube to obtain a clear yellow solution. The reducing agents were weighed within the glovebox and added into the Schlenk tube, directly or added in the fume hood under argon flow. Then, they were stirred well and the reactions were systematically monitored.

<u>Low-temperature reactions</u> : 1,4-dihydro-1,4-phosphasiline derivative **21b** (50 mg, 0.08 mmol) was dissolved in 0.5 mL of the solvent in a Schlenk tube to obtain a clear yellow solution. The reducing agents were weighed inside the glovebox in a Schlenk tube and prepared homogenous solutions in 0.5 mL of the solvent. Then, both flasks were cooled down to − 80 °C and the reducing agents were transferred either by using a stainless steel cannula (phosphanes were directly added under argon flow using a syringe). Then, they were stirred well and warmed up to room temperature.

Table 10.17.1. Reduction conditions of **21b**.

Reaction Code	Reducing agent used (Amount, mmol)	Solvent	Conditions
MR-586, MR-623, MR-622	n-Bu$_3$P (0.02 mL, 0.08 mmol)	DCM	– 80 °C
MR-589	Et$_3$P (0.01 mL, 0.08 mmol)	DCM	– 80 °C
MR-767	t-BuLi (0.05 mL, 0.08 mmol)	THF	– 80 °C
MR-634	1,4-dihydro-1,4-bis(trimethylsilyl)pyrazine (23 mg, 0.102 mmol)	DCM	– 80 °C
MR-625	n-Bu$_3$P (0.03 mL, 0.12 mmol)	DCM	Room Temperature
MR-743	KC$_8$ (16.2 mg, 0.12 mmol)	Et$_2$O	Room Temperature
MR-644	Tetrakis(dimethylamino)ethylene (0.02 mL, 0.08 mmol)	Et$_2$O	Room Temperature

References

(1) *Kirk-Othmer Encyclopedia of Chemical Technology*; Wiley, New York, **2000**.

(2) Trofimov, B. A.; Arbuzova, S. N.; Gusarova, N. K. *Russ. Chem. Rev.* **1999**, *68*, 215–227.

(3) Berlin, K. D. *Science* **1973**, *181*, 649.

(4) Gusarova, N. K.; Malysheva, S. F.; Arbuzova, S. N.; Trofimov, B. A. *Russ. Chem. Bull.* **1998**, *47*, 1645–1652.

(5) Pignolet, L. H. *Homogeneous Catalysis with Metal Phosphine Complexes*; Springer US, New York, **1983**.

(6) Guo, H.; Fan, Y. C.; Sun, Z.; Wu, Y.; Kwon, O. *Chem. Rev.* **2018**, *118*, 10049–10293.

(7) Horner, L.; Jurgeleit, W.; Klüpfel, K. *Justus Liebigs Ann. Chem.* **1955**, *591*, 108–117.

(8) Winterfeldt, E.; Dillinger, H.-J. *Chem. Ber.* **1966**, *99*, 1558–1568.

(9) Pitzer, K. S. *J. Am. Chem. Soc.* **1948**, *70*, 2140–2145.

(10) Mulliken, R. S. *J. Am. Chem. Soc.* **1950**, *72*, 4493–4503.

(11) Gier, T. E. *J. Am. Chem. Soc.* **1961**, *83*, 1769–1770.

(12) Dimroth, K.; Hoffmann, P. *Angew. Chem. Int. Ed. Engl.* **1964**, *3*, 384.

(13) Recker, G. *Z. Anorg. Allg. Chem.* **1976**, *423*, 242–254.

(14) Klebach, T. C.; Lourens, R.; Bickelhaupt, F. *J. Am. Chem. Soc.* **1978**, *100*, 4886–4888.

(15) Yoshifuji, M.; Shima, I.; Inamoto, N.; Hirotsu, K.; Higuchi, T. *J. Am. Chem. Soc.* **1981**, *103*, 4587–4589.

(16) Yoshifuji, M.; Shima, I.; Inamoto, N.; Hirotsu, K.; Higuchi, T. *J. Am. Chem. Soc.* **1982**, *104*, 6167.

(17) Becker, G.; Gresser, G.; Uhl, W. *Z. Naturforsch.* **1981**, *36*, 16–19.

(18) Märkl, G. *Angew. Chem. Int. Ed. Engl.* **1966**, *5*, 846–847.

(19) Regitz, M.; Scherer, O. J. *Multiple bonds and low coordination in phosphorus chemistry*; Georg Thieme Verlag, Stuttgart, **1990**.

(20) Mathey, F. *Phosphorus-Carbon Heterocyclic Chemistry*; Elsevier, **2001**.

(21) Gudat, D.; Niecke, E.; Sachs, W.; Rademacher, P. *Phosphorus and Sulfur and the Related Elements* **1987**, *30*, 796.

(22) Geoffroy, M.; Jouaiti, A.; Terron, G.; Cattani-Lorente, M.; Ellinger, Y. *J. Phys. Chem.* **1992**, *96*, 8241–8245.

(23) Jouaiti, A.; Al Badri, A.; Geoffroy, M.; Bernardinelli, G. *J. Organomet. Chem.* **1997**, *529*, 143–149.

(24) Lejeune, M.; Grosshans, P.; Berclaz, T.; Sidorenkova, H.; Besnard, C.; Pattison, P.; Geoffroy, M. *New J. Chem.* **2011**, *35*, 2510.

(25) Sasamori, T.; Tokitoh, N.; Streubel, R. π-Electron Redox Systems of Heavier Group 15 Elements. *Organic Redox Systems*; Nishinaga, T., Ed.; John Wiley & Sons, Inc, Hoboken, New Jersey, **2016**; 563–578.

(26) Çetinkaya, B.; Hitchcock, P. B.; Lappert, M. F.; Thorne, A. J.; Goldwhite, H. *J. Chem. Soc., Chem. Commun.* **1982**, *0*, 691–693.

(27) Culcasi, M.; Gronchi, G.; Escudie, J.; Couret, C.; Pujol, L.; Tordo, P. *J. Am. Chem. Soc.* **1986**, *108*, 3130–3132.

(28) Sasamori, T.; Mieda, E.; Nagahora, N.; Sato, K.; Shiomi, D.; Takui, T.; Hosoi, Y.; Furukawa, Y.; Takagi, N.; Nagase, S.; Tokitoh, N. *J. Am. Chem. Soc.* **2006**, *128*, 12582–12588.

(29) Crabtree, R. H. *Synthesis and Reactivity in Inorganic and Metal-Organic Chemistry* **1982**, *12*, 959–960.

(30) Appel, R.; Poppe, M. *Angew. Chem. Int. Ed. Engl.* **1989**, *28*, 53–54.

(31) Toyota, K.; Masaki, K.; Abe, T.; Yoshifuji, M. *Chem. Lett.* **1995**, *24*, 221–222.

(32) Toyota, K.; Tashiro, K.; Yoshifuji, M. *Chem. Lett.* **1991**, *20*, 2079–2082.

(33) Toyota, K.; Tashiro, K.; Yoshifuji, M.; Miyahara, I.; Hayashi, A.; Hirotsu, K. *J. Organomet. Chem.* **1992**, *431*, 39-C41.

(34) Yoshifuji, M.; Toyota, K.; Murayama, M.; Yoshimura, H.; Okamoto, A.; Hirotsu, K.; Nagase, S. *Chem. Lett.* **1990**, *19*, 2195–2198.

(35) Gajare, A. S.; Toyota, K.; Yoshifuji, M.; Ozawa, F. *J. Org. Chem.* **2004**, *69*, 6504–6506.

(36) Ikeda, S.; Ohhata, F.; Miyoshi, M.; Tanaka, R.; Minami, T.; Ozawa, F.; Yoshifuji, M. *Angew. Chem. Int. Ed.* **2000**, *39*, 4512–4513.

(37) Appel, R.; Winkhaus, V.; Knoch, F. *Chem. Ber.* **1987**, *120*, 243–245.

(38) FLOCH, P. *Coord. Chem. Rev.* **2006**, *250*, 627–681.

(39) Müller, C.; Vogt, D. *Dalton Trans.* **2007**, 5505–5523.

(40) Müller, C.; Broeckx, L. E. E.; Krom, I. de; Weemers, J. J. M. *Eur. J. Inorg. Chem.* **2013**, *2013*, 187–202.

(41) Regulska, E.; Romero-Nieto, C. *Dalton Trans.* **2018**, *47*, 10344–10359.

(42) Coles, N. T.; Sofie Abels, A.; Leitl, J.; Wolf, R.; Grützmacher, H.; Müller, C. *Coord. Chem. Rev.* **2021**, *433*, 213729.

(43) Ashe, A. J. *J. Am. Chem. Soc.* **1971**, *93*, 3293–3295.

(44) Mao, Y.; Mathey, F. *Chemistry (Weinheim an der Bergstrasse, Germany)* **2011**, *17*, 10745–10751.

(45) Rosa, P.; Le Floch, P.; Ricard, L.; Mathey, F. *J. Am. Chem. Soc.* **1997**, *119*, 9417–9423.

(46) Chen, X.; Alidori, S.; Puschmann, F. F.; Santiso-Quinones, G.; Benkő, Z.; Li, Z.; Becker, G.; Grützmacher, H.-F.; Grützmacher, H. *Angew. Chem. Int. Ed.* **2014**, *53*, 1641–1645.

(47) Alkorta, I.; Elguero, J. *Magn. Reson. Chem.* **2010**, *48 Suppl 1*, S32-7.

(48) Müller, C.; Wasserberg, D.; Weemers, J. J. M.; Pidko, E. A.; Hoffmann, S.; Lutz, M.; Spek, A. L.; Meskers, S. C. J.; Janssen, R. A. J.; van Santen, R. A.; Vogt, D. *Chemistry (Weinheim an der Bergstrasse, Germany)* **2007**, *13*, 4548–4559.

(49) Huy, N. H. T.; Donnadieu, B.; Mathey, F. *Organometallics* **2007**, *26*, 6497–6500.

(50) Ashe, A. J. *J. Am. Chem. Soc.* **1971**, *93*, 6690–6691.

(51) Ashe, A. J.; Diephouse, T. R.; El-Sheikh, M. Y. *J. Am. Chem. Soc.* **1982**, *104*, 5693–5699.

(52) Ishii, T.; Suzuki, K.; Nakamura, T.; Yamashita, M. *J. Am. Chem. Soc.* **2016**, *138*, 12787–12790.

(53) Doux, M.; Ricard, L.; Mathey, F.; Floch, P. L.; Mézailles, N. *Eur. J. Inorg. Chem.* **2003**, *2003*, 687–698.

(54) Nief, F.; Fischer, J. *Organometallics* **1986**, *5*, 877–883.

(55) Streubel, R. 1λ^5-Phosphinines. *Science of Synthesis* **2005**; *15*, 1157–1179.

(56) Baum, G.; Massa, W. *Organometallics* **1985**, *4*, 1572–1574.

(57) Dave, T.; Berger, S.; Bilger, E.; Kaletsch, H.; Pebler, J.; Knecht, J.; Dimroth, K. *Organometallics* **1985**, *4*, 1565–1572.

(58) Märkl, G.; Martin, C. *Angew. Chem. Int. Ed. Engl*. **1974**, *13*, 408–409.

(59) Moores, A.; Ricard, L.; Le Floch, P.; Mézailles, N. *Organometallics* **2003**, *22*, 1960–1966.

(60) Moores, A.; Ricard, L.; Le Floch, P. *Angew. Chem.* **2003**, *115*, 5090–5094.

(61) Bruce, M.; Meissner, G.; Weber, M.; Wiecko, J.; Müller, C. *Eur. J. Inorg. Chem.* **2014**, *2014*, 1719–1726.

(62) Zhang, Y.; Tham, F. S.; Nixon, J. F.; Taylor, C.; Green, J. C.; Reed, C. A. *Angew. Chem. Int. Ed.* **2008**, *47*, 3801–3804.

(63) Dimroth, K. *Phosphorus-carbon double bonds*; Springer-Verlag, Berlin, **1973**.

(64) Dimroth, K.; Steuber, F. W. *Angew. Chem.* **1967**, *79*, 410–411.

(65) Choua, S.; Dutan, C.; Cataldo, L.; Berclaz, T.; Geoffroy, M.; Mézailles, N.; Moores, A.; Ricard, L.; Le Floch, P. *Chemistry (Weinheim an der Bergstrasse, Germany)* **2004**, *10*, 4080–4090.

(66) Gerson, F.; Merstetter, P.; Pfenninger, S.; Märkl, G. *Magn. Reson. Chem.* **1997**, *35*, 384–388.

(67) Cataldo, L.; Choua, S.; Berclaz, T.; Geoffroy, M.; Mézailles, N.; Ricard, L.; Mathey, F.; Le Floch, P. *J. Am. Chem. Soc.* **2001**, *123*, 6654–6661.

(68) Mézailles, N.; Mathey, F.; Le Floch, P, The Coordination Chemistry of Phosphinines: Their Polydentate and Macrocyclic Derivatives, *Progress in Inorganic Chemistry*; John Wiley & Sons, New York, **2001**; 455–550.

(69) Le Floch, P.; Mathey, F. *Coord. Chem. Rev.* **1998**, *178-180*, 771–791.

(70) Mézailles, N.; Le Floch, P.; Waschbüsch, K.; Ricard, L.; Mathey, F.; Kubiak, C. P. *J. Organomet. Chem.* **1997**, *541*, 277–283.

(71) Deberitz, J.; Nöth, H. *J. Organomet. Chem.* **1973**, *55*, 153–163.

(72) Vahrenkamp, H.; Nöth, H. *Chem. Ber.* **1973**, *106*, 2227–2235.

(73) Nainan, K. C.; Sears, C. T. *J. Organomet. Chem.* **1978**, *148*, C31-C34.

(74) Deberitz, J.; Nöth, H. *Chem. Ber.* **1970**, *103*, 2541–2547.

(75) Vahrenkamp, H.; Nöth, H. *Chem. Ber.* **1972**, *105*, 1148–1157.

(76) Elschenbroich, C.; Baer, F.; Bilger, E.; Mahrwald, D.; Nowotny, M.; Metz, B. *Organometallics* **1993**, *12*, 3373–3378.

(77) Mao, Y.; Lim, K. M. H.; Li, Y.; Ganguly, R.; Mathey, F. *Organometallics* **2013**, *32*, 3562–3565.

(78) Reetz, M. T.; Bohres, E.; Goddard, R.; Holthausen, M. C.; Thiel, W. *Chem. Eur. J.* **1999**, *5*, 2101–2108.

(79) Schmid, B.; Venanzi, L. M.; Albinati, A.; Mathey, F. *Inorg. Chem.* **1991**, *30*, 4693–4699.

(80) Arce, A. J.; Deeming, A. J.; Sanctis, Y. de; Manzur, J. *J. Chem. Soc., Chem. Commun.* **1993**, 325.

(81) Knoch, F.; Kremer, F.; Schmidt, U.; Zenneck, U.; Le Floch, P.; Mathey, F. *Organometallics* **1996**, *15*, 2713–2719.

(82) Breit, B.; Winde, R.; Mackewitz, T.; Paciello, R.; Harms, K. *Chem. Eur. J.* **2001**, *7*, 3106–3121.

(83) Baber, R. A.; Haddow, M. F.; Middleton, A. J.; Orpen, A. G.; Pringle, P. G.; Haynes, A.; Williams, G. L.; Papp, R. *Organometallics* **2007**, *26*, 713–725.

(84) Reetz, M. T.; Li, X. *Angew. Chem. Int. Ed.* **2005**, *44*, 2962–2964.

(85) Doux, M.; Mézailles, N.; Melaimi, M.; Ricard, L.; Le Floch, P. *Chem. Commun.* **2002**, 1566–1567.

(86) Reetz, M. T.; Mehler, G. *Tetrahedron Lett.* **2003**, *44*, 4593–4596.

(87) van den Winkel, Y.; van der Laarse, J.; Kanter, F. J. J. de; van der Does, T.; Bickelhaupt, F.; Smeets, W. J. J.; Spek, A. L. *Heteroatom Chem.* **1991**, *2*, 17–28.

(88) Böhm, D.; Knoch, F.; Kummer, S.; Schmidt, U.; Zenneck, U. *Angew. Chem. Int. Ed. Engl.* **1995**, *34*, 198–201.

(89) Kobayashi, Y.; Kumadaki, I.; Ohsawa, A.; Hamana, H. *Tetrahedron Lett.* **1976**, *17*, 3715–3716.

(90) Koner, A.; Pfeifer, G.; Kelemen, Z.; Schnakenburg, G.; Nyulászi, L.; Sasamori, T.; Streubel, R. *Angew. Chem. Int. Ed.* **2017**, *56*, 9231–9235.

(91) Begum, I.; Schnakenburg, G.; Kelemen, Z.; Nyulászi, L.; Boeré, R. T.; Streubel, R. *Chem. Commun.* **2018**, *54*, 13555–13558.

(92) Sharma, M. K.; Ebeler, F.; Glodde, T.; Neumann, B.; Stammler, H.-G.; Ghadwal, R. S. *J. Am. Chem. Soc.* **2021**, *143*, 121–125.

(93) Sharma, M. K.; Rottschäfer, D.; Glodde, T.; Neumann, B.; Stammler, H.-G.; Ghadwal, R. S. *Angew. Chem. Int. Ed.* **2021**, *60*, 6414–6418.

(94) Rottschäfer, D.; Glodde, T.; Neumann, B.; Stammler, H.-G.; Andrada, D. M.; Ghadwal, R. S. *Angew. Chem. Int. Ed.* **2021**, *60*, 15849–15853.

(95) Steffenfauseweh, H.; Rottschäfer, D.; Vishnevskiy, Y. V.; Neumann, B.; Stammler, H.-G.; Szczepanik, D. W.; Ghadwal, R. S. *Angew. Chem. Int. Ed.* **2023**, e202216003.

(96) Koner, A. *On the imidazole-2-thione-based route to tricyclic 1,4-diphosphinines: synthesis, structures and reactions*; Universitäts- und Landesbibliothek, Bonn, **2018**.

(97) Welideniya, D.; Ramachandran, M. R. K.; Kalisch, T.; Streubel, R. *Dalton Trans.* **2021**, *50*, 9345–9366.

(98) Gese, A.; Kermanshahian, S.; Schnakenburg, G.; Kelemen, Z.; Nyulaszi, L.; Ferao, A. E.; Streubel, R. K. *Inorg. Chem.* **2021**, *60*, 13029–13040.

(99) Märkl, G.; Weber, W.; Weiß, W. *Chem. Ber.* **1985**, *118*, 2365–2395.

(100) Koner, A.; Sauerbrey, S.; Schnakenburg, G.; Bauzá, A.; Frontera, A.; Streubel, R. *Eur. J. Inorg. Chem.* **2018**, *2018*, 904–916.

(101) Koner, A.; Kunz, M.; Schnakenburg, G.; Streubel, R. *Eur. J. Inorg. Chem.* **2018**, *2018*, 3778–3784.

(102) Rottschäfer, D.; Neumann, B.; Stammler, H.-G.; Sergeieva, T.; Andrada, D. M.; Ghadwal, R. S. *Chemistry (Weinheim an der Bergstrasse, Germany)* **2021**, *27*, 3055–3064.

(103) Bélanger-Chabot, G.; Braunschweig, H.; Roy, D. K. *Eur. J. Inorg. Chem.* **2017**, *2017*, 4353–4368.

(104) Liu, Z.; Marder, T. B. *Angew. Chem. Int. Ed.* **2008**, *47*, 242–244.

(105) Bosdet, M. J.; Piers, W. E. *Can. J. Chem.* **2009**, *87*, 8–29.

(106) Drescher, R.; Lin, S.; Hofmann, A.; Lenczyk, C.; Kachel, S.; Krummenacher, I.; Lin, Z.; Braunschweig, H. *Chem. Sci.* **2020**, *11*, 5559–5564.

(107) Barnard, J. H.; Brown, P. A.; Shuford, K. L.; Martin, C. D. *Angew. Chem. Int. Ed.* **2015**, *54*, 12083–12086.

(108) Yang, W.; Krantz, K. E.; Dickie, D. A.; Molino, A.; Wilson, D. J. D.; Gilliard, R. J. *Angew. Chem. Int. Ed.* **2020**, *59*, 3971–3975.

(109) Märkl, G.; Dorfmeister, G. *Tetrahedron Lett.* **1987**, *28*, 1093–1096.

(110) Märkl, G.; Dörges, C.; Riedl, T.; Klärner, F.-G.; Lodwig, C. *Tetrahedron Lett.* **1990**, *31*, 4589–4592.

(111) Märk, G.; Dorsch, S. *Tetrahedron Lett.* **1995**, *36*, 3839–3842.

(112) Märkl, G.; Matthes, D. *Angew. Chem. Int. Ed. Engl.* **1972**, *11*, 1019–1020.

(113) Bieger, K.; Tejeda, J.; Reau, R.; Dahan, F.; Bertrand, G. *J. Am. Chem. Soc.* **1994**, *116*, 8087–8094.

(114) Nakamura, T.; Suzuki, K.; Yamashita, M. *J. Am. Chem. Soc.* **2014**, *136*, 9276–9279.

(115) Ashe, A. J.; Al-Ahmad, S.; Kampf, J. W. *Angew. Chem. Int. Ed. Engl.* **1995**, *34*, 1357–1359.

(116) Nakamura, T.; Suzuki, K.; Yamashita, M. *Organometallics* **2015**, *34*, 1806–1808.

(117) Nakamura, T.; Suzuki, K.; Yamashita, M. *Chem. Commun.* **2017**, *53*, 13260–13263.

(118) Märkl, G.; Schlosser, W. *Angew. Chem. Int. Ed. Engl.* **1988**, *27*, 963–965.

(119) Thomas J. Barton/Dennis S. Banasiak. *J. Am. Chem. Soc.* **1977**, *99*, 5199–5200.

(120) Tokitoh, N.; Wakita, K.; Okazaki, R.; Nagase, S.; Ragué Schleyer, P. von; Jiao, H. *J. Am. Chem. Soc.* **1997**, *119*, 6951–6952.

(121) Wakita, K.; Tokitoh, N.; Okazaki, R.; Nagase, S. *Angew. Chem. Int. Ed.* **2000**, *39*, 634–636.

(122) Nakata, N.; Takeda, N.; Tokitoh, N. *Organometallics* **2001**, *20*, 5507–5509.

(123) Nakata, N.; Takeda, N.; Tokitoh, N. *J. Am. Chem. Soc.* **2002**, *124*, 6914–6920.

(124) Mizuhata, Y.; Noda, N.; Tokitoh, N. *Organometallics* **2010**, *29*, 4781–4784.

(125) Mizuhata, Y.; Fujimori, S.; Noda, N.; Kanesato, S.; Tokitoh, N. *Dalton Trans.* **2018**, *47*, 14436–14444.

(126) Kaiya, C.; Suzuki, K.; Yamashita, M. *Angew. Chem. Int. Ed.* **2019**, *58*, 7749–7752.

(127) Han, J. S.; Sasamori, T.; Mizuhata, Y.; Tokitoh, N. *Dalton Trans.* **2010**, *39*, 9238–9240.

(128) Sugahara, T.; Guo, J.-D.; Hashizume, D.; Sasamori, T.; Nagase, S.; Tokitoh, N. *Dalton Trans.* **2018**, *47*, 13318–13322.

(129) Sugahara, T.; Guo, J.-D.; Sasamori, T.; Nagase, S.; Tokitoh, N. *Angew. Chem. Int. Ed.* **2018**, *57*, 3499–3503.

(130) Sasamori, T.; Sugahara, T.; Agou, T.; Guo, J.-D.; Nagase, S.; Streubel, R.; Tokitoh, N. *Organometallics* **2015**, *34*, 2106–2109.

(131) Sugahara, T.; Guo, J.-D.; Hashizume, D.; Sasamori, T.; Tokitoh, N. *J. Am. Chem. Soc.* **2019**, *141*, 2263–2267.

(132) Tashkandi, N. Y.; Pavelka, L. C.; Caputo, C. A.; Boyle, P. D.; Power, P. P.; Baines, K. M. *Dalton Trans.* **2016**, *45*, 7226–7230.

(133) Sugahara, T.; Sasamori, T.; Tokitoh, N. *Dalton Trans.* **2019**, *48*, 9053–9056.

(134) Zhu, Z.; Wang, X.; Olmstead, M. M.; Power, P. P. *Angew. Chem. Int. Ed.* **2009**, *48*, 2027–2030.

(135) Baumgartner, T.; Réau, R. *Chem. Rev.* **2006**, *106*, 4681–4727.

(136) Shameem, M. A.; Orthaber, A. *Chem. Eur. J.* **2016**, *22*, 10718–10735.

(137) Pfeifer, G.; Chahdoura, F.; Papke, M.; Weber, M.; Szűcs, R.; Geffroy, B.; Tondelier, D.; Nyulászi, L.; Hissler, M.; Müller, C. *Chem. Eur. J.* **2020**, *26*, 10534–10543.

(138) Regulska, E.; Hindenberg, P.; Romero-Nieto, C. *Eur. J. Inorg. Chem.* **2019**, *2019*, 1519–1528.

(139) Gerson, F.; Plattner, G.; Ashe, A. J.; Maerkl, G. *Mol. Phys.* **1974**, *28*, 601–615.

(140) Jongsma, C.; Graaf, H. G. de; Bickelhaupt, F. *Tetrahedron Lett.* **1974**, *15*, 1267–1270.

(141) Märkl, G.; Kreitmeier, P.; Daffner, R. *Tetrahedron Lett.* **1993**, *34*, 7045–7048.

(142) Tohmé, A.; Grelaud, G.; Argouarch, G.; Roisnel, T.; Labouille, S.; Carmichael, D.; Paul, F. *Angew. Chem. Int. Ed.* **2013**, *52*, 4445–4448.

(143) Shah, S.; Burdette, S. C.; Swavey, S.; Urbach, F. L.; Protasiewicz, J. D. *Organometallics* **1997**, *16*, 3395–3400.

(144) Kuhn, N.; Kratz, T. *Synthesis* **1993**, *1993*, 561–562.

(145) Majhi, P. K.; Koner, A.; Schnakenburg, G.; Kelemen, Z.; Nyulászi, L.; Streubel, R. *Eur. J. Inorg. Chem.* **2016**, *2016*, 3559–3573.

(146) Schneider, H.; Schmidt, D.; Radius, U. *Chemistry (Weinheim an der Bergstrasse, Germany),* **2015**, *21*, 2793–2797.

(147) Ren, Y.; Linder, T.; Baumgartner, T. *Can. J. Chem.* **2009**, *87*, 1222–1229.

(148) Blinka, T. A.; Helmer, B. J.; West, R. *Advances in Organometallic Chemistry*; Elsevier, **1984**; 193–218.

(149) Passarelli, V.; Carta, G.; Rossetto, G.; Zanella, P. *Dalton Trans.* **2003**, 413–419.

(150) Uhl, W.; Tannert, J.; Layh, M.; Hepp, A.; Grimme, S.; Risthaus, T. *Organometallics* **2013**, *32*, 6770–6779.

(151) Ramachandran, M. R. K.; Schnakenburg, G.; Majumdar, M.; Kelemen, Z.; Gál, D.; Nyulászi, L.; Boeré, R. T.; Streubel, R. K. *Inorg. Chem.* **2022**, *61*, 4639–4646.

(152) Kuhn, N.; Kratz, T. *Synthesis* **1993**, *1993*, 561–562.

(153) Bygdén, A. *Ber. Dtsch. Chem. Ges.* **1915**, *48*, 1236–1242.

(154) Maier, G.; Mihm, G.; Baumgärtner, R. O. W.; Reisenauer, H. P. *Chem. Ber.* **1984**, *117*, 2337–2350.

(155) Toulokhonova†, I.; Zhao, R.; Kozee, M.; West, R. *Main Group Metal Chemistry,* **2001**, *24*.

(156) West, R. *J. Am. Chem. Soc.* **1954**, *76*, 6012–6014.

(157) Yamaguchi, S.; Jin, R.-Z.; Tamao, K. *J. Organomet. Chem.* **1998**, *559*, 73–80.

(158) Denk, M.; Lennon, R.; Hayashi, R.; West, R.; Belyakov, A. V.; Verne, H. P.; Haaland, A.; Wagner, M.; Metzler, N. *J. Am. Chem. Soc.* **1994**, *116*, 2691–2692.

(159) Driess, M.; Yao, S.; Brym, M.; van Wüllen, C.; Lentz, D. *J. Am. Chem. Soc.* **2006**, *128*, 9628–9629.

(160) Kira, M.; Ishida, S.; Iwamoto, T.; Kabuto, C. *J. Am. Chem. Soc.* **1999**, *121*, 9722–9723.

(161) Kira, M. *Chem. Commun.* **2010**, *46*, 2893–2903.

(162) Atwell, W. H.; Weyenberg, D. R. *J. Am. Chem. Soc.* **1968**, *90*, 3438–3443.

(163) Atwell, W. H. *Organometallics* **2009**, *28*, 3573–3586.

(164) Mizuhata, Y.; Sasamori, T.; Tokitoh, N. *Chem. Rev.* **2009**, *109*, 3479–3511.

(165) Shan, C.; Yao, S.; Driess, M. *Chem. Soc. Rev.* **2020**, *49*, 6733–6754.

(166) Granucci, G.; Toniolo, A. *Chem. Phys. Lett.* **2000**, *325*, 79–85.

(167) Perrin, D. D.; Armarego, W. L. F.; Perrin, D. R. *Purification of Laboratory Chemicals*; Pergamon Press, Oxford, **1988**.

(168) Lunn, G.; Sansone, E. B. *Destruction of hazardous chemicals in the laboratory*, Fourth edition; John Wiley & Sons, **2023**.

(169) Sheldrick, G. M. *Acta crystallographica. Section A, Foundations and advances* **2015**, *71*, 3–8.

(170) Dolomanov, O. V.; Bourhis, L. J.; Gildea, R. J.; Howard, J. A. K.; Puschmann, H. *J Appl Crystallogr.* **2009**, *42*, 339–341.

(171) Bourhis, L. J.; Dolomanov, O. V.; Gildea, R. J.; Howard, J. A. K.; Puschmann, H. *Acta crystallographica. Section A, Foundations and advances* **2015**, *71*, 59–75.

(172) Gritzner, G.; Kuta, J. *Pure Appl. Chem.* **1984**, *56*, 461–466.

(173) Punji, B.; Mague, J. T.; Balakrishna, M. S. *Inorg. Chem.* **2007**, *46*, 10268–10275.

(174) Chantrell, P. G.; Pearce, C. A.; Toyer, C. R.; Twaits, R. *J. Appl. Chem.* **1964**, *14*, 563–564.

(175) King, R. B.; Sadanani, N. D. *Synthesis and Reactivity in Inorganic and Metal-Organic Chemistry* **1985**, *15*, 149–153.

(176) Reetz, M. T.; Maier, W. F. *Justus Liebigs Ann. Chem.* **1980**, *1980*, 1471–1473.

(177) Campbell, M.; Snieckus, V.; Baxter, E. W. Lithium 2,2,6,6-Tetramethylpiperidide, *Encyclopedia of Reagents for Organic Synthesis*; John Wiley & Sons, Ltd, **2001**.

(178) Roy, G.; Jayaram, P. N.; Mugesh, G. *Chem. Asian J.* **2013**, *8*, 1910–1921.

(179) Nishinaga, T., Ed. *Organic Redox Systems: synthesis, properties and applications*; John Wiley & Sons, Inc, Hoboken, New Jersey, **2016**.

Abbreviations

Å	Ångström (1x10–10 m)		K	Kelvin
°	angle in degree		KHMDS	Potassium hexamethyldisilazide
Ar	Aromatic substituent		KO*t*-Bu	Potassium *tert*-butoxide
APCI	Atmospheric Pressure Chemical Ionizatio		LDA	Lithium Diisopropylamide
ATR	Attenual Total Reflexion		LIFDI	Liquid Injection Field Desorption Ionization
au	Atomic Unit		LiTMP	Lithium tetramethylpiperidide
br	broad signal		LUMO	Lowest Unoccupied Molecular Orbital
n-Bu	*n*-butyl		m	multiplet
calc.	calculated		mg	milligram
°C	Degree Celsius		mL	millilitre
$CDCl_3$	Deuterated chloroform		mmol	millimole
CD_2Cl_2	Deuterated dichloromethane		MS	mass spectrometry
C_6D_6	Deuterated benzene		m/z	mass to charge ratio
cm	Centimeter		NICS	Nucleus Independent Chemical Shift
CSD	Cambridge Structural Database		nm	nanometre
CV	Cyclic voltammetry		NMR	Nuclear Magnetic Resonance
DCM	Dichloromethane		PE	petrol ether (40/60)
DEPT	Distortionless Enhancement by Polarization		Ph	phenyl (C6H5)
δ	chemical shift in ppm		ppm	parts per million

Δδ	chemical shift difference	*n*-Pr	*n*-Propyl
EI	Electron Impact ionization	q	quartet
ESI	Electrospray Ionization	quin	quintet
Et	ethyl	R, R´, R$_1$	organic substituent
Et$_2$O	diethyl ether	r.t.	room temperature
eq.	Equivalent	s	singlet
eV	Electron volt	T	temperature
FWHM	Full Width at Half Maximum	*t*	tertiary
g	gram	TD-DFT	Time-dependent Density-Functional Theory
h	Hour	*tert*	tertiary
HMBC	Heteronuclear Multiple Quantum Correlation	THF	Tetrahydrofuran
HOMO	Highest Occupied Molecular Orbital	THF-*d*8	Deuterated tetrahydrofuran
HR-MS	High Resolution Mass Spectrometry	TMEDA	Tetramethylethylenediamine
HSQC	Heteronuclear Single Quantum Coherence	Toluene-*d*8	Deuterated toluene
Hz	Hertz	TMP	Tetramethylpiperidide
IR	Infra Red	Ø	diameter
$^{n}J_{X,Y}$	coupling constant (between the elements X,Y over n bonds) in Hz	X	halogen or leaving group

Appendix

11.1 Crystal data and structure refinement for compound 10a
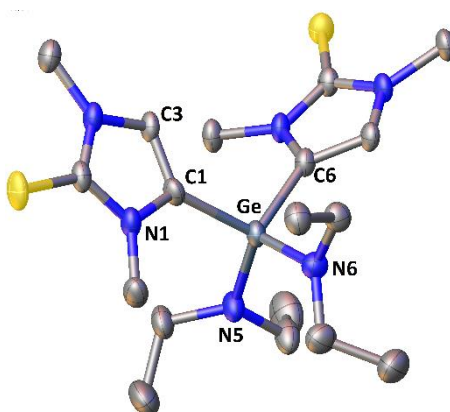
Identification code	GSTR799, MR-391 // GXray7148
Crystal Habitus	clear colorless needle
Device Type	STOE STADIVARI
Empirical formula	$C_{40}H_{78}Ge_2N_{12}OS_4$
Moiety formula	2(C18 H34 Ge N6 S2), C4 H10 O
Formula weight	1016.56
Temperature/K	100
Crystal system	Triclinic
Space group	P-1
a/Å	10.4910(7)
b/Å	15.5099(8)
c/Å	17.3593(10)
α/°	75.118(4)
β/°	72.831(5)
γ/°	81.836(5)
Volume/Å^3	2601.5(3)
Z	2
ρ_{calc}g/cm^3	1.298
μ/mm^{-1}	3.251
F(000)	1076.0
Crystal size/mm^3	0.4 × 0.1 × 0.05
Absorption correction	multi-scan
Tmin; Tmax	0.2573; 0.4835
Radiation	CuKα (λ = 1.54186)

2Θ range for data collection/°	8.846 to 135.468°
Completeness to theta	0.989
Index ranges	-10 ≤ h ≤ 12, -18 ≤ k ≤ 13, -20 ≤ l ≤ 20
Reflections collected	56715
Independent reflections	9314 [R_{int} = 0.0777, R_{sigma} = 0.0480]
Data/restraints/parameters	9314/20/570
Goodness-of-fit on F^2	1.020
Final R indexes [I>=2σ (I)]	R_1 = 0.0545, wR_2 = 0.1396
Final R indexes [all data]	R_1 = 0.0769, wR_2 = 0.1582
Largest diff. peak/hole / e Å^{-3}	0.62/-0.87

Bond Lengths

Atom	Atom	Length/Å	Atom	Atom	Length/Å
Ge	N5	1.809(4)	Ge1A	C6A	1.928(4)
Ge	N6	1.823(3)	S1A	C2A	1.689(4)
Ge	C1	1.936(4)	S2A	C7A	1.694(4)
Ge	C6	1.945(4)	N1A	C1A	1.396(5)
S1	C2	1.683(4)	N1A	C2A	1.366(5)
S2	C7	1.677(4)	N1A	C4A	1.456(5)
N1	C1	1.404(5)	N2A	C2A	1.360(5)
N1	C2	1.363(5)	N2A	C3A	1.378(5)
N1	C4	1.451(6)	N2A	C5A	1.466(5)
N2	C2	1.365(5)	N3A	C6A	1.411(5)
N2	C3	1.382(5)	N3A	C7A	1.358(5)
N2	C5	1.455(5)	N3A	C9A	1.450(5)
N3	C6	1.397(5)	N4A	C7A	1.356(5)
N3	C7	1.365(5)	N4A	C8A	1.390(5)
N3	C9	1.458(5)	N4A	C10A	1.452(5)
N4	C7	1.366(5)	N5A	C11A	1.479(5)
N4	C8	1.369(5)	N5A	C13A	1.455(6)
N4	C10	1.465(5)	N6A	C15A	1.451(6)
N5	C11	1.466(5)	N6A	C17A	1.471(7)
N5	C13	1.451(6)	N6A	C17S	1.44(2)
N6	C15	1.448(5)	C1A	C3A	1.356(6)
N6	C17	1.465(5)	C6A	C8A	1.349(6)
C1	C3	1.352(6)	C11A	C12A	1.497(7)
C6	C8	1.362(5)	C13A	C14A	1.496(8)
C11	C12	1.516(6)	C15A	C16A	1.506(7)
C13	C14	1.499(7)	C17A	C18A	1.498(10)
C15	C16	1.512(7)	C17S	C18S	1.502(10)

C17	C18	1.501(9)	O00J	C20	1.432(6)
Ge1A	N5A	1.828(3)	O00J	C21	1.416(7)
Ge1A	N6A	1.809(4)	C19	C20	1.502(8)
Ge1A	C1A	1.937(4)	C21	C22	1.516(9)

Atom	Atom	Atom	Angle/°	Atom	Atom	Atom	Angle/°
N5	Ge	N6	107.68(16)	N6A	Ge1A	C1A	112.58(17)
N5	Ge	C1	112.31(17)	N6A	Ge1A	C6A	109.76(17)
N5	Ge	C6	106.89(16)	C6A	Ge1A	C1A	105.66(17)
N6	Ge	C1	110.96(15)	C1A	N1A	C4A	126.2(3)
N6	Ge	C6	111.58(16)	C2A	N1A	C1A	110.9(3)
C1	Ge	C6	107.38(16)	C2A	N1A	C4A	122.8(3)
C1	N1	C4	126.7(3)	C2A	N2A	C3A	109.8(3)
C2	N1	C1	110.2(3)	C2A	N2A	C5A	125.7(3)
C2	N1	C4	123.1(3)	C3A	N2A	C5A	124.3(3)
C2	N2	C3	109.2(3)	C6A	N3A	C9A	125.5(3)
C2	N2	C5	124.3(3)	C7A	N3A	C6A	110.5(3)
C3	N2	C5	126.5(3)	C7A	N3A	C9A	123.8(3)
C6	N3	C9	127.0(3)	C7A	N4A	C8A	109.7(3)
C7	N3	C6	110.8(3)	C7A	N4A	C10A	124.4(3)
C7	N3	C9	122.2(3)	C8A	N4A	C10A	125.9(3)
C7	N4	C8	110.2(3)	C11A	N5A	Ge1A	115.4(3)
C7	N4	C10	123.8(3)	C13A	N5A	Ge1A	120.6(3)
C8	N4	C10	126.0(3)	C13A	N5A	C11A	115.3(3)
C11	N5	Ge	117.9(3)	C15A	N6A	Ge1A	123.6(3)
C13	N5	Ge	122.3(3)	C15A	N6A	C17A	119.3(4)
C13	N5	C11	116.2(4)	C17A	N6A	Ge1A	117.0(4)
C15	N6	Ge	122.4(3)	C17S	N6A	Ge1A	130.3(10)
C15	N6	C17	116.3(3)	C17S	N6A	C15A	100.5(10)
C17	N6	Ge	118.3(3)	N1A	C1A	Ge1A	128.8(3)
N1	C1	Ge	125.4(3)	C3A	C1A	Ge1A	124.9(3)
C3	C1	Ge	128.8(3)	C3A	C1A	N1A	105.2(3)
C3	C1	N1	105.6(3)	N1A	C2A	S1A	126.5(3)
N1	C2	S1	127.2(3)	N2A	C2A	S1A	128.2(3)
N1	C2	N2	106.0(3)	N2A	C2A	N1A	105.3(3)
N2	C2	S1	126.8(3)	C1A	C3A	N2A	108.8(3)
C1	C3	N2	108.9(3)	N3A	C6A	Ge1A	124.9(3)
N3	C6	Ge	125.6(3)	C8A	C6A	Ge1A	129.4(3)
C8	C6	Ge	129.0(3)	C8A	C6A	N3A	105.4(3)
C8	C6	N3	105.4(3)	N3A	C7A	S2A	127.6(3)
N3	C7	S2	127.8(3)	N4A	C7A	S2A	126.5(3)

N3	C7	N4	105.1(3)	N4A	C7A	N3A	105.9(3)
N4	C7	S2	127.1(3)	C6A	C8A	N4A	108.5(3)
C6	C8	N4	108.5(4)	N5A	C11A	C12A	115.0(4)
N5	C11	C12	116.5(4)	N5A	C13A	C14A	114.4(5)
N5	C13	C14	114.9(4)	N6A	C15A	C16A	115.5(4)
N6	C15	C16	113.7(4)	N6A	C17A	C18A	111.7(6)
N6	C17	C18	116.1(5)	N6A	C17S	C18S	111(2)
N5A	Ge1A	C1A	110.66(16)	C21	O00J	C20	111.4(4)
N5A	Ge1A	C6A	106.91(17)	O00J	C20	C19	109.6(4)
N6A	Ge1A	N5A	110.99(16)	O00J	C21	C22	108.3(5)

11.2 Crystal data and structure refinement for compound 12a
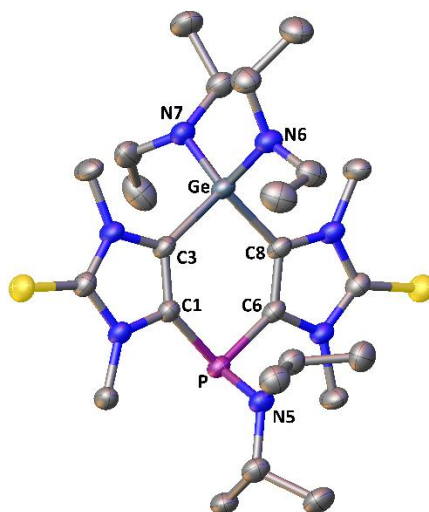
Identification code	GSTR800, MR-445 // GXray7152
Crystal Habitus	clear colorless block
Device Type	STOE STADIVARI
Empirical formula	$C_{24}H_{46}GeN_7PS_2$
Moiety formula	C24 H46 Ge N7 P S2
Formula weight	600.36
Temperature/K	100
Crystal system	triclinic
Space group	P-1
a/Å	8.9922(3)
b/Å	10.9651(3)
c/Å	15.4675(5)
α/°	87.642(3)
β/°	81.540(3)
γ/°	79.789(3)
Volume/Å^3	1484.44(8)
Z	2
ρ$_{calc}$g/cm^3	1.343
μ/mm^{-1}	3.423
F(000)	636.0
Crystal size/mm^3	0.21 × 0.15 × 0.05
Absorption correction	multi-scan
Tmin; Tmax	0.3874; 0.5059
Radiation	CuKα (λ = 1.54186)
2Θ range for data collection/°	9.958 to 140.974°
Completeness to theta	0.992

Index ranges	$-10 \leq h \leq 10, -13 \leq k \leq 13, -18 \leq l \leq 6$
Reflections collected	35661
Independent reflections	5589 [R_{int} = 0.0516, R_{sigma} = 0.0321]
Data/restraints/parameters	5589/0/328
Goodness-of-fit on F^2	1.071
Final R indexes [I>=2σ (I)]	R_1 = 0.0547, wR_2 = 0.1473
Final R indexes [all data]	R_1 = 0.0697, wR_2 = 0.1599
Largest diff. peak/hole / e Å^{-3}	1.57/-0.45

Bond Lengths

Atom	Atom	Length/Å	Atom	Atom	Length/Å
Ge	N6	1.810(3)	N4	C8	1.398(5)
Ge	N7	1.815(3)	N4	C10	1.463(5)
Ge	C3	1.936(4)	N5	C11	1.489(5)
Ge	C8	1.938(4)	N5	C14	1.487(5)
S1	C2	1.679(4)	N6	C17	1.468(5)
S2	C7	1.684(4)	N6	C19	1.474(5)
P	N5	1.689(3)	N7	C21	1.451(5)
P	C1	1.835(4)	N7	C23	1.481(5)
P	C6	1.830(4)	C1	C3	1.376(5)
N1	C1	1.396(5)	C6	C8	1.366(5)
N1	C2	1.371(5)	C11	C12	1.531(6)
N1	C4	1.460(5)	C11	C13	1.519(6)
N2	C2	1.356(5)	C14	C15	1.523(6)
N2	C3	1.403(5)	C14	C16	1.523(6)
N2	C5	1.450(5)	C17	C18	1.530(6)
N3	C6	1.402(5)	C19	C20	1.523(6)
N3	C7	1.361(5)	C21	C22	1.510(7)
N3	C9	1.454(5)	C23	C24	1.509(6)
N4	C7	1.365(5)			

Atom	Atom	Atom	Angle/°	Atom	Atom	Atom	Angle/°
N6	Ge	N7	105.19(15)	C23	N7	Ge	117.5(3)
N6	Ge	C3	118.23(16)	N1	C1	P	119.5(3)
N6	Ge	C8	107.45(15)	C3	C1	P	133.3(3)
N7	Ge	C3	109.47(15)	C3	C1	N1	106.9(3)
N7	Ge	C8	118.76(15)	N1	C2	S1	127.6(3)
C3	Ge	C8	98.39(15)	N2	C2	S1	127.1(3)
N5	P	C1	105.08(17)	N2	C2	N1	105.4(3)
N5	P	C6	103.06(16)	N2	C3	Ge	126.5(3)

C6	P	C1	98.69(16)	C1	C3	Ge	127.1(3)
C1	N1	C4	126.3(3)	C1	C3	N2	106.0(3)
C2	N1	C1	110.5(3)	N3	C6	P	119.9(3)
C2	N1	C4	123.2(3)	C8	C6	P	133.7(3)
C2	N2	C3	111.2(3)	C8	C6	N3	106.4(3)
C2	N2	C5	123.1(3)	N3	C7	S2	127.7(3)
C3	N2	C5	125.7(3)	N3	C7	N4	105.5(3)
C6	N3	C9	125.5(3)	N4	C7	S2	126.8(3)
C7	N3	C6	110.7(3)	N4	C8	Ge	125.1(3)
C7	N3	C9	123.7(3)	C6	C8	Ge	127.8(3)
C7	N4	C8	110.4(3)	C6	C8	N4	107.0(3)
C7	N4	C10	123.5(3)	N5	C11	C12	112.1(3)
C8	N4	C10	126.1(3)	N5	C11	C13	111.9(4)
C11	N5	P	120.0(3)	C13	C11	C12	108.4(4)
C14	N5	P	118.7(3)	N5	C14	C15	113.5(3)
C14	N5	C11	119.6(3)	N5	C14	C16	113.1(4)
C17	N6	Ge	117.3(3)	C15	C14	C16	112.2(4)
C17	N6	C19	115.6(3)	N6	C17	C18	112.9(4)
C19	N6	Ge	121.1(3)	N6	C19	C20	112.2(4)
C21	N7	Ge	118.4(3)	N7	C21	C22	116.5(4)
C21	N7	C23	115.8(3)	N7	C23	C24	113.7(4)

11.3 Crystal data and structure refinement for compound 13a
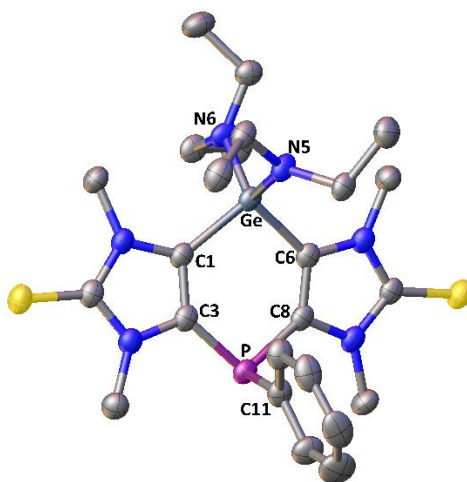
Identification code	GSTR798, MR-446 // GXray7147
Crystal Habitus	clear yellowish colorless block
Device Type	STOE STADIVARI
Empirical formula	$C_{52}H_{84}Ge_2N_{12}OP_2S_4$
Moiety formula	2(C24 H37 Ge N6 P S2), C4 H10 O
Formula weight	1228.71
Temperature/K	100
Crystal system	monoclinic
Space group	$C2/c$
a/Å	19.4838(7)
b/Å	11.2254(3)
c/Å	30.2357(11)
α/°	90.00
β/°	112.700(3)
γ/°	90.00
Volume/Å^3	6100.7(4)
Z	4
ρ_{calc}g/cm^3	1.338
μ/mm^{-1}	3.352
F(000)	2584.0
Crystal size/mm^3	0.3 × 0.3 × 0.1
Absorption correction	multi-scan
Tmin; Tmax	0.1971; 0.3168
Radiation	CuKα (λ = 1.54186)
2Θ range for data collection/°	6.338 to 140.984°
Completeness to theta	1.000
Index ranges	-20 ≤ h ≤ 23, -10 ≤ k ≤ 13, -36 ≤ l ≤ 36

Reflections collected	35811
Independent reflections	5798 [R_{int} = 0.0562, R_{sigma} = 0.0281]
Data/restraints/parameters	5798/0/339
Goodness-of-fit on F^2	1.042
Final R indexes [I>=2σ (I)]	R_1 = 0.0460, wR_2 = 0.1228
Final R indexes [all data]	R_1 = 0.0498, wR_2 = 0.1271
Largest diff. peak/hole / e Å^{-3}	0.92/-0.83

Bond Lengths

Atom	Atom	Length/Å	Atom	Atom	Length/Å
Ge	N5	1.8092(18)	N4	C10	1.458(3)
Ge	N6	1.8176(18)	N5	C17	1.463(3)
Ge	C1	1.939(2)	N5	C19	1.463(3)
Ge	C6	1.932(2)	N6	C21	1.454(3)
S1	C2	1.683(2)	N6	C23	1.468(3)
S2	C7	1.680(2)	C1	C3	1.368(3)
P	C3	1.809(2)	C6	C8	1.361(3)
P	C8	1.818(2)	C11	C12	1.389(4)
P	C11	1.847(2)	C11	C16	1.390(4)
N1	C1	1.399(3)	C12	C13	1.395(4)
N1	C2	1.358(3)	C13	C14	1.383(5)
N1	C4	1.465(3)	C14	C15	1.376(5)
N2	C2	1.367(3)	C15	C16	1.395(4)
N2	C3	1.395(3)	C17	C18	1.517(4)
N2	C5	1.457(3)	C19	C20	1.524(4)
N3	C6	1.395(3)	C21	C22	1.523(4)
N3	C7	1.360(3)	C23	C24	1.521(4)
N3	C9	1.452(3)	O	C26	1.423(4)
N4	C7	1.371(3)	O	C26^1	1.423(4)
N4	C8	1.390(3)	C25	C26	1.490(5)

Bond Angles

Atom	Atom	Atom	Angle/˚	Atom	Atom	Atom	Angle/˚
N5	Ge	N6	107.69(9)	N1	C2	S1	127.40(18)
N5	Ge	C1	115.71(9)	N1	C2	N2	106.08(19)
N5	Ge	C6	109.00(9)	N2	C2	S1	126.52(19)
N6	Ge	C1	108.57(9)	N2	C3	P	118.84(17)
N6	Ge	C6	117.61(9)	C1	C3	P	133.41(19)
C6	Ge	C1	98.42(10)	C1	C3	N2	107.7(2)
C3	P	C8	99.91(11)	N3	C6	Ge	126.02(17)
C3	P	C11	101.18(11)	C8	C6	Ge	127.42(17)

C8	P	C11	101.00(10)	C8	C6	N3	106.48(19)
C1	N1	C4	125.6(2)	N3	C7	S2	126.91(18)
C2	N1	C1	110.67(19)	N3	C7	N4	105.42(19)
C2	N1	C4	123.65(19)	N4	C7	S2	127.64(18)
C2	N2	C3	109.5(2)	N4	C8	P	120.34(17)
C2	N2	C5	124.1(2)	C6	C8	P	132.18(17)
C3	N2	C5	126.3(2)	C6	C8	N4	107.4(2)
C6	N3	C9	125.39(19)	C12	C11	P	122.86(19)
C7	N3	C6	110.66(19)	C12	C11	C16	119.6(2)
C7	N3	C9	123.95(19)	C16	C11	P	117.53(19)
C7	N4	C8	110.02(19)	C11	C12	C13	119.7(3)
C7	N4	C10	122.84(19)	C14	C13	C12	120.6(3)
C8	N4	C10	127.1(2)	C15	C14	C13	119.6(2)
C17	N5	Ge	122.92(15)	C14	C15	C16	120.4(3)
C17	N5	C19	116.11(18)	C11	C16	C15	120.0(3)
C19	N5	Ge	119.03(14)	N5	C17	C18	112.3(2)
C21	N6	Ge	122.72(14)	N5	C19	C20	114.3(2)
C21	N6	C23	116.13(18)	N6	C21	C22	112.5(2)
C23	N6	Ge	117.94(16)	N6	C23	C24	113.7(2)
N1	C1	Ge	127.50(17)	C26	O	C26[1]	111.3(3)
C3	C1	Ge	125.46(17)	O	C26	C25	110.0(3)
C3	C1	N1	106.0(2)				

11.4 TD-DFT results at B3LYP/6-311G**//M06-2X/6-311+G** level of theory (first 7 excited state) of 2a'ᐟ.

Excited state	Wavelength	Oscillator strength	Transition	Contribution
1	1005 nm	0.0871	β-HOMO-β-LUMO	0.99153
2	682 nm	0.0000	β-HOMO-3-β-LUMO	-0.13499
			β-HOMO-1-β-LUMO	0.98415
3	658 nm	0.0047	β-HOMO-3-β-LUMO	0.40247
			β-HOMO-2-β-LUMO	0.89461
			β-HOMO-1-β-LUMO	0.13453
4	656 nm	0.0042	β-HOMO-3-β-LUMO	0.90050
			β-HOMO-2-β-LUMO	-0,40329
5	453 nm	0.0125	α-HOMO-α-LUMO+1	0.20231
			β-HOMO-4-β-LUMO	0.96571
6	401 nm	0.0117	α-HOMO-α-LUMO	-0.21044
			β-HOMO-5-β-LUMO	0.95549
7	389 nm	0.0079	α-HOMO-1-α-LUMO+1	0.17393
			α-HOMO-α-LUMO	0.88698
			β-HOMO-5-β-LUMO	0.25533

11.5 Stacked plots of K[14b] (1 mM) with v = 0.05, 0.2, 0.5, 1 V/s.

11.6 Stacked plots of 15b (1 mM) with v = 0.05, 0.2, 0.5, 1 V/s

List of figures, schemes and tables